Journal of Pathology Informatics 15 (2024) 100357

Contents lists available at ScienceDirect

Journal of Pathology Informatics

journal homepage: www.elsevier.com/locate/jpi

Review Article

Computational pathology: A survey review and the way forward☆

Mahdi S. Hosseini [a,*], Babak Ehteshami Bejnordi [b,1], Vincent Quoc-Huy Trinh [c], Lyndon Chan [d], Danial Hasan [d], Xingwen Li [d], Stephen Yang [d], Taehyo Kim [d], Haochen Zhang [d], Theodore Wu [d], Kajanan Chinniah [d], Sina Maghsoudlou [a], Ryan Zhang [d], Jiadai Zhu [d], Samir Khaki [d], Andrei Buin [e], Fatemeh Chaji [a], Ala Salehi [f], Bich Ngoc Nguyen [g], Dimitris Samaras [h], Konstantinos N. Plataniotis [d]

[a] Department of Computer Science and Software Engineering (CSSE), Concordia Univeristy, Montreal, QC H3H 2R9, Canada
[b] Qualcomm AI Research, Qualcomm Technologies Netherlands B.V., Amsterdam, The Netherlands
[c] Institute for Research in Immunology and Cancer of the University of Montreal, Montreal, QC H3T 1J4, Canada
[d] The Edward S. Rogers Sr. Department of Electrical & Computer Engineering (ECE), University of Toronto, Toronto, ON M5S 3G4, Canada
[e] Huron Digitial Pathology, St. Jacobs, ON N0B 2N0, Canada
[f] Department of Electrical and Computer Engineering, University of New Brunswick, Fredericton, NB E3B 5A3, Canada
[g] University of Montreal Hospital Center, Montreal, QC H2X 0C2, Canada
[h] Department of Computer Science, Stony Brook University, Stony Brook, NY 11794, United States

ARTICLE INFO

Keywords:
Digital pathology
Whole slide image (WSI)
Deep learning
Computer aided diagnosis (CAD)
Clinical pathology
Survey

ABSTRACT

Computational Pathology (CPath) is an interdisciplinary science that augments developments of computational approaches to analyze and model medical histopathology images. The main objective for CPath is to develop infrastructure and workflows of digital diagnostics as an assistive CAD system for clinical pathology, facilitating transformational changes in the diagnosis and treatment of cancer that are mainly address by CPath tools. With evergrowing developments in deep learning and computer vision algorithms, and the ease of the data flow from digital pathology, currently CPath is witnessing a paradigm shift. Despite the sheer volume of engineering and scientific works being introduced for cancer image analysis, there is still a considerable gap of adopting and integrating these algorithms in clinical practice. This raises a significant question regarding the direction and trends that are undertaken in CPath. In this article we provide a comprehensive review of more than 800 papers to address the challenges faced in problem design all-the-way to the application and implementation viewpoints. We have catalogued each paper into a model-card by examining the key works and challenges faced to layout the current landscape in CPath. We hope this helps the community to locate relevant works and facilitate understanding of the field's future directions. In a nutshell, we oversee the CPath developments in cycle of stages which are required to be cohesively linked together to address the challenges associated with such multidisciplinary science. We overview this cycle from different perspectives of data-centric, model-centric, and application-centric problems. We finally sketch remaining challenges and provide directions for future technical developments and clinical integration of CPath. For updated information on this survey review paper and accessing to the original model cards repository, please refer to GitHub. Updated version of this draft can also be found from arXiv.

Contents

☆ This work is dedicated to the beloved memories of Kuanhou Fang, Shahnaz Habibpanah, Zakiyeh Khaliji-Oskoui, James Liang, Mahsa MohammadiMoghaddam, Vily Panoutsakopoulou, Athanasia Samara, Huoyuan Yu, Dexi Zhang and all people around the world who have lost their lives because of cancer.

* Corresponding author.
E-mail address: mahdi.hosseini@concordia.ca (M.S. Hosseini).

[1] Qualcomm AI Research is an initiative of Qualcomm Technologies, Inc.

http://dx.doi.org/10.1016/j.jpi.2023.100357
Received 15 October 2023; Received in revised form 21 December 2023; Accepted 23 December 2023
Available online 14 January 2024

1. Introduction

April 2017 marked a turning point for digital pathology when the Philips IntelliSite digital scanner received the US Food & Drugs Administration (FDA) approval (with limited use case) for diagnostic applications in clinical pathology.[1,2] A subsequent validation guideline was created to help ensure the produced Whole Slide Image (WSI) scans could be used in clinical settings without compromising patient care, while maintaining similar results to the current gold standard of optical microscopy.[3–6] The use of WSIs offers significant advantages to the pathologist's workflow: digitally captured images, compared to tissue slides, are immune from accidental physical damage and maintain their quality over time.[7,8] Clinics and practices can share and store these high-resolution images digitally enabling asynchronous viewing/collaboration worldwide.[9,10] The

development of *digital pathology* shows great promise as a framework to improve work efficiency in the practice of pathology.[10,11] Adopting a digital workflow also opens immense opportunities for using computational methods to augment and expedite their workflow–the field of *Computational Pathology (CPath)* is dedicated to researching and developing these methods.[12–17]

However, despite the aforementioned advantages, the adoption of digital pathology, and hence computational pathology, has been slow. Some pathologists consider the analysis of WSIs as opposed to glass slides as an unnecessary change in their workflow[9,18–20] and recent surveys indicate that the switch to digital pathology does not provide enough financial incentive.[8,21–25] This is where advances from CPath can address or overpower many of the concerns in adopting a digital workflow. For example, CPath models to identify morphological features that correlate with breast cancer[26] provide substantial benefits to clinical accuracy. Further, CPath models that identify lymph node metastases with better sensitivity while reducing diagnostic time[27] can streamline workflows to increase pathologist throughput and generate more revenue.[28,29]

Similar to digital pathology, the adoption of CPath methods has also lagged despite the many benefits it offers to improve efficiency and accuracy in pathology.[2,30–32] This lack of adoption and integration into clinical practice raises a significant question regarding the direction and trends of current work in CPath. This survey looks to review the field of CPath in a systematic fashion by breaking down the various steps involved in a CPath workflow and categorizing CPath works to both determine trends in the field and provide a resource for the community to reference when creating new works.

Existing survey papers in the field of CPath can be clustered into a few groups. The first focuses on the design and applications of smart diagnosis tools.[15–17,33–43] These works focus on designing novel architectures for artificial intelligence (AI) models with regards to specific clinical tasks, although they may briefly discuss clinical challenges and limitations. A second group of works focus on clinical barriers for AI integration discussing specific certifications and regulations required for the development of medical devices under clinical settings.[44–49] Lastly, the final group focuses on both the design and the integration of AI tools with clinical applications.[12–14,29,50–56] These works speak to both the computer vision and pathology communities in developing machine learning (ML) models that can satisfy clinical use cases.

Our work is situated in this final group as we breakdown the end-to-end CPath workflow into stages and systematically review works related to and addressing those stages. We oversee this as a workflow for CPath research that breaks down the process of problem definition, data collection, model creation, and clinical validation into a cycle of stages. A visual representation of this cycle is provided in Fig. 1. We review over 700 papers from all areas of the CPath field to examine key works and challenges faced. By reviewing the field so comprehensively, our goal is to layout the current landscape of key developments to allow computer scientists and pathologists alike to situate their work in the overall CPath workflow, locate relevant works, and facilitate an understanding of the field's future directions. We also adopt the idea of generating model cards from[57] and designed a card format specifically tailored for CPath. Each paper we reviewed was catalogued as a model card that concisely describes (1) the organ of application, (2) the compiled dataset, (3) the machine learning model, and (4) the target task. The complete model card categorization of the reviewed publications is provided in Appendix A.12 for the reader's use.

In our review of the CPath field, we find that two main approaches emerge in works: 1) a data-centric approach and 2) a model-centric approach. Considering a given application area, such as specific cancers, e.g. breast ductal carcinoma in-situ (DCIS), or a specific task, e.g. segmentation of benign and malignant regions of tissue, researchers in the CPath field focus generally on either improving the data or innovating on the model used.

Works with data-centric approaches focus on collecting pathology data and compiling datasets to train models on certain tasks based on the

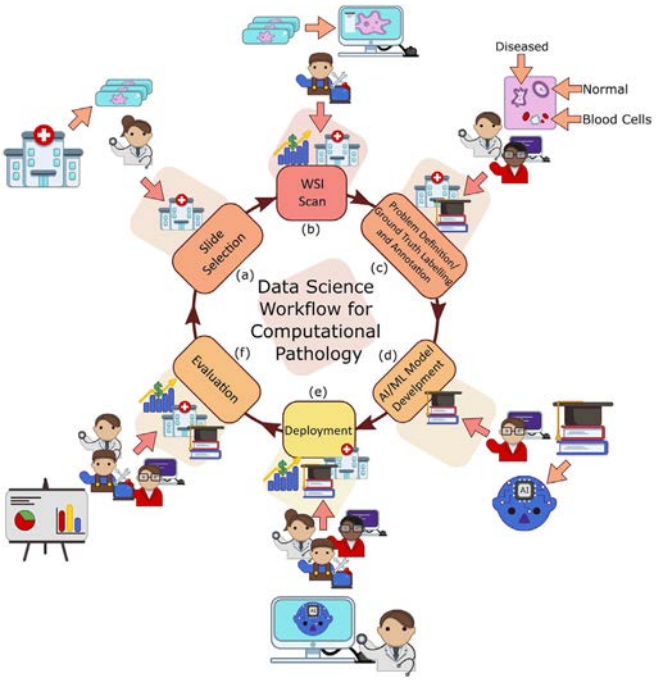

Fig. 1. We divide the data science workflow for pathology into multiple stages, wherein each brings a different level of experience. For example, the annotation/ground truth labelling stage (c) is where domain expert knowledge is consulted as to augment images with associated metadata. Meanwhile, in the evaluation phase (e), we have computer vision scientists, software developers, and pathologists working in concert to extract meaningful results and implications from the representation learning.

premise that the transfer of domain expert knowledge to models is captured by the process of collecting and labeling high-quality data.[51,58,59] The motivation behind this approach in CPath is driven by the need to 1) address the lack of labeled WSI data representing both histology and histopathology cases due to the laborious annotation process[24] and 2) capture a predefined pathology ontology provided by domain expert pathologists for the class definitions and relations in tissue samples. Regarding the lack of labeled WSI data our analysis reveals that there are a larger number of datasets with granular labels, but there is a larger total amount of data available for a given organ and disease application that have weakly supervised labels at the Slide or Patient-level. Although some tasks, such as segmentation and detection, require WSI data to have more granular labels at the region-of-interest (ROI) or image mosaic/tiles (known as patch) levels, to capture more precise information for training models, there is a potential gap to leverage the large amount of weakly-supervised data to train models that can be later used downstream on smaller strongly-supervised datasets for those tasks. When considering the ontology of pathology as compared to the field of computer vision, we note that pathology datasets have far fewer classes than computer vision (e.g. ImageNet-20K contains 20,000 class categories for natural images[60] whereas CAMELYON17 has four annotated classes for breast cancer metastases[61]), but has much more variation within each of these classes in terms of representations and fuzzy boundaries around the *grade* of cancers which subdivides each class into many more in reality. There are also very rare classes in the form of rare diseases and cancers, as presented in Fig. 12 and discussed in Section 2, which present a class imbalance challenge when compiling data or training models. If one considers the complexities involved in representational learning of related tissues and diseases, it raises the question of whether there is a clear understanding and consensus in the field of how an efficient dataset should be compiled for model development. Our survey analyzes the availability of CPath datasets along with what area of application they address and their annotation level in detail in Section 3.3,

and the complete table of datasets we have covered is available in Appendix A.9. Section 4 goes into more depth about the various levels of annotation, the annotation process, and selecting the appropriate annotation level for a task.

The model-centric approach, by contrast, is favoured by computer scientists and engineers, who design algorithmic approaches based on the available pathology data. Selection of a modelling approach, such as self-supervised, weakly-supervised, or strongly-supervised learning, is dictated directly by the amount of data available for a given annotation level and task. Currently, many models are developed on datasets with strongly-supervised labels at the ROI, Patch, or Pixel-levels to address tasks such as tissue type classification or disease detection. However, a recent trend is developing to apply self-supervised and weakly-supervised learning methods to leverage the large amount of data with Slide and Patient-level annotations.[62] Models are trained in a self or weakly supervised manner to learn representations on a wider range of pathology data across organs and diseases, which can be leveraged for other tasks requiring more supervision but without the need for massive labeled datasets.[63–65] This trend points to the future direction of CPath models following a similar trend to that in computer vision, where large-scale models are being pre-trained using self-supervised techniques to achieve state-of-the-art performance in downstream tasks.[66,67]

Although data and model centric approaches are both important in advancing the performance of models and tools in CPath, we note a need for much more *application* centric work in CPath. We define a study to be application centric if the primary focus is on addressing a particularly impactful task or need in the clinical workflow, ideally including clinical validation of the method or tool. To this end, Section 2 details the clinical pathology workflow from specimen collection to report generation, major task categories in CPath, and specific applications per organ. Particularly, we find that very few works focus on the pre or post-analytical phases of the pathology workflow where many errors can occur, instead focusing on the analytical phase where interpretation tasks take place. Additionally, certain types of cancer with deadly survival rates are underrepresented in CPath datasets and works. Very few CPath models and tools have been validated in a clinical setting by pathologists, suggesting that there may still be massive barriers to actually using CPath tools in practice. All of this points to a severe oversight by the CPath community towards considering the actual application and implementation of tools in a clinical setting. We suspect this to be a major reason as to why there is a slow uptake in adopting CPath tools by pathology labs.

The contributions of this survey include the provision of an end-to-end workflow for developing CPath work which outlines the various stages involved and is reflected within the survey sections. Further, we propose and provide a comprehensive conceptual model card framework for CPath that clearly categorizes works by their application of interest, dataset usage, and model, enabling consistent and easy comparison and retrieval of papers in relevant areas. Based on our analysis of the field, we highlight several challenges and trends, including the availability of datasets, focus on models leveraging existing data, disregard of impactful application areas, and lack of clinical validation. Finally, we give suggestions for addressing these aforementioned challenges and provide directions for future work in the hopes of aiding the adoption and implementation of CPath tools in clinical settings.

The structure of this survey closely follows the CPath data workflow illustrated in Fig. 1. Section 2 begins by outlining the clinical pathology workflow and covers the various task domains in CPath, along with organ specific tasks and diseases. The next step of the workflow involves the processes and methods of histopathology data collection, which is outlined in Section 3. Following data collection, Section 4 details the corresponding annotation and labeling methodology and considerations. Section 5 covers deep learning designs and methodologies for CPath applications. Section 6 focuses on regulatory measures and clinical validation of CPath tools. Section 7 explores emerging trends in recent CPath research. Finally, we provide our perceived challenges and future outlook of CPath in Section 8.

2. Clinical applications for CPath

The field of CPath is dedicated to the creation of tools that address and aid steps in the clinical pathology workflow. Thus, a grounded understanding of the clinical workflow is of paramount importance before development of any CPath tool. The outcomes of clinical pathology are diagnostics, prognostics, and predictions of therapy response. Computational pathology systems that focus on diagnostic tasks aim to assist the pathologists in tasks such as tumour detection, tumour grading, quantification of cell numbers, etc. Prognostic systems aim to predict survival for individual patients while therapy response predictive models aid personalized treatment decisions based on histopathology images. Fig. 3 visualizes the goals pertaining to these tasks. In this section, we provide detail on the clinical pathology workflow, the major application areas in diagnostics, prognostics, and therapy response, and finally detail the cancers and CPath applications in specific organs. The goal is to outline the tasks and areas of application in pathology where CPath tools and systems can be developed and implemented.

2.1. Clinical pathology workflow

This subsection provides a general overview of the clinical workflow in pathology covering the collection of a tissue sample, its subsequent processing into a slide, inspection by a pathologist, and compilation of the analysis and diagnosis into a pathology. Fig. 2 summarizes these steps at a high level and provides suggestions for corresponding CPath applications. The steps are organized under the conventional pathology phases for samples: pre-analytical, analytical, and post-analytical. These phases were developed to categorize quality control measures, as each phase has its own set of potential sources of errors,[68] and thus potential sources of corrections during which CPath and healthcare artificial intelligence tools could prove useful. For details about each step of the workflow, please refer to the Appendix A.1.

Pre Analytical Phase The first step of the *pre-analytical* phase is a biopsy performed to collect a tissue sample, where the biopsy method is dependent on the type of sample required and the tissue characteristics. Sample collection is followed by accessioning of the sample which involves entering of the patient and specimen information into a Laboratory Information System (LIS) and linking to the Electronic Medical Records (EMR) and potentially a Slide Tracking System (STS). After accessioning, smaller specimens that have not already been preserved by fixation in formalin are fixated. Once the basic specimen preparation has occurred, the tissue is analyzed by the pathology team without the use of a microscope; a step called grossing. Grossing involves cross-referencing the clinical findings and the EMR reports, with the operator localizing the disease, locating the pathological landmarks, describing these landmarks, and measuring disease extent. Specific sampling of these landmarks is performed, and these samples are then put into cassettes for the final fixation. Subsequently, the samples are then sliced using a microtome, stained using the relevant stains for diagnosis, and covered with a glass slide.

Analytical Phase After a slide is processed and prepared, a pathologist views the slide to analyze and interpret the sample. The approach to interpretation varies depending on the specimen type. Interpretation of smaller specimens is focused on diagnosis of any disease. Analysis is performed in a decision-tree style approach to add diagnosis-specific parameters, e.g. esophagus biopsy → type of sampled mucosa → presence of folveolar-type mucosa → identify Barrett's metaplasia → identify degree of dysplasia. Once the main diagnosis has been identified and characterized, the pathologist sweeps the remaining tissue for secondary diagnoses which can also be characterized depending on their nature. Larger specimens are more complex and usually focus on characterizing the tissue and identifying unexpected diagnoses beyond the prior diagnosis from a small specimen biopsy. Microscopic interpretation of large specimens is highly dependent on the quality of the grossing and the appropriate detection and sampling of landmarks. Each landmark (e.g., tumor surface, tumor at deepest point, surgical margins, lymph node in mesenteric fat) is

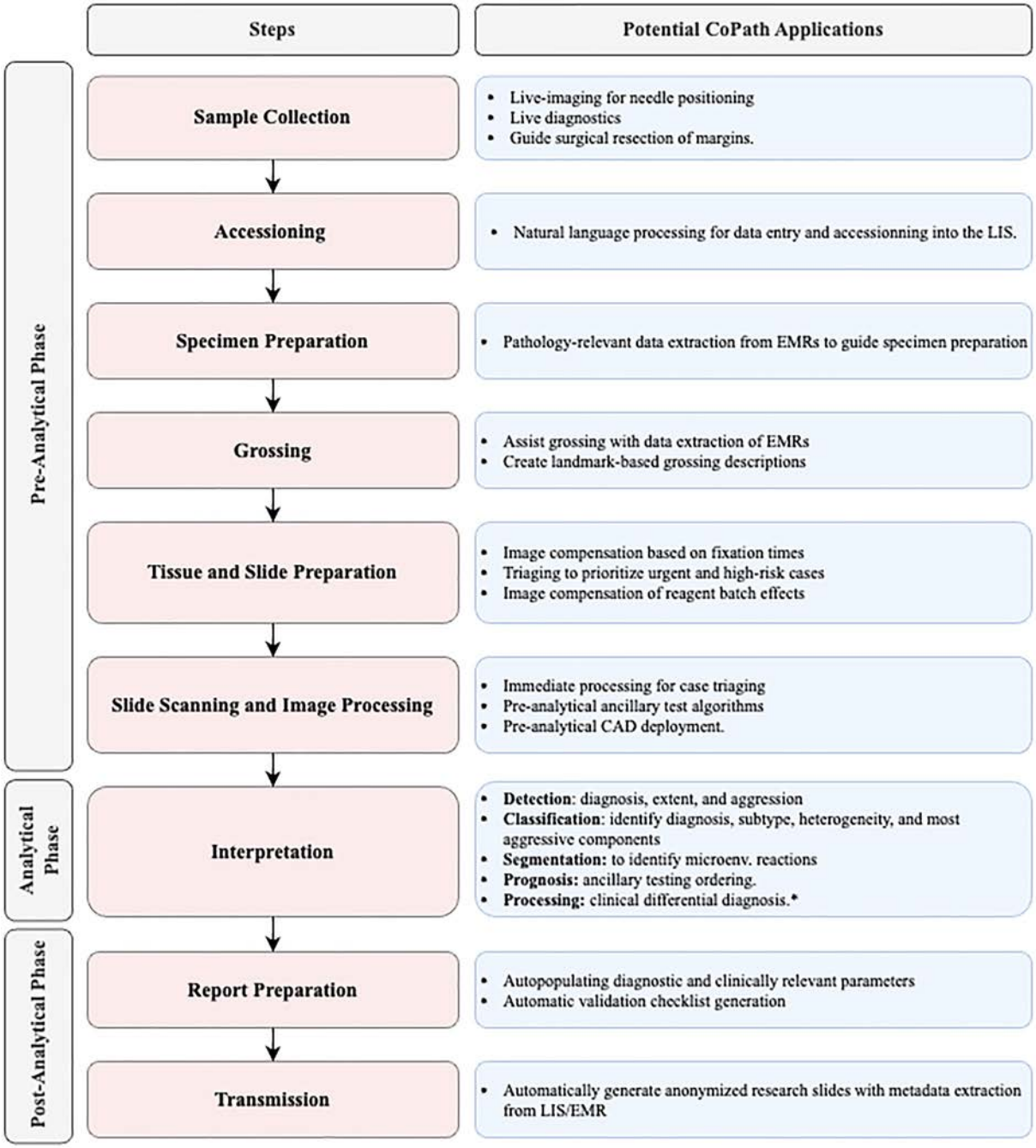

Fig. 2. Quality assurance and control phases developed by pathologists to oversee the clinical pathology workflow into three main phases of pre-analytical, analytical, and post-analytica phases. We further show how each of these processes can be augmented under the potential CPath applications in an end-to-end pipeline.

characterized either according to guidelines, if available, or according to the pathologist's judgment. After the initial microscopic interpretation additional deeper cuts ("levels"), special stains, immunohistochemistry (IHC), and/or molecular testing may be performed to hone the diagnosis by generating new material or slides from the original tissue block.

Post-Analytical Phase The pathologist synthesizes a diagnosis by aggregating their findings from grossing and microscopic examination in combination with the patient's clinical information, all of which are included in a final pathology report. The classic sections of a pathology report are patient information, a list of specimens included, clinical findings, grossing report, microscopic description, final diagnosis, and comment. The length and degree of complexity of the report again depends on the specimen type. Small specimen reports are often succinct, clearly and unambiguously listing relevant findings which guide treatment and follow-up. Large specimen reports depend on the disease, for example, in cancer resection specimens the grossing landmarks are specifically targeted at elements that will guide subsequent treatment.

In the past, pathology reports had no standardized format, usually taking a narrative-free text form. Free text reports can omit necessary data, include irrelevant information, and contain inconsistent descriptions.[69] To combat this, synoptic reporting was introduced to provide a structured and standardized reporting format specific to each organ and cancer of interest.[69,70] Over the last 15 years, synoptic reporting has enabled pathologists to communicate information to surgeons, oncologists, patients, and researchers in a consistent manner across institutions and even countries. The College of American Pathologists (CAP) and the International

Collaboration on Cancer Reporting (ICCR) are the two major institutions publishing synoptic reporting protocols. The parameters included in these protocols are determined and updated by CAP and ICCR respectively to remain up-to-date and relevant for diagnosis of each cancer type. For the field of computational pathology, synoptic reporting provides a significant advantage in dataset and model creation, as a pre-normalized set of labels exist across a variety of cases and slides in the form of the synoptic parameters filled out in each report. Additionally, suggestion or prediction of synoptic report values are a possible CPath application area.

2.2. Diagnostic tasks

Computational pathology systems that focus on diagnostic tasks can broadly be categorized as: (1) disease detection, (2) tissue subtype classification, (3) disease diagnosis, and (4) segmentation. These tasks are visually depicted in Fig. 3. Note how the detection tasks all involve visual analysis of the tissue in WSI format. Thus computer vision approach is primarily adopted towards tackling diagnostic tasks in computer aided diagnosis (CAD). For additional detail on some previous works on these diagnostic tasks, we refer the reader to Appendix A.2

Detection We define the detection task as a binary classification problem where inputs are labeled as positive or negative, indicating the presence or absence of a certain feature. There may be variations in the level of annotation required, e.g. slide-level, patch-level, pixel-level detection depending on the feature in question. Although detection tasks may not provide an immediate disease diagnosis, it is a highly relevant task in many pathology workflows as pathologists incorporate the presence or absence of various histological features into synoptic reports that lead to diagnosis. Broadly, detection tasks fall into two main categories: (1) screening the presence of cancers and (2) detecting histopathological features specific to certain diagnoses.

Cancer detection algorithms can assist the pathologists by filtering obviously normal WSIs and directing pathologist's focus to metastatic regions.[71] Although pathologists have to review all the slides to check for multiple conditions regardless of the clinical diagnosis, an accurate cancer detection CAD would expedite the workflow by pinpointing the ROIs and summarizing results into synoptic reports, ultimately leading to a reduces time per slide. Due to this potential impact, cancer detection tasks have been explored in a broad set of organs. Additionally, the simple labeling in binary detection tasks allows for deep learning methods to generalize across different organs where similar cancers form.[72–74]

Tissue Subtype Classification Treatment and patient prognosis can vary widely depending on the stage of cancer, and finely classifying specific tissue structures associated with a specific disease type provides essential diagnostic and prognostic information.[75] Accordingly, accurately classifying tissue subtypes is a crucial component of the disease diagnosis process. As an example, discriminating between two forms of glioma (a type of brain cancer), glioblastoma multiforme and lower grade glioma, is critical as they differ by over 45% in patient survival rates.[76] Additionally, accurate classification is key in colorectal cancer (CRC) diagnosis, as high morphological variation in tumor cells[77] makes certain forms of CRC difficult to diagnose by pathologists.[78] We define this classification of histological features as tissue subtype classification.

Disease Diagnosis The most frequently explored design of deep learning in digital pathology involves emulating pathologist diagnosis. We define this multi-class diagnosis problem as a disease diagnosis task. Note the similarity with detection–disease diagnosis can be considered a fine-grained classification problem which subdivides the general positive

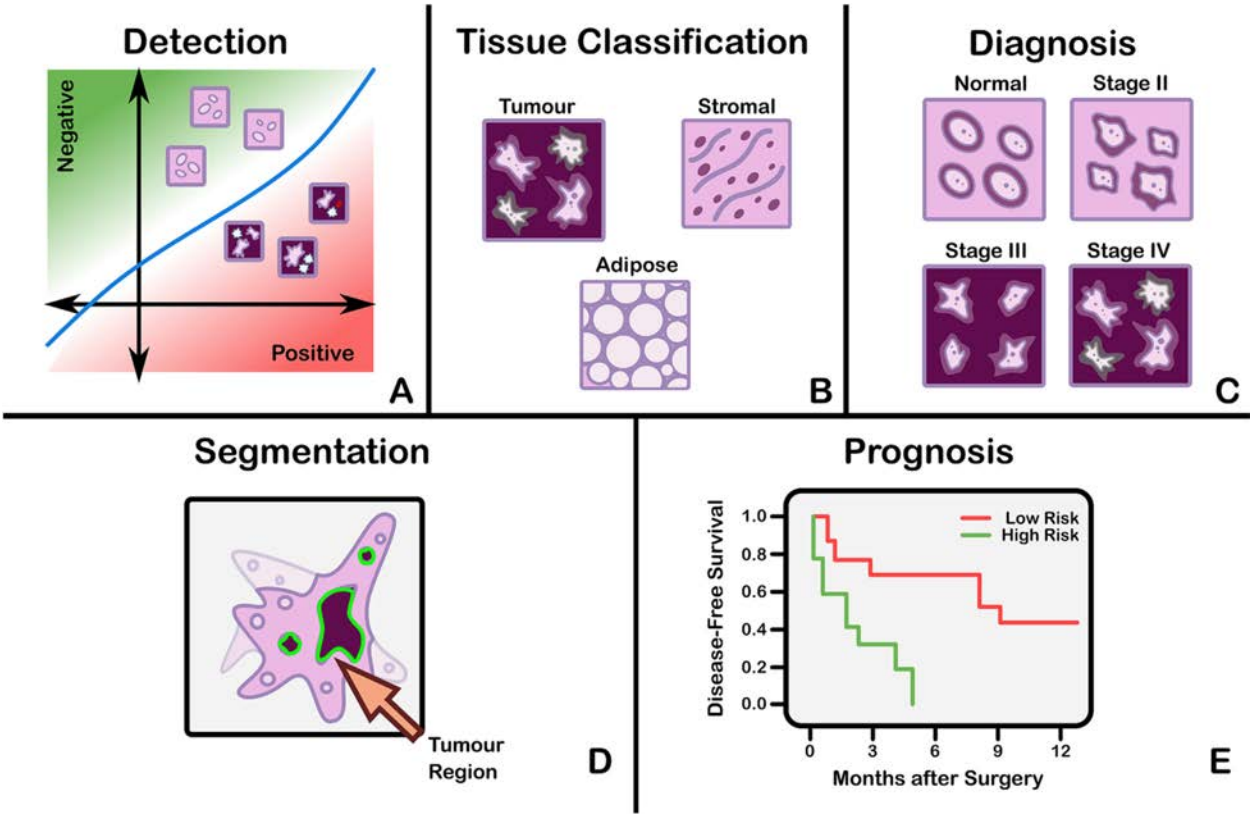

Fig. 3. The categorization of diagnostic tasks in computational pathology along with examples A) **Detection:** common detection task such as differentiating positive from negative classes like malignant from benign, B) **Tissue Subtype Classification:** classification task for tumorous tissue, Stroma, and adipose tissue, C) **Disease Diagnosis:** common disease diagnosis task like cancer staging, D) **Segmentation:** tumor segmentation in WSIs, and E) **Prognosis tasks:** shows a graph comparing survival rate and months after surgery.

disease class into finer disease-specific labels based on the organ and patient context.

Segmentation The segmentation task moves one step beyond classification by adding an element of spatial localization to the predicted label (s). In semantic segmentation, objects of interest are delineated in an image by assigning class labels to every pixel. These class labels can be discrete or non-discrete, the latter being a more difficult task.[79] Another variant of the segmentation task is instance segmentation, which aims to achieve both pixel-level segmentation accuracy as well as clearly defined object (instance) boundaries. Segmentation approaches can accurately capture many morphological statistics[80] and textural features,[81] both of which are relevant for cancer diagnosis and prognosis. Most frequently, segmentation is used to capture characteristics of individual glands, nuclei, and tumor regions in WSIs. For instance, glandular structure is a critical indicator of the severity of colorectal carcinoma,[82] thus accurate segmentation could highlight particularly abnormal glands to the pathologist as demonstrated in.[82–84] Overall, segmentation provides localization and classification of cancer-specific tumors and of specific histological features that can be meaningful for the pathologist's clinical interpretation.

2.3. Prognosis

Prognosis involves predicting the likely development of a disease based on given patient features. For accurate survival prediction, models must learn to both identify and infer the effects of histological features on patient risk. Prognosis represents a merging of the diagnosis classification task and the disease-survivability regression task.

Training a model for prognosis requires a comprehensive set of both histopathology slides and patient survival data (i.e. a variant of multi-modal representation learning). Despite the complexity of the input data, ML models are still capable of extracting novel histological patterns for disease-specific survivability.[85–87] Furthermore, strong models can discover novel prognostically-relevant histological features from WSI analysis.[88,89] As the quality and comprehensiveness of data improves, additional clinical factors could be incorporated into deep learning analysis to improve prognosis.

2.4. Prediction of treatment response

With the recent advances in targeted therapy for cancer treatment, clinicians are able to use treatment options that precisely identify and attack certain types of cancer cells. While the number of options for targeted therapy are constantly increasing, it becomes increasingly important to identify patients who are potential therapy responders to a specific therapy option and avoid treating non-responding patients who may experience severe side effects. Deep learning can be used to detect structures and transformations in tumour tissue that could be used as predictive markers of a positive treatment response. Training such deep learning models usually requires large cohorts of patient data for whom the specific type of treatment option and the corresponding response is known.

2.5. Organs and diseases

This section presents an overview of the various anatomical application areas for computational pathology grouped by the targeted organ. Each organ section gives a brief overview of the types of cancers typically found and the content of the pathology report as noted from the corresponding CAP synoptic reporting outline (discussed at 2.1). Fig. 4 highlights the intersection between the major diagnostic tasks and the anatomical focuses in state-of-the-art research. The majority of papers are dedicated to the four most common cancer sites: breast, colon, prostate, and lung.[90] Additionally, a significant amount of research is also done on cancer types with highest mortality, brain and liver.[90] Note that details of some additional works that may be of interest for each organ type can be found in Appendix A.7 (see Fig. 5).

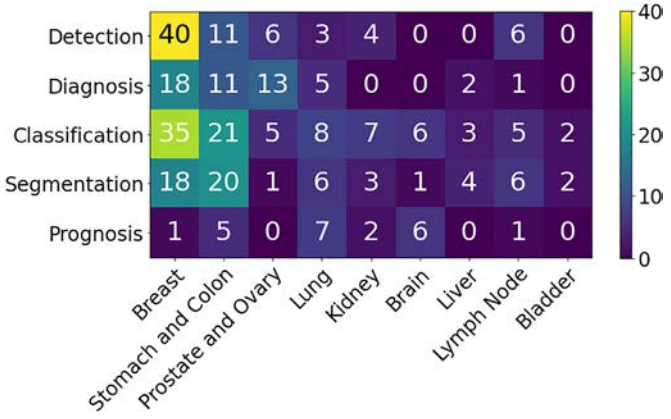

Fig. 4. Distribution of diagnostic tasks in CPath for different organs from Table 9.11. This distribution includes more than 400 cited works from 2018 to 2022 inclusive. The x-axis covers different organs, the y-axis displays different diagnostic tasks, and the height of the bars along the vertical axis measures the number of works that have examined the specific task and organ. Please refer to Table 9.11 in the supplementary section for more information.

Breast Breast cancers can start from different parts of the breast and majorly consist of 1) Lobular cancers that start from lobular glands, 2) Ductal cancers, 3) Paget cancer which involves the nipple, 4) Phyllodes tumor that stems from fat and connective tissue surrounding the ducts and lobules, and 5) Angiosarcoma which starts in the lining of the blood and lymph vessels. In addition, based on whether the cancer has spread or not, breast cancers can be categorized into *in situ* or *invasive/infiltrating* forms. DCIS is a precancerous state and is still confined to the ducts. Once the cancerous cells grow out of the ducts, the carcinoma is now considered *invasive* or *infiltrative* and can metastasize.[91]

Synoptic reports for breast cancer diagnosis are divided based on the type of cancers mentioned above. For DCIS and invasive breast cancers, synoptic reports focus on the histologic type and grade, along with the nuclear grade, evidence of necrosis, margin, involvement of regional lymph nodes, and biomarker status. Notably, architectural patterns are no longer a valuable predictive tool compared to nuclear grade and necrosis to determine a relative ordering of diagnostic importance for DCIS.[92] In contrast to DCIS and invasive cancers, Phyllodes tumours vary due to their differing origin in the fat and connective tissue, focusing on analyzing the stroma characteristics, existence of heterologous elements, mitotic rate, along with the involvement of lymph nodes. Finally, to determine therapy response and treatments, biomarker tests for Estrogen, Progesterone[93] and HER-2[94] receptors are recommended, along with occasional tests for Ki67 antigens.[95,96]

Most breast cancer-focused works in CPath propose various solutions for carcinoma detection and metastasis detection, an important step for assessing cancer stage and morbidity. Metastasis detection using deep learning methods was shown to outperform pathologists' exhaustive diagnosis by 9% free-response receiver operating characteristic (FROC) in.[97]

Prostate Prostate cancer is the second most prevalent cancer among the total population and the most common cancer among men (both excluding non-melanoma skin cancers). However, most prostate cancers are not lethal. Prostate cancer can occur in any of the three prostate zones: Central (CZ), Peripheral (PZ), and Transition (TZ), in increasing order of aggressiveness. Prostate cancers are almost always adenocarcinomas, which develop from the gland cells that make prostate fluid. The other types of prostate cancers are small cell carcinomas, neuroendocrine tumors, transitional cell carcinomas, isolated intraductal carcinoma, and sarcomas (which are very rare). Other than cancers, there are multiple conditions that are important to identify or diagnose as precursors to cancer or not. Prostatic intraepithelial neoplasia (PIN) is diagnosed as either low-grade PIN or high-grade PIN. Men with high-grade PIN need closely monitored follow-up sessions to screen for prostate cancer. Similarly, atypical small

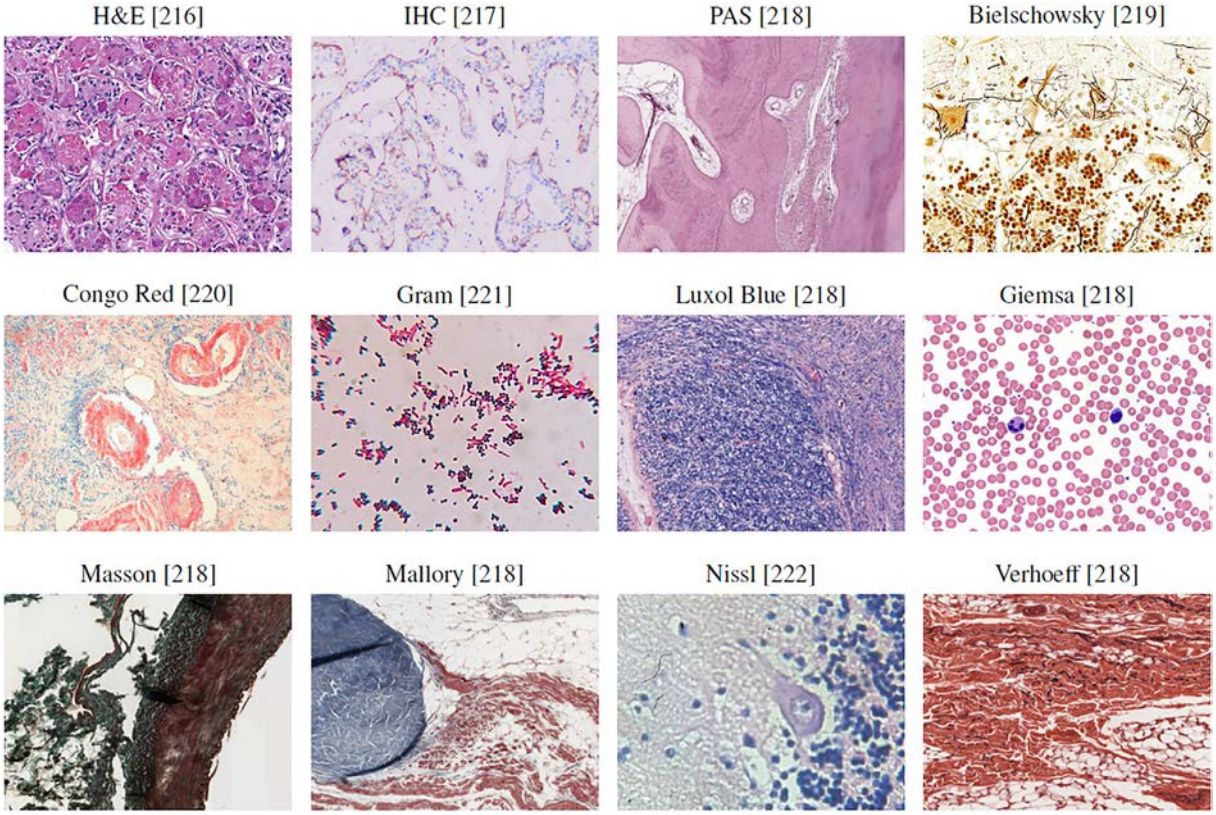

Fig. 5. WSI tissue images with different types of histological stains. Each stain highlights different areas and structures of the tissue in order to aid in visualizing underlying characteristics. Amongst this diversity, there is Hematoxylin and Eosin or H&E which is mainly used in studies as most histopathological processes can be understood from this stain. All images provided are under a Creative Commons license, specifics on the license can be found in the references.

acinar proliferation (ASAP) is another precancerous condition requiring follow-up biopsies.[98]

To grade and score tumours, pathologists use a Tumor, Nodes, Metastasis (TNM) framework. In the synoptic report, pathologists identify and report the histologic type and grades, and involvement of regional lymph nodes to help grade and provide prognosis for any tumours. Specifically for prostate analysis, tumour size and volume are both important factors in prognosis according to multiple studies.[99–102] Similarly, location is important to note for both prognosis and therapy response.[103] Invasion to nearby (except perineural invasion) tissues is noted and can correlate to TMN classification.[104] Additionally, margin analysis is especially important in prostate cancers as the presence of a positive margin increases the risk of cancer recurrence and metastasis.[105] Finally, intraductal carcinoma (IDC) must be identified and distinguished from PIN and PIA; as it is strongly associated with a high Gleason score, a high-volume tumor, and metastatic disease.[106–110]

After a prostate cancer diagnosis is established, pathologists assign a Gleason Score to determine the cancer's grade: a grade from 1 to 5 is assigned to the two most common areas and those two grades are summed to make a final Gleason Score.[111] For Gleason scores of 7, where survival and clinical outcomes demonstrate large variance, the identification of Cribriform glands is key in helping to narrow possible outcomes.[112,113]

Ovary Ovarian cancer is the deadliest gynecologic malignancy and accounts for more than 14, 000 deaths each year.[114] Ovarian cancer manifests in three types: 1) epithelial cell tumors that start from the epithelial cells covering the outer surface of the ovary, 2) germ cell tumors which start from the cells that produce eggs, and 3) stromal tumors which start from cells that hold the ovary together and produce the hormones estrogen and progesterone. Each of these cancer types can be classified into benign, intermediate and malignant categories. Overall, epithelial cell tumors are the most common ovarian cancer and have the worst prognosis.[115]

When compiling a synoptic report for ovarian cancer diagnosis, pathologists focus on histologic type and grade, extra-organ involvement, regional lymph nodes, T53 gene mutations, and serous tubal intraeptithelial carconma (STIC). Varying histologic tissue types are vital to determine the pathology characteristics and determining eventual prognosis. For example, generally endometrioid, mucinous, and clear cell carcinomas have better outcomes than serous carcinomas.[116] Additionally, lymph node involvement and metastasis in both regional and distant nodes has a direct correlation to patient survival, grading, and treatment. Determining the presence of STICs correlates directly to the presence of ovarian cancer, as 60% of ovarian cancer patients will also have an associated STIC.[114] Finally, T53 gene mutations are the most common in epithelial ovarian cancer; which has the worst prognosis among ovarian cancers, so determining their presence is critical to patient cancer risk and therapy response.[117,118] There are not a large number of works dedicated to the ovary specifically, but most works on ovary focus on classification of its five most common cancer subtypes: high-grade serous (HGSC), low-grade serous (LGSC), endometriod (ENC), clear cell (CCC), and mucinous (MUC).[119,120]

Lung Lung cancer is the third most common cancer, next to breast and prostate cancer.[121] Lung cancers mostly start in the bronchi, bronchioles, or alveoli and are divided into two major types, non-small cell lung carcinomas (NSCLC) (8085%) and small cell lung carcinomas (SCLC) (1015%). Although NSCLS cancers are different in terms of origin, they are grouped because they have similar outcomes and treatment plans. Common NSCLS cancers are 1) adenocarcinoma, 2) squamous cell carcinoma 3) large cell carcinoma, and some other uncommon subtypes.[122]

For reporting, histologic type helps determine NSCLC vs SCLC and the subtype of NSCLC. Although NSCLC generally has favourable survival rates and prognosis as compared to SCLC, certain subtypes of NSCLC can have lower survival rates due to co-factors.[123] Histologic patterns are applicable in adenocarcinomas, consisting of favourable types: lepidic, intermediate: acinar and papillary, and unfavourable: micropapillary and solid.[124]

Grading each histologic type aids in categorization but is differentiated based on each type, and thus is out of scope for this paper. Importantly for lung cancers, tumour size is an independent prognostic factor for early cancer stages, lymph node positivity, and locally invasive disease. Additionally, the size of the invasive portion is an important factor for prognosis of nonmucinous adenocarcinoma with lepidic pattern.[123,125–129] Other important lung specific features are visceral pleural invasion, which is associated with worse prognosis in early-stage lung cancer even with tumors <3cm,[130] and lymphatic invasion which indicates an unfavourable prognostic finding.[125,131]

Colon and Rectum Colorectal cancers are two of the five most common cancer types.[90] Cancer cells usually start to develop in the innermost layer of the colon and rectum walls, known as the mucosa, and continue their way up to other layers. In other layers, there are lymph and blood vessels that can be used by cancer cells to travel to nearby lymph nodes or other organs.[132] Colorectal cancers usually start with the creation of different types of polyps, each possessing a unique risk of developing into cancer. Most colorectal cancers are adenocarcinomas, which are split into three well-studied subtypes: classic adenocarcinoma (AC), signet ring cell carcinoma (SRCC), and mucinous adenocarcinoma (MAC). In most cases, AC has a better prognosis than MAC or SRCC. Other types, albeit uncommon, of colorectal cancers are: carcinoid tumors, gastrointestinal stromal tumors (GISTs), lymphomas, and sarcomas.[133]

As in other cancers, histologic grade is the most important factor in cancer prognosis along with regional lymph node status and metastasis. The tumor site is also important in determining survival rates and prognosis.[134] Vascular invasion of both small and large vessels are important factors in adverse outcomes and metastasis,[135–137] and perineural invasion has been shown in multiple studies to be an indicator of poor prognosis.[137–139] Additionally, microsatellite instability (MSI) is shown to be a good indicator of prognosis and is divided into three stages in decreasing adversity of Stable (MSI-S), Low (MSI-L), and High (MSI-H).[140] Finally, some studies have indicated the usefulness of biomarkers in colorectal cancer treatment, with biomarkers such as BRAF mutations, KRAS mutations, MSI, APC, MicroRNA, and PIK3CA.[141]

Works are relatively well-distributed among various tasks including disease diagnosis, segmentation, and detection. Expanding on colorectal cancer detection, work from[142] used feature analysis for colorectal and mucinous adenocarcinomas using heatmap visualizations. They discovered that adenocarcinoma is often detected by ill-shaped epithelial cells and that misclassification can occur due to lumen regions that resemble the malformed epithelial cells. Similarly for mucinous carcinoma, the model again recognizes the dense epithelium, but this time ignores the primary characteristic of the carcinoma (abundance of extracellular mucin). These findings suggest that a thorough analysis of class activation maps can be helpful for improving the classifier's accuracy and intuitiveness.

Bladder There are several layers within the bladder wall with most cancers starting in the internal layer, called the urothelium or transitional epithelium. Cancers remaining in the inner layer are non-invasive or carcinoma in situ (CIS) or stage 0. If they grow into other layers such as the muscle or fatty layer, the cancer is now *invasive*. Nearly all bladder cancers are urothelial carcinomas or transitional cell carcinomas (TCC). However, there are other types of cancer such as squamous cell carcinomas, adenocarcinomas, small cell carcinomas, and sarcomas which all are very rare. In the early stages, all types of bladder cancers are treated similarly but as their stage progresses, and chemotherapy is needed, different drugs might be used based on the type of the cancer.[143] As with other organs, histologic type and grade also play a role in prognosis and treatment,[144] and lymphovascular invasion is independently associated with poor prognosis and recurrence.[145]

Works focusing on the bladder display promising results that could lead to rapid clinical application. For example, a prediction method for four molecular subtypes (basal, luminal, luminal p53, and double negative) of muscle-invasive bladder cancer was proposed in,[146] outperforming pathologists by 30% in classification accuracy when restricted to a tissue morphology-based assessment. Further improvements in accuracy could help expedite diagnosis by complementing traditional molecular testing methods.

Kidney Each kidney is made up of thousands of glomeruli which feed into the renal tubules. Kidney cancer can occur in the cells that line the tubules (renal cell carcinoma (RCC)), blood vessels and connective tissue (sarcomas), or urothelial cells (Urothelial carcinoma). RCC accounts for about 90% of kidney cancers and comes in two types: 1) clear cell renal carcinoma, which are most common and 2) non-clear cell renal carcinoma consisting of papillary, chromophobe and some very rare subtypes.[147] The CAP's cancer protocol template for the kidney is solely focused on RCCs,[148] likely due to their high probability. Tumour size is directly associated with malignancy rates, with 1cm size increase resulting in 16% increase in malignancy chance.[149] Additionally, the RCC histologic type is correlated with metastasis, with clear cell, capillary, collecting ducts (Bellini), and medullary being the most aggressive ones.[150]

Many works are focused on glomeruli segmentation, as the number of glomeruli and glomerulosclerosis constitute standard components of a renal pathology report.[151] In addition to glomeruli detection, some works have also detected other relevant features such as tubules, Bowman's capsules, and arteries.[152] The results display strong performance on PAS-stained nephrectomy samples and tissue transplant biopsies, and there seems to be a strong correlation between the visual elements identified by the network and those identified by renal pathologists.

Brain There are two main types of brain tumors: malignant and non-malignant. Malignant tumors can be classified as primary tumors (originating from the brain) or secondary (metastatic).[153,154] The most common type of brain cancers is gliomas, occurring 50.4% of the time, and are classified into four grades.[155] In the synoptic reporting, tumour location is noted as it has some impact on the prognosis, with parietal tumours showing better prognosis compared to other locations.[153] Additionally, focality of glioblastomas (a subtype of gliomas) is important to determine as multifocal glioblastoma is far more aggressive and resistant to chemotherapy as compared to unifocal.[154] A recent summary of the World Health Organization's (WHO) classification of tumors of the central nervous system has indicated that biomarkers as both ancillary and diagnostic predictive tools.[156] Additionally, in a recent WHO edition of classification of tumours of the central nervous system, molecular information is now integrated with histologic information into tumor diagnosis for cases such as diffuse gliomas and embryonal tumors.[157]

Accordingly, most works focus on gliomas and more specifically glioblastoma, the most aggressive and invasive form of glioma. Due to glioblastoma's extremely low survival rate of 5% after 5 years, compared to a low grade glioma's survival rate of over 50% after 5 years,[76,158] it is critical to distinguish the two forms for improved patient care and prognosis.

Liver Liver cancer is one of the most common causes of cancer death.[159] In particular, hepatocellular carcinoma (HCC) is the most common type of primary liver cancer and has various subtypes, but they generally have little impact on treatment.[160] Histogolical grade is divided into nuclear features and differentiation, which directly correlate to tumour size, presentation, and metastatic rate.[161,162] Notably, high-grade dysplastic nodules are included in synoptic reports for HCC but are difficult to assess and have high inter-observer disagreement,[163] and thus is an area where CAD systems could be leveraged to normalize assessments. Current grading of this cancer suffers from an unsatisfactory level of standardization,[164] likely due to the diversity and complexity of the tissue. This could explain why relatively low number of works are dedicated to liver disease diagnosis and prognosis. Instead, most works focus on the segmentation of cancerous tissues.

Lymph Nodes There are hundreds of lymph nodes in the human body that contain immune cells capable of fighting infections. Cancer manifests in lymph nodes in two ways: 1) cancer that originates in the lymph node itself known as lymphoma and 2) cancer cells from different origins that invade lymph nodes.[165] As mentioned in the prior organ sections, lymphocytic infiltration is correlated with cancer recurrence on multiple

organs and lymph nodes are the most common site for metastasis. The generalizable impact to multiple organs and importance of detecting lymphocytic infiltration is why many works focused on lymph nodes address metastasis detection.[166]

Organ Agnostic The remaining papers focus on segmentation, diagnosis, and prognosis tasks that attempt to generalize to multiple organs, or target organ agnostic applications. An interesting approach to increase the generalization capability of deep learning in histopathology is proposed in.[167] Currently, publicly available datasets with thorough histological tissue type annotations are organ specific or disease specific and thus constrain the generalizability of CPath research. To fill this gap, a novel dataset called Atlas of Digital Pathology (ADP) is proposed.[167] This dataset contains multi-label patch-level annotations of Histological Tissue Types (HTTs) arranged in a hierarchical taxonomy. Through supervised training on ADP, high performance on multiple tasks is achieved even on unseen tissue types.

3. Data collection for CPath

One of the first steps in the workflow for any CPath research is the collection of a representative dataset. This procedure often requires large volumes of data that should be annotated with ground-truth labels for further analysis.[62,64,168] However, creating a meaningful dataset with corresponding annotations is a significant challenge faced in the CPath community.[62,64,168–170]

This section outlines the entire process of the data-centric design approach in CPath, including tissue slide preparation and WSI scanning–the first two stages in the proposed workflow shown in Fig. 1. Additionally, the trend in dataset compilation across the 700 papers surveyed is discussed regarding dataset sizes, public availability, and annotation types; see Table 9.11 in the Supplementary Material for information regarding the derivations and investigation of said trends.

3.1. Tissue slide preparation

For the application development stages in CPath, the creation of a new WSI dataset must begin with selection of relevant glass slides. High quality WSIs are required for effective analysis, however, considerations must be made for potential slide artifacts and variations inherently present. As described in Section 2.1, pathology samples are categorized as either biopsy or resection samples, with most samples being prepared as *permanent* samples and some intra-operative resection samples being prepared as *frozen* samples.

Variations and Irregularities Throughout the slide sectioning process, artifacts and irregularities can occur which reduce the slide quality, including: uncovered portions, air bubbles in between the glass seal, tissue chatter artifacts, tissue folding and tears, ink markings present on the slide, and dirt, debris, microorganisms, or cross-contamination of slides by unrelated tissue from other organs.[171–173] Frozen sections can present unique irregularities and variations, such as freezing artifacts, cracks in the tissue specimen block, or delay of fixation causing drying artifacts.[174,175] Beyond these irregularities, glass slides may vary in stain colouring, occurring due to differences in slide thickness, tissue thickness, fixation, tissue processing schedule, patient variation, stain variation, and lab variation.[174,176–180]

All such defects and variations are important to keep in mind when selecting glass slides for the development and application process in CPath, as they can both reduce the quality of the WSI as well as impact the performance of developed CAD tools trained with these WSIs.[171,172,177] A more detailed discussion on the surveyed works in CPath which seek to identify and correct issues in slide artifacts and colour variation in WSIs is found in Section 3.2. However, prior to digitization, artifacts, and irregularities can be kept at a minimum by following good pathology practices. While an in-depth discussion of this topic is outside the scope of this paper, some research provides an extensive list of recommendations for reducing such errors in slide sectioning.[173]

3.2. Whole slide imaging (WSI)

WSI Scan Once a glass slide is prepared, it must be digitized into a WSI. The digitization and processing workflow for WSIs can be summarized as a four-step process[181]: (1) Image acquisition via scanning; (2) Image storage; (3) Image editing and annotation; (4) Image display.[182] As the first two steps of the digitization workflow are the most relevant for WSI collection and with regards to the CPath workflow, they are discussed to a greater extent below.

Slide scanning is carried out through a dedicated slide scanner device. A plethora of such devices currently exist or are in development; see Appendix Table 1 for a collection of commercially available WSI scanners. Additionally, some research has investigated and compared the capabilities and performances of various WSI scanners.[183–186]

In order to produce a WSI that is in focus, which is especially important for CPath works, appropriate focal points must be chosen across the slide either using a depth map or by selecting arbitrarily spaced tiles in a subset.[187] Once focal points are chosen, the image is scanned by capturing tiles or linear scans of the image, which are stitched together to form the full image.[180,187] Slides can be scanned at various magnification levels depending on the downstream task and analysis required, with the vast majority being scanned at $20\times$ ($\sim 0.5\mu m$/pixel) or $40\times$ ($\sim 0.25\mu m$/pixel) magnification.[180]

WSI Storage and Standards WSIs are in giga-pixel dimension format.[30,188] For instance a tissue in $1cm \times 1cm$ size scanned @$0.25\mu m$/pixel resolution can produce a 4.8GB image (uncompressed) with $50,000 \times 50,000$ pixels. Due to this large size, hardware constraints may not support viewing entire WSIs at full resolution, thus WSIs are most often stored in a tiled format so only the viewed portion of the image (tile) is loaded into memory and rendered.[189] When building CAD tools for CPath, this large WSI dimensionality must be taken into account in determining how much compute is required to analyze a WSI. Alongside the WSI, metadata regarding patient, tissue specimen, scanner, and WSI information is stored for reference.[30,188,190] Due to their clinical use, it is important to develop effective storage solutions for WSI images and metadata, allowing for robust data management, querying of WSIs, and efficient data retrieval.[191,192] Further details on WSI image formats and storage methods are discussed in Appendix A.6.

To develop CPath CAD tools in a widespread and general manner, a standardized format for WSIs and their corresponding metadata is essential.[188] However, there is a general lack of standardization for WSI formats outputted by various scanners, as shown in Table 1, especially regarding metadata storage. The Digital Imaging and Communications in Medicine (DICOM) standard provides a format for CPath image formatting and data management through Supplement 145,[190,193] and has been shown in research to allow for efficient access and interoperability of data between varying medical centers and devices.[188] However, few scanners are DICOM-compliant and thus there are challenges to using different models of scanners, thus different image formats and metadata structures, in the context of dataset aggregation and processing.

Apart from storage format, a general framework for storing and distributing WSIs is also an important pillar for CPath. In other medical imaging fields such as radiology, images are often stored in a picture archiving and communications systems (PACS) in a standardized DICOM format, with DICOM storage and retrieval protocols to interface with other systems.[189] The need for standardization persists in pathology for WSI storage solutions; few works have proposed solutions to incorporate DICOM-based WSIs in a PACS, although some research has successfully implemented a WSI PACS consistent using the DICOM standard using a web-based service for viewing and image querying.[189]

WSI Defects and Variations Certain aspects of the slide scanning process can introduce unfavorable irregularities and variations.[194] A major source of defects is out-of-focus regions in a generated WSI; often caused by glass slide artifacts, such as air bubbles and tissue folds, which interfere with selection of focus points for a slide.[171,195] Out-of-focus regions degrade WSI quality and are detrimental to the performance of CAD tools developed

with these WSIs, presenting concerns for performance with studies showing high false-positive errors.[196,172] Additionally, as WSIs are scanned in strips or tiles, any misalignment between sections can introduce striping/stitching errors in the final image.[197] Another source of error may appear during tissue-background segmentation where the scanner may misidentify some tissue regions as background, potentially missing crucial tissue areas on the glass slide from being digitized.[198]

Variations in staining refers to differences in colour and contrast of the tissue structures in the final WSI occurring due to differences in the staining process, staining chemicals, and tissue state. Variations in colour can lead to difficulty in generalizing CAD tools to WSIs from different labs, institutions, and settings.[199,200] Even identical staining techniques can yield different WSIs due to scanner differences in sensor design, light source and calibration,[180,201] creating challenges for cross-laboratory dataset generation. These additional sources of variation add layers of complexity to the WSI processing workflow, and must be kept in mind during slide selection and dataset curation for CAD tool development and deployment.

Addressing Irregularities and Variations Much work has gone into identifying areas of irregularities within WSIs, most notably blur and tissue fold detection.[195,196] Some research has explored automated deep learning tools to identify these irregularities at a more efficient pace than manual inspection.[195,196] Developing techniques for addressing staining variation has also been a significant research area[177,202–207] as the use of techniques addressing stain variation is important for all future works. We list some computational approaches proposed to address these issues: An example method proposed in[202] uses a stain normalization technique, attempting to map the original WSI onto a target color profile. In this technique, a color deconvolution matrix is estimated to convert each image to a target hematoxylin and eosin (H&E) color space and each image is normalized to a target image colour profile through spline interpolation.[202] A second approach applies color normalization using the H channel with a threshold on the H channel on a Lymphocyte Detection dataset.[205] Recent studies have shown promise in having deep neural networks accomplish the stain normalization in contrast to the previous classical approaches,[203,208–210] commonly applying generative models such as generative adversarial networks (GANs) to stain normalization. Furthermore, Histogram Equalization (HE) technique for contrast enhancement is used in,[211] where novel preprocessing technique is proposed to select and enhance a portion of the images instead of the whole dataset, resulting in improved performance and computational efficiency.

An alternative approach to address the impact of stain variation on training CAD tools is data augmentation. Such methods augment the data with duplicates of the original data, containing adjustments to the color channels of the image, creating images of varying stain coloration, and training train models that are accustomed to stain variations.[200] This method has been frequently used as a pre-processing step in the development of training datasets for deep learning.[212–214] A form of medically-irrelevant data augmentation based on random style transfer, called STRAP, was proposed by researchers and outperformed stain normalization.[206] Similar to style transfer,[215] proposes stain transfer which allows one to virtually generate multiple types of staining from a single stained WSI.

3.3. Cohort selection, scale, and challenges

The data used to create/train CPath CAD tools can greatly impact the performance and success of the tool. Curating the ideal dataset, and thus selecting the ideal set of WSIs for the development of a CAD tool is a non-trivial task. Several works suggest that datasets for deep learning in CPath should include a large quantity of data with a degree of variation and artifacts in the WSIs.[62,172] Some works also recommend the inclusion of difficult or rarely diagnosed cases; other works indicate that inclusion of extremely difficult cases may decrease the performance of advanced models.[172,216]

A study highlighting the results of the 2016 Dataset Session at the first annual Conference on Machine Intelligence in Medical Imaging outlines several key attributes to create an ideal medical imaging dataset,[217] including: having a large amount of data to achieve high performance on the desired task, quality ground truth annotations, and being reusable for further efforts in the field. While the scope of this conference did not include CPath, many of the points made regarding medical imaging datasets are also relevant to the development of CPath datasets. The session also outlined the impact that class imbalances can have on ML models, an issue also prevalent in CPath as healthy or benign regions often outnumber diseased regions by a significant margin.[218]

Our survey of past works in the literature reveals some trends in CPath datasets. Currently, the majority of datasets presented in the literature for CAD tool development are small-scale datasets,[62] using a small number of images, and/or images from a small number of pathology laboratories. Examples of these smaller datasets include a dataset with 596 WSIs (401 training, 195 testing) from four centres for breast cancer detection[219] and the Breast Cancer Histology (BACH2018) dataset, which has 500 ROI images (400 training, 100 testing) and 40 WSIs (30 training, 10 testing).[220] Although curating a dataset from fewer pathology laboratories may be simpler, these smaller scale datasets may not be able to effectively generalize to data from other pathology centres.[199,120] An example of this can be seen in which data from different pathology centres are clustered disjointly in a t-distributed stochastic neighbor embedding (t-SNE) representation demonstrated in.[172] Another alternative was proposed in[221]: using a swarm learning technique multiple AI models were trained on different small data sets separately and then unified into one central model.

Additionally, stain variations, slide artifacts, and variation of disease prevalence may sufficiently shift the feature space such that a deep learning model may not sustain high performance on unseen data in new settings.[120,222] As artifacts in WSIs are inevitable, with some artifacts, such as ink mark-up on glass slides, being an important part of the pathology workflow,[223] the ability of CAD tools to become robust to these artifacts through exposure to a diverse set of images is an important consideration.

Compared to the number of studies conducted on small-scale datasets, relatively fewer studies have been performed using large-scale, multi-centre datasets.[62,224,172] One study uses over 44,715 WSIs from three organ types, with very little curation of the WSIs for multi-instance learning detailed in.[62] Stomach and colon epithelial tumors were classified using 8,164 WSIs in.[224] A similar study uses 13,537 WSIs from three laboratories to test a machine learning model trained on 5,070 WSIs and achieves high performance.[62]

Despite some advancements, there exist major barriers to using such large, multi-centre datasets in CAD development. Notably, for strongly supervised methods of learning, an immense amount of time is needed to acquire granular ground truth annotations on a large amount of data.[224] To combat this, some researchers have implemented weakly-supervised learning by harvesting existing slide level annotations to forego the need for further annotation.[62] Additionally, it may be difficult to aggregate data from multiple pathology centres due to regulatory, privacy, and attribution concerns, despite the improvements that diverse datasets offer. Section 5 discusses model architectures and training techniques that harness curated datasets of various annotation levels.

Dataset Availability In general computer vision, progress can be tracked by the increasing size and availability of datasets used to train models, e.g. ImageNet grew from 3.2 million images and 5000 classes in 2009 to 14 million images and 21,000 classes in 2021.[225] We infer a similar trend in dataset growth and availability indicates progress in CPath. In our survey of over 700 CPath papers, we determine the current landscape by noting the dataset(s) used in work, along with dataset details such as the organ(s) of interest, annotation level, and stain type, tabulating the results into Table 9.11 of the supplementary materials, with summarized findings from Table 9.11 are shown in Fig. 6.

From Fig. 6 we can clearly see that the majority of datasets used for research developments in computational pathology are privately sourced or require additional registration/request. With organs represented in a small number of datasets, such as the liver, thyroid, brain, etc, having a smaller proportion of freely accessible datasets as compared to the Breast,

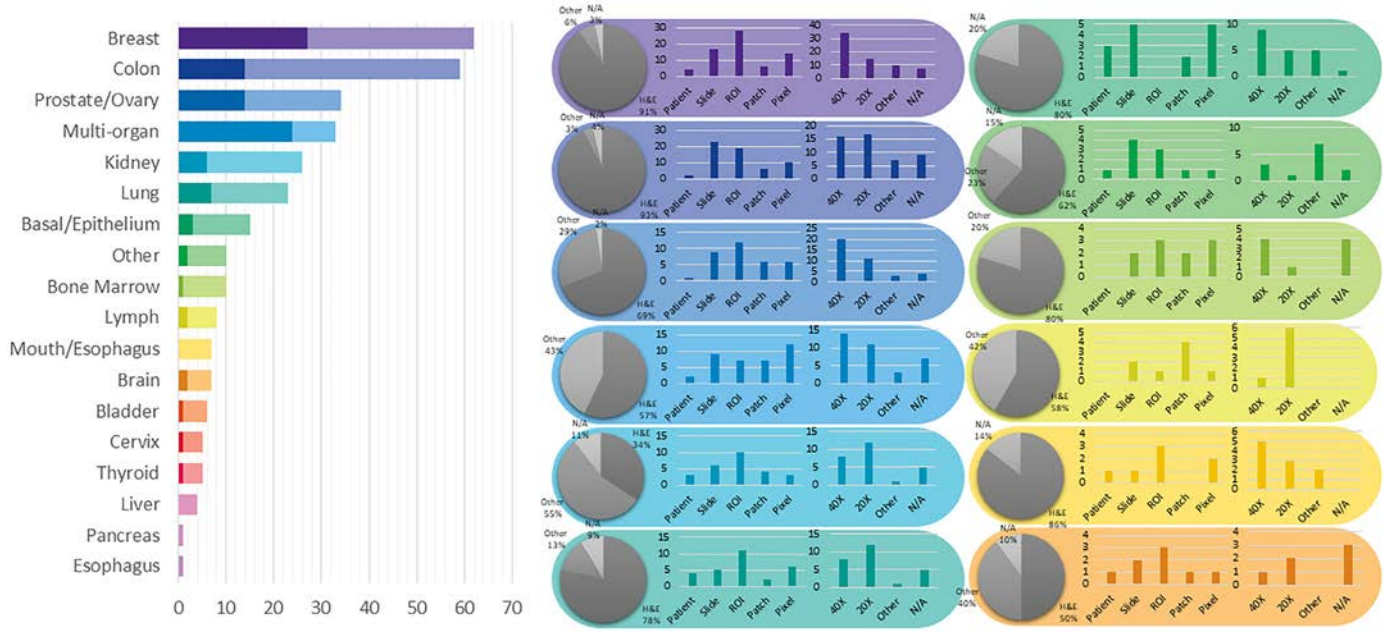

Fig. 6. (left) shows the distribution of datasets per organ as a capture of the current trend in datasets, although the number of datasets can change over time an understanding of what organs have more available data is important for developing CAD tools. Along the vertical axis, we list different organs, while the horizontal axis shows the number of datasets; wherein the darker color denotes public availability while the light color includes unavailable or by request statuses. (right) Distribution of staining types, annotation levels, and magnification details per organ color coded consistently with the bar graph. Organs have been sorted based on the abundance of datasets. For more details, please refer to Table 9.11 in the supplementary section.

Colon, or Porstate. This can be problematic when trying to create CAD tools for cancers in these organs due to a lack of accessible data. We additionally note that although data sets requiring registration/request for access can be easily accessible, as in the case of Breast Cancer Histopathological Database (BreakHis)[226] being used in multiple works,[227–229] the need for registration presents a barrier to access as requests may go unanswered or take much time to review.

In our categorization of CPath datasets, we find that a few prominent datasets have been released publicly for use by the research community. Many such datasets are made available through grand challenges in computational pathology,[230] such as the CAMELYON16 and CAMELYON17 challenges for breast lymph node metastases detection,[61,231,232] and the Gland Segmentation in Colon Histology Images Challenge (GLaS) competition for colon gland segmentation in conjunction with Medical Image Computing and Computer Assisted Intervention (MICCAI) 2015.[233,234] Notable amongst publicly available data repositories is the cancer genome atlas (TCGA),[235] a very large-scale repository of WSI-data containing many organs and diseases, along with covering a variety of stain types, magnification levels, and scanners. Data collected from TCGA has been used in a large number of works in the literature for the development of CAD tools.[200,236,237] As such, TCGA represents an essential repository for the development of computational pathology. While patient confidentiality is a general concern when compiling and releasing a CPath dataset, large-scale databases such as TCGA prove that it is possible to provide relatively unrestricted data access without compromising patient confidentiality. Further evaluating public source datasets, it seems that the majority of them use data extracted from large data repositories, such as TCGA, without specifying the IDs of the images used, which provides a challenge in comparing datasets or CAD tool performance across works. However, there are a few datasets that are exceptions to that phenomenon.[64,238–240]

Fig. 6 also provides some insights on the dataset breakdown by organ, stain type, and annotation level. Per organ, it can be seen that the breast, colon, prostate/ovary, and lung tissue datasets are amongst the most common, understandably since cancer occurrence in these regions is the most frequent[90]–complying with cancer statistics findings in 9.5. Multi-organ datasets are the other most common type, where we have designated a dataset to be multi-organ if it compiles WSIs from several different organs. To note, multi-organ datasets are especially useful for the development of generalized image analysis tools in computational pathology. The annotation level provided in the datasets did not indicate any pattern across most organs.

Dataset Bias It is also important to note the potential for bias in datasets that may influence the ability of any deep learning algorithm to generalize on unseen data.[241,242] This problem is a prevalent issue in general machine learning applications,[243–246] and CPath is not immune to it. The survey review in[247] reviews a large number of other examples in machine learning that exhibit such bias, both from a dataset-standpoint and an algorithm-standpoint.

Such a lack of generalizability in CPath can impact the ability of machine learning models trained on biased data to meet the needs of patients. As noted in,[241] minority groups may be disproportionately negatively impacted if care is not taken in curating a diverse dataset that adequately reflects the relevant demographics for the problem to be solved.

Several works have delved into the issue of dataset bias in CPath specifically.[248,249] A notable example is in,[249] where the study was able to demonstrate that deep learning models trained on WSIs from TCGA were able to infer the organization that contributed the slide sample. Notably, some features, such as genetic ancestry, patient prognosis, and several key genomic markers were significantly correlated with the site the WSI was provided from. As the vast majority of data in TCGA is acquired from 24 origin centers,[248] such site-specific factors may impact the ability of a DL model to perform well on patient data from different sites.

As discussed previously, having a large set of diverse data may help to mitigate generalization issues.[120,199,241] Additionally, the study[249] makes the suggestion that training data should be from separate sites than validation data, and that per-site performance of a model should be reported when validating a model. In doing this, the robustness of the model to site-specific variation, including both stain and demographic related variation, can be evaluated.

4. Domain expert knowledge annotation

A primary goal of CPath is to capture and distill domain expert knowledge, in this case the expertise of pathologists, into increasingly efficient and accurate CAD tools to aid pathologists everywhere. Much of the domain knowledge transfer is encompassed within the process of human experts, in this case pathologists, generating diagnostically-relevant annotations and labels for WSIs. It must be emphasized, that without some level of label, a WSI dataset is not directly usable to train a model for most CAD tasks that involve the generation of diagnoses, prognoses, or suggestions for pathologists. Thus, the process of obtaining and/or using annotations at the appropriate granularity and quality is paramount in the field. This section focuses on describing various types of ground-truth annotation to cover the spectrum of weak to strong supervision of labels, discussing the practicality of labeling across this supervision spectrum, and how a labeling workflow can be potentially designed to optimize related annotation tasks.

4.1. Supervised annotation

In contrast to general computer vision, computer scientists do not have expert-level knowledge of histopathology and thus they are not as efficient at generating annotations or labels of pathology images. Further, labels cannot be easily obtained by outsourcing the task to the general public. As a result, pathologists must be leveraged to obtain labels at some stage of the data collection and curation process, and in many annotation pipelines the first step involves recruiting the help of pathologists for their expertise in labelling.

Obtaining Expert Domain Knowledge The knowledge of pathologists is essential in the development of accurate ground truth annotations–a process most commonly completed by encircling ROI.[219] However, there are studied instances of inter-observer variance between pathologists when determining a diagnosis.[250–252] As obtaining the most correct label is essential when training a model for CAD, this issue must be addressed and a review of the data by several pathologists can result in higher quality ground truth data as compared to that of a single pathologist. As a result, most datasets are curated by involving a group of pathologists in the annotation process. If there exists a disagreement between the expert pathologists on the annotation of a ground truth, one of several methods is usually employed to rectify the discrepancy. A consensus can be reached on the annotation label through discussion amongst pathologists, as is done in the triple negative breast cancer (TNBC-CI) dataset,[253] the Breast Cancer Surveillance Consortium (BCSC) dataset[254] and the minimalist histopathology image analysis dataset (MHIST) dataset.[255] Alternatively, images, where disagreements occur, can be discarded, as is done in some works.[256,257] Further, the disagreement between annotators can be recorded to determine the difficulty level of the images, as is done in the MHIST dataset.[216] This extra metadata aids in the development of CAD tools for analysis.

Pathologists can also be involved indirectly in dataset annotation. Both the Multi-organ nuclear segmentation dataset (MoNuSeg)[258] and ADP[167] have non-expert labelers annotate their respective datasets. A board-certified pathologist is then tasked with reviewing the annotations for correctness. Alternatively, some researchers have employed a pathologist in performing quality control on WSIs for curating a high-quality dataset with minimal artifacts.[87,259] To enable the large scale collection of accurate annotated data, Lizard[260] was developed using a multi-stage pipeline with several significant "pathologist-in-the-loop" refinement steps.

Existing pathological reports, along with the metadata that comes from public large-scale databases like TCGA, can also be leveraged as additional sources of task-dependent annotations without the use of further annotation. For example, TCGA metadata was used to identify desirable slides in,[26] while pathological diagnostic reports were used for breast ductal carcinoma in-situ grading in.[261]

To note, there are some tasks where manual annotation by pathologists can be bypassed altogether. For instance, IHC was applied to generate mitosis figure labels using a Phospho-Histone H3 (PHH3) slide-restaining approach in,[262] while immunofluorescence staining was used as annotations to identify nuclei associated with pancreatic adenocarcinoma.[263] These works parallel the techniques that pathologists often use in clinical practice, such as the use of IHC staining as a supplement to H&E stained slides for difficult to diagnose cases.[264] They demonstrate high performance on their respective tasks wherein the top-performing models on the Tumor Proliferation Assessment Challenge 2016 (TUPAC16)[265] dataset were achieved.[262] Importantly, these techniques still utilize supervision, albeit weakly, by leveraging lab techniques that have been developed and refined to identify the desired regions visually.

Ground-Truth Diagnostic Information Understanding different annotation levels and their impact on the procedural development of ML pipelines is an important step in solving tasks within CPath. There are five possible levels of annotation, in order of increasing granularity (from weakly-supervised to fully-supervised): patient, slide, ROI, patch, and pixel. Fig. 7

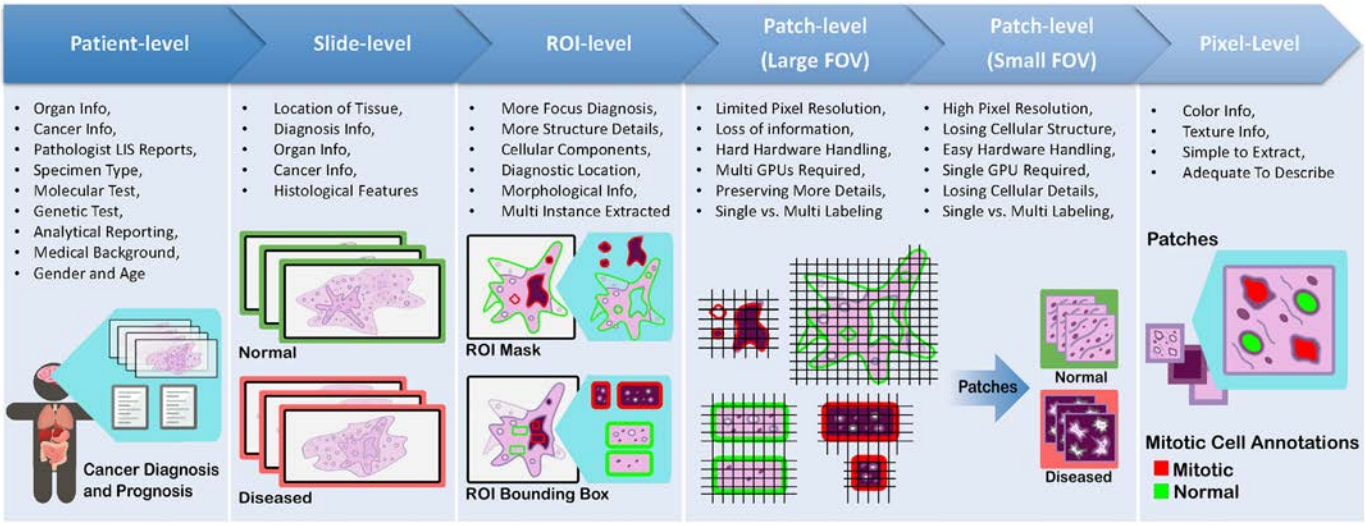

Fig. 7. Details of the five different types of annotations in computational pathology. From left to right: a) **Patient-level annotations:** can include high level information about the patient like status of cancer, test results, etc. b) **Slide-level:** are annotations associated with the whole slide, like a slide of normal tissue or a diseased one c) **ROI-level annotations:** are more focused on diagnosis and structure details d) **Patch-level:** are separated into Large FOV (field of view) and small FOV, each having different computational requirements for processing, and finally e) **Pixel-level:** includes information about color, texture and brightness

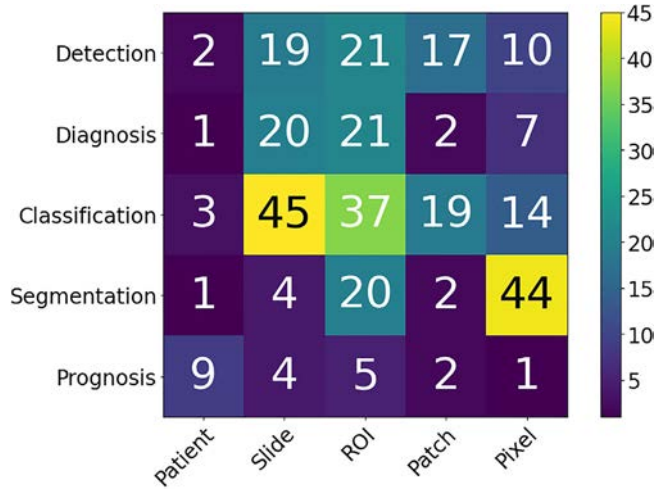

Fig. 8. A snapshot of the distribution of different annotation levels based on the CPath task being addressed in the surveyed literature for the purposes of highlighting the trend of datasets. The x-axis displays the different annotation levels studied in the papers (from left to right): Patient, Slide, ROI, Patch, and Pixel. The y-axis shows the different tasks (top to bottom): Detection, Diagnosis, Classification, Segmentation, and Prognosis. The height of the bars along the vertical axis measures the number of works that have examined the specific task and annotation level.

overviews the benefits and limitations of each level. For additional information regarding each annotation level please refer to Appendix A.8.

Picking the Annotation Level Selecting an annotation level depends largely on the specific CPath task being addressed, as shown in Fig. 8. For example, segmentation tasks tend to favor pixel-level annotations as they require precise delineation of a nucleus or tissue ROI. Conversely, disease diagnosis tends to favor datasets with ROI-level annotations, as diagnosis tasks are predominantly associated with the classification of diseased tissue, the higher-level annotations may provide a sufficient level of detail and context for this task.[266]

Fig. 8 shows that tasks that use stronger supervision are more likely to be used in CAD tool model development. However, due to the high cost of pixel-level annotation, fully supervised annotations are challenging to develop. Even patch-based annotations often require the division and analysis of a WSI into many small individual sub-images resulting in a similar problem to pixel-based annotations.[63,212] In contrast, WSI data is most often available with an accompanying slide-level pathology report regarding diagnosis thus making such weakly labeled information at the WSI level significantly more abundant than ROI, patches, or pixel-level data.[267,268] Different levels of annotation can be leveraged together, as demonstrated by a framework to use both pixel and slide level annotations to generate pseudo labels in.[269] Additionally, it is common in CPath to further annotate the slide-level WSIs on an ROI or patch level structure.[32,85,270,271]

Active Learning Tools Active learning annotation tools bridge the gap between the need for highly supervised labels and the current abundance of less informative annotations. Such works seek to ease the annotation process by using computational approaches to assist the human annotator. For example, in,[168] a platform was developed for creating nuclei and gland segmentation ground truth labels quickly and efficiently. A convolutional neural network (CNN), trained on similar cohort data, was used to segment nuclei and glands with different mouse actions.[168] Alternatively, Awan et al.[169] presented the HistoMapr™ platform to assist in diagnosis and ground truth data collection. Through this tool, a pathologist selects one of several proposed classes for each given ROI, thus mitigating the need for hand-drawn annotations or manual textual input.[169] Similarly, an active learning model called the Human-Augmenting Labeling System (HALS)[272] was developed to increase data efficiency by guiding annotators to more informative slide sections. Quick Annotator (QA)[273] is another tool which provides an easy-to-use online interface for annotating ROIs and was designed to create a significant improvement in the annotation efficiency of histological structures by several orders of magnitude. There are other active learning annotation tools proposed for different applications in computer vision that can be investigated for use in the pathology datasets. Such examples include methods to produce object segmentation masks for still images[274,275] as well as video.[276] One notable example is DatasetGAN[275]; the model is proposed as a training data creator, and it is shown that the model can produce segmentation masks with a small number of labelled images in the training data. While these systems are for general computer vision, they may be adoptable in computational pathology, and would facilitate the necessary relationship between pathologists and computer scientists in the development of CAD tools. As such, they may prove to be a valuable contributor to the CAD system development workflow.

Tissue-Class and Disease Complexity Much of the current CPath research operates under the umbrella of supervised learning tasks, and correspondingly uses labeled data to develop automated CAD tools. We refer to supervised learning to include a diverse spectrum of annotation i.e. weak-supervision (e.g. patient-level) all the way to strong-supervision (e.g. pixel-level). Classes within a dataset can be task-dependent, for example as shown in Table 9.11 of the supplementary material, datasets primarily used for segmentation such as MoNuSeg[258] and CPM-17[277] have classes for each annotated pixel indicating the presence or absence of nuclei. However, classes need not be task-dependent; datasets such as CAMELYON16[231] outline metastases present in WSIs that can be used for a variety of applications, including disease detection[231] and segmentation tasks.[278]

The current paradigm for dataset compilation in computational pathology, particularly for disease detection and diagnosis, treats different disease tissue types as separate independent classes. For example, BreakHis divides all data into benign/malignant breast tumours.[226] At the ROI level, GLaS divides colon tissue into five classes: healthy, adenomatous, moderately differentiated, moderately-to-poorly differentiated, and poorly differentiated.[233] So far, this approach to class categorization has resulted in high-performing CAD tools.[80,83,84,228,229,279] However, the treatment of different disease tissue types as an independent class is perceived differently in computer vision domain where the representation learning of normal objects is done differently compared to anomalies. A similar synergy can be found by differentiating healthy tissue classes from diseased ones and one should be mindful about defining meaningful tissue ontology for annotation and labeling.

4.2. Optimum labeling workflow design

This section focuses on the steps required for compilation of a CPath dataset which is broken into three main sub-tasks: Data Acquisition, Data Annotation, and Data Management, as per Fig. 9. Each sub-task is discussed below with reference to its individual components in the hierarchical structure in Fig. 9.

Data Acquisition Database compilation starts from data acquisition. When collecting data, it is vital that there are large amounts of data,[280] along with having sufficient diversity.[62,172] Specifically, diversity in CPath data occurs in multiple ways, such as staining methods, tissue types and regions, laboratory processes, and digital scanners. We advise that CPath researchers consult expert pathologists on the diversity of data required for various tasks. Ideally, all the data acquired in pathology should be perfect without any irregularity and artifacts. However, some level of artifacts and irregularity are unavoidable and introducing realistic artifacts that are representative of real-world scenarios into the data increases the robustness and generalizability of CAD tools.

Data Annotation After collecting sufficient data, the next task is annotation of the data. Data annotation is a costly process in both time and money, thus a budget and schedule should always be established when

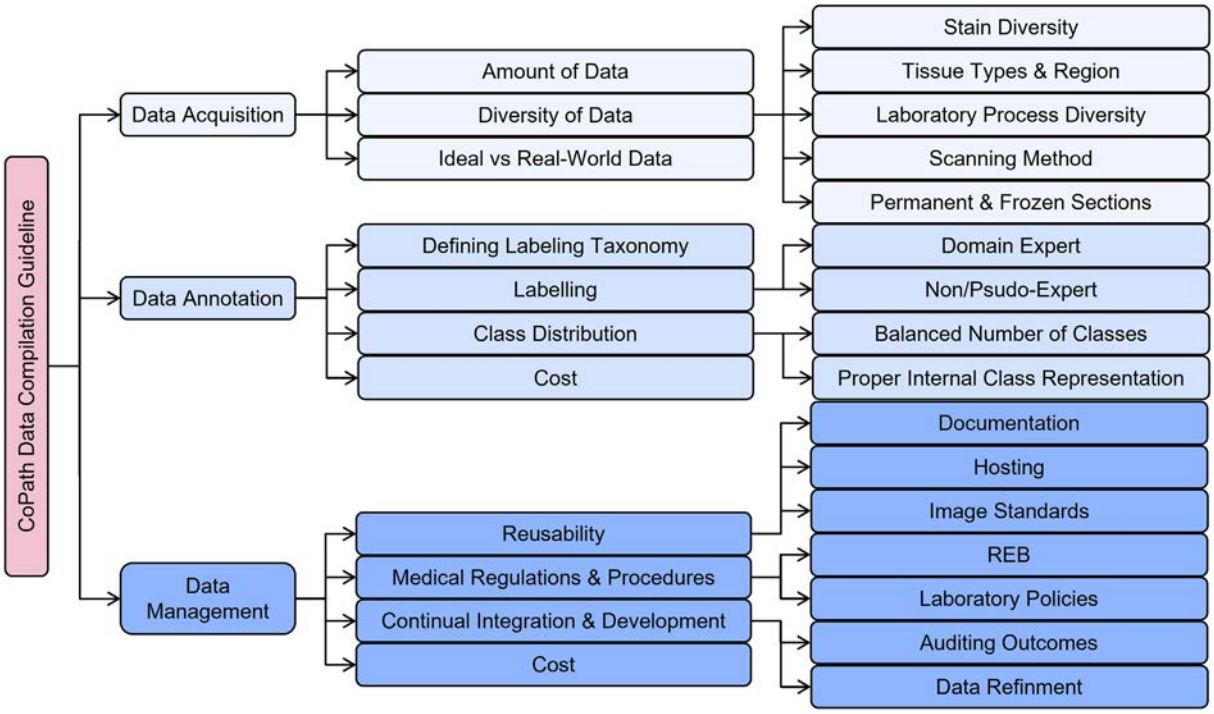

Fig. 9. Tree diagram for the optimum labeling workflow, where a CPath dataset is divided into tasks and sub-tasks based on its initial characteristics.

generating labels. There are often various approaches for annotating different structures,[281] so a specific labelling taxonomy should be defined *a priori*. As mentioned previously, annotation should involve expert pathologists due to the domain knowledge requirement and importance of label correctness. A table of commonly used commercially available annotation software for annotating different slide formats are show in Table 2, along with their compatible image formats which is important to note when trying to build compatible and accessible datasets.

Once the ontology of class-definitions is defined (in collaboration with expert pathologists), there will be two ways to generate labels or annotations in general: domain expert labelling or non-expert labelling. The domain expert labelling refers to having pathologists annotate data that they are specialized at, which is labor-extensive. On the other hand, non-expert labelling can use crowdsourcing techniques to generate weak labels or have non-experts, such as junior pathologists or students, label the data. This process is cheaper and quicker, but it may be harder to maintain the same level of quality as domain expert labeling.[281] Regardless of the labelling methodology used, labels generated from both should be validated. Finally, to determine the sufficiency of label quantity, one should consider the balance between the number of classes, representation size of each class, and complexity of class representation. Techniques from active-learning could be also leveraged to compensate for lack of resource management as well as maintain the quality of labeling as discussed above.

Data Management Data management is an important aspect of any dataset creation process, and is the one that is most likely to be overlooked. Proper data management should have considerations for reusability, medical regulations/procedures, and continuous integration and development.

Reusability can be broken down into detailed documentation of the data, accessible and robust hosting of data, and consideration for image standards. Poor cross-organizational documentation can lead to missing metadata, ultimately resulting in discarding entire datasets.[282] Adherence to an established image standard, such as DICOM, can help resolve some of these issues in reusability. Medical regulations/procedures can be broken down into the construction of a Research Ethics Board (REB) and proper consideration for whom is curating the data. Through incentives for data excellence for medical practitioners, the issue of misaligned priorities between data scientists, domain experts, and field partners can be resolved.[282] To ensure that models used on actual patients remain relevant and hidden errors do not propagate, continuous integration/development (CI/CD) must be implemented. These systems must include at least two components, a method to audit predictions from the model, as well as a way to refine the training data accounting for discrepancies found through auditing. Several algorithms deployed in high-risk environments, including medical diagnosis, proved to only work well when data was updated after initial deployment.[283,282] Throughout the data management process, consultation with domain experts is a vital step in ensuring the success of data compilations.[284]

5. Model learning for CPath

Once an application domain and corresponding dataset have been chosen, the next step of developing a CPath tool involves designing of an appropriate model and representation learning paradigm. Representation learning refers to a set of algorithmic techniques dedicated to learning feature representations of a certain data domain that can be used in downstream tasks.[285] In CPath, the amount of data available for a given annotation level and task are the key determinants to designing a model and learning technique. The last decade has shown neural network architectures to become the dominant method in many machine-learning domains because they are rich enough to avoid handcrafted features and offer superior performance.[286] The annotation level of the data pertaining to the task corresponds to the level of supervision for the learning technique applied. This relationship between data annotation level and learning supervision level is surveyed in Fig. 11.

This section details the various types of models and learning techniques, along with the tasks they have been applied to in CPath. Fig. 10 highlights the most common backbone architectures used for feature encoding in SOTA research, based on the corresponding tasks. More details are provided in Table 9.11 from the supplementary materials. The selection of architectures is then compared to draw useful insights into accuracy, computational complexity, and limitations. Lastly, existing challenges in model design are investigated.

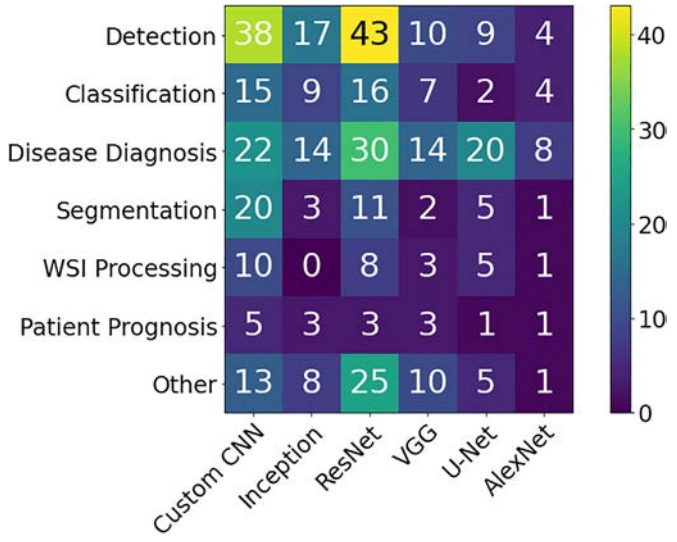

Fig. 10. Distribution of the most common Neural Network architectures used in the surveyed literature, based on the CPath task. The x-axis displays the Neural Network architectures used in the papers (from left to right): Custom CNN, Inception, ResNet, VGG, U-Net, and AlexNet. The y-axis shows the different tasks (top to bottom): Detection, Classification, Disease Diagnosis, Segmentation, WSI Processing, Patient Prognosis, and Others. For more details, please refer to Table 9.11 in the supplementary section.

5.1. Classification architectures

In CPath, general classification architectures are the most prevalent due to their straightforward applicability to a wide range of tasks including tissue subtype classification, disease diagnosis and detection (more details in Section 2 and Fig. 4). Architectures commonly used for natural images, in particular CNNs, are widely adopted for CPath. To maximize model performance, it is a common approach to pre-train the model on large datasets like ImageNet before subsequent fine-tuning them to perform well for the specific CPath task, a task known as transfer learning.[64,86,87,206,250,261,267,287–312] Transfer learning for CPath allows for: 1) improved generalizability, particularly for tasks with limited amount of data; and 2) improved ease in finetuning a model compared to training from scratch.[313]

Graph Convolutional Neural Networks (GCN)[314,315] is an alternative architecture that can be used to improve the learning of context-aware features across the WSI. GCNs typically consist of nodes representing elements and edges defining relationships between nodes. In,[316] a GCN was defined on a WSI, where the nodes represent patches and edges represent the connections among patches; this work obtained remarkable results on cancer prognosis task outperforming the SOTA in four out of five cancer types.[316]

Vision Transformers (ViT),[317] have recently emerged as a direct application of Transformer models[318] to the image domain. In ViT, images are sub-patched and flattened into a 1D embedding along with a positional encoding which is then classified by an MLP head. By using the positional encoding, the model's attention mechanism can focus computation on the most relevant areas of the image. ViT models have been applied with great success to CPath tasks, especially in conjunction with pre-trained CNN models.[319] We refer the reader to a comprehensive survey of transformer methods in medical image analysis for more details.[320]

General classification architectures are also commonly used as a foundation for novel architectural designs. For example, Squeeze-and-Excitation (SE) modules were introduced to reduce the number of parameters in ResNet and DenseNet blocks while maintaining high accuracy.[321,229] A fully-connected conditional random field (CRF) was incorporated on top of a CNN encoder to improve performance while maintaining the same level of computational complexity.[322] Lastly, patch sampling and pooling were used with AlexNet to perform slide-level disease diagnosis and segmentation.[142]

Finally, in order to achieve superior performance, many researchers often rely on ensemble or multi-stage techniques which combine the predictive power or feature extraction abilities of multiple models to form a final output. These approaches have shown performance improvements compared to traditional single model classifiers.[323–328] However, this often comes at the expense of higher computational requirements.

5.2. Segmentation architectures

Segmentation is widely used in CPath, as shown in Fig. 4, and enable localizing the area of interest at the pixel level.[329] U-Net was initially developed for neuronal structure segmentation in electron microscopy image

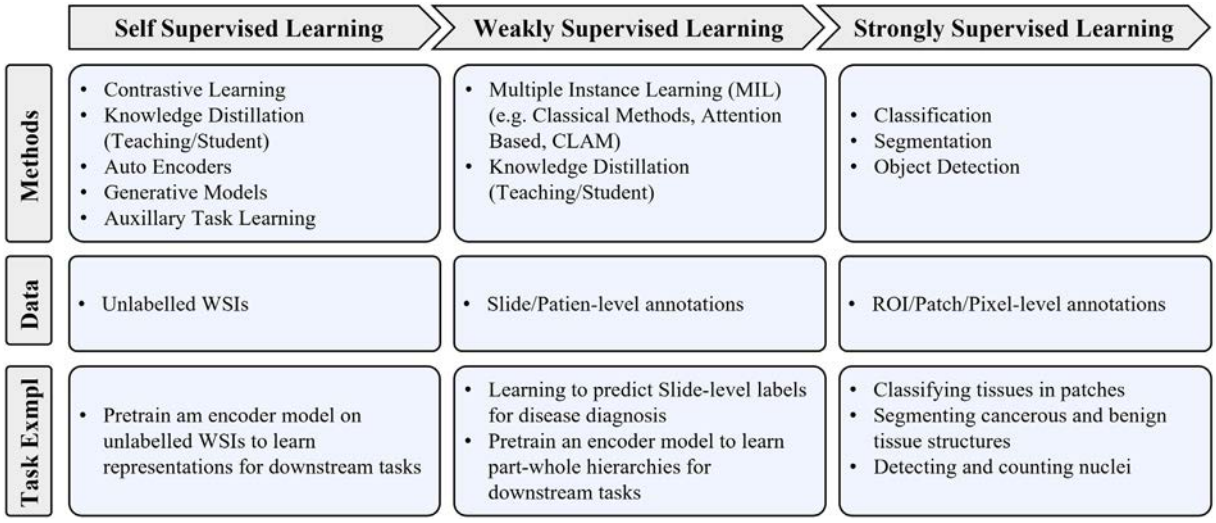

Fig. 11. Details of types of learning using varying levels of supervision. Note that the types of tasks each type of learning can address vary based on the data that is available, as noted in the *Example Task* portion of the figure. However, from left to right, models trained with less supervision can still learn salient representations of the data that can be used to fine-tune models for tasks requiring more supervision. In that sense, for CPath there is a *spectrum* of supervision from self to strongly supervised learning that aligns well with the annotation levels shown in Fig. 7.

stacks,[329] but has become one of the most common architectures for segmentation in CPath.[152,205,207,237,273,278,304,323,330–349] U-Net has an encoder-decoder structure: an encoder to contract features spatially and a decoder to expand them again to capture semantically related context and generate pixel-level predictions.[329] The U-Net model has been used to segment nuclei for creating a novel dataset with unsupervised learning,[237] but it should be noted that this process also relies on the Mask R-CNN framework and pathologists for quality-checking purposes.

Another common approach for segmentation is to use fully convolutional networks (FCNs),[80,84,198,258,270,349–355] customized architectures constructed by combining multiple components of various architectures, or introducing new components to pre-existing architectures.[84,168,234,259,266,269,300,309,343,344,356–369] For example, one work used a custom CNN to predict whether each pixel was benign or malignant, while a second CNN was used to refine the initial prediction through probability fusion.[84]

5.3. Object detection architectures

In this section, we specifically focus on architectures that are used for object detection in CPath, where bounding boxes are predicted around regions of interest. A major CPath application for object detection is mitosis detection with the primary goal for counting the number of mitosis instances. To this end, a large number of studies has been dedicated to this application.[199,200,218,262,337,343,370–379] Object detection has been additionally applied for nuclei,[77,380–385] colorectal gland[80,341,386] and glomeruli detection[387–389]; however, it can also be applied to the detection of a variety of histopathological objects including tumor-infiltrating lymphocytes[390] or keratin pearls.[364]

In CPath, object detection employs a combination of pre-existing off-the-shelf architectures and customized neural networks to perform object detection tasks, as shown in Fig. 10. A model called CircleNet, which uses a deep layer aggregation network as a backbone, was proposed to detect round objects.[388] Their approach involves using an anchor-free "center point localization" framework in order to output a heatmap with center points followed by a conversion into a bounding circle for the detection of kidney glomeruli. A multi-stage deep learning detection model based on Fast R-CNN was proposed in.[372] First, a modified Fast R-CNN generated region proposals, then a ResNet-50 model eliminated false positives, and a Feature Pyramid Network detected mitosis in sparsely annotated images using a ResNet backbone.[378]

5.4. Multi-task learning

Multi-task models are individual models predicting for multiple tasks at once (e.g. classification and segmentation), as defined in Section 2. Multi-task learning (MTL) can be beneficial over independent task learning because sharing representations between related tasks can create more generalizable representations and encourage the task heads to make logically consistent predictions. This type of model, however, is uncommon in CPath, as it requires annotating multiple tasks for each image.[32,82,120,377,391–393] We discuss some of these papers in further detail below.

In one work, a ResNet-50 backbone followed by independent decoders (a pyramid scene parsing network for segmentation and a fully-connected layer for classification) was used to solve 11 different tasks (4 segmentation based and 7 classification based).[120] With significantly less computation, the MTL model achieved comparable or better results to single task learning in classification, but comparatively worse results in segmentation. Similarly, in,[82] a ResNet-50 with two parallel branches to perform segmentation and classification, was able to achieve comparable results on both tasks through an MTL approach.

While the results are impressive, there is still work to be done in this field. One work found that model performance may be sensitive to the number and type of tasks used during training.[391] If the tasks are unrelated, this could deteriorate the performance compared to a single-task setting. How to weigh different task objectives and select optimal tasks to be trained together is yet an active area of research.[394,395] MTL represents an interesting field of research in CPath as it may reduce the necessity to train multiple deep neural networks to perform different tasks.

5.5. Multi-modal learning

As opposed to multi-task networks where multiple tasks are learned simultaneously, the multi-modal approach involves using network input features from multiple domains/modalities at once.[396] In the case of CPath, modalities can be represented as pathologists' reports, gene expression data, or even WSI images. Most commonly, immunohistochemistry (IHC) stains alongside the H&E stain to better visualize specific proteins.[397–399] As a result, models can learn better unified/shared latent representations which capture correlations from multiple indicators, since some information may not be captured by individual indicators.[400] This approach can be viewed as adding hand-crafted features to boost performance. While the use of deep learning normally implies using learned features to replace hand-crafted ones, using hand-crafted features can nonetheless improve performance compared to strictly deep learning approaches when data is limited.[401] Indeed, many works have obtained best performance by combining manual and learned features.[371,383,402] This was demonstrated in the case of mitotic cell classification when an ensembled classifier model using hand-crafted features set a new record for the MITOS-ATYPIA 2014 challenge with an F-score of 86%.[403] However, where data is plentiful, CNNs alone can outperform all other hand-crafted features. In the same MITOS-ATYPIA 2014 challenge, the previous record was broken this way with a new F-score of 96%.[404] Although one cannot compare these two works directly as they use different classifier heads and dataset balancing methods, one can argue that the optimal choice of approaches from deep learning, classical ML, and different modalities should depend on the situation. Multi-modal approaches are gaining traction in CPath for specific problems, especially where useful additional data is available.[405,406] For example, gene expression data and WSI images are often combined to improve cancer prognosis prediction.[407,408]

5.6. Vision-language models

Following its successful use in the natural image domain, vision-language data (consisting of histopathology images paired with relevant natural language text) is becoming increasingly prominent in CPath. Whether it be the development of foundational models[409] extending to CPath, or fine tuning state-of-art large large models for use in downstream tasks,[410–412] leveraging the semantic information embedded in the natural language data is becoming more evidently beneficial. It was only recently that foundational language models advanced enough to become useful in CPath, and this has triggered an explosion of interest into building models at the intersection of visual and language information. At the moment, language data is primarily used to address Multi-Instance Learning, although this is still an extremely new field and we anticipate that future works will surely address more advanced tasks (see Section 7.4 for further discussion).

5.7. Sequential models

Recurrent Neural Networks (RNNs) are typically used in tasks with temporally-correlated sequential data, such as speech or time series.[413] Since RNNs consider the past through the hidden state, they are suited for handling contextual information. While images are the default data format in CPath (and hence poorly-suited for RNNs), some works opt to combine RNNs with CNNs as a feature extractor,[62,88,414,213,224,257,259,415–420] most commonly by aggregating patches or processing feature sequences.[62,224,259,418,421] Another application of RNNs is to consider spatial relations between patches, which can be lost after extracting from the slide.[213,257]

A particularly exciting use of RNNs is in deciding which region within an image should be examined next.[417,422] In the "Look, Investigate, and Classify" 3-stage model, an long short-term memory (LSTM) was used to classify the ROI cropped from the current patch and predict the next region to be analyzed, and achieved good performance while only using 15% of pixels from the original image.[417] Similarly, an LSTM network was used to better predict ROIs by treating state features similar to time-series data, thus identifying only relevant examples to use for training.[422] And an LSTM transformer with "Feature Aware Normalization" (FAN) units for stain normalization was used in parallel with a VGG-19 network.[318] More recently, transformers using attention mechanisms have been used to allow parallelization and better sequence translation compared to older RNNs or LSTM networks.[423]

5.8. Synthetic data and generative models

With annotated data difficult to obtain in CPath, especially with granular labels (see Section 3.3 for more discussion), this is problematic for training generalizable models. Hence, generating *synthetic* data from a controlled environment (either via simulation or a trained model) for augmenting the available training set of annotated data shows much promise. Originally developed for visual style transfer in general computer vision, generative models learn to create novel instances of samples from a given data distribution - they form the dominant approach in CPath.

Initial works primarily utilized Generative Adversarial Networks (GANs) for patch synthesis,[330,424–426] stain normalization,[206,208–210,427,428,] style transfer,[206,429–431] and various other tasks.[212] One unsupervised pipeline relied on a non-GAN model to create an initial patch that was refined by a GAN.[330] In another work, one CycleGAN generated tumor images and another non-tumor, in order to train a classification network.[432] One work used neural image compression to learn the optimal encoder to map image patches to spatially consistent feature vectors.[212] Another work first classified bone marrow cell representations and then used an unsupervised GAN to generate more instances from each cluster.[433] A self-supervised CycleGAN was also used for stain normalization, and shown to improve model performance in subsequent detection and segmentation tasks.[210] Similarly, a CycleGAN pipeline was applied to perform artificial IHC re-staining.[434] Recent works in GANs attempt to model spatial awareness of tissues and improve the realism of the generated samples.[435]

Lately, diffusion models have become the SOTA in general computer vision and now produce far more semantically plausible and noise-free images than GANs. These improvements promise to make synthetic data finally accepted by pathologists and the broader CPath community as reliable training data and significantly improve the generalizability of models trained on them.[436]

5.9. Multi-instance learning (MIL) models

Multi-instance learning (MIL) involves training from data that is labelled as high-level bags consisting of numerous unlabelled instances. In the context of CPath, these labelled bags often represent annotated slides of far more unlabelled patch instances.[437] As labels at the WSI level are much easier to obtain (and hence more prevalent) than patch-level annotations, MIL has been applied to CPath by a significant number of papers.[62–64,267,268,308,316,418,437–456] Since both utilize coarser annotations for training on massive images, MIL is similar to weakly-supervised learning. However, weak supervision predicts at a finer level (e.g. pixel segmentation from labelled patches) than the provided annotation while MIL prediction is typically at the same level.

One notable work used a two stage approach to first encode patches with a CNN from a slide into feature vectors and then pass the most cancer-likely ones to an slide-level classification RNN. A similar work first detected abnormal regions in the WSI before adaptively fusing the instance-level features with an importance coefficient.[439] Adding additional instance-specific attributes tends to improve MIL performance. One work applied a nuclei grading network to provide a cell-level prediction for each patch, and demonstrate this out-performs hand-crafted cell features for overall slide classification.[319] Recent works explore the morphological and spatial relationships between instances, which conforms with pathologist diagnostic intuitions and have demonstrably improved performance, especially with unbalanced data.[456]

As not all instances are equally relevant to the bag label, many works focus on building attention mechanisms to adaptively focus on more relevant instances. One work used such a mechanism to highlight regions of interest and improve localization relative to other SOTA CNNs.[437] MIL models can be improved by considering multi-scale information: one work notably used embeddings from different magnification levels and self-supervised contrastive learning to learn WSI classifiers.[268] Some works explicitly encode the patient-slide-patch hierarchy in the attention mechanism,[457,458] with one work using a cellular graph for top-down attention.[459] Graph Neural Networks (GNNs) have been explored to leverage intra- and inter-cell relationships, enabling cancer grading,[460] classification,[461] and survival prediction.[462,463] These hierarchy- and morphology-aware models are the current SOTA and pave the way for future improvements.

One persistent challenge with using MIL in CPath, compared to natural image computer vision, is the lack of large-scale WSI datasets.[464] One recent work addressed issues related to small sample cohorts by splitting up large bags (and their labels) into smaller ones through pseudo-bags.[465]

5.10. Contrastive self-supervised learning for few-shot generalization

The idea of using contrastive learning (CL) for self-supervised learning (SSL) dates back to 2005, yet only recently gained momentum in CPath.[268,306,466–471] By using a contrastive loss, a feature embedding is learned to ensure similar (positive) examples are close in vector space, while dissimilar (negative) examples are distant.[466,467] Contrastive learning is an attractive approach for CPath because when used as self-supervision for few-shot learning,[268,306,468] it does not require labelling the massive self-supervision image set but only labelling the small subset used for training on the downstream task, an approach that has recently achieved SOTA performance in a wide array of tasks in CPath.[306] SimCLR was originally proposed to learn representations invariant to different augmentation transforms (such as crop, noise) for natural images,[66] and when applied to CPath, was found to match or outperform SOTA supervised techniques.[306] Self-supervised pre-training has been shown to perform best against fully-supervised pre-training when applied to small but visually-diverse datasets.[306] Recent works have focused on transferring the self-supervised representations to the downstream task more intelligently: through latent space transfers,[472] with an awareness of the patient-slide-patch hierarchy,[473,474] or with semi-supervised pseudo-label guidance.[475]

5.11. Novel CPath architectures

In this section, we discuss papers that made significant changes to the model design or completely designed an architecture from scratch for CPath tasks.[64,277,357,361,382,476–479] Typically, model architectures are adapted from the natural image domain and minor changes applied for CPath tasks, rather than being designed from scratch for CPath directly. Unfortunately, general computer vision architectures typically require large computational resources not necessarily available in clinical settings and are prone to overfitting on smaller CPath training sets.[476]

More importantly, CPath tasks often comprise of multiple specialized sub-tasks not addressed by common architectures - in such cases, CPath-specific architectures perform better. "PlexusNet" achieved SOTA performance with significantly fewer parameters[476] and "Hover-Net" used a three-branched architecture for nuclei classification and instance segmentation.[277] Path R-CNN similarly used one branch to generate epithelial region proposals and another to segment tumours.[382]

In other cases, custom architectures are designed to obtain better performance with respect to certain metrics[85,295,338,377,388] or improve computational efficiency and speed,[196] where since model inference can be a bottleneck for WSI processing. To automate architecture design, neural architecture search (NAS) is often used. This is an umbrella term covering evolutionary algorithms (EA), deep learning (specifically Reinforcement Learning), and gradient-based NAS searches. There are two approaches to EA: (1) Neuroevolution, which more generally optimizes at the neuron-level to find optimal weights, and (2) Evolutionary-Algorithms based NAS (EANAS), which searches for optimal combinations of mid-sized neural network blocks and conducts training after this architectural search.[480,481] In CPath, reinforcement learning-based NAS has designed models for cancer prediction which were found to train faster, have fewer parameters, and perform comparably with manually designed models.[482] Another work demonstrated that a significantly smaller model can outperform existing SOTA models on a variety of CPath tasks using an adaptive optimization strategy.[479]

We hypothesize that NAS has yet to be explored significantly in CPath due to the lack of annotated data (see Section 3.3) and its relative recency as a research area. According to the "no free lunch theorems",[483,484] no single model can perform best on all tasks. However, computationally efficient but performant models are crucial for CPath applications, and NAS is the most promising approach to computationally design such architectures without manual engineering.

5.12. Model comparison

The various model architectures and types discussed above can and should be compared on common benchmarks to determine the best models for a given task.[485] Numerous papers have conducted such benchmarking work on CNNs. One work comparing GoogLeNet, AlexNet, VGG16, and FaceNet on breast cancer metastasis classification found that deeper networks (i.e. GoogLeNet) predictably performed better.[199] Another work found that using ResNet-34 with a custom gradient descent performed best.[387] Finally, VGG-19 performed best in colorectal tissue subtype clasification, showing that deeper SOTA networks do not necessarily perform better universally. Which CNN performs best depends on the task, the nature of the data, the metrics used, training time, hyperparameters, and/or hardware constraints.

Likewise, third parties have organized "grand-challenges" to facilitate the fair comparison of different techniques on a common CPath task and dataset. In some cases, SOTA CNNs achieve the best results, such as the adapted GoogLeNet that obtained the highest AUC[231] and the AlexNet that achieved highest accuracy[486] for breast cancer detection in the CAMELYON16 challenge. Likewise, SqueezeNet, which is an existing SOTA network performs best in colorectal tissue subtype classification.[487] On the contrary, the best performing models for mitosis detection in the TUPAC16[199] and MITOS12[338] challenges both relied on custom CNN architectures. For breast cancer diagnosis, a novel Hybrid CNN achieved the best results in the BACH18 (ICIAR18) dataset[488] while the two teams achieving the best classification accuracy in the BreakHis dataset used differing approaches: one directly used ResNet-50[291] and the other used an ensemble of VGG networks.[489] For nuclei segmentation on the Kumar-TCGA dataset, a novel framework using ResNet and another existing model achieved the highest F1-score.[357] Lastly, a custom CNN achieved the best results for gladn segmentation on the GLaS dataset.[168]

However, as mentioned in Section 3.3, many grand challenges use private datasets or even extract data from larger public repositories without referencing the original WSIs used. Furthermore, benchmark datasets address different tasks and lack standardization. As models that are hyper-optimized to for specific sets of data continue to be released, the lack of more standardized benchmark datasets and model comparison studies make it impossible to systematically compare new models against existing ones or assess their robustness in clinical settings, thus impeding model development in CPath.

6. Evaluation and regulations

6.1. Clinical validation

Within the domain of CPath, clinical validation is essential for substantiating the decisions produced by deep learning models so that they are more readily accepted by the medical community. Generally, acceptable clinical criteria are determined by authoritative professional guidelines, consensus, or evidence-based sources. However, in CPath, prediction results are generated by the computer scientists and engineers who build the model, and may not be completely aware of where their work fits into the clinical pathology workflow–the clinical implications of this arrangement are often unknown.[169] By incorporating pathologist expertise, clinical validation can better align the technical work with clinical objectives.

Despite the importance of this step for real-world deployment, very few works have performed clinical validation with expert pathologists. We identify three prominent types of clinical validation in the CPath literature: (1) direct performance comparison of CAD tools with pathologists on a similar task, (2) impact of CAD tool assistance on pathologist performance, and (3) pathologist validation of CAD tool outputs. Each topic is further discussed in the sections alongside notable results.

Direct Performance Comparison with Pathologists To validate the benefits of deep learning methods, it is desirable that they equal or surpass the performance humans to gain the trust of pathologists in their decisions and their willingness to use them as a second opinion.[490] With this in mind, many papers directly compared their models with pathologists in tasks such as prognosis and diagnosis.

One study on cancer detection found that the top computational models from the CAMELYON16 challenge out-performed the 11 pathologists with a two-hour time constraint and performed similarly to the expert pathologist without a time constraint.[231] This suggests that deep learning models could be particularly useful in clinical scenarios with excessive numbers of time-critical cases to diagnose. Similarly, for tissue subtype classification, another study performed similarly to, or slightly better than individual pathologists. The proposed model agreed with all pathologists 66.6% of the time and agreed with two-thirds of pathologists 76.7% of the time.[75] An additional study claimed their deep learning model outperformed pathologists without gynecology-specific training in ovarian carcinoma classification.[119] This pushes the idea that CAD predictions can be used as a second opinion due to the potential for human error by individual pathologists.

One paper on diagnosis[256] demonstrated that deep learning models can correctly classify images that even individual pathologists failed to correctly identify. However, another paper found that 50% of the examples misclassified by their model were also misclassified by at least one pathologist.[491] This suggests that deep learning models can aid pathologists in decision-making, but as they tend to achieve a specificity and sensitivity similar to pathologists, they must be applied cautiously to avoid reinforcing the biases or errors of individual pathologists.

Deep learning models for prognosis have been shown to achieve performance similar to or better than experts as well.[238,289,381] In one study, the best model for renal clear cell carcinoma classification achieved 83% accuracy, outperforming the inter-pathologist accuracy of 80%.[289] This shows that deep learning models and pathologists may perform similarly on patient prognosis.

Overall, AI approaches are not perfect but have approached expert-level ability in a variety of tasks. Deep learning could play an important role as a second opinion and in democratizing the knowledge distilled from many pathologists to other pathology centres. Specifically, deep learning models appear to be best used as a tool to enhance the pathologist workflow, and could provide aid in making quick decisions with high accuracy.[14]

Impact of CAD Tool Assistance Much of CPath research is conducted under the assumption that the resulting AI tools will be intuitive, usable, and beneficial to pathologists and patients. However, CAD tools that are developed without feedback from pathologists could fail to integrate into a realistic pathologist workflow or impact the most significant diagnostic tasks.

Thus, a valuable validation experiment is to compare and comprehend the performance of expert pathologists in clinical tasks before and after being given the assistance of a CAD tool.

In one study, a CAD system called Paige Prostate Alpha leveraged a weakly-supervised algorithm to highlight patches in a WSI with the highest probability of cancer.[62] When used by pathologists, the model significantly improved sensitivity, average review time, and accuracy over unaided diagnosis. Likewise, another study using the LYNA algorithm examined the performance of six pathologists on breast cancer tumor classification before and after being able to see the LYNA-predicted patch heatmaps. The results indicate using LYNA substantially improved sensitivity, average review time, and the subjective "obviousness" score for all breast cancer types.[72,27]

These studies suggest that integrating CAD tools into the clinical workflow will greatly improve pathologist efficiency. However, there is a general lack of research on the impact of CAD tools on pathology efficiency. Such studies would shed more light on the impact of CAD tools and identify approaches for implementation in clinical settings.

6.2. FDA regulations

Despite the ongoing development of CAD tools in CPath and its potential for triaging cases and providing second opinions, the regulations regarding this technology pose an obstacle to the testing and deployment of these devices. The FDA currently provides three levels of clearance on AI/ML-based medical technologies: 510(k) clearance, premarket approval, and the De Novo pathway. While one source lists 64 AI/ML-based medical solutions that are currently FDA-approved or cleared, none of these are in the field of CPath.[492] A few companies, such as Paige AI, hold the 510 (k) clearance for their digital pathology image viewer; however, an automated diagnostic system has yet to be approved. This may indicate a reluctance to change, and the lack of clarity in the process of FDA approval has prevented numerous impactful technologies from being deployed. There is a need for collaboration between researchers, doctors, and governmental bodies to establish a clear pathway for these novel technologies to be validated and implemented in clinical settings.

7. Emerging trends in CPath research

Computational pathology research has seen a sudden shift of focus in the past year of 2023. Driven by recent technological advances in the field of computer vision for natural images and the release of capable foundational models in natural language processing, formerly difficult research problems in CPath have been solved, opening up exciting new avenues of research, especially the difficulty of training models on adequate annotated data. We will discuss the main research trends below in further detail and make simple predictions of where the field is headed.

7.1. Contrastive self-supervised learning becomes mainstream

Data annotation for CPath is a persistent problem - it is easy to collect large amounts of visual data but much harder to annotate them. Transfer learning can help but it is difficult to transfer a model trained on one dataset to generalize to another. Whereas past efforts focused on carefully engineered methods, the recent development of contrastive self-supervised learning[66] means that it has become the mainstream approach in CPath.[268,306,468] Not only does it utilize the massive amounts of unlabelled images typically available in CPath, but it also as a result only requires finetuning on a small set for the downstream task. We anticipate that this will lead to the development of general-use foundational models in the future to perform the most common CPath tasks, as more pathology images are collected and models become more advanced.

7.2. Prediction becoming increasingly high-level

We noticed that recent research works are increasingly addressing higher level prediction tasks than before. Whereas patch classification[267,287–290] or pixel segmentation[237,329–333] was formerly mainstream, these problems appear to have been largely solved, and now there is far more research into higher-level problems dominate, such as multiple-instance learning.[62,437,457–459] As computational methods continue to improve, it is natural that they are applied not merely as attention aids for pathologists (i.e. at the pixel or patch level), but furthermore are used to make intelligent slide- and patient-level decisions on their own. Indeed, they promise to vastly improve pathologist efficiency when used with human pathologists in the loop to validate the automated decisions, especially when paired with modern natural language capabilities.

7.3. Spatial and hierarchical relationships receiving attention

Inspired by the approach taken for natural image computer vision, the mainstream approach in CPath currently requires breaking up large WSIs into smaller patches and perceiving them independently (see Fig. 7). However, this ignores the spatial relationships between cells and tissues or between the patches and their parent slides in histopathology images, which are often relevant or even crucial when making decisions. Many works have recently found success in explicitly encoding an awareness of these inter-cell relationships[460,462,463] and the patch-slide-patient hierarchy,[457–459] especially using Graph neural networks, but these suffer from higher latency than conventional CNNs. We anticipate future works will seek to speed up GNNs for tasks where spatial and hierarchical relationships are important and continue developing hierarchy-aware attention for MIL techniques.

7.4. Vision-language models for explainable predictions

One persistent problem in CPath has been developing models that can explain their decisions for human validation. One obvious route is to develop models that produce natural language output (and even converse with the human user to explain their decisions), but until recently, this would have required collecting massive amounts of pathology text paired with images. With foundational vision-language models widely available and able to generalize to great effect in the natural image domain,[493–495] recent works have shown that they perform excellently when applied with minimal re-training to CPath images.[410–412] Further advances require collecting more pathology-specific data, but we anticipate that crowd sourcing of public pathology annotations will become mainstream and this will lead to the development of foundational vision-language models. As natural language capabilities continue improving, we also anticipate that synoptic report automation will become feasible and reinforcement learning from human feedback (RLHF)[496] will become common for improving CPath language models.

7.5. Synthetic data now realistic enough

Whereas one way to combat the difficulty of annotating CPath data is to develop models that require fewer annotations, another trend is to generate more annotated data for training. Whereas concerns were previously raised about their realism, new advances in generative image models have now been leveraged to produce realistic histopathology images and pixel-accurate annotations simultaneously. However, current works are limited by specific tissues, organs, diseases,[212,330,432,433] or stains[210,434] and are limited by their inability to easily expand to other histopathology content. We note that generating synthetic data via game engines and 3D model assets is a recent trend in the natural image domain,[497–499] but visual modelling of histopathology entities is little explored. We anticipate that future works will attempt to improve synthetic histopathology image generation by: (1) attempting to create generative models that can generalize to a broad variety of histopathology images and (2) create simulation software to generate realistic histopathology images without learned models.

8. Existing challenges and future opportunities

8.1. CPath as anomaly detection

Typically in computer vision, the various classes represent distinct normative entities, such as airplanes or bears.[500,501] There exist abundant "normal" samples and potentially few "anomalous" samples, which are considered data points significantly dissimilar to the majority within a given class.[502] These anomalies are not only out of distribution from the samples in a dataset, there is also a lack of consensus on understanding anomalous representations as effectively identifying anomalies requires ML models to learn a feature space encompassing all "normal" samples within each class.[502]

In other words, in general computer vision, each class cannot simply be considered as an anomalous version of any other class. However, in CPath, since each class is often considered a different disease state on a single tissue type, diseased classes are essentially extensions of the "normal" healthy class into the "anomalous" zone. From a pathologist's perspective, similar to the general computer vision approach, the curriculum learning process of a resident pathologist first involves training on histology and gaining a mastery of normal tissue identification, and then train on diseased tissues, so they are able to flag the sample as anomalous and follow up with possible diagnosis.

In light of this, it may be illuminating to approach the problem from an anomaly detection viewpoint: provided a model has sufficient variety of healthy tissue, any anomalies must then be diseased. The output of such an anomaly detection algorithm is dependent on the task at hand. One source describes several meaningful output types that may be produced[502]: an anomaly score which describes how anomalous a sample is and a binary label indicating whether a sample is normal or anomalous. If only identifying anomalous samples is enough, a binary classification procedure may be sufficient. However, if it is necessary to identify the particular stage of progression of a disease type, then a more granular approach in assigning some *anomaly score* may be more appropriate as explored in a previous work.[503] This work found that the confidence score in tissue classification was inversely correlated with disease progression, thus the confidence score may act as a proxy for an anomaly score. Theoretically, such approaches may better replicate the behaviour of pathologists. While several works have used an anomaly detection approach on medical image data outside of CPath,[504–506] few works tackle the problem for WSI data in CPath.

8.2. Leveraging existing datasets

As mentioned in Section 3.3 of this paper, a minority of datasets in CPath are available to be freely used by the public. Additionally, the level of annotations varies for each dataset. However as can be noted in Table 9.11 of the supplementary material, for prominent public datasets such as CAMELYON16, CAMELYON17, GlaS, BreakHis, and TCGA, there is far more available data annotated at the slide level as opposed to more granular predictions. For example, considering breast datasets, there are 399 WSIs annotated at the Slide and ROI levels in CAMELYON16[507] and 1399 WSIs annotated at the Patient, Slide, and ROI levels in CAMELYON17,[61] in contrast, the TCGA-BRCA dataset contains 1163 diagnostic slides and 1978 tissue slides that are accompanied with labels at the Patient and Slide levels and diagnostic reports with labels for tissue features and tumor grades.[235]

The lack of publicly available datasets with granular annotations is a major challenge in CPath. To address this lack some training data, techniques have been proposed to efficiently obtain labels, such as an active deep learning frameworks that use a small amount of labelled data to suggest the most pertinent unlabelled samples to be annotated.[508] Alternatively, other works propose models to synthetically create WSI patches, usually with the use of GANs. For example, Hou et al.[330] introduced an unsupervised pipeline that was capable of synthesizing annotated data at a large scale, noting that even pathologists had difficulty distinguishing between real and synthesized patches. However, despite these promising results, the issue of acquiring accurate and large datasets remains a prevalent issue within CPath.

Generally, tasks such as tissue classification or gland segmentation require labels at the ROI, Patch, or Pixel levels. However, existing data annotated at the patient and slide levels can be used for these tasks by leveraging weakly supervised techniques such as MIL,[64,437] or by learning rich representations using self-supervised techniques such as DINO[65,509] and contrastive learning[306] that can be used in downstream tasks. Specifically, work is being done to develop training methodologies and architectures that are more data efficient for patient- and slide-level annotations, such as CLAM, which is a MIL technique that is used to train a performant CPath model with as little as 25% of the training data to get over 0.9 AUC.[64] Another recent work used self-supervised learning on WSIs without labels to train a hierarchical vision transformer and used the learned representations to finetune for cancer subtyping tasks. This finetuned model outperformed other SOTA methods that used supervised learning methods on both the full training set and when all models used only 25% of the training set. These examples demonstrate a recent trend in the application of weakly and self-supervised learning techniques to leverage pre-existing and available data with weak labels, showcasing that a large amount of granular labels are not necessarily required for achieving SOTA performance. We urge researchers in the CPath field to follow this trend and focus on how to leverage existing weakly labelled datasets, especially to learn rich representations as a pre-training step for learning on smaller strongly labelled datasets.

8.3. Creating new datasets

Although we mention the availability of many datasets and comment on how to leverage this existing data, there is still a need for new CPath datasets that address overlooked clinical and diagnostic areas. Therefore, creation of new CPath datasets should focus on addressing two main goals: (1) tasks that are not addressed adequately by existing datasets and (2) accumulating as large a dataset as possible with maximal variety.

Regarding the first goal, there are still organs, diseases, and pathology tasks without freely available data or sufficient annotations to develop CAD tools. For example, in Fig. 6, we see that whereas breast tissue datasets are abundant, there are few public datasets for the brain and none for the liver. Collecting and releasing datasets for these organs would have significant impact in enabling further works focusing on these applications. Further, analysis of specific organ synoptic reports can guide CPath researchers to build CAD tools to identify or discriminate the most impactful diagnostic parameters. In the case of the prostate, which is discussed in Section 2.5, the synoptic report requires distinguishing IDC from PIN and PIA as it correlates to high Gleason scores. This is important, as high-grade PIN is a cancer precursor requiring follow-up sessions for screenings. These parameters are identified and noted in the report by the pathologist and factor into the final diagnosis and grading. Thus, collecting annotated datasets for such parameters can be crucial to developing CAD tools that are relevant to clinical workflows and can enrich learned representations.

The second goal is concerned with the scaling laws of deep learning models with respect to the amount of data available and their application to diverse clinical settings. As seen in the general computer vision domain, larger datasets tend to improve model performance, especially when used to learn rich model representations through pre-training that can be used for downstream tasks such as classification and semantic segmentation.[510] Additionally, ensuring that datasets capture the underlying data distribution and thus sufficiently encompass the test distribution has been shown to be especially important in the medical domain.[511] For CPath, this means ensuring a dataset captures the expected variations in tissue structure, disease progression, staining, preparation artifacts, scanner types, and image processing. Collecting a sufficiently large dataset continues to

be problematic, however, so recent works have focused on using crowd sourcing to annotate histopathology data posted publicly on Twitter and YouTube,[409,411] a practice that is similar to that commonly used for natural images.

8.4. Pre- and post-analytical CAD tools

In recent years, advances in image analysis, object detection, and segmentation have motivated new approaches to support the analytical phase of the clinical workflow, especially in the two steps where CAD tools could significantly increase efficiency and accuracy: (1) specimen registration and (2) pathology reports. This need is highlighted by a study determining that the pre-analytical and post-analytical phases (as shown in Fig. 2 account for up to 77% of medical errors in pathology.[512] Likewise, Meier et al. classify 14% of medical errors as diagnostic errors, with an even smaller proportion being misinterpreted diagnoses in their study.[513] Other authors attribute approximately 1525% of diagnostic errors to slide interpretation.[514–518] These results reinforce the need for CPath applications that address more than just the analytical phase.[519] Considering post-analytical step of compiling a pathology report, a few natural language processing efforts have been used to analyze completed pathology reports,[520–522] extract primary site codes from reports,[523] and generate of captions or descriptive texts for WSI patches.[415] However, to the best of our knowledge, there are no works that reliably extract clinical data from service requests and electronic medical records to automatically generate synoptic or text reports. Developing such a tool that could explicitly identify the most significant parameters for its decisions would directly improve clinical workflow and increase the interpretability of the results at the same time. We encourage the field of CPath to expand its efforts in creating tools for the pre- and post-analytical steps in order to reduce the large proportion of clinical errors attributed to those phases, and suggest some potential applications in Fig. 2.

8.5. Multi domain learning

Despite being particularly well-suited for CPath, multi-domain learning (MDL) is still a relatively unexplored topic. MDL aims to train a unified architecture that can solve many tasks (e.g. lesion classification, tumour grading) for data coming from different domains (e.g. breast, prostate, liver). During inference, the model receives an input image and the corresponding domain indicator and is able to solve the corresponding task for the given domain. There are two reasons that make MDL attractive for CPath. The first is that the additional information from a source domain (coming from a related organ such as the stomach) can be informative for improving performance in the target domain (e.g. colon). By sharing representations between related domains, the model is enabled to generalize to other domains. The second motivation is to alleviate the data sparsity problem where one domain has a limited number of labeled data. Through MDL, the domain with limited data can benefit from the features that are jointly learned with other related tasks/domains.[524,525]

8.6. Federated learning for multi-central CPath

Data-driven models require a large amount of data to yield strong performance. In CPath, this requires incorporating diverse datasets with varying tissue slide preparations, staining quality, and scanners. An obvious solution to train such models is to accumulate the data from multiple medical centers into a centralized repository. However, in practice, data privacy regulations may not permit such data sharing between medical institutions, especially between countries. A possible solution lies in privacy-preserving training algorithms, such as federated learning,[526,527] which can make use of decentralized data from multiple institutions while maintaining data privacy. In federated learning, training starts with a generic machine learning model in a centrally located server. But instead of transferring data to a centralized server for training, copies of the model are sent to individual institutions for training on their local data. The learning updates are encrypted and sent to the central server and then aggregated across the institutions. Ming Lu et al.[447] demonstrated the feasibility and effectiveness of applying federated, attention-based weakly supervised learning for general-purpose classification and survival prediction on WSIs using data from different sites. Using such algorithms for CPath can facilitate cross-institutional collaborations and can be a viable solution for future commercial solutions that need to continuously augment and improve their ML models using decentralized data.

8.7. CPath-specific architecture designs

Many deep learning architectures are not designed for CPath specifically, which raises a serious question about the optimality of using "borrowed" architectures from general computer vision. For instance,[476] notes that traditional CV architectures may not be well suited for CPath due to a large number of parameters that risk overfitting. Additionally, the field of pathology has much domain-specific knowledge that should be taken into account before choosing an ML model. For example, under varying magnifications different morphological patterns are captured, from cellular-level details to tissue architecture features.[328] Naively applying an architecture without considering such details could discard key visual information and lead to deteriorated performance.

Unlike natural images, WSIs exhibit translational, rotational, and reflective symmetry[528] and CNNs for general vision applications do not exploit this symmetry. The conventional approach to overcome this issue is to train the model with augmented rotations and reflections, but this increases training time and does not explicitly restrict CNN kernels to exploit those symmetries. Rotation-equivariant CNNs, which are inherently equivariant to rotations and reflections were introduced for digital pathology,[528] significantly improving over a comparable CNN on slide level classification and tumor localization. Similarly, Lafarge et al.[376] designed a group convolution layer leveraging the rotational symmetry of pathology data to yield superior performance in mitosis detection, nuclei segmentation, and tumor classification tasks. These results motivate the application and further research of rotation-equivariant models for CPath.

In general, we note that the SOTA computer vision architectures used in computational pathology have tended to lag behind those used for natural images by a couple of years. This delay in knowledge propagation from the mainline computer vision research in natural images may be due to the data-centric nature of the CPath field. As data labelling is specialized and expensive to conduct, annotating more data or clever training tweaks to finetune established architectures is more attractive than developing advanced, specialized architectures. However, we recommend that CPath researchers should still use the most powerful relevant models available for the simple reason that they tend to perform best given the computational resources available. While computational efficiency is generally not as important during training, it is imperative at inference time if models are to be run in real-time on medical devices with limited computational resources.

8.8. Digital and computational pathology adoption

Despite the numerous advantages to the clinical workflow and applications offered by using digital pathology and CPath, the adoption of digital pathology remains the first barrier to clinical use. A major reason for adoption hesitancy is the common opinion that digital slide analysis is an unnecessary step in a pathologist's workflow which has been refined over decades to produce reproducible and robust diagnoses without digitization.[9,18–20] In terms of clinical efficiency, studies have shown mixed results, with two finding that digitization actually decreased

efficiency (by increasing turnaround time by 19%).[529,530] However, another study demonstrated a clear increase in productivity and reduction of turnaround-time.[24] One of the co-authors (B.N.) has implemented digital pathology at a public tertiary institution, which began as a pilot study over three years including three experienced academic pathologists and showed that digitization reduced turnaround time by 18% for biopsies and 25% for resections, and increased case output by 17%. These trial results led to all pathologists not retiring within two years to transition to a digital pathology workflow in 2019. Due to the varied nature of results and outcomes in studies analyzing the effectiveness of digital pathology there is more work to be done to have a multi-institution and lab analysis for more general and concrete results.

A major factor in the adoption of digital or computational pathology practices is the source of funding and the pay structure of pathologists. A few cost-analysis studies show that the transition to digital pathology becomes financially advantageous in 2 years, with savings projected to be up to $5M after 5 years in a sizeable tertiary center.[9,531–533] The financial impact will also be viewed differently in public vs private healthcare settings. Public healthcare is primarily limited by funding and universal access to healthcare whereas for private lab networks improvements in processes and services are directly linked to the prospects of obtaining additional contracts and increased profitability. However, studies considering multiple institutions and funding settings are still required to fully characterize the financial impact compared to clinical benefit. Additionally, on an individual pathologist level, compensation structures can affect buy in for implementation. For example, at our co-authors' B.N. and V.Q.T institution, a fee-for-service structure is used to compensate pathologists thus an increase in throughput and productivity has a direct correlation to increased pay. We propose that this fee-for-service model contributes to the widespread embracement of DP at this institution. In contrast, pathologists in a salary-based environment are paid based based on a combined package of services which includes diagnostics, research, teaching, administration, quality control, etc. An increase in clinical productivity would technically not benefit them directly, as it would translate to a high number of rendered diagnostics over the same amount of time.

Integration CPath into the clinical workflow is relatively understudied as few papers have actually deployed, or performed clinical validation of their results. Works in this area have either proposed methods to deploy their models in the clinic or developed tools to enable the use of their research in the clinic.[287,490,534] However, as a primary goal of CPath is the use of CAD tools in clinical settings, more works should consider how to integrate models and tools into the clinical workflow, especially in conjunction with expert clinicians.

8.9. Institutional challenges

Several institutional challenges may affect the implementation of CPath tools, and similar challenges in implementing digital pathology workflows at medical institutions have been well-described by many studies.[535–539] As noted by multiple studies considering the digital transition of pathology laboratories,[535–539] the importance of a common shared goal and frequent communication between the involved parties is necessary to successfully deploy a digital system. These lessons are likely extendable in the context of CPath and CAD development as well. Specifically, Cheng et al.[538] reported on their experiences and lessons learned as a 7-point-based system to efficiently deploy a digital pathology system in a large academic center. We believe similar systematic approaches will need to be developed to implement CPath applications in a clinical setting.

Another institutional challenge concerns the regulatory oversight at the departmental, institutional, accrediting agencies, pathology association, state/provincial, and federal levels. Regulatory measures underlying WSI scanners are well established, as well as the technical and clinical validation of their use.[540–542] On the other hand, patient confidentiality, ethics, medical data storage regulations, and data encryption laws are equally, if not more, time-consuming and intensive to comply with. These issues can be mitigated by deploying a standardized digital pathology system throughout multiple institutions at the state/provincial level. For example, our co-author (B.N.) has obtained governmental approval and funding to distribute a set of digital pathology systems throughout the province's public anatomical pathology laboratories. Similarly, a unified set of standards for processing and digitizing slides, along with unifying storage and access to WSIs for research use in collaborative efforts is paramount in moving forward in both the development and implementation of CAD systems.

8.10. Clinical alignment of CPath tasks

Researchers in the CPath field must ensure that the CAD tools they create are clinically relevant and applicable to pathology so that effort and resources are not allocated towards extraneous or clinically irrelevant tasks. For example, certain CADs have been proposed to facilitate case triaging and reduce turnaround time for critical diagnoses.[72–74,543,544] However, several regulatory agencies in pathology aim for 90% of cases to be completed within a timeframe of 72 hours for signing-out resection specimens and up to 48 hours for biopsies.[545,546] In this context, triaging becomes extraneous, as signing out cases faster than 48-72 hours has no clinical impact. However, in the context of an institution operating at longer turnaround times or struggling to keep up with the caseload, this method could be lifesaving. Alternatively, identifying mitotic figures and counting positive Ki-67 nuclei are appreciated tools already in use in multiple digital pathology settings, despite these tools being seldom applied to the large caseload proportion of most practicing pathologists.

As noted previously, the overall number of pathologists in the USA has decreased 17% from 2007 to 2017 and caseloads have increased by 41.7%.[547] This trend places further emphasis of developing CAD tools towards specific challenges encountered by pathologists and where subspecialists may not be readily available. For example, a large consortium generated a prostate cancer CAD that achieved a 86.8% concordance with expert genitourinary pathologists,[548] a significant breakthrough for healthcare settings where prostate biopsies are not signed out by subspecialists. Additionally, targeting specific diagnoses with high rates of medical errors and inter-observer variance, notably in dermatological, gynecological, and gastrointestinal pathology, should be prioritized and integrated into practice quickly to support patient care.[549] Finally, advanced CAD tools capable of diagnosing features out of reach by conventional pathology could have a great impact. For example, identifying the origin of metastases from morphological cues on the WSIs without added IHC[448] or CADs capable of calculating the exact involvement of cancer on a biopsy core for prognostic purposes.[548]

8.11. Concluding remarks

Bringing pathologists and computer scientists together and initiating meaningful collaborations with shared gains between all parties is likely the most efficient path forward for CPath and CAD integration. Opportunities to facilitate collaborations should be promoted by parties such as the Pathology Innovation Collaborative Community and the Digital Pathology Association. Furthermore, we encourage involved pathologists and computer scientists to communicate and collaborate on studies towards the common goal of providing patients with fast, reproducible, and high-quality care.

Declaration of competing interest

The authors declare that they have no known competing financial interests or personal relationships that could have appeared to influence the work reported in this paper.

Acknowledgment

Authors would like to thank Huron Digital Pathology for providing support and insightful discussions related to digital pathology hardware infrastructures. Authors would like to also thank Xin Zhao, Koosha E. Khorasani, Mona Sharifi, Kiana Abtahi, Alejandra Zambrano Luna, Cassandre Notton, Tomas Pereira, and Amirhossein Mohammadi for their help in initial preparation of our model-cards. This work was partly supported from NSERC-CRD (CRDPJ515553-17) funding grant and MITACS-Elevate award (Ref. IT14369).

Appendix

A.1. Clinical pathology workflow

Sample Collection Tissue samples are categorized into two general types a) *small specimens*, normally obtained to diagnose disease and guide subsequent treatment and b) *large specimens*, surgically removed to treat the disease after diagnosis. *Small specimen* biopsies are performed by different specialties in different settings, which can vary from family doctors sampling skin lesions to head and neck specialists performing panendoscopic biopsies under anesthesia. Based on the type of sample required and its originating site, small specimen samples are obtained by different methods: 1) core biopsies, 2) cytological specimens, 3) small excisions, and 4) pincer biopsies. In contrast, *large specimens* are mostly resections performed by surgeons for treatment purposes once the diagnosis has already been obtained. Large specimens are significantly more complex than small specimens and require a high-level of expertise to process before reaching the microscopic interpretation step.

Accessioning The patient-care team fills out request forms which are tagged to the pathology specimen and sent along with the sample to the pathology department to enter the specimen and patient information into the laboratory information system (LIS). Depending on the institution, the LIS can then be linked to the electronic medical records (EMR) system to populate basic demographic data, and to a slide tracking system (STS) to locate and time each event in pathology. Ensuring that accessioning is done correctly is essential, as specimen mix-ups or incorrect data entry from request forms are a large source of errors in the worfklow.[512]

Specimen Preparation Most samples arrive at the pathology lab having already been preserved in a 4% formalin solution. Other preservation media are used for specific pathology objectives; notably using Roswell Park Memorial Institute medium (RPMI) to preserve cells for flow cytometry and glutaraldehyde preservation for electronic microscopy.[550] Sometimes, the samples are sent to the pathology lab without a preservation medium, and in this "fresh" state the tissue will undergo cold ischemia changes until the pathologist can assess the sample, perform specimen preparation, and fix the tissue in the preservation media. Indeed, each of these events has an impact on the quality of the tissue, which in turn significantly affects the quality of the final WSI. Specifically, large specimens are almost always processed by a pathologist who will open the container, take basic measurements, and open the organ to ensure uniform formalin penetration.

At some medical centers, intra-operative consultations for resection samples are processed in a frozen section procedure, which allows for more rapid diagnosis of the tissue specimens while trading off diagnostic accuracy when compared to fixation in formalin.[551,552] Frozen section samples will be rapidly frozen after the proceeding *grossing* step, therefore they arrive in the lab unprocessed and remain unprocessed until after grossing, undergoing the aforementioned cold ischemia changes in the meantime.

Grossing Once the basic specimen preparation has occurred, the tissue is analyzed by the pathology team without the use of a microscope; a step called grossing. Smaller specimens are often grossed by technicians who fill out a template-based description notably highlighting the number, size, and appearance of the fragments. After grossing, the tissue fragments are placed into tissue cassettes for final fixation. Grossing larger specimens is much more complex, and is usually performed by pathologists, pathologist-assistants, medical residents, or fellows who have undergone extensive training. The grossing starts by orienting the specimen according to the surgical procedure. By cross-referencing the clinical findings and the EMR reports, the operator will localize the disease, locate the pathological landmarks, describe these landmarks, and measure the extent of the disease. Specific sampling of these landmarks is performed, and these samples are then put into cassettes for the final fixation.

Final Tissue and Slide Preparation For non-frozen section samples, the final fixation step will accrue all the samples put into cassettes and will add a last phase of fixation in formalin. Afterwards, the tissue cassettes are removed from formalin and inserted into a tissue processor which dehydrates the tissue through alcohol gradients, subsequently replacing the liquid with melted paraffin wax. These samples are removed from the tissue processor and placed into a mold filled with paraffin which solidifies into a block. A technician then cuts the blocks with a microtome into $4\mu m$ slices and places them onto positively charged slides. Slides are then deparaffinized, rehydrated by an inverse alcohol gradient, and stained with pigments such as Hematoxylin and Eosin (H&E), or further processed for ancillary testing by immunohistochemistry. Once these steps are complete, the tissue is dehydrated, cleared, and mounted with a coverslip. Note that significant variations will affect the final quality of the slides based on the performance of the prior steps, the experience of the technician who cut the slides, and batch effects from the reagents which are often reused for multiple slides prior to being replaced–known as cross-contamination.

Frozen section samples are rapidly frozen using a freezing medium such as liquid nitrogen, dry ice, or isopentane.[174,175,551,552] After freezing, the tissue is cut using a microtome and fixed immediately, most often with formalin.[174,175] Slides are then stained and covered with a glass coverslip and stored at 80°C.[175]

Slide Scanning and Image Processing The stained slides are cleaned of excess mounting media and scanned with a whole-slide scanner. They are then loaded onto the image management software, which has previously been linked to the LIS and the STS.[553]

Interpretation After a slide is processed and prepared, a pathologist views the slide to analyze and interpret the sample. The approach to interpretation varies depending on the specimen type. Interpretation of smaller specimens is focused on diagnosis of any disease. Analysis is performed in a decision-tree style approach to add diagnosis-specific parameters, e.g. esophagus biopsy → type of sampled mucosa → presence of folveolar-type mucosa → identify Barrett's metaplasia → identify degree of dysplasia. Once the main diagnosis has been identified and characterized, the pathologist sweeps the remaining tissue for secondary diagnoses which can also be characterized depending on their nature. Larger specimens are more complex and focus on the focus is on characterizing the tissue and identifying unexpected diagnoses beyond the prior diagnosis from a small specimen biopsy. Microscopic interpretation of large specimens is highly dependent on the quality of the grossing and the appropriate detection and sampling of landmarks. Each landmark (e.g., tumor surface, tumor at deepest point, surgical margins, lymph node in mesenteric fat) is characterized either according to guidelines, if available, or according to the pathologists' judgment. After the initial microscopic interpretation additional deeper cuts ("levels"), special stains, immunohistochemistry, and/or molecular testing may be performed to hone the diagnosis by generating new material or slides from the original tissue block.

Pathology Report The pathologist synthesizes a diagnosis by aggregating their findings from grossing and microscopic examination in combination with the patient's clinical information, all of which are included in a final pathology report. The classic sections of a pathology report are patient information, a list of specimens included, clinical findings, grossing report, microscopic description, final diagnosis, and comment. The length and degree of complexity of

the report again depends on the specimen type. Small specimen reports are often succinct, clearly and unambiguously listing relevant findings which guide treatment and follow-up. Large specimen reports depend on the disease, for example, in cancer resection specimens the grossing landmarks are specifically targeted at elements that will guide subsequent treatment.

In the past, pathology reports had no standardized format, usually taking a narrative-free text form. Free text reports can omit necessary data, include irrelevant information, and contain inconsistent descriptions.[69] To combat this, synoptic reporting was introduced to provide a structured and standardized reporting format specific to each organ and cancer of interest.[69,70] Over the last 15 years, synoptic reporting has enabled pathologists to communicate information to surgeons, oncologists, patients, and researchers in a consistent manner across institutions and even countries. The College of American Pathologists (CAP) and the International Collaboration on Cancer Reporting (ICCR) are the two major institutions publishing synoptic reporting protocols. The parameters included in these protocols are determined and updated by CAP and ICCR respectively to remain up-to-date and relevant for diagnosis of each cancer type. For the field of computational pathology, synoptic reporting provides a significant advantage in dataset and model creation, as a pre-normalized set of labels exist across a variety of cases and slides in the form of the synoptic parameters filled out in each report. Additionally, suggestion or prediction of synoptic report values are a possible CPath application area.

A.2. Diagnostic tasks

Here we provide some examples of diagnostic tasks where CPath has been applied, for the reader to understand the variety of diagnostic problems that CPath can be used to address.

Detection A machine learning framework for detecting cancerous tissue regions and predicting scan-level diagnosis is proposed in,[266] wherein thresholding and statistical analysis used to abstain from making a decision in uncertain cases.In contrast to directly predicting the presence of cancers, feature-focused detection tasks can be highly useful in patient diagnosis and treatment planning. For example, identifying microsatellite instability is a crucial factor in determining if immunotherapy will be effective on a patient, and deep learning methods were shown to be effective at detecting microsatellite instability in.[287] Similarly, the detection of fibrous regions in liver WSIs is a precursor step to liver tumor classification and a computational approach to detection was demonstrated in.[554] Furthermore, the first automatic detection algorithm for keratin pearls, which are valuable biomarkers for oral squamous cell carcinoma grading is presented in.[364] Future research into automated detection methods for similar cancer biomarkers could be a valuable step towards developing AI-based pathologist support tools. As an example, lymphocytes, a type of white blood cell, can be detected and quantified to assess the overall health of the immune system. However, manually detecting these cells is a time-consuming task and pathologists rarely identify and count lymphocytes. Thus several computational approaches, including open source tools such as QuPath[555] and deep learning based approaches, are used to provide lymphocyte counts to pathologists.[205] Likewise, counting nuclei can contribute towards diagnoses, however, nuclei detection is a difficult task because of the large variations in the shape of different types of nuclei, such as nuclear clutter, heterogeneous chromatin distribution, and irregular and fuzzy boundaries. Addressing these issues, for example, spatially constrained context-aware correlation filters with hierarchical deep features extracted from multiple layers of a pre-trained network were proposed to accurately detect nuclei in.[385]

Tissue Subtype Classification Deep neural networks have been shown to be effective at extracting molecular tumor features from histopathology images, opening new avenues for deep learning applications in computational pathology.[556] As an extension of the tissue subtype classification task, ML models are often able to identify important correlations between tissue structures and disease. Work on nuclei classification suggests that features regarding the nuclear inner texture are most relevant for high classification accuracy.[554] Additionally, a classifier discovered unique chromatin patterns associated with specific types of thyroid follicular lesions in.[557] The potential discovery of similar associations makes tissue subtype classification a relevant task to pursue. Another work presented a computational pathology framework that can localize well-known morphological features on WSIs without the need for spatial labels for each feature using attention-based multiple-instance learning on WSI classification.[64] This method outperforms standard weakly-supervised classification algorithms and is adaptable to independent test cohorts, biopsy/resection samples, and varying tissue content. Additionally, the co-representation learning for classification (CoReL) framework is proposed in[379] to improve state-of-the-art classification performance for nuclei classification, mitosis detection, and tissue type classification with less data.[379]

Disease Diagnosis As stated in 2, disease diagnosis can be considered a fine-grained classification problem which subdivides the general positive disease class into finer disease-specific labels based on the organ and patient context. Under this paradigm, research tends to be focused on maximizing performance for reliable clinical applications.[415,490,558] Recently, works have begun implementing different emulations of pathologist behaviour in their proposed models. For instance, multi-scale receptive fields were proposed for use in networks to simulate the pathologist viewing process of slides at varying zoom levels.[328] Alternatively, weighted slide-level features were used to classify Barett's esophagus and esophageal adenocarcinoma, similar to a pathologist assessing the overall impact of various cancer biomarkers.[288] To emulate how pathologists isolate and focus on salient regions of the slide, the concept of visual attention can be applied to identify the most important regions of tissue slides, thus ignoring diagnostically-irrelevant image regions.[417,422,437] Such methods indicate a positive step towards the clinical implementation of AI-based CAD tools by reinforcing and emulating tested methodologies in pathology. Further, differential diagnoses in complicated cases of metastatic tumors and cancer of unknown primary (CUPs) can require many clinical tests to narrow a differential diagnosis, and a method called Tumor Origin Assessment via Deep Learning (TOAD) is introduced as an assistive tool to assign a differential diagnosis.[302] This work uses digitized H&E slides of tumors with known primary origins to train a model with transfer learning and weakly supervised multitask learning to simultaneously identify the tumorous or metastatic regions and predicts the site of origin.

Segmentation Segmentation CAD tools can capture characteristics of individual glands, nuclei, and tumor regions. The wide generalizability of this task to various disease types makes it a particularly suitable tool for computational pathology, on which many studies have been conducted.[277,330–332,350] For example, models that use segmentation to determine nuclear characteristics including size and shape can help pathologists distinguish between various cell types and consequently, disease severity.[207,234] In,[349] a generalized deep learning-based framework was proposed which uses a sequence of novel techniques forin the preprocessing, training, and inference steps which in conjunction improve the efficiency and the generalizability of model. Similarly, a new framework for WSI analysis in colonoscopy pathology, including lesion segmentation and tissue diagnosis was developed and includes an improved U-Net with a VGG net as the backbone, as well as two training and inference schemes to address the challenge of high resolution images analysis.[304]

There are also some instances of segmentation in different organs. For example, an interactive segmentation model was proposed in which the user-provided squiggles guide the model toward semantic segmentation of tissue regions.[367] Also, they proposed four novel techniques to automatically extract minimalistic and human-drawn-like guiding signals from Ground Truth (GT) masks so that they can be used during the model's training. Similarly for the

eye, macular edema (ME) is a common disease where analyzing the fluid lesions is a critical stage of the diagnostic process. The optical coherence tomography (OCT) technique can potentially investigate three fluid types and a novel pipeline for segmentation of the three types of fluid lesions in OCT was proposed in.[355] They presented a multi-layer segmentation to detect the ROI and presented an FCN architecture with attention gate (AG) and spatial pyramid pooling (SPP) module to improve the feature extraction. To predict cellular composition from images, ALBRT is proposed in,[470] using contrastive learning to learn a compressed and rotation-invariant feature representation which first detects the presence of different cell types in an image patch and then provides cell counts for each type. Another novel deep learning model was developed for simultaneous nuclei instance segmentation in.[369] The model is based on an encoder-decoder architecture design that performs nuclei segmentation by predicting the distance of pixels from their nuclei centers along with the nuclei probability masks and predicts nuclei classes when nuclei type annotations are available. Another work in nuclei segmentation is the hard-boundary attention network (HBANet), which identifies hard-boundaries between nuclei, a difficult problem due to overlapped nuclei.[559] It presents a background weaken module (BWM) to improve the model's attention to the foreground, and integrates low-level features containing more detailed information into deeper feature layers. Furthermore, a gradient-based boundary adaptive strategy (GS) is designed to generate boundary-weakened data as extra inputs and train the model in an adversarial manner. Finally, segmentation has also been applied to delineate tumorous tissue regions for a variety of cancer types, such as breast,[278,560] colorectal,[142,363] and prostate cancer.[476,561] Such works assist in the efficient isolation of tumor tissue, which is a crucial task for making accurate disease predictions.

A.3. Prognosis

Prognostic models must predict the likely development of a disease based on patient features. For instance, a prognostic model was developed by adjusting a tumor microenvironment-based spatial map with clinical variables such as patient age, gender, health history, and cancer stage.[534] This multi-domain data analysis approach is advanced by another work, which uses both histopathological image data and cancer genomic data in their novel deep learning framework.[477,562] In,[563] the authors discussed the correlation between platelets and other haematological measures to cancer by assessing patient status and considering the patient features in the primary care dataset, such as age and sex. They demonstrate the model performance with the plot of survival analysis per age group for platelets. Experiments on the publicly available TCGA data demonstrates that prognostic accuracy was maximized when both forms of data were simultaneously considered. Merging information from multiple WSIs of a patient allowed a hybrid aggregation network (HANet), consisting of a self-aggregation module and a WSI-aggregation module, to predict survival risks.[564]

A.4. Prediction of treatment response

Oral epithelial dysplasia (OED) segmentation is critical for early identification and effective treatment and HoVer-Net+ is a model to simultaneously perform nuclear instance segmentation (and classification) and semantic segmentation of epithelial layers based on H&E stained histopathology slides of the oral mucosa.[365] This model achieves the state-of-the-art performance in both tasks (0.839 dice score) and is the first method for simultaneous nuclear instance segmentation and semantic tissue segmentation.

A.5. Cancer statistics

Cancer remains the leading cause of global mortality in 2020, claiming nearly 10 million lives or approximately 1 in 6 deaths.[583] The grey circle in Fig. 12 illustrates the prominence of Breast, Prostate, Colon, and Rectum, as well as Lung cancers, which collectively account for half of all diagnosed cases. The mounting volume of pathology cases poses a significant challenge in clinical workflows. This underscores the pivotal role of computational pathology in streamlining processes, aiding pathologists in coping with overwhelming workloads. Notably, certain cancers not only exhibit high prevalence but also contribute substantially to the overall mortality rates. Lung cancer, for instance, represents approximately 12% of cancer cases in the United States, with its prognosis falling within the lowest range, as depicted in Fig. 12 (030%). Computational pathology proves instrumental, particularly in lung cancer, by facilitating classification and prognosis tasks due to distinct variations among its types in terms of presentation, prognosis, and treatment strategies. Conversely, there are less prevalent cancers like liver cancer characterized by poor prognoses. CPath's ability to compile specialized datasets for such cancers not only aids pathologists but also supports clinicians in devising personalized treatment plans. Understanding disease statistics and severity is paramount when designing a Computer-Aided Diagnosis (CAD) tool in Computational Pathology (CPath) or curating datasets. By factoring in disease prevalence, mortality rates, and severity across various cancer types, CAD tools can be optimized to prioritize detection, prognosis, and treatment planning for the most prevalent and severe cases, aligning computational pathology advancements with the urgent needs of patients and healthcare practitioners.

A.6. Whole slide imaging

Generally, a WSI scanning device is composed of four major components[180]: (1) a light source; (2) a slide stage; (3) an objective lens; and (4) a digital camera. In order to produce a WSI that is in focus, which is especially important for CPath works, appropriate focal points must be chosen across the slide either using a depth map or by selecting arbitrarily spaced tiles in a subset.[187] Once focal points are chosen, the image is scanned by capturing tiles or linear scans of the image, these individual components are then stitched together to form the full image known as the big flat TIFF image.[180,187] To reduce the area needed to be scanned, a segmentation algorithm can be used within the scanner to separate tissue regions from extraneous background regions.[198] Additionally, slide can also be scanned at various magnification levels depending on the downstream task and analysis required. The vast majority of WSIs are scanned at $20\times$ ($\sim 0.5\mu m$/pixel) or $40\times$ ($\sim 0.25\mu m$/pixel) magnification as these are the most useful in practice for general pathologist.[180]

WSI Storage and Standards

WSIs are in giga-pixel dimension format.[30,188] For instance a tissue in $1cm \times 1cm$ size scanned @$0.25\mu m$/pixel resolution can produce a 4.8GB image (uncompressed) with a $50,000 \times 50,000$ pixels. Due to this large size, hardware constraints may not support viewing entire WSIs at full resolution.[189] Therefore, WSIs are most often stored in a tiled format, so that only the viewed portion of the image (tile) is loaded into memory and rendered.[189]

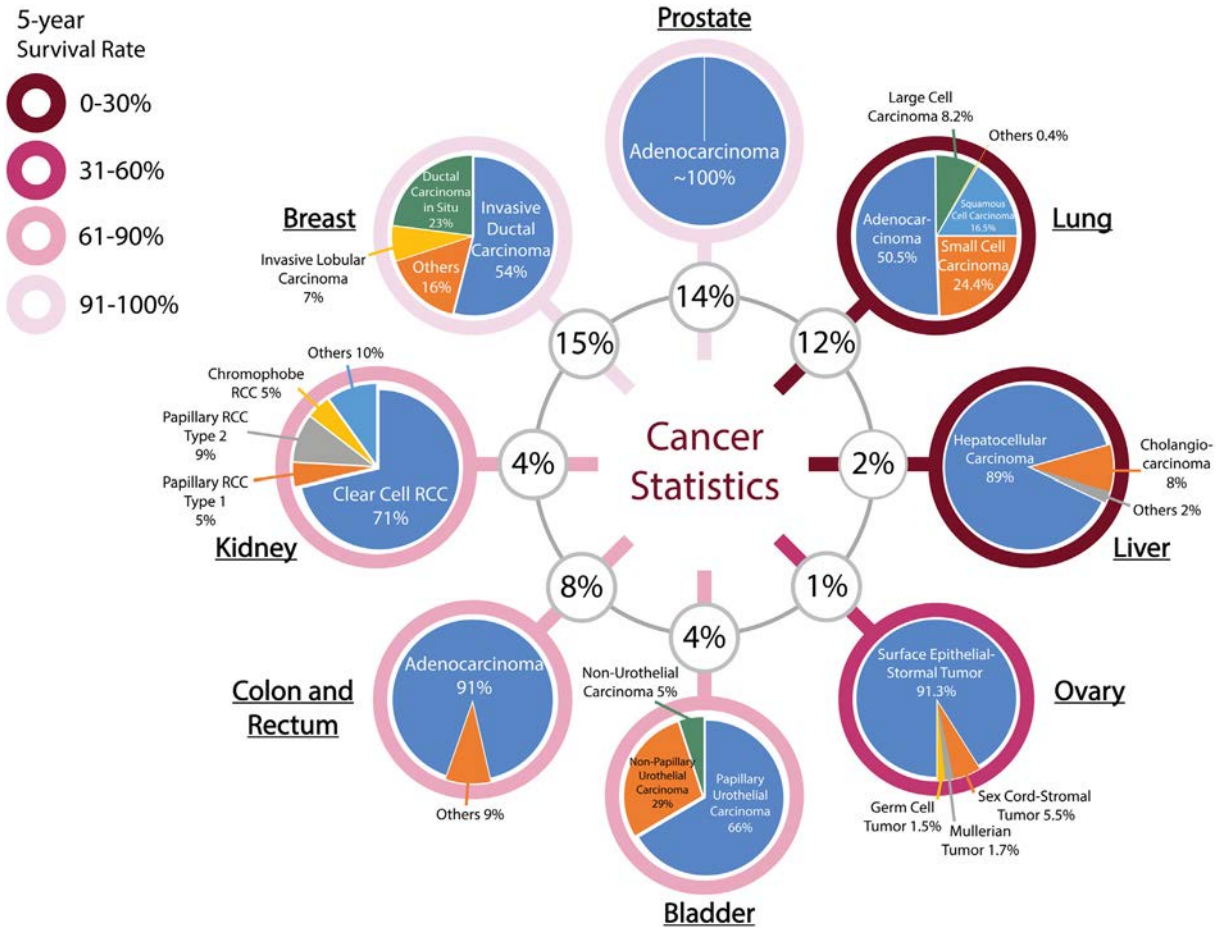

Fig. 12. Demonstration of the cancer statistics, featuring both the 5-Year Survival Rate and Incidence of each cancer in addition to incidence percentage of each subtype. The grey inner circle shows the incidence percentage of the respective cancer. The colored circle around each cancer corresponds to the respective 5-Year Survival Rate bin, showcasing the severity of the cancer. Darker shades (lower survival rate) means fewer people will survive the cancer after 5 years period and the cancer has poor prognosis. On the other hand, lighter shades (higher survival rates) mean more people will survive after 5 years and the cancer has good prognosis.[98,565–582]

Table 1
The following table lists commercially available WSI Scanners grouped by manufacturing company and their respective available compression slide formats.

Company: Scanner Model (Slide Format)
Leica Biosystems: Aperio AT2 / CS2 / GT450 (TIFF (SVS))
Hamamatsu: Nanozoomer SQ / S60 / S360 / S210 (JPEG)
F. Hoffmann-La Roche AG: Ventana DP200 / iScan HT / iScan Coreo (BIF, TIFF, JPG2000, DICOM)
Huron Digital Pathology: TissueScope IQ / LE / LE120 (BigTIFF, DICOM compliant)
Philips: Ultra-Fast Scanner(iSyntax Philips proprietary file)
3DHistech: Pannoramic Series (MRXS, JPG, JPG2000)
Mikroscan Technologies: SL5 (TIFF)
Olympus: SL5 (JPEG, vsi, TIFF)
Somagen Diagnostics: Sakura VisionTek (BigTIFF, TIFF, JPG2000)
Akoya Biosciences: Vectra Polaris (JPEG, single-layer TIFF, BMP, or PNG)
Meyer Instruments: EASYSCAN PRO 6 (SVS, MDS, JPEG, JPEG2000)
Kfbio: KF-PRO (JPEG, JPEG2000, BMP, TIFF)
Motic: EasyScan Pro (JPEG, JPEG2000, Aperio Compatible)
Precipoint: PreciPoint O8 (GTIF)
Zeiss: Zeiss Axio (Not specified)
Objective Imaging: Glissando (SVS, BigTIFF)
Microvisioneer: manualWSI (Not specified)

Additionally, to support efficient zooming, WSIs are stored in a pyramidal structure, where higher levels of the pyramid represent lower magnification levels. The highest level of the pyramid is generally a very low resolution thumbnail snapshot of the WSI, while the lowest is the full resolution image (i.e. big-flat TIFF). In this way, different zoom levels can be captured and displayed in a WSI format efficiently–artificially replicating different zooming levels from optical microscopy.[189,193] Additionally, WSIs can be compressed before storage to reduce their filesize, often using JPEG, JPEG 2000, or LZW algorithms, which can reduce an image size by more than seven times.[180] Alongside the WSI, metadata regarding patient, tissue specimen, scanner, and WSI information is stored for reference.[30,188,190] Due to their clinical use and importance, it is important to develop effective storage solutions for these WSI data files and metadata, allowing for robust data management, querying of WSIs, and efficient data retrieval.[191,192]

To develop CPath CAD tools in a widespread and general manner, a standardized format for WSIs and their corresponding metadata is essential.[188] However, there is a general lack of standardization for WSI formats outputted by various scanners, as shown in Table 1, especially regarding metadata storage. The Digital Imaging and Communications in Medicine (DICOM) standard provides a framework for biomedical image format and data management and has been extended to the CPath field through Supplement 145.[190,193] Some research has shown that the use of the DICOM standard allows for efficient data access and greater interoperability between different centres and different CPath-related devices.[188] However there is currently a lack of widespread adoption,[30,188,190,584] reflected in Table 1 where only two recorded scanners are DICOM-compliant. Notably, with regards to metadata, DICOM provides a systematic format detailing a variety of relevant medical information, consistent with DICOM standards in other medical imaging fields.[190] The expansion through Supplement 145 also adds pyramid-tiling for WSIs, a format that is directly beneficial to creation of CPath and CAD tools. While many scanners have adopted the pyramid-type scheme for image data, they have not fully adopted the DICOM image format, outputting in either TIFF, BigTIFF format, or in TIFF-derivatives such as SVS or GTIFF. While the TIFF format allows for semi-structured metadata,[189] the consistency in metadata structure offered by DICOM is an advantage over the former.[190]

Apart from storage format, a general system for storing and distributing WSIs is also an important pillar for CPath. Whereas in other medical imaging fields such as radiology, images are often stored in a picture archiving and communications systems (PACS) in a standardized DICOM format, with DICOM storage and retrieval protocols,[189] the need for standardization persists in pathology for WSI storage solutions. Few works have proposed solutions to incorporate DICOM-based WSIs in a PACS, although some research has successfully implemented a WSI PACS consistent using the DICOM standard using a web-based service for viewing and image querying.[189]

A.7. Organs and diseases

The following Appendix section is a supplement to Section 2.5. Details are provided for several notable works in CPath for the organ types listed in the subsection.

Breast

- A subset of breast-focused research studies the correlation between tissue morphology and molecular differences. Molecular testing can often be preferred over tissue morphology assessments when selecting breast cancer treatments as it provides objective and reproducible disease classifications. For instance, the connection between epithelial patterns with various molecular predictions and heatmaps was used to clearly visualize this correlation in.[429]
- In[342] a proposed U-NET based architecture called piNET is used for cell detection and classification in order to calculate the proliferation index (PI) of the Ki67 biomarker. The network classifies cells as Ki67 + /Ki67- and uses this classification to calculate the PI. The architecture is able to achieve a PI accuracy of 85.2%, higher than the accuracies of other models.[342]
- A two-stage CNN, one for patch-level feature extraction and the other for classification, was proposed and achieved 95% accuracy for classifying normal, benign, in situ carcinoma, and invasive carcinomas.[585]
- In,[586] several well-known models (DenseNet121, ResNet50, VGG16, and Xception), are compared with their own CNN model named lightweight convolutional neural network (LCNN) for the detection of breast cancer metastasis to axillary lymph nodes (ALN).
- Further research has proposed an automated patient-level tumor segmentation and classification system that takes full use of diagnosis information hints from pathologists.[366] A multi-level view DeepLabV3 + (MLV-DeepLabV3 +) was created to investigate the differentiating aspects of cell characteristics between tumor and normal tissue for tumor segmentation. Furthermore, expert segmentation models were chosen and merged using Pareto-front optimization to mimic expert consultation and provide a flawless diagnosis.

Prostate

- Most works focus on prostate aim to classify cancer based on Gleason scoring. To aid in that effort, a U-Net model for object semantic segmentation is created in,[347] with the goal of precisely labeling each pixel in an image as belonging to either foregrounds, which may contain glands, or background.
- A method is proposed in[382] that trains a model on both epithelial cell detection and Gleason grade prediction tasks to achieve better performance in both tasks than models trained on either of the tasks alone. Further, some works have investigated epithelial cell detection to explore data augmentation and stain/color normalization techniques[199,204] which demonstrates the importance of epithelial cell features as an indicator for prostate cancer detection.
- Work in[587] focused on classifying glands, gland boundary regions, and stroma. The authors opted for two classic classifiers: support vector machines (SVM) and Convolutional Neural Networks (CNNs), finding the SVM to perform best by offering high accuracy and good indicators of regions which are present with high probability. The output of the SVM classifier could help pathologists locate existing glands, saving them a significant amount of time from actively searching for them.

Lung

- To further aid diagnosis, prognosis, and treatment decisions, a novel method for nuclei detection and characterization is introduced in[234] using an unsupervised autoencoder network to learn without the use of any annotations. The unsupervised autoencoder is used to construct a CNN that only requires 5% of training data to generate comparable results to the SOTA on supervised lymphocyte and nuclei tasks, thereby reducing the need for extremely large annotated datasets.
- In,[491] the work not only classifies adenocarcinoma and squamous cell carcinoma, but also predicts the 10 most commonly mutated genes in adenocarcinoma. The findings indicate the presence of genotype-phenotype correlations for lung cancer tissues, and paves the way for cancer classification and mutation predictions of other types of less common lung cancers.

Colon and Rectum

- An interesting detection application for MSI is implemented in.[287] In this work, ResNet-18 is used to predict MSI from H&E slides with an AUC of 0.84, although performance was reduced with tissue samples from different ethnicities. As MSI requires extensive additional testing which is not always performed,[287] the study highlights the applicability of deep learning in detecting this important prognosis indicator.
- The work in[428] presents a weakly-supervised model named the Slide Level Annotation Model (SLAM) based on ShuffleNet[588] that can be trained to detect genetic/molecular changes, including MSI or BRAF mutation, in colorectal WSIs. The results show improvement over SOTA models, and a visualization heatmap is generated which allow for improved result interpretability and analysis.

Bladder

- In,[415] bladder cancer grade classification is explored using a large dataset of 915 WSIs which ends up outperforming 17 pathologists by an average of 10%. The model in this study has been integrated into an end-to-end diagnostic tool that provides interpretable cellular-level ROI visualization and natural language descriptions of histology slides. However, there was also a diagnostic disagreement of 23% between the system and pathologists, which could hinder the diagnostic process and consequently limit the overall productivity.

Kidney

- For effective patient prognosis, tissue microarray analysis is typically used to identify biomarkers. Currently, this process is time-consuming and prone to error, especially due to the heterogeneity of nuclei. A random forest classifier was proposed to more efficiently detect cancerous nuclei in MIB-1 stained tissue micro-array spots and predict the survival rate for renal cell carcinoma (RCC) patients in.[381] The results show that there is a significant difference in survival times for patients with high and low proliferating tumors, and further state MIB-1 staining as a key prognostic factor for the survival chance of RCC.
- To aid in determing donor organ acceptance in kidney transplants,[84] uses frozen kidney sections as input data to identify the percentage of glomerulosclerosis.

Brain

- The achieved state-of-the-art SOTA classification accuracy on the 2014 MICCAI Grand Challenge dataset was achieved in.[76] However, on completely unseen datasets, performance varied from 84% to 93%. This shows the complexity of the diseases; low grade glioma (LGG) versus glioblastoma multiforme (GBM) classification is not a trivial task. Not only do their appearances vary in pathological samples, the diagnosis is often made from a few distinct features in a small slide region.[76]

Liver

- A notable work for liver cancer classification evaluates a pathologist's performance using a liver cancer diagnostic tool for the diagnosis of HCC and cholangiocarcinoma.[490] Despite lower performance than pathologists, the tool's decisions directly affected pathologists' decisions. Correct model predictions increased pathologists' average accuracy, while incorrect predictions lowered average accuracy. Furthermore, pathologists frequently consulted the model's predictions for difficult cases. This confirms the potential use of deep learning models as an AI diagnostic tool to provide knowledgeable second opinions.

Lymph Nodes

- One of the earliest histopathology challenges, ICPR2010, targets lymphocyte and centroblast counting.[589]
- The importance of the lymph nodes in cancer diagnosis is notably addressed in the CAMELYON16 and CAMELYON17 Challenges, in which participants classify lymph node metastases.[264] Metastases in breast regional lymph nodes are classified based on size: micrometastasis, macrometastasis, and isolated tumour cells (ITCs). The ITC classification accuracy was less than 40% for all top teams. This indicates that there was extreme difficulty in detecting ITCs, most likely due to the small size and variability. These results suggest that further improvements can be made by introducing more true positives of ITC data, or incorporating IHC stain information as an additional layer of information to improve detection robustness.

Organ Agnostic

- Nuclei segmentation of epithelial, inflammatory, fibroblast and miscellaneous tissues is performed across seven different organs in.[277] The method attempts to generalize across a large variety of datasets for increased usability and scalability in a clinical setting.

A.8. Ground truth labelling and annotation

Patient-level Annotation Patient-level annotations assign a single label to a single patient and come from case reports that can address multiple WSIs from a primary organ site. In addition to the WSIs, the Laboratory Information System (LIS) may also contain additional metadata, diagnostic information, and analytical or synoptic report information.[590] Notably, the LIS can store specimen type, molecular and genetic tests, patient medical history, and clinical variables such as the patient's age and gender.[591,592]

Slide-level Annotation Slide-level annotations designate labels for a single WSI, which encompasses diagnosis and cancer information.[268,302] In comparison to the patient-level, this level of focus provides a more precise tissue location for the provided diagnosis.[316,450,593]

ROI-level Annotation ROI-level annotation identifies regions within a slide that can be of either diagnostic or analytical relevance to a pathologist. Regions themselves can be designated using two methods: (1) bounding boxes[169,213,219] or (2) pixel-wise masks that are augmented on the WSIs.[61,220,594]

Importantly, each ROI is considered to be a single class,[595] but the labels represent more detailed tissue structures providing more specific and detailed diagnostic information than patient and slide levels,[64] ultimately being more applicable in disease diagnosis tasks.[365]

Patch-level Annotation Patch-level annotation is done on mosaic tiles (usually in a square shape) extracted from the WSI/ROI with a given field of view (FOV). Most deep-learning models are trained at the patch level, which contains anatomical structures of tissues and cells. Patches are either single-labeled or multi-labeled according to the taxonomical labeling workflow.[380] One key aspect for patch-level annotation is determining the optimum FOV to encompass enough tissue classes,[596] as considering smaller or bigger FOV can provide different advantages, as demonstrated in Fig. 7 for the patch-level.

Patch-Size Selection The choice of the patch size is limited by the computational complexity of the hardware that is used for training CAD tools. For instance, the majority of deep learning pipelines accept image sizes of less than 300×300 pixels.[64,468,597–599,] The size of the FOV needs to be determined such that acceptable levels of morphological tissues will be covered within that patch. Accordingly, the pixel resolution is determined given a certain FOV and patch size. Given the above factors, if a larger FOV is required, then pixel resolution is limited which translates to information loss. In comparison, if higher pixel resolution is required, then the FOV will be limited accordingly which may exclude cellular/architectural relevance pertaining to the underlying class representation.[379] To mitigate this tradeoff, larger image dimensions are required which consequently increases the computational power required for patch processing (e.g. high RAM GPU memory or parallelized multi-GPU processing).[596]

Pixel-level Sizing Pixel-level annotation requires labelling each pixel as a specified class. In this level, features are simple to extract and sufficient for describing the images as they encompass color and texture information.[600] However, there is a lack of biological interpretability as the other levels of annotation more appropriately describe characteristics of the cellular and tissue structures.[269] A solution based on human-interpretable image features can include histological knowledge and expert annotations that can describe different cell anatomies such as the stroma, the nuclei of the cells, and the size and shape of tumor regions, as well as the texture of the tissues and the location of tumor-infiltrating lymphocytes.[601]

Table 2
Commercially available annotation software along with their manufacturing company and available input slide formats.

Company: Annotation Tool (Input Format)
Leica Biosystems: Aperio eSlide Manage (JFIF, JPEG2000, PMM)
Pathcore: Sedeen Viewer (Aperio SVS, Leica SVN, TIFF, JPEG2000)
Indica: Halo (TIFF/SVS)
Objective Pathology: MyObjective (Scanner-wide compatibility)
ASAP: ASAP (Multiple formats through OpenSlide)
SiliconLotus: SiliconLotus (Not specified)
Augmentiqs: Annotation Software Suite (Not specified)
QuPath: QuPath (Multiple formats, Bio-formats and OpenSlide)
Proscia: Concentriq (Not specified)
Visiopharm A/S: VisioPharm (Not specified)
Hamamatsu: NDP (JPEG)
Roche: Ventana Companion Image Analysis (BIF, TIFF, JPG2000, DICOM compliant)
Huron: HuronViewer (BigTIFF, FlatTIFF, DICOM compliant)
Philips: Intellisite (iSyntax Philips proprietary file)
3DHistech: CaseViewer (JPG, PNG, BMP, TIFF)
AnnotatorJ[269]: AnnotatorJ (JPG, PNG, TIFF)
NuClick[347]: NuClick (Not specified)

Pixel-wise masks are differentiated from pixel-level annotations in that when an ROI mask of this type is tiled into multiple instances (i.e. patches), each sample is considered a single class. The ROI-level is in contrast to the pixel-level annotations, wherein the latter is defined to include all annotations where each patch can contain several class types.

A.9. Surveyed datasets

A.9.1. Table creation details

For each dataset recorded in the literature, a collection of information was collected. This information was organized into 10 categories, listed below. The full table is given in Table 9.11:

1. *Dataset Name*: The name of the dataset, if given. If no name is given, then a name was given for book-keeping purposes.
2. *References*: The works that use this dataset are listed.
3. *Availability*: A hyperlink to the dataset, when publicly available or available for request directly is provided.
4. *Stain type*: The type of stain used.
5. *Size*: Describes the number of WSIs, where this information is available, or the number of patches present in the dataset.
6. *Resolution (μm)/ Magnification*: Presents the resolution, in micrometers along with the magnification in the format μm/Magnification. If a piece of information is unavailable (either resolution or magnification) this information is omitted from the table.
7. *Annotation Type*: Describes the annotation granularity present in the dataset (patient, slide, ROI/ROI mask, patch, pixel) where available.
8. *Label Structure*: Whether each image in the dataset has a single label associated with it, or multiple. Datasets, where each image has only a single label associated with it, are labeled with *S*, whereas those with multiple labels are labeled with *M*.
9. *Classes*: The number of classes available, where this count is meaningful. Where it is more helpful to describe the format of ground truth (ex. nucleus pixel locations), this is written instead.
10. *Class Balance (CB)*: Datasets which are balanced are marked with a *B*, whereas those which are imbalanced are marked as *I*. Those where this information is unavailable are marked with an *U*.

A.10. Organ overview

For each paper recorded in the literature, a collection of information about their specific goal was collected. This information was categorized by organ and arranged into a table, the organs being: Basal/Epithelium, Bladder, Brain, Mouth/Esophagus, Breast, Liver, Lymph Node, Prostate/Ovary, Kidney, Lung, Pancreas, Thyroid, Stomach/Colon. Below will be the explanation of each column in Table 9.11:

1. *References:* Reference number of the paper that involved the specified task.
2. *Tasks:* Specific target goal that the work wanted to achieve, this range from different types of detection, classification, and segmentation to prognosis and diagnosis.
3. *Disease Specification:* Describes the pathology of the target goal of the paper.
4. *Methods:* Define the different machine learning methods used to achieve the proposed target task of the paper.

A.11. Technicalities by task

For each paper recorded in the literature, a collection of information on the Neural Network architectures used was organized and categorized by its specific task. It was found that across the majority of papers, the following five tasks were the most prevalent: Detection, Disease Diagnosis, Segmentation, WSI Processing, and Patient Prognosis. At the end of the table, an **Other Task** section was added to attach other works that don't follow the selected tasks. Below will be the explanation of each column in Table 9.11:

1. *References:* Reference number of the paper that involved the specified task.
2. *Tasks Specification:* Describes the pathology of the target goal of the paper.
3. *Architecture:* Defines the different Neural Network architectures used to achieve the proposed target task of the paper.
4. *Datasets:* Name of the datasets used for the specified task (see Table 9.11 for information on datasets).

Compilation of all the datasets carefully studied in this survey with its respective information (see Table Creation Details).

Dataset Name	References	Availability	Stain Type	Size	Res(μm)/ Mag	Annotation	Label	Class	CB
Basal/Epithelium									
NKI-VGH	[602]	Link	H&E	158 ROIs	N/A	Pixel	S	2	U
AJ-Epi-Seg	[543]	Link	H&E	42 ROIs	20×	Pixel	S	2	U
TCGA-Phil	[270]	TCGA	H&E	50 WSIs	40×	Pixel	S	4	I
MOIC	[594]	N/A	N/A	6 610 MOIs	10×	Slide	S	2	U
MOIS	[594]	N/A	N/A	1 436 MOIs	10×	Pixel	S	2	U
Jiang et al.	[594]	N/A	N/A	128 WSIs	40×	Pixel	S	2	U
MIP	[603]	N/A	H&E	108 Patients	40×	Patient	S	2	I
YSM	[603]	N/A	H&E	104 Patients	40×	Patient	S	2	I
GHS	[603]	N/A	H&E	51 Patients	40×	Patient	S	2	I
DKI	[297]	N/A	H&E	695 WSIs	40×	Slide	S	2	I
Y/CSUXH-TCGA	[604]	N/A	H&E	2 241 WSIs	0.275/40×, 0.5/20×, 1/10×, 5/4×	Slide	S	4	U
BE-Hart	[605]	N/A	H&E	300 WSIs	40×	Patch	S	2	I
BE-Cruz-Roa	[606]	N/A	H&E	308 ROI, 1 417 Patches	10×	Patch	S	2	U
DLCS	[172]	N/A	H&E	5 070 WSIs	0.25/40×	Slide	S	4	U
BE-TF-Florida-MC	[172]	N/A	H&E	13 537 WSIs	0.24/20×, 0.5/20×, 0.55/20×	Slide	S	4	U
Bladder									
TCGA + UFHSH	[415]	By Req.	H&E	913 WSIs	40×	Slide, ROI	S	2	I
TCGA-Woerl	[146]	TCGA	H&E	407 WSIs	40×	ROI	S	4	I
Bla-NHS-LTGU	[380]	N/A	IF	75 ROIs	N/A	Pixel	S	2	U
CCC-EMN MIBC	[146]	N/A	H&E	16 WSIs	40×	ROI	S	4	I
UrCyt	[607]	N/A	ThinStrip	217 WSIs	40×	Pixel	S	3	U
AACHEN-BLADDER	[485]	N/A	H&E	183 Patients	N/A	Patient	S	2	I
Brain									
TCGA-Shirazi	[85]	N/A	H&E	654 WSIs, 849 ROIs	0.5	ROI	M	4	I
TCGA-GBM-Tang	[608]	TCGA	N/A	209 Patients, 424 WSIs	0.5/20×	Patient	S	2	I
MICCAI14	[76,609]	N/A	H&E	45 WSIs	N/A	Slide	S	2	B
M-Qureshi	[341]	N/A	H&E	320 ROIs	N/A	ROI	S	4	B
Lai et al.	[592]	N/A	Amyloid-β antibody	30 WSIs	20×	Slide, Pixel	S	2, 3	I, U
Vessel	[610]	Link	H&E, PAS-H, Masson tri-chome, Jones	226 WSIs	0.25/40×	ROI	M	3	I
WCM	[611]	N/A	H&E	87 WSIs	N/A	Patch	S	2	U
Esophagus									
ESO-DHMC	[288]	N/A	H&E	180 WSIs, 379 ROIs	20×	ROI	S	4	U
Kidney									
AIDPATHA	[389,612]	Link	PAS	31 WSIs	20×	Pixel	S	3	U
AIDPATHB	[389,612]	Link	PAS	2 ~ 340 Patches	20×	Patch	S	2	B

(continued on next page)

(*continued*)

Dataset Name	References	Availability	Stain Type	Size	Res(μm)/ Mag	Annotation	Label	Class	CB
M-Gadermayr	[613]	N/A	PAS	24 WSIs	20×	ROI	S	2	U
TCGA-RCC-Lu	[64]	TCGA	H&E	884 WSIs	20×, 40×	Slide	S	3	I
BWH-CRCC	[64]	N/A	H&E	135 WSIs	10×, 20×	Slide	S	3	I
BWH-BRCC	[64]	N/A	H&E	92 WSIs	40×	Slide	S	3	I
BWH-RCC	[64]	N/A	H&E	135 WSIs	40×	Slide	S	3	I
Kid-Wu	[387]	N/A	N/A	1 216 Patients, 60 800 Patches	N/A	Patch	S	2	U
UHZ-Fuchs	[381]	N/A	MIB-1	133 Patients	0.23/40×	Patient	S	9	I
WUPAx	[84]	N/A	H&E	48 WSIs	0.495	ROI	S	2	I
Pantomics	[614]	N/A	H&E	21 349 Patches	0.5/20×	Patch	S	2	U
RUMC	[152]	N/A	PAS	50 WSIs	0.24/20×	Pixel	S	10	I
Mayo	[152]	N/A	PAS	10 WSIs	0.49/20×	Pixel	S	10	I
UHZ-RCC	[289]	N/A	MIB-1	1 272 Patches	N/A	Patch	S	2	I
Kid-Cicalese	[615]	N/A	PAS	1 503 ROIs	N/A	ROI	S	2	I
Kid-Yang	[388]	N/A	H&E, PAS, Jones	949 WSIs	0.25	ROI	S	2	U
Kid-BWH-TCGA	[447]	N/A	H&E	1 184 WSIs	20×	Slide	S	3	I
WTH	[421]	N/A	N/A	3 734 Patients	N/A	Patient	S	3	I
TCGA-RCC-Chen	[616]	N/A	N/A	45K ROIs	20×	ROI	S	3	B
BWH-RCC-Chen	[616]	N/A	N/A	1 661 ROIs	20×	ROI	S	3	I
MC-Gallego	[344]	N/A	H&E, PAS	20 WSIs, 1 184 ROIs	20×, 40×	ROI	S	2	I
AACHEN-RCC	[485]	N/A	H&E	249 Patients	N/A	Patient	S	3	I
ANHIR	[617]	Link	H&E, MAS, PAS, and PASM	50 WSIs	0.1 to 0.2/40×	Slide	S	8	I
Glomeruli renal biopsies	[618]	N/A	H&E, PAS or Jones	42 WSIs	0.25	ROI	S	2	I
Hubmap Glom	[619]	Link	H&E, PAS, PAS-H, Silver, Jones, Van Gieson, etc	3712 WSIs	0.13 to 0.25/40×	ROI	S	2	U
KPMP	[619]	Link	PAS-H	26 WSIs	0.25/40×	ROI	M	2	U
Breast									
BreakHis	[226,228]	By Req.	H&E	82 Patients, 7 909 ROIs	40×, 100×, 200×, 400×	ROI	S	2	I
CAMELYON 16	[61,231,507]	link	H&E	399 WSIs	0.243/20×, 0.226/40×	Slide, ROI	S	3	I
BACH18	[220,585]	Link	H&E	40 WSIs, 400 Patches	0.42, 0.467	Patch, Pixel	S	4	B
TUPAC16	[265]	Link	H&E	821 WSIs	40×	Slide	S	3	I
TUPAC16-Mitoses	[265]	Link	H&E	73 WSIs	0.25/40×	ROI	S	2	U
TUPAC16-ROIs	[265]	Link	H&E	148 WSIs	40×	ROI	S	2	U
CAMELYON 17	[61,232,620]	Link	H&E	1 399 WSIs	0.23, 0.24, 0.25	Patient, Slide, ROI	S	5, 4, 3	I
BioImaging	[256,621]	N/A	H&E	285 WSIs	0.42/200×	Slide	S	4	B
Ext-BioImaging	[257]	N/A	H&E	1 568 WSIs	0.42/200×	Slide	S	4	I
MITOS-ATYPIA14	[374,622]	Link	H&E	1 696 HPFs	40×	Pixel	S	2	U
MITOS12	[374,623]	Link	H&E	50 HPFs	0.185/40×, 0.2273/40×, 0.22753/40×, 0.2456/40×	Pixel	S	2	U
AJ-Lymphocyte	[390,543]	Link	H&E	100 ROIs	40×	Pixel	S	2	U
MSK	[62,624,625]	Link	H&E	130 WSIs	0.5/20×	Slide	S	2	I
CCB	[350]	Link	H&E	33 Patches	40×	Pixel	S	2	U
BIDMC-MGH	[26]	Link	H&E	167 Patients, 167 WSIs	0.25/40×	Patient	S	4	I
PUIH	[213]	N/A	H&E	4 020 WSIs	100×, 200×	Slide	S	4	I
HASHI	[219]	Link	H&E	584 WSIs	0.2456/40×, 0.23/40×	ROI	S	2	U
TNBC-CI	[253]	Link	H&E	50 Patches	40×	Pixel	S	2	U
AP	[626,627]	Link	H&E	300 ROIs	40×	ROI	S	3	I
KIMIA Path24	[628]	Link	N/A	28 380 Patches	0.5/20×, 0.25/40×	Patch	S	24	U
BCSC	[254,438]	By Req.	H&E	240 WSIs	40×	Slide, ROI	M	14	I
AJ-IDC	[295,543,629]	Link	H&E	162 WSIs, 277 524 Patches	40×	Patch	S	2	I
PCam	[528]	Link	H&E	327 680 Patches	10×	Patch	S	2	I
AJ-N	[630]	N/A	H&E	141 ROIs	40×	Pixel	S	2	U
TCGA-Cruz-Roa	[631]	TCGA	H&E	195 WSIs	0.25/40×	ROI	M	5	U
TCGA-Jaber	[632]	TCGA	H&E	1 142 WSIs	20×	Patch	S	2	I
TCGA-Corvò	[633]	TCGA	H&E	91 WSIs	N/A	ROI	S	4	U
TCGA-Lu-Xu	[390]	TCGA	H&E	1K WSIs	N/A	ROI	S	2	I
AMIDA13	[373,634]	N/A	H&E	606 ROIs	0.25/40×	Pixel	S	2	U
MICCAI16/17	[330]	N/A	H&E	64 WSIs	N/A	Pixel	S	2	U
MICCAI18	[330]	N/A	H&E	33 WSIs	N/A	Pixel	S	2	U
RUMC-Litjens	[71]	N/A	H&E	271 WSIs	0.24/20×	ROI	S	2	U
ABCTB	[429]	N/A	H&E	2 531 WSIs	20×	Patient	S	3	U
NHO-1	[97]	N/A	H&E	110 WSIs	40×	Slide	S	2	I
RUMC-Bejnordi	[635]	N/A	H&E	221 WSIs	0.243/20×	Slide, ROI	S	3	I
UVLCM-UVMC	[636]	N/A	H&E	2 387 WSIs	0.455/20×	Slide	S	6	I
HUP	[631]	N/A	H&E	239 WSIs	0.25/40×	ROI	M	5	U
UHCMC-CWRU	[631]	N/A	H&E	110 WSIs	0.23/40×	ROI	M	5	U
CINJ	[631]	N/A	H&E	40 WSIs	0.25/40×	ROI	M	5	U

(*continued*)

Dataset Name	References	Availability	Stain Type	Size	Res(μm)/ Mag	Annotation	Label	Class	CB
Bre-Steiner	[27]	N/A	H&E, IHC	70 WSIs	0.25	Slide	S	4	I
NMCSD	[72]	N/A	N/A	108 WSIs	0.24	Slide	S	4	I
BC-Priego-Torres	[560]	N/A	H&E	12 WSIs	0.2524/40×	Pixel	S	2	U
BIRL-SRI	[637]	N/A	H&E	65 WSIs, 5 151 Patches	2/5 ×, 1/10×	ROI	S	2	U
BWH-Lymph	[64]	N/A	H&E	133 WSIs	40×	Slide	S	2	B
NHS-Wetstein	[340]	N/A	H&E	92 WSIs	0.16/40×	ROI	S	3	U
BRE-Parvatikar	[252]	N/A	H&E	93 WSIs, 1 441 ROIs	0.5/20×	ROI	S	2	I
BWH-TCGA-Breast	[447]	N/A	H&E	2 126 WSIs	20×	Slide	S	2	I
Bre-Brieu	[380]	N/A	H&E	30 ROIs	N/A	Pixel	S	2	U
Duke	[591]	N/A	H&E	140 WSIs	0.5/20×	ROI	S	2	U
TransATAC	[591]	N/A	H&E	30 WSIs	0.45/20×	ROI	S	2	U
BRACS	[638–640]	By req.	H&E	547 WSIs, 4 539 ROIs	0.25/40×	Slide, ROI	S	7	I
Post-NAT-BRCA	[641]	Link	H&E	138 Patients	40×	Patient	S	3	I
BCSS	[642]	Link	H&E	151 WSIs, 20K ROIs	0.25	ROI	M	20	I
Amgad et al.	[367]	N/A	H&E	151 WSIs, 20 340 ROIs	0.25/40×	ROI	S	5	U
SMH + OVC	[342]	N/A	Ki67	30 TMAs, 660 Patches	20×	Pixel	S	2	U
DeepSlides	[342]	Link	Ki67	452 Patches	40×	Pixel	S	2	U
Protein Atlas	[342,643]	Link	Ki67	56 TMAs	20×	Slide	S	3	U
Yale HER2	[342]	N/A	H&E	188 WSIs	20×	ROI	S	3	U
Yale Response	[342]	N/A	H&E	85 WSIs	N/A	ROI	S	2	U
TCGA-Farahmand	[342]	N/A	H&E	187 WSIs	N/A	ROI	S	2	U
Breast Histopathology Images	[644]	Link	H&E	162 WSIs	40×	Patch	S	2	I
Colsanitas	[645]	N/A	H&E	544 WSIs	0.46/40×	ROI	M	4	I
Pancreas									
Pan-Bai	[334]	N/A	Ki67 IHC	203 TMAs	Ma×. of 20×	Pixel	S	3	I
Liver									
SUMC	[490]	N/A	H&E	80 WSIs	0.25/40×	Slide	S	2	B
MGH	[646]	N/A	H&E	10 WSIs	0.46/20×	ROI	S	4	U
Liv-Atupelage	[554]	N/A	H&E	305 ROIs	20×	ROI	S	5	I
IHC-Seg	[336]	N/A	H&E, PD1, CD163/CD68, CD8/CD3, CEA, Ki67/CD3, Ki67/CD8, FoxP3, PRF/CD3	77 WSIs	20×	Pixel	S	4	I
Lung									
TCGA-Gertych	[240]	IDs	H&E	27 WSIs, 209 ROIs	0.5/20×, 0.25/40×	ROI, Pixel	S	4	I
TCGA-Brieu	[380]	TCGA	H&E	142 ROIs	N/A	Pixel	S	2	U
TCGA-Wang	[534,625,647]	TCGA	H&E	1 337 WSIs	20×, 40×	ROI	S	3	U
NLST-Wang	[534,648]	By Req.	H&E	345 WSIs	40×	ROI	S	3	U
TCGA-Wang-Rong	[214,625,647]	TCGA	H&E	431 WSIs	40×	ROI	S	6	U
NLST-Wang-Rong	[214,648]	By Req.	H&E	208 WSIs	40×	Pixel	S	7	U
SPORE	[534,649]	N/A	H&E	130 WSIs	20×	ROI	S	3	U
CHCAMS	[534]	N/A	H&E	102 WSIs	20×	ROI	S	3	U
TCGA-Hou-2	[234]	TCGA	H&E	23 356 Patches	0.5/20×	Patch	S	2	I
TCGA-LUSC-Tang	[608]	TCGA	N/A	98 Patients, 305 WSIs	0.5/20×	Patient	S	2	I
TCGA-CPTAC-Lu	[64]	TCGA, CPTAC	H&E	1 967 WSIs	20×, 40×	Slide	S	2	I
DHMC	[75]	N/A	H&E	422 WSIs, 4 161 ROIs, 1 068 Patches	20×	Slide, ROI, Patch	M, S, S	6	I
Lung-NHS-LTGU	[380]	N/A	IF	29 ROIs	N/A	Pixel	S	2	U
CSMC	[240]	N/A	H&E	91 WSIs, 703 ROIs	0.5/20×	ROI, Pixel	S	4	I
MIMW	[240]	N/A	H&E	88 WSIs, 1 026 ROIs	0.389/20×	ROI, Pixel	S	4	I
NSCLC-Wang	[89]	N/A	H&E	305 Patients	20×	Patient	S	2	I
ES-NSCLC	[650]	N/A	H&E	434 Patients, 434 TMAs	20×	Patient	S	2	I
BWH-NSCLC-CL	[64]	N/A	H&E	131 WSIs	20×	Slide	S	2	I
BWH-NSCLC-BL	[64]	N/A	H&E	110 WSIs	40×	Slide	S	2	B
BWH-NSCLC-RL	[64]	N/A	H&E	131 WSIs	20×, 40×	Slide	S	2	I
VCCC	[563]	N/A	N/A	472 Patients	N/A	Patient	S	3	I
Dijon + Caen	[651]	N/A	HES	197 WSIs	20×	ROI	S	2	U
PKUCH + TMUCH	[345]	N/A	IHC	239 WSIs, 677 ROIs	20×	ROI	S	2	U

(*continued on next page*)

(*continued*)

Dataset Name	References	Availability	Stain Type	Size	Res(μm)/ Mag	Annotation	Label	Class	CB
Lymph Nodes									
LYON19	168,652,653	Link	IHC	441 ROIs	0.24	Pixel	S	2	U
AJ-Lymph	543,654	Link	H&E	374 WSIs	40×	Slide	S	3	I
TUCI-DUH	558	N/A	H&E	378 WSIs	0.24/20×	Slide	S	2	I
Thagaard-2	655	N/A	H&E, IHC	56 Patches	20×	Patch	S	2	I
Thagaard-3	655	N/A	H&E, IHC	135 Patches	20×	Patch	S	2	B
Thagaard-4	655	N/A	H&E, IHC	81 Patches	20×	Patch	S	2	I
Thagaard-5	655	N/A	H&E, IHC	60 Patches	20×	Patch	S	2	I
Zhongshan Hospital	166	N/A	H&E	595 WSIs	0.5/20×	ROI	M	2	I
Mouth/Esophagus									
SKMCH&RC	656	N/A	H&E	70 WSIs, 193 ROIs	0.275/40×	ROI	S	2	I
SKMCH&RC-M	656	N/A	H&E	30 WSIs	0.275/40×	ROI	S	4	U
ECMC	210	N/A	H&E	143 WSIs	0.172/40×, 0.345/20×, 0.689/10×	Pixel	S	7	U
BCRWC	364	N/A	N/A	126 WSIs	1.163/50×	Pixel	S	4	U
LNM-OSCC	32	N/A	H&E	217 WSIs	0.2467/20×, 0.25/40×	ROI	S	2	U
OP-SCC-Vanderbilt	650	N/A	H&E	50 Patients	40×	Patient	S	2	B
Sheffield University	365	N/A	H&E	43 WSIs	0.4952/20×	Slide	S	4	I
Prostate/Ovary									
PCa-Bulten	657	Link	H&E, IHC	102 WSIs, 160 ROIs	0.24/20×	Pixel	S	2	U
OV-Kobel	658	Link	H&E, Ki-67, Mammoglobin B, ER, Mesothelin, MUC5, WT1, p16, p53, Vimentin, HNF-1b	168 WSIs, 88 TMAs	N/A	Slide	S	6	I
TCGA-Tolkach	659	TCGA	H&E	389 WSIs	0.25/40×	ROI	S	3	U
UHZ	660	Link	H&E	886 TMAs	0.23/40×	ROI	S	5	U
SMS-TCGA	476	N/A	H&E	310 WSIs	20×, 40×	ROI	S	2	U
TCGA-Arvaniti	661	TCGA	H&E	447 WSIs	20×, 40×	Slide	S	2	I
TCGA-Yaar	443	TCGA	H&E	220 Patients	20×	Patient	S	2	I
Pro-RUMC	71	N/A	H&E	225 WSIs	0.16/40×	ROI	S	2	B
UHZ-PCa	289	N/A	MIB-1	826 Patches	N/A	Patch	S	2	I
SUH	208	N/A	H&E	230 WSIs, 1 103 160 Patches	10×	ROI	S	4	I
CSMC	382,442	N/A	H&E	513 Patches	0.5/20×	Pixel	S	4	U
HUH	73	N/A	H&E	28 WSIs	0.22	Pixel	S	2	U
RCINJ	662	N/A	H&E	83 WSIs	20×	Slide	S	2	I
Pro-Raciti	418	N/A	H&E	304 WSIs	0.5/20×	Slide, ROI	S	2	I, U
VPC	663	N/A	H&E	333 TMAs	40×	Pixel	S	4	U
Pro-Campanella	195	N/A	H&E	137 376 Patches	20×	Patch	S	6	U
UPenn-Yan	664	N/A	H&E	43 WSIs	40×	ROI	S	2	U
Pro-Doyle	665	N/A	H&E	12K ROIs	0.25/40×	ROI	S	2	U
UPenn-Doyle	666	N/A	H&E	214 WSIs	40×	ROI	S	7	U
RUMC-Bulten	267	N/A	H&E	1 243 WSIs	0.24	Slide	S	2	U
VGH	119	N/A	H&E	305 WSIs	N/A	ROI	S	5	U
NMCSD + MML + TCGA	667	N/A	H&E	1 557 WSIs	0.25/40×, 0.5/20×	Slide, ROI	S	4	I, U
OVCARE	668	N/A	H&E	354 WSIs	40×	ROI	S	5	U
CWU	669	Link	H&E	478 WSIs, 120K Patches	0.504/20×	Patch	S	3	I
UHC	669	Link	H&E	157 WSIs, 120K Patches	0.231/40×	Patch	S	3	I
HWN	669	Link	H&E	51 WSIs, 120K Patches	0.264/40×	Patch	S	3	I
CSMC	347	N/A	N/A	625 Patches	N/A	Pixel	S	4	U
DiagSet-A	266	By Req.	H&E	2 604 206 Patches	5×, 10×, 20×, 40×	Patch	S	9	I
DiagSet-B	266	By Req.	H&E	4 675 WSIs	0.25/40×	Slide	S	2	I
DiagSet-C	266	By Req.	H&E	46 WSIs	0.25/40×	Slide	S	3	U
SICAPv2	384,670	Link	H&E	182 WSIs	40×	Slide, Pixel	S	4	I, U
OVCARE-Farahani	671	N/A	H&E	485 Patients, 948 WSIs	40×	Patient, Slide	S	5	I
University of Calgary	671	N/A	H&E	60 Patients, 60 WSIs	40×	Patient, Slide	S	5	I
PANDA	672	Link	H&E	11 000 WSIs	40×	ROI	S	5	I
Thyroid									
UPMC	557	N/A	Feulgen	10-20 WSIs	0.074	Pixel	S	3	U
Chen et al.	346	N/A	N/A	600 WSIs	40×	Slide	S	3	I
TCGA-Hoehne	454	TCGA	H&E	482 WSIs	40×	Slide	S	4	I
DEC	454	N/A	H&E	224 WSIs	40×	Slide	S	4	I
ACQ	454	N/A	H&E	100 WSIs	40×	Slide	S	4	I
Stomach & Colon									
UMCM	220,673	Link	H&E	5K Patches	0.495/20×	Patch	S	8	B

(*continued*)

Dataset Name	References	Availability	Stain Type	Size	Res(μm)/ Mag	Annotation	Label	Class	CB
GLaS	83,674	Link	H&E	165 WSIs	0.62/20×	ROI	S	5	I
CRCHistoPhenotypes	77,277	Link	H&E	10 WSIs, 100 Patches	0.55/20×	Pixel	S	4	I
DACHS	428	N/A	H&E	3 729 WSIs	20×	Slide	S	3	I
NCT-CRC-HE-100K	86,468,673	Link	H&E	86 WSIs, 100K Patches	0.5	Patch	S	9	I
NCT-CRC-HE-7K	86,468,673	Link	H&E	25 WSIs, 7 180 Patches	0.5	Patch	S	9	I
CoNSeP	277	Link	H&E	16 WSIs, 41 Patches	40×	Pixel	S	7	I
OSU	432	Link	H&E, Pan-Cytokeratin	115 WSIs	0.061/40×	ROI	S	2	U
Warwick-CRC	169,675	Link	H&E	139 ROIs	20×	ROI	S	3	I
HUH	676	Link	EGFR	27 TMAs, 1 377 ROIs	20×	ROI	S	2	I
CRAG	169	N/A	H&E	38 WSIs, 139 Patches	0.275/20×	Patch	S	3	I
ULeeds	677,678	Link	H&E	27 WSIs	N/A	Slide	S	3	B
Kather et al.	287	Link	H&E	11 977 Patches	0.5	Patch	S	3	U
ZU	142	By Req.	H&E	717 ROIs	0.226/40×	ROI	S	6	I
KCCH	287	N/A	H&E	185 Patients	N/A	Patient	S	3	I
SC-Takahama	278	N/A	H&E	1 019 WSIs	Ma× . of 20×	Pixel	S	2	U
HUCH	88	N/A	H&E	420 Patients	0.22	Patient	S	2	I
RC-Ciompi	679	N/A	H&E	74 WSIs	0.455/200×	ROI	S	9	U
DHMC-Korbar	78	N/A	H&E	1 962 WSIs	200×	Slide	S	6	U
CRC-TP	279	N/A	H&E	20 WSIs, 280K Patches	20×	ROI	S	7	U
CRC-CDC	279	N/A	H&E	256 Patches	20×	Pixel	S	5	I
SC-Xu	440	N/A	N/A	60 WSIs	N/A	ROI	S	2	U
FAHZU-Xu	441	N/A	H&E	13 838 WSIs	40×	Slide	S	2	I
Bilkent	83,680	N/A	H&E	72 Patches	20×	Pixel	S	2	U
DHMC-Wei	293	N/A	H&E	1 230 WSIs	20×	Slide	S	3	I
Warwick-UHCW	363	N/A	H&E	75 WSIs	0.275/40×	ROI	S	2	U
Warwick-Osaka	363	N/A	H&E	50 WSIs	0.23/40×	Slide	S	6	I
GNUCH	328	N/A	H&E	94 WSIs, 343 ROIs	N/A	Slide, ROI	S	4, 2	I
SPSCI	681	N/A	H&E	55 WSIs, 251 ROIs	0.19/40×	ROI	S	5	I
WSGI	439	N/A	H&E	608 WSIs	0.2517/40×	Slide, Pixel	S	3, 2	I, U
TBB	682	N/A	H&E	44 TMAs	N/A	Slide	S	3	I
UV	683	N/A	H&E	456 WSIs	40×	Slide	S	4	U
SC-Sali	684	N/A	H&E	1 150 WSIs	N/A	Slide	S	7	I
SC-Holland	296	N/A	H&E	10 WSIs, 1K Patches	40×, 100×	Slide	S	2	B
SC-Kong	685	N/A	H&E	272 WSIs	40×	ROI	S	2	U
SSMH-STAD	236	N/A	H&E	50 WSIs	N/A	Slide	S	2	B
HIUH	224	N/A	H&E	8 164 WSIs	20×	Slide, ROI	S	3	I
HAH	224	N/A	H&E	1K WSIs	20×	Slide	S	3	I
SC-Galjart	391	N/A	H&E	363 Patients, 1 571 WSIs	0.25	Slide	S	2	U
SC-Zheng	420	N/A	H&E	983 WSIs, 10 030 ROIs	0.96/10×	ROI	S	5	U
CRC-I-Chikontwe	445	N/A	H&E	173 WSIs	40×	Slide	S	2	I
CRC-II-Chikontwe	445	N/A	H&E	193 WSIs	40×	Slide	S	2	I
PLAGH	686	N/A	H&E	2 123 WSIs	0.238/40×	Pixel	S	4	U
QUASAR	687	N/A	H&E	106 268 ROIs	0.5	ROI	S	2	U
CGMH	303	N/A	H&E	297 WSIs	0.229/40×	ROI	S	2	U
AOEC-RUMC-I	453	N/A	H&E	2 131 WSIs	5×-10×	Slide	M	5	I
AOEC-RUMC-II	453	N/A	H&E	192 WSIs	5×-10×	Slide, ROI	M, S	4	I, U
Lizard	260	Link	H&E	291 WSIs,	0.5/20×	Pixel	S	6	I
YCR-BCIP	428	N/A	H&E	889 WSIs	20×	Slide	S	2	I
MHIST	255	By Req.	H&E	3 152 Patches	40×	Patch	S	2	I
YSMH	368	N/A	H&E	390 WSIs	20×	Slide, ROI	S	5	I, U
ColonPredict-Plus-2	343	N/A	H&E	200 Patients, 2 537 Patches	N/A	Pixel	S	2	U
PAIP	688	By Req.	H&E	47 WSIs	N/A	ROI	S	2	U
Li et al.	269	N/A	N/A	10 894 WSIs, 200 Patches	0.5/20×	Slide, Pixel	S	2	I
Stanford Hospital	311	Link	H&E, p53 IHC	70 WSIs	20×	Slide	S	2	U
IMP Diagnostics Lab.	689,690	By Req.	H&E	1133 WSIs	40×	Slide	S	3	I
Chaoyang	691	Link	H&E	6 160 patches	N/A	Patch	S	8	I
BERN-GASTRIC-MSI	485	N/A	H&E	302 Patients	N/A	Patient	S	2	I
BERN-GASTRIC-EBV	485	N/A	H&E	304 Patients	N/A	Patient	S	2	I
Bone Marrow									
BM-MICCAI15	692	Link	H&E	11 WSIs	N/A	Pixel	S	3	U
MICCAI15-Hu	433	N/A	H&E	11 WSIs, 1 995	N/A	Patch	S	4	I

(*continued on next page*)

(*continued*)

Dataset Name	References	Availability	Stain Type	Size	Res(μm)/ Mag	Annotation	Label	Class	CB
				Patches					
FAHZU-Hu	433	N/A	H&E	24 WSIs, 600 Patches	N/A	Patch	S	3	B
BM-Hu	433	N/A	H&E	84 WSIs	N/A	Slide	S	2	I
RUMC-Eekelen	354	N/A	PAS	24 WSIs	0.25	Pixel	S	6	U
MSKCC	339	N/A	H&E	1 578 WSIs	0.5025, 0.5031/20×	Pixel	S	7	I
EUH	693	N/A	Wright's Stain	9 230 ROIs	0.25/40×	ROI	S	12	I
Frankel et al.	694	N/A	H&E	424 WSIs	40×	Slide	S	9	I
Internal-STAD	695	N/A	H&E	203 WSIs	0.25/40×	ROI	S	N/A	U
MultiCenter-STAD	695	N/A	H&E	417 WSIs	0.46/40×	ROI	S	N/A	U
Cervix									
TCGA-Idlahcen	261	TCGA	H&E	10 WSIs	2.5×-40×	Slide	S	2	B
XH-FMMU	696	N/A	H&E	800 WSIs	4×-40×	ROI	S	2	U
Pap-Cytology	168	N/A	N/A	42 ROIs	20×	Pixel	S	2	U
Chen et al.	346	N/A	N/A	372 WSIs	40×	Slide	S	2	I
OAUTHC	451	N/A	H&E	1 331 ROIs	N/A	ROI	S	2	I
Multi-organ									
MoNuSeg	258	Link	H&E	30 WSIs	40×	Pixel	S	2	U
UHN	250	Link	H&E	1 656 WSIs, 838 644 Patches	0.504/20×	Slide, Patch	S	74	I
CPM-15	277	Link	H&E	15 Patches	20×, 40×	Pixel	S	2	U
CPM-17	277	Link	H&E	32 Patches	20×, 40×	Pixel	S	2	U
ADP	167,300	By Req.	H&E	100 WSIs, 17 668 Patches	0.25/40×	Patch	M	57	I
Bándi-Dev-Set	198	Link	H&E, Sirius Red, PAS, Ki-67, AE1AE3, CK8-18	100 WSIs	0.2275, 0.2278, 0.2431, 0.25, 0.2525, 0.5034	Pixel	S	6	U
Bándi-Dis-Set	198	Link	H&E, Alcian Blue, Von Kossa, Perls, CAB, Grocott	8 WSIs	0.2431	ROI	S	4	U
PanNuke	697,698	Link	H&E	20K WSIs, 205 343 ROIs	40×	ROI	S	5	I
Salvi-SCAN	656	Link	H&E	270 ROIs	10×, 20×, 40×	Pixel	S	2	U
TCGA-Nuclei	330,625,699	Link	H&E	5 060 WSIs, 1 356 Patches	0.25/40×	Pixel	S	14	U
MO-Khoshdeli	356	Link	H&E	32 WSIs, 32 Patches	0.5	Pixel	S	2	U
FocusPath	196	Link	H&E, Trichrome, IRON(FE), Mucicarmine, CR, PAS, AFB, Grocott	9 WSIs, 8 640 Patches	0.25/40×	Patch	S	15	U
Cheng-Jiang	700	Link	H&E, TCT, IHC	20 521 WSIs	10×	Slide	4	S	I
Stanford-TMA	290,701	By Req.	H&E, IHC	6 402 TMAs	N/A	Slide	S	4	I
TCGA-Courtiol	87	TCGA	H&E	56 Patients, 56 WSIs	N/A	Patient, Slide	S	3	I
BreCaHAD	74	link	H&E	170 ROIs	40×	ROI	S	2	U
TCGA-Hegde	702	TCGA	H&E	60 WSIs	10×	ROI	S	10	U
TCGA-Diao	703	TCGA	H&E	2 917 WSIs	20×, 40×	ROI, Pixel	S	4, 6	I
TCGA-Levine	668	TCGA	H&E	668 WSIs	N/A	ROI	S	5	U
TCGA@Focus	196	Link	H&E	1K WSIs, 14 371 Patches	N/A	Patch	S	2	I
TCGA-Shen	704	TCGA	H&E	1 063 WSIs	20×	Patch	S	3	U
TCGA-Lerousseau	444	TCGA	H&E	6 481 WSIs	20×	Pixel	S	3	U
TCGA-Schmauch	705	TCGA	H&E	10 514 WSIs	N/A	Slide	S	28	I
MO-Khan	202	N/A	H&E	60 WSIs	20×, 40×	Pixel	S	3	U
MESOPATH/MESOBANK	87	N/A	HES	2 981 Patients, 2 981 WSIs	40×	Patient, Slide	S	3	U
Mo-Campanella	195	N/A	H&E, SDF-1, TOM20	249 600 Patches	20×	Patch	S	6	U
BWH-TCGA-MO	448	N/A	H&E	25 547 WSIs	N/A	Slide	S	18	I
BWH-Lu	302	N/A	H&E	19 162 WSIs	20×, 40×	Slide	2	I	
Feng et al.	471	N/A	H&E, IHC	500 WSIs	20×	Slide	S	10	B
SegSet	266	N/A	H&E	30 WSIs	0.25/40×	Pixel	S	2	U
LC25000	706	Link	H&E	25 000 Patches	N/A	Patch	S	5	B
OCELOT-CELL	707	Link	H&E	306 WSIs, 673 Patches	0.2	ROI	S	2	I
OCELOT-TISSUE	707	Link	H&E	306 WSIs, 673 Patches	0.2	Pixel	S	3	I
Other									
MUH	468,708	N/A	N/A	18 365 Patches	14.14/100×	Patch	S	15	I
UPenn	709	N/A	H&E	209 Patients	20×	Patient	S	2	I
CMTHis	299	N/A	H&E	352 ROIs	40×, 100×, 200×, 400×	ROI	S	2	I
Heidelberg University	710	N/A	H&E	431 WSIs	N/A	ROI	S	2	U
CHOA	711	N/A	H&E	43 WSIs	10×	Slide	S	4	I
Han-Wistar Rats	452	N/A	H&E, ISH	349 WSIs	40×	Slide	S	2	U
Osteosarcoma	479	Link	H&E	1 144 ROIs	10×	ROI	S	3	I
UPenn + OSU + UH	712	N/A	H&E	2 358 WSIs	40×	Slide	S	4	I

(*continued*)

Dataset Name	References	Availability	Stain Type	Size	Res(μm)/ Mag	Annotation	Label	Class	CB
Kaggle 2018 Data Science Bowl	[713]	Link	DAPI, Hoechst, H&E	670 WSIs	N/A	Pixel	S	2	U
ALL-IDB2	[714,715]	By Req.	N/A	260 ROIs	300× - 500×	Slide	S	2	B

Compilation of tasks found in different Co-Path papers categorized by organ (see 9.10)

References	Tasks	Disease Specification	Methods
Basal/Epithelium			
[594]	Detection	Metastasis	End-to-end classifier using cascaded CNNs
[606]	Detection	Metastasis	Unsupervised learning via auto-encoder
[604]	Disease diagnosis	Melanoma, intra-dermal, compound, junctional nevus	CNN-based patch classifier
[716]	Nuclei subtype classification	lymphocyte, stromal, artefact, cancer	CRImage and TTG/CNx for cell identification and classification
[717]	Tissue subtype classification	Epithelial, stromal tissues, Spitz, conventional melanocytic lesions	Integration of CNN and HFCM segmentation
[605]	Tissue subtype classification	Epithelial, stromal tissues, Spitz, conventional melanocytic lesions	CNN-based classifier with transfer learning
[87]	Patient prognosis	Epithelioid, sarcomatoid, biphasic in mesothelium, distant metastatic recurrence	ResNet classifier with transfer learning
[259]	Patient prognosis	Epithelioid, sarcomatoid, biphasic in mesothelium, distant metastatic recurrence	Combination of DNN and RNN for feature processing
[270]	Tumor segmentation	Tumor, epidermis, dermis, background	FCN based segmentation
[297]	Classification	Nevi, melanoma	CNN-based classifier
Bladder			
[415]	Classification	Papillary urothelial carcinoma LG/HG	Combination of CNN and LSTM
[380]	Segmentation	Voronoi objects, edges, background regions	CycleGAN with U-Net segmentation
[258]	Nuclei Segmentation	Nuclear, Non-nuclear, Boundary	CNN-based classifier with AJI evaluation
[146]	Tissue Subtype Classification	Double negative, basal, luminal, luminal p53-like	ResNet variation classifier
Brain			
[76]	Classification	Glioblastoma multiforme, LG glioma	Elastic net classifier with weighted voting
[718]	Classification	LGG Grade II/III, GBM	Modular CNN-ensemble network
[142]	Classification	LGG and GBM	CNN-based classifier with transfer learning
[719]	Classification	Glioma grading III, IV, V	SVM classifier
[250]	Classification	Tissue feature correlation analysis	CNN-based classifier with transfer learning
[611]	Patient prognosis	Tissue feature correlation analysis	Densenet121 classifiers, initialized with imageNet pre-trained weights
[238]	Patient prognosis	IDH mutation	Survival CNN with genetic biomarker data integration
[85]	Patient prognosis	Survival period for glioblastoma	CNN-based patch classifier
[477]	Patient prognosis	GBM prognostic index	Fusion network of genome, histopathology, and demography
[608]	Patient prognosis	Glioblastoma Multiforme	Custom CNN classifier
[556]	Patient prognosis/Tissue subtype classification	Oligodendroglioma, IDH-mutant/wild type astrocytoma	CNN-based classifier
[592]	Segmentation	Superior Middle Temporal Gyri in the temporal cortex	Semi-supervised active learning(SSL)
Mouth/Esophagus			
[720]	Tissue subtype classification	Stroma, lymphocytes, tumor, mucosa, kerClassificationatin pearls, blood, adipose	Modified AlexNet patch classifier with active learning
[288]	Disease Diagnosis	Barrett esophagus no dysplasia, esophageal adenocarcinoma, normal, Barrett esophagus with dysplasia	Attention based classifier
[721]	Patient prognosis	Oropharyngeal squamous cell carcinoma	Computational cell cluster graph
[365]	Segmentation	Oral epithelial dysplasia (OED)	HoVer-Net+, a deep learning framework consists of an encoder branch, and three decoder branches
Breast			
[199,489]	Detection	Benign, malignant	CNN-based patch classifier
[299,722,723]	Detection	Benign, malignant	CNN classifier with transfer learning
[631]	Detection	Benign, malignant	CNN-based pixel classifier
[508]	Detection	Benign, malignant	Pre-trained AlexNet with automatic label query
[724]	Detection	Benign, malignant	Pre-trained AlexNet with Bi-LSTM classifier
[323]	Detection	Benign, malignant	Combination of CNN classifier and U-Net segmentation
[725]	Detection	Benign, malignant	CNN-based classifier
[417]	Detection	Benign, malignant	3 stage LSTM-RNN classifier
[437]	Detection	Benign, malignant	Attention-based MIL model
[295]	Detection	Benign, malignant	Tri-branched ResNet model
[227]	Detection	Benign, malignant	Combination of CNN and hand-crafted features
[219]	Detection		Custom CNN classifier with Quasi-Monte Carlo sampling
[390]	Detection, Patient Prognosis	Tumor, Normal/ Tumor-infiltrating lymphocytes	U-Net based classifier
[338]	Detection	Mitosis	Multi-scale custom CNN classifier
[644]	Detection	Invasive Ductal Carcinoma	Bayesian Convolution Neural Networks
[586]	Binary classification	Breast cancer to axillary lymph nodes (ALNs)	Pre-trained architectures: DenseNet121, ResNet50, VGG16, Xception and lightweight convolutional neural network

(*continued on next page*)

(*continued*)

References	Tasks	Disease Specification	Methods
			(LCNN)
366	Tumor Segmentation and Classification	Breast Cancer Metastases	SOTA methods, designed MLVDeepLabV3 +
641	Segmentation	Segmentation of the malignant nuclei within each tumor bed	Mask regional convolutional neural network (Mask R-CNN)
726	Segmentation	Segmentation of multiple subtypes on breast images	Deep Multi Magnification Network (DMMN), CNN architecture
298	Detection	Metastasis/ Micro, Macro	CNN-based pixel classifier
419	Detection	Metastasis/ Micro, Macro	Resnet with transfer learning
727	Detection	Metastasis/ Micro, Macro	Combination of CNNs with LSTM-RNN, DCNN-based classifier
322	Detection	Cancer metastasis detection	MIL + RNN classifier, Neural conditional random field
728	Detection	Cancer metastasis detection	CNN with attention mechanism
486	Detection	Metastasis in sentinel lymph node	CNN with Random Forest classifier
729	Detection	Invasive ductal carcinoma	CNN-based patch classifier
291	Detection	Invasive ductal carcinoma	ResNet with transfer learning
629	Detection	Invasive ductal carcinoma	CNN-based random forest classifier
654	Detection	Invasive ductal carcinoma	Autoencoder network
72	Detection	Macrometastasis, micrometastasis, isolated tumor cells, negative	Customized InceptionV3 classifier
218	Detection	Mitosis detection	CNN classifier with two-phase training
262	Detection	Mitosis detection	Task-based CNN ensemble
371	Detection	Mitosis detection	CNN-based random forest classifier
337	Detection	Mitosis detection	CNN classifier with transfer learning
372	Detection	Mitosis detection	Multi-stage RCNN classifier
373	Detection	Mitosis detection	FCN classifier
374	Detection	Mitosis detection	Adaptive Mask RCNN
375	Detection	Mitosis detection	CNN-based patch classifier
200	Detection	Mitosis detection	Combination of DCNN network
377	Detection	Mitosis detection	R2U-Net based regression model
228	Classification	Epithelium, Stroma	Magnification invariant CNN classifier
229	Classification	Benign, malignant	CNN classifier interleaved with squeeze-excitation modules (SENet)
730	Classification	Adenosis, fibroadenoma, phyllodes tumors, tubular adenoma, ductal, lobular, mucinous, papillary	Inception Recurrent Residual Convolutional Neural Network (IRRCNN)
731	Classification	Adenosis, fibroadenoma, phyllodes tumors, tubular adenoma, ductal, lobular, mucinous, papillary	Custom DenseNet classifier
645	Classification	normal tissue, benign lesion, in situ carcinoma, and invasive carcinoma	Custom multiclass dense layer classifier based on Xception network
732	Disease diagnosis	Adenosis, fibroadenoma, phyllodes tumors, tubular adenoma, ductal, lobular, mucinous, papillary	Two-stage ResNet classifier (MuDeRN)
324	Disease diagnosis	Benign, malignant	Ensemble of CNN classifiers
294	Disease diagnosis	Adenosis, fibroadenoma, phyllodes tumors, tubular adenoma, ductal, lobular, mucinous, papillary	CNN-based classifier with transfer learning
733	Disease diagnosis	Adenosis, fibroadenoma, phyllodes tumors, tubular adenoma, ductal, lobular, mucinous, papillary	Class structured DCNN
422	Disease diagnosis	Adenosis, fibroadenoma, phyllodes tumors, tubular adenoma, ductal, lobular, mucinous, papillary	Two stage classification and selection network
734	Disease diagnosis	Adenosis, fibroadenoma, phyllodes tumors, tubular adenoma, ductal, lobular, mucinous, papillary	Domain adaptation based on representation learning
735	Disease diagnosis	Benign, in-situ, invasive carcinoma	CNN-based classifier with gravitational loss
736	Disease diagnosis	Benign, in-situ, invasive carcinoma	CNN ensemble with LightGBM
737	Disease diagnosis	Benign, in-situ, invasive carcinoma	InceptionV3 classifier using dual path network
26	Disease diagnosis	Usual ductal hyperplasia, ductal carcinoma in situ	Logistic regression with Lasso regularization
362	Disease diagnosis	Proliferation score (1, 2, or 3)	Encoder-decoder with Gaussian Mixture model
252	Disease diagnosis	Low risk/High risk	Logistic regression using morphological features
488	Disease diagnosis	normal, benign, in situ carcinoma, invasive carcinoma	Hybrid CNN classifier
636	Disease diagnosis	Proliferative without atypia, atypical hyperplasia, ductal / lobular carcinoma in situ, invasive carcinoma	Cascade of VGG-Net like classifier
738	Disease diagnosis	Benign, malignant	CNN-based classifier with fourier pre-processing
414	Disease diagnosis	Benign, malignant	Combination of CNN and LSTM classifiers
739	Disease diagnosis	Tumour, normal	Metric learning using similarities
220	Classification	Clinically relevant classes	CNN-based patch classifier with aggregation
256	Classification	Benign, in-situ, invasive carcinoma	Scale-based CNN classifier
585	Classification	Normal, benign, in situ, invasive carcinoma	Combination of patch and image level CNN
635	Classification	Normal, benign, DCIS, invasive ductal carcinoma (IDC)	Context-aware stacked CNN
740	Classification	Benign, in-situ, invasive carcinoma	CNN-based classifier with dimensionality reduction
63	Classification	Benign, in-situ, invasive carcinoma	MIL with auto-regression
416	Classification	Benign, in-situ, invasive carcinoma	Parallel network with CNN-RNN
257	Classification	Benign, in-situ, invasive carcinoma	Hybrid Convolutional and Recurrent NN
301	Classification	Benign, in-situ, invasive carcinoma	CNN-based patch classifier
741	Classification	Benign, in-situ, invasive carcinoma	Convolutional capsule network
621	Classification	Benign, in-situ, invasive carcinoma	Combination of residual and spatial model
742	Classification	Benign, in-situ, invasive carcinoma	Custom CNN patch classifier
213	Classification	Benign, in-situ, invasive carcinoma	CNN classifier with bidirectional LSTM
743	Classification	Tumor, non-tumor	Custom CNN-based classifier
330	Nuclei segmentation	N/A	UNet segmentation with GAN patch refinement

(*continued*)

References	Tasks	Disease Specification	Methods
[380]	Nuclei segmentation	N/A	UNet segmentation with CycleGAN domain transfer
[350]	Nuclei segmentation	N/A	Ensemble of several CNNs with different architectures
[258]	Nuclei segmentation	Normal, malignant, dysplastic epithelial, fibroblast, muscle, inflammatory, endothelial, miscellaneous	Sequential CNN network
[630]	Nuclei segmentation	Normal, malignant, dysplastic epithelial, fibroblast, muscle, inflammatory, endothelial, miscellaneous	Custom encoder-decoder model
[591]	Detection, Segmentation	DCIS and invasive cancers	IM-Net for DCIS detection and segmentation
[278]	Tumour segmentation	Tumor, Normal	U-Net segmentation with GoogleNet patch level feature extraction
[361]	Tumour segmentation	Normal, benign, in situ carcinoma or invasive carcinoma	Global and local ResNet feature extractors, FCN with auto zoom
[353]	Tumour segmentation	Normal, benign, in situ carcinoma or invasive carcinoma	Global and local ResNet feature extractors, FCN with auto zoom
[367]	Segmentation	Breast cancer	U-Net, Residual Multi-Scale (RMS)
[342]	Segmentation	Ki67 detection for breast cancer	U-NET, piNET
[560]	Tumour segmentation	Non-tumor, ductal carcinoma in situ (DCIS), invasive ductal carcinoma (IDC), lobular carcinoma in situ (LCIS), invasive lobular carcinoma (ILC)	Ensemble of CNN with atrous spatial pyramid encoding
[305]	Classification	Prediction of HER2 status and trastuzumab response	CNN classifier with Inception v3, Transfer learning
[308]	Tissue subtype classification	Classifying cancerous tissues	weakly supervised approach, Multiple Instance Learning (MIL) model, Transfer learning pre-trained models (Trans--AMIL), VGG, DenseNet, ResNe
[628]	Tissue subtype classification	24 different tissues	Ensemble of different CNN architectures with transfer learning
[438]	Tissue subtype classification	Proliferative without atypia, atypical hyperplasia, ductal / lobular carcinoma in situ, invasive carcinoma	Multi-class MIL
[638]	Disease Diagnosis	Normal, Benign, Atypical, Ductal Carcinoma In Situ, Invasive	CNN-based classifier using graphical representation
[429]	Tissue subtype classification	Estrogen, Progesterone, Her2 receptor	Style invariant ResNet classifier
[27]	Tissue subtype classification	Negative, micrometastasis, macrometastasis, isolated tumor cell cluster (ITC)	Custom CNN-based classifier
[340]	Tissue subtype classification	Adipose regions, TDLU regions, acini centroid	UNet based CNN classifier
[639]	Classification, Segmentation	Benign, Atypical (flat epithelial atypia, atypical ductal hyperplasia), Malignant (ductal, in situ, invasive)	Graphical neural networks
[632]	Tissue subtype classification	Basal-like, HER2-enriched, Luminal A, and Luminal B	CNN-based classifier with PCA
[744]	Classification	Malignant, normal	CNN classifier with transfer learning
[209]	Segmentation	Stain normalization	Style transfer using CycleGAN, Relevance vector machine
[425]	Segmentation	Realistic patch generation	GAN based architecture
[745]	Classification	Processing technique comparison	Comparison of color normalization methods
[325]	Classification	19 histological types, HER2-, HER2 + , PR + , PR-	Graph CNN slide level classifier
[327]	Classification	normal, benign, in situ, and invasive	Dynamic Deep Ensemble CNN
[456]	Binary Classification	Breast cancer	Transformer based MIL (TransMIL)
Liver			
[554]	Disease diagnosis, Nuclei segmentation	G0, G1, G2, G3, G4 (HCC grade)	BoF-based classifier
[490]	Disease diagnosis	Hepatocellular/cholangio carcinoma	CNN-based end to end diagnostic tool
[607]	Nuclei segmentation	N/A	CycleGAN based segmentation
[336]	Tissue segmentation	Background, tumor, tissue and necrosis	UNet with color deconvolution
[746]	Tissue segmentation	Steatosis droplet	Mask-RCNN segmentation
[646]	Classification	Stain normalization	Relevance vector machine
[430]	Classification	Hematoxylin, eosin, unstained RBC	Linear discriminant classifier
[431]	Classification	Stain style transfer	CycleGAN based architecture, CycleGAN with perceptual embedding consistency loss
Lymph Nodes			
[205]	Detection	Detection and quantification of Lymphocytes	U-Net and SegNet with VGG16 and Resnet50 and pre-trained weights of ImageNet
[231]	Detection	Metastasis	Ensemble of CNNs with different architectures
[747]	Detection	Metastasis	Custom CNN for discrimitive feature learning
[264]	Detection	Metastasis	DCNN classifier
[97]	Detection	Metastasis	CNN-based patch classifier
[748]	Detection	Metastasis (Isolated / micro / macro)	Variants of ResNet/GoogleNet
[558]	Disease diagnosis	Hyperplasia, small B cell lymphomas	Bayesian NN with dropout variance
[364]	Tissue segmentation	Keratin, subepithelial, epithelial, background	Custom CNN model
[360]	Tumor segmentation	normal, metastatic	Representation-Aggregation Network with LSTM
[749]	Classification, Segmentation	Domain shift analysis for breast tumour	Comparison of CNN models, data augmentation, and normalization techniques
[203]	Classification, Segmentation	Stain normalization	Deep Gaussian mixture color normalization model
[427]	Classification, Segmentation	Stain normalization	GAN, stain-style transfer network
[750]	Classification, Segmentation	Similar image retrieval	Siamese network
[469]	Classification	metastatic tissue	Contrastive predictive coding, Autoregressor PixelCNN

(continued on next page)

(*continued*)

References	Tasks	Disease Specification	Methods
[166]	Prognosis of lymph node metastasis	lymph node metastasis of papillary thyroid carcinoma	Transformer-Guided Multi-instance Learning, Attention-based mutual knowledge distillation
Prostate/Ovary			
[587]	Tissue subtype classification	Gland, Gland border region, or Stroma	SVM with RBF kernel, CNN classifiers
[347]	Tissue subtype classification	stromal areas (ST), benign/normal (BN), low-grade pattern (G3) and high-grade pattern (G4) cancer	CNN classifiers using a modified U-Net architecture
[348]	Detection	Tumor, No-tumor	Generative Adversarial Network named GAN-CS
[73,267]	Detection	Tumor, Normal	CNN-based classifier with transfer learning, MIL model
[263]	Detection	Pancreatic adenocarcinoma	Custom CNN classifier
[665]	Detection	Probabilistic boosting tree with active learning	
[669]	Detection	benign glandular, nonglandular, tumor tissue	Pre-trained and validated model based on InceptionResNetV2 convolutional architecture
[382]	Disease diagnosis	Prostate cancer (benign, LG, HG)	Region based CNN classifier
[751]	Disease diagnosis	Gleason Score (G6-G10)	Comparison of commonly used CNN models
[751]	Disease diagnosis	Gleason Score (0-5)	Active Learning Framework
[659]	Disease diagnosis	Invasive carcinoma, Benign (glandular, non-glandular, stromal, seminal vesicles, ejaculatory ducts, high-grade prostatic intraepithelial neoplasia, HGPIN), intraductal carcinoma	NASNetLarge classifier with transfer learning
[661]	Disease diagnosis	Gleason grading (3, 4, 5)	ResNet classifier with symmetric domain adaptation
[667]	Disease diagnosis	Gleason grading (3, 4, 5)	Two-stage deep learning system
[752]	Disease diagnosis	Gleason grading (3, 4, 5)	Multi-scale U-Net for pixel-wise Gleason score prediction
[208]	Disease diagnosis	Gleason grading (3, 4, 5)	CNN classifier with CycleGAN
[442]	Disease diagnosis	Gleason grading (3, 4, 5)	Attention-based MIL classifier
[663]	Disease diagnosis	Benign, Gleason Grades 3-5	Ensemble of CNN classifiers
[664]	Disease diagnosis	Gleason grades 1-5	K-NN classifier using statistical representation of Homology Profiles
[119]	Disease diagnosis	High-grade serous ovarian, clear cell ovarian, endometrioid (ENOC), low-grade serous, mucinous carcinoma	Two-staged CNN with RF classifier
[753]	Disease diagnosis	Low risk Gleason score (6-7), high risk (8-10)	Information retrieval using TF-IDF
[561]	Gland segmentation	Gleason Score (1-5)	Image analysis using mathematical morphology
[266]	Tissue subtype classification	Diagset A : scan background (BG), tissue background (T), normal, healthy tissue (N), acquisition artifact (A), or one of the 1-5 Gleason grades (R1-R5), Diagset B: presence of cancerous tissue on the scan (C) or lack thereof (NC), Diagset C:containing cancerous tissue (C), not containing cancerous tissue (NC), or uncertain and requiring further medical examination (IHC)	CNNs, a variant of fully-convolutional VDSR networks, AlexNet, VGG16/19, ResNet50, InceptionV3
[204]	Tissue subtype classification	Epithelial, stromal	Multiresolution segmentation
[666]	Tissue subtype classification	Gleason grade 3-5, Benign Epithelium (BE), Benign stroma (BS), Tissue atrophy (AT), PIN	Cascaded approach
[418]	Clinical validation	Cancer, non-cancerous	Two-stage MIL-RNN classifier
[443]	Prediction of treatment response	Positive, negative (response to platinum chemotherapy)	Ensemble of RBF + SVM and MIL-based CNN classifier
Kidney			
[614]	Detection	Tumor, normal	DCNN based classifier
[615]	Detection	Antibody mediated rejection	CNN-based classifier
[421]	Classification	Abnormalities of blood chemistry, Kidney function and dehydration	k Nearest Neighbour (kNN), Long short-term memory (LSTM)
[344]	Classification, Segmentation	Cancer	Modified U-Net CNN model
[388]	Detection	Glomeruli boundaries	CNN-based classifier with center point localization
[754]	Detection	Glomeruli and Nuclei	Anchor Free Backbone + center point localization
[381]	Prognosis	Survival rate for renal cell carcinoma	Random forest classifier for nuclei detection
[755]	Prognosis	Survival rate	Kaplan-Meier analysis
[84]	Classification	Sclerosed glomeruli, tubulointerstitium	Laplacian-of-Gaussian method for blob detection
[387]	Classification	Glomerulus, lymphocytes	Different architectures of standard CNN with patient privacy preservation
[389]	Classification	Non-glomerular tissue, normal glomeruli, sclerosed glomeruli	U-Net based classifier
[315]	WSI representation and classification	Kidney Chromophobe Renal Cell Carcinoma (KICH), Kidney Renal Clear Cell Carcinoma (KIRC) and Kidney Renal Papillary Cell Carcinoma(KIRP)	hierarchical global-to-local clustering, weakly-supervised
[613]	Segmentation	Glomeruli	Cascaded UNet model
[152]	Segmentation	Glomeruli, sclerotic glomeruli, empty Bowman's capsules, proximal tubuli, distal tubuli, atrophic tubuli, undefined tubuli, capsules, arteries, interstitium	Ensemble of U-Net
[456]	Multiple Classification	3 cancer types	Transformer based MIL (TransMIL)
Lung			
[234]	Detection	Lymphocyte richness	Unsupervised classifier using convolutional autoencoder
[332]	Segmentation, Classification	Mitosis, ND, LUAD, LUSC	Deep residual aggregation network with U-Net
[651]	Classification	Squamous and nonsquamous nonsmall cell	Inception V3
[345]	Detection	Tumor, cell Detection	U-Net
[563]	Classification	Cancer	Decision Tree, AdaBoost and XGBoost
[491]	Disease diagnosis	LUAD, LUSC	Deep CNN with transfer learning
[756]			CNN ensemble with random forest aggregation

(*continued*)

References	Tasks	Disease Specification	Methods
251			ML models with Cox hazard model
332			Deep residual aggregation with U-Net
446	Prognosis	Malignant, Normal	MIL-based CNN classifier
75	Disease diagnosis	Lepidic, acinar, papillary, micropapillary, solid, benign	CNN-based patch classifer
240	Disease diagnosis	Acinar, micropapillary, solid, cribriform, non-tumor	CNN-based classifier
491	Prognosis	STK11, EGFR, SETBP1, TP53, FAT1, KRAS, KEAP1, LRP1B, FAT4, NF1	Deep CNN with transfer learning
757	Segmentation	Characterizing spatial arrangement features of the immune response	Watershed-based model
214,330,380	Segmentation	N/A Nuclei of tumor cells, stromal cells, lymphocytes, macrophages, blood cells, karyorrhexis	UNet segmentation with GAN patch refinement, UNet segmentation with CycleGAN domain transfer Mask-RCNN based classifier
534	Classification	Tumor cell, stromal cell, lymphocyte	CNN
758	Classification	LUAD, LUSC	Pre-trained DenseNet
315	WSI representation and classification	Lung Adenocarcinoma (LUAD) and Lung Squamous Cell Carcinoma (LUSC)	hierarchical global-to-local clustering, weakly-supervised
251	Prognosis	Pathology grade, non-small cancer Recurrence prediction for non-small cell cancer	Various ML models with Cox hazard model
89		Lung squamous cell carcinoma Tumor cell, stromal cell, lymphocyte	CNN-based classifier
251			Custom CNN
332			Cox regression model
564	Prognosis	Squamous cell	Self-supervised pre-trained model, HANet
318	Segmentation	Stain normalization	CNN, LSTM based feature aware normalization
759	Classification	Cancer, normal	High resolution heatmaps from CNN
456	Binary Classification	LUSC/LUAD subtypes classification	Transformer based MIL (TransMIL)
456	Detection	carcinomas and benign tissue	Transfer Learning
Paneras			
250	Classification	Feature correlation analysis Nuclei, antigen, cytoplasm, blood, ECM	CNN-based classifier with transfer learning Non-linear tissue component discrimination
334	Classification	Immunopositive tumor, immunonegative tumor, non-tumor	U-Net
326	Tissue Classification	benign lung tissues (LN), lung adenocarcinomas (LAC), lung squamous cell carcinomas (LSCC), benign colonic tissues (CN), and colon adenocarcinomas (CAC)	Pyramid Deep-Broad Learning
Thyroid			
557	Classification	Follicular lesion (FA, FTC), normal	Radial based SVM classifier
454	Classification, Detection	Unknown/have mutation(BRAF +), dont have mutation (BRAF-)/ have fusion (NTRK +), dont have fusion (NTRK-)	Attention-based deep multiple instance learning classifier, DenseNet121
455	Classification, Detection	Tumor, Healthy/papillary, follicular, poorly differentiated, anaplastic/have mutation(BRAF +), dont have mutation (BRAF-)	Multi Instance Learning (MIL)
Stomach/Colon			
432,440,441	Detection	Cancer	Combination of CNN and MIL, InceptionV3 classifier with conditional GANs, Generalized mean model with parallel MIL
287	Detection	Microsatellite instability	ResNet with transfer learning
446	Prognosis	Malignant, normal	MIL-based CNN classifier
77	Detection	Nucleus	Space-constrained CNN
236	Detection	Adenocarcinoma, normal	CNN-based classifier
296	Detection	Carcinoma, benign	CNN-based classifier
686	Detection	High-grade intraepithelial neoplasia	Deep learning classifier with ResNet backbone
269	Detection	Gastric cancer	DLA34, Hybrid and Weak supervision Learning method
428	Detection	Tumor-bearing tissue, Non-tumor tissue	SuffleNet with end-to-end learning method
221	Detection	BRAF mutational status and microsatellite instability	Swarm Learning
468	Classification	N/A	Encoder, Resnet18
343	Classification	Colorectal carcinoma, Colorectal cancer	Weakly supervised neural network named comparative segmentation network (CompSegNet), U-Net
326	Classification of tissue	Cadipose (ADI), background (BACK), debris (DEB), lymphocytes (LYM), mucus (MUC), smooth muscle (MUS), normal colon mucosa (NORM), cancer-associated stroma (STR), and colorectal adenocarcinoma epithelium (TUM)	Pyramid Deep-Broad Learning
368	Segmentation	colorectal cancer	CNN, Sliding window method, U-Net + +
304	Segmentation, Classification	Colorectal cancer	U-Net16/19 network with a VGG-16/19 net as backbone
681	Disease diagnosis	Non-epithelial normal, normal gastric epithelium, neoplastic gastric epithelium/-tubular gastric adenocarcinoma, solid-type gastric adenocarcinoma, diffuse/-discohesive gastric carcinoma	Custom CNN classifier
142	Disease diagnosis	Adenocarcinoma, mucinous carcinoma, serrated carcinoma, papillary carcinoma, and cribriform comedo-type carcinoma	CNN-based classifier with transfer learning
224	Disease diagnosis	Adenocarcinoma, adenoma, non-neoplastic	CNN classifier with RNN aggregation
675	Disease diagnosis	Colorectal cancer	CNN
293	Disease diagnosis	Celiac disease, nonspecific duodenitis	ResNet patch classifier
445	Disease diagnosis	Cancer	Multiple instance learning
328	Disease diagnosis	Adenocarcinoma, poorly cohesive carcinoma, normal gastric mucosa	Multi-scale receptive field model
439	Disease diagnosis	Dysplasia, Cancer	Multi-instance deep learning classifier
82	Disease diagnosis	Healthy, adenomatous, moderately differentiated, moderately-to- poorly differentiated, and poorly differentiated	Multi-task classifier
678	Disease diagnosis	Adenocarcinoma (AC), tubulovillous adenoma (AD), healthy (H)	Downstream classifiers (ResNet18, SVM)
80,83,84	Segmentation	Benign, malignant	Deep contour-aware networks using transfer learning, CNN
81,359	Segmentation	Carcinoma	Random polygon model, Multi-scale CNN with minimal information loss

(*continued on next page*)

(*continued*)

References	Tasks	Disease Specification	Methods
82,760	Segmentation	Lumen, cytoplasm, nuclei	SVM classifier with RBF kernel, Regions containing glandular structures, Multi-task classifier
386,761	Segmentation	Colorectal Cancer	Two-parallel-branch DNN
368	Segmentation	Colon: adenocarcinoma, high-grade adenoma with dysplasia, low-grade adenoma with dysplasia, carcinoid, and hyperplastic polyp	Ensemble method, wavelet transform (WWE)
260	Segmentation, Classification	Epithelial cell, Connective tissue cell, Lymphocytes, Plasma cells, Neutrophils, Eosinophils	ResNet-34 network with contrastive learning, HoVerNet
688	Segmentation, Classification	high/ low mutation density, microsatellite instability/ stability, chromosomal instability/ genomic stability, CIMP-high/ low, BRAF mutation/wild-type, TP53 mutation/ wild-type, KRAS wild-type/ mutation	ResNet-18 network/ Adapted ResNet34/ HoVerNet, Weakly supervised learning
303	Classification	Colorectal Cancer	customized CNNs, pretrained model VGG, ResNet, Inception, IRV2
383	Segmentation	Epithelial, inflammatory, fibroblast, miscellaneous, unassigned	Spatially Constrained CNN
278	Segmentation	Tumour	U-Net segmentation with GoogleNet patch level feature extraction, Custom CNN with random forest regression
292	Segmentation	Gastric cancer	CNN models with transfer learning
363	Segmentation	colon/ adenoma, adenocarcinoma, signet, and healthy cases	combination of PHPs, CNN features
687	Classification	tumor, stroma	random forests
86	Prognosis	Stroma	CNN based on neuronal activation in tissues
88	Prognosis	Five year survival rate	CNN/LSTM bassed regression classifier
695	Prognosis	EBV-associated gastric cancer	deep convolutional neural network backboned by ResNet50
453	Classification	cancerous, high-grade dysplasia, low-grade dysplasia, hyperplastic polyp, normal glands	CNN based classifier with a Multi-Scale Task Multiple Instance Learning (MuSTMIL)
78,762–765	Classification	Hyperplastic polyp, sessile serrated polyp, traditional serrated / tubular / tubulovillous / villous adenoma	Radial based SVM classifier, CNN classifier with dropout variance and active learning, SqueezeNet with transfer learning ResNet patch classifier
763,764	Classification	tumor epithelium, simple stroma, complex stroma, immune cell conglomerates, debris and mucus, normal mucosal glands, adipose tissue, background	Bilinear CNN classifier, Convolutional networks (ConvNets)
682	Classification	Normal epithelium, normal stroma, tumor	VGG16, hierarchical neural network
224	Classification	Adenocarcinoma, adenoma, or non-neoplastic	InceptionV3 patch classifier
279	Classification	Epithelial, Spindle-shaped, Necrotic, Inammatory	SC-CNN with Delaunay Triangulation
766	Segmentation	Colorectal cancer, Gastroesophageal junction (dysplasic) lesion, Head and neck carcinoma	DCNN with residual blocks
678	Classification	Adenocarcinoma, corresponding to noticeable CRC, Tubulovillous adenoma, a precursive lesion of CRC, Healthy tissue	Bayesian CNNs (B-CNNs),
311	Classification	cancer, non-cancer	Transfer Learning
420	Disease diagnosis	Gastric cancer	GCN-RNN based feature extraction and encoding
767	Segmentation	Tumor	GAN
768	Prognosis	Adenocarcinoma, disease-specific survival time	ECA histomorphometric-based image classifier
426	Synthesis of large highresolution images	Colorectal Cancer	Novel framework called SAFRON (Stitching Across the FROntier Network)
Multi-Organ			
289	Classification	Benign, malignant	CNN based classifier
64	Classification	Kidney, Lymph nodes, Lung/ Chromophobe, clear cell carcinoma, papillary	Weakly supervised ResNet50 with transfer learning
277	Segmentation	Bladder, Breast, Kidney, Liver, Prostate, Stomach/ Normal, malignant, dysplastic epithelial, fibroblast, muscle, inflammatory, endothelial, miscellaneous	Modified Preact-ResNet50
258	Segmentation	Nuclear, non-nuclear, boundary	CNN-based classifier with AJI evaluation
476	Detection	Liver, Prostate/ Tumor, normal	Custom CNN architecture
676	Classification	Epithelial, stromal tissues	DCNN classifier
769	Classification	Brain, Breast, Kidney/ DCIS, ERBB2 +, triple negative	Transfer learning using multi-scale convolutional sparse coding
290	Detection	Bladder, Breast, Lymph nodes, Lung	CNN-based classifier with transfer learning
62	Detection	Basal, Breast, Prostate/ Cell carcinoma, Metastasis	RNN classifier with multiple instance learning
71	Classification	Micro/Macro metastasis	RNN classifier with MIL
685	Detection	Breast, Stomach/ Tumor, normal	Custom CNN classifier
370	Segmentation	Bladder, Breast, Liver, Prostate, Kidney, Stomach/ Edge, foreground, background	Domain-Adversarial Neural Network
332	Segmentation, Classification	Brain, Lung, Esophagus/ Mitosis, Lymphocyte richness, LUAD, LUSC	Deep residual aggregation network with U-Net segmentation
202	Segmentation	Breast, Esophagus, Liver/ Stain normalization	Relevance vector machine
770	Classification	colon, kidney, ovarian cancer, lung adenocarcinoma, gastric mucosa, astrocytoma, skin cutaneous melanoma, breast cancer/ Nuclei, antigen, cytoplasm, blood, ECM	Non-linear tissue component discrimination
452	Classification	Different organs of rats/Exploring the morphological changes in tissue to biomarker level	CNN, MIL, multi-task learning
307	Classification	Adrenal gland, Bladder, Breast, Liver, Lung, Ovary, Pancreas, Prostate, Testis, Thyroid, Uterus, Heart	CNN models with transfer learning/ ResNet-152 pretrained on ImageNet and GTEx
206	Classification	Colon, Breast/molecular fingerprint of a deficient mismatch (Microsatellite stability (MSS)/ Microsatellite instability (MSI)	CNN models with transfer learning method
306	Classification, Segmentation	blood, breast, lymph, colon, bone, prostate, liver, pancreas, bladder, cervix, esophagus, head, neck, kidney, lung, thyroid, uterus, bone marrow, skin, brain, stomach, and ovary	Unsupervised contrastive learning, residual networks pretrained with self-supervised learning
356	Segmentation	Brain, Breast/ Nuclei	Custom encoder-decoder model
271	Prognosis	Bladder/ Lung, Low TMB, Medium TMB, High TMB	Deep transfer learning, SVM with Gaussian kernel
771	Classification	Bladder, Brain, Breast, Bronchus and lung, Connective, subcutaneous and other soft tissues, Kidney, Liver and intrahepatic bile ducts, Pancreas, Prostate gland, Thyroid gland/ Cancer	ResNet18, self-supervised BYOL method, Clustering tiles using k-means clustering

(*continued*)

References	Tasks	Disease Specification	Methods
[349]	Segmentation, Classification	Colon, Liver, lymph node sections	An ensemble of FCNs architectures/U-Net with DenseNet, ResNet
[772]	Segmentation cellular nuclei	Multiple	Cross-patch Dense Contrastive Learning
[562]	Prognosis, Cancer Grade Classification	brain and kidney	CNN, GCN, SNN
[773]	Segmentation	Colon, Lymph Node	Kullback-Leibler (KL) divergence with classifier
[479]	Segmentation	Breast, Bone, Tissue	Performing Neural architecture search(NAS)
[774]	Segmentation of nuclei and cytoplasm	Lung, Bladder	Multi-task model
[775]	Classification	Axillary lymph nodes, Breast/Metastasis, Colorectal cancer	Adversarial autoencoder, Progressive growing algorithm for GANs, Resnet18 with pre-trained ImageNet weights
[601]	Classification, Detection	Skin/ cutaneous melanoma(SKCM), Stomach/ adenocarcinoma(STAD), Breast/ cancer(BRCA), Lung/ adenocarcinoma(LUAD), Lung/ squamous cell carcinoma (LUSC)	Convolutional neural networks(CNNs), Birch clustering
[776]	Classification of tissue	Stomach, Colon, Rectum	CNN + Pathology Deformable Conditional Random Field
[472]	Classification of tissue	Liver, Lung, Colon, Rectum	Contrastive learning (CL) with latent augmentation (LA)
[777]	Classification	Stomach, Intestine, Lymph node, Colon	label correction + NSHE scheme
[778]	Detection	Renal/ cell carcinoma (RCC), lung/nonsmall cell cancer (NSCLC), Breast/cancer lymph node metastasis	Attention-based learning, Instance-level clustering
[779]	Classification	Breast, Colon /Tumor metastasis and Tumor cellularity quantification	ResNet-18
[379]	Classification, Detection	Breast cancer, Colorectal adenocarcinoma, Colorectal cancer	Co-representation learning (CoReL), Neighborhood-aware multiple similarity sampling strategy
[341]	segmentations	Nuclei in pancreatic, tubules in colorectal, epithelium in breast	U-net
[450]	Classification	Brain, Endocrine, Gastro, Gynaeco, Liver, pancreas, Urinary tract, Melanocytic, Pulmonary, Prostate Cancer	DenseNet121, KimiaNet
[780]	Detection	cell nuclear	Robust Self-Trained Network(RSTN) trained on distance maps(DMs)
[384]	Segmentation, Classification	Nuclei in the breast, prostate/Benign, ADH, DCIS	GNN models
[309]	Classification, Segmentation	Lung and Skin/nuclei	ResGANet
[650]	Prognosis	HPV +, HPV-, survival class	MIL classifier with discriminant analysis
[448]	Detection	18 primary organ/Tumor	MIL with attention pooling
[239]	Detection	Tumor, normal	Sparse coding and transfer learning
[74]	Detection	Tumor, normal from 23 cohorts	CNN-based classifier with transfer learning
[704]	Detection	Loose non-tumor tissue, dense non-tumor tissue, normal tumor tissue	Custom CNN classifier
[376]	Detection	Mitosis centroid	G-CNN for rotational invariance
[312]	Detection, Segmentation	Colon, Rectum	Concept Contrastive Learning
[302]	Disease diagnosis	Lung, Breast, Colorectal, Glioma, Renal, Endometrial, Skin, Head and neck, Prostate, Bladder, Thyroid, Ovarian, Liver, Germ cell, Cervix, Adrenal/metastatic tumors and Cancer	MIL
[273]	Segmentation	Breast, Pancreatic, Colon/Cell Nuclei, Tubules, Epithelium	u-net
[207]	Segmentation	prostate, colon, breast, kidney, liver, bladder, stomach/Nuclei	U-Net
[471]	Segmentation	Bladder, Breast, Colorectal, Endometrial, Ovarian, Pancreatic, Prostate/Nuclei	Hovernet on tiles, Nuc2Vec with a ResNet34 with contrastive learning method
[619]	Segmentation	Brain, Kidney,	semantic segmentation + Xception
[559]	Segmentation	Breast, liver, kidney, prostate, bladder, colon, stomach/Cell boundary pixels, Nuclei	Hard-boundary Attention Network (HBANet) with background weaken module (BWM)
[369]	Segmentation, Classification	Bladder, Breast, Colorectal, Endometrial, Ovarian, Pancreatic, Prostate/Nucleus boundaries/Normal epithelial, malignant/dysplastic epithelial, fibroblast, muscle, inflammatory, endothelial, miscellaneous	CNN pretrained on ImageNe/End-to-end learning
[346]	Classification	Thyroid frozen sections, Colonoscopy tissue, Cytological cervical pap smear/ benign, non-benign	VGG16bn, ResNet50, U-net, with stochastic selection and attention fusion
[781]	Classification	Colon, Breast/ non-discriminative and discriminative regions	CNN classifier, ResNet18, Weakly supervised learning, Max-Min uncertainty
[376]	Classification, Segmentation	Nuclear boundaries, Benign, malignant	G-CNN for rotational invariance
[172]	Classification	Basaloid, Melanocytic, Squamous	Multi-stage CNN classifier
[782]	Classification	Colorectal glands, Tumor, normal	Dense steerable filter CNN for rotational invariance
[444]	Segmentation	Contoured tumor regions	Resnet classifier with transfer learning
[703]	Classification	Skin melanoma, stomach adenocarcinoma, breast cancer, lung adenocarcinoma, lung squamous cell carcinoma	Custom CNN using human-interpretable image features (HIF)
[783]	Classification	20 classes for muscle, epithelial, connective tissue	Inception Residual Recurrent CNN
[32]	Tissue subtype classification	Adipose (ADI), background (BACK), debris (DEB), lymphocytes (LYM), mucus (MUC), smooth muscle (MUS), normal colon mucosa (NORM), cancer-associated stroma (STR), colorectal adenocarcinoma epithelium (TUM)	ResNet based classifier
[385]	Nuclei segmentation	Breast, Colon, Liver, Prostate, Kidney, Stomach, Colorectal, Bladder, Ovarian	CNN model, VGG-19 network
[268]	Segmentation	Lung, Breast	Multiple Instance Learning (MIL), self-supervised contrastive learning in SimCLR setting, feature vector aggregation
[316]	Prognosis	Prediction of cancer rate survival in the Bladder, Breast, Lung, Uterus, Brain	Graph Convolutional Neural Net(GCN)

(continued on next page)

(*continued*)

References	Tasks	Disease Specification	Methods
[207]	Nuclei segmentation	prostate, colon, breast, kidney, liver, bladder, stomach	A convolutional U-Net architecture
[333]	Nuclei segmentation	Nuclear boundaries	U-net based architecture
[478]	Nuclei segmentation	Nuclear boundaries	Modified HoVer-Net segmentation
[351]	Nuclei segmentation	Nuclear boundaries	CNN-based attention network
[300]	Segmentation	3-level hierarchy of histological types	Pixel level semantic segmentation
[198]	Segmentation	Tissue, background, edge artifacts, inner artifacts, inner/external margin	Custom FCNN
[259]	Segmentation	Lymphocytes, necrosis	Semantic segmentation CNN classifier
[169]	Disease diagnosis	usual ductal hyperplasia, ductal carcinoma in-situ	Deep-learning based CAD tool for pathologists
[424]	Nuclei segmentation	Positive/negative in nuclei boundaries	Conditional GAN
[358]	Nuclei segmentation	Nuclear boundaries	CNN-based Boundary-assisted Region Proposal Network
[357]	Nuclei segmentation	Nuclei, other	CNN-based multi-branch network classifier
[199]	Detection	Mitosis and metastasis detection	U-Net based normalization
[168,331]	Nuclei segmentation	normal epithelial, myoepithelial, invasive carcinoma, fibroblasts endothelial, adipocytes, macrophages, inflammatory	U-Net with regression loss
[335]	Nuclei segmentation	Nuclei body, nuclei boundary, background Background removal Nuclei boundary	UNet based classifier with self-supervised learning UNet with transfer learning Custom encoder-decoder network
[120]	Tissue subtype classification	60 types of tissues from a various datasets	ResNet50 feature encoder/decoder for 11 tasks
[655]	Detection	Tumor, normal	ResNet based patch classifier
[616]	Classification	Skin/Skin lesions, Chest/ Benign, malignant, Kidney/Chromophobe, clear cell, papillary carcinoma	Conditional Progressive Growing GAN (PG-GAN/ResNet-50)
[212]	Classification	Neural image compression for Rectal carcinoma	CNN classifier with encoder compression network
[392]	Pathology report information extraction	Tumor description relating to primary cancer site, laterality, behavior, histological type, and histological grade	Ensemble of multi-task CNN
[195]	Detection	Blur detection	Combination of CNN and Random Forest regressor
[196]	Classification	15 types based on focus level	Lightweight CNN
[705]	Segmentation	Molecular feature extraction	Multi-layer perceptron with aggregation
[700]	Classification	Deblurring	Encoder-decoder with VGG-16 blur type classifier
[689]	Classification	WSI Classification	Multi-scale Context-aware MIL, Multi-level Zooming
[65]	Classification	BRCA subtyping, NSCLC subtyping, RCC Subtyping	Vision Transformer
[784]	Classification	Classification of glioma and non-small-cell lung carcinoma cases into subtypes	Two-level model consisting of an Expectation Maximization based method combined with CNN and a decision fusion model
[65]	Prognosis	Survival prediction of IDC, CCRCC, PRCC, LUAD, CRC, and STAD cancer types	Vision Transformer
[785]	WSI Processing	Stain normalization	Combination of segmentation and clustering for nuclear/stroma detection
[210]	WSI Processing	Stain normalization	Self-supervised cycleGAN
[352]	WSI Processing	Stain normalization	Modified Wasserstein Barycenter approach for multiple referencing
[668]	WSI Processing	Patch synthesis	Progressive GAN model
[786]	WSI Processing	Similar image retrieval	Classifier based on ANN with K-means clustering
Other			
[787]	Detection	Heart/rejection and nonrejection tissue tiles	Progressive Generative Adversarial Network + Inspirational Image Generation with a VGG-19 as a classifier
[709]	Detection	Heart failure	CNN based patch classifier
[712]	Classification	Heart/Endomyocardial disease	CACHE-Grader, SVM and K-means clustering
[710]	Classification	Skin/Cancer	random forest ensemble learning method, feature extractor using ResNeXt50
[355]	Detection	Eye/Macular edema	Fully convolutional neural network (FCN), Improved attention U-Net architecture (IAUNet)
[447]	Prognosis	N/A	Custom MIL framework with attention modules
[433]	Classification	Bone marrow/Neutrophil, myeloblast, monocyte, lymphocyte	GAN-based classifier
[693]	Classification, Detection	Bone marrow/nonneoplastic, myeloid leukemia, myeloma	Two-stage detection and classification model
[788]	Detection	Bone marrow/aspirate pathology synopses	BERT-based NLP mode, Active learning
[339]	Segmentation	Viable tumor, necrosis with/without bone, normal bone, normal tissue, cartilage, blank	UNet-based multi-magnification network
[789]	Diseases diagnosis	Bacterial disease	CNN-based classifier
[354]	Segmentation	Bone marrow/Myelopoietic cells, erythropoietic cells, matured erythrocytes, megakaryocytes, bone, lipocytes	Custom CNN
[699]	Segmentation	10 Cancer types	U-Net, Mask R-CNN for quality control
[167]	Classification	Level 1 (Epithelial, Connective Proper, Blood, Skeletal, Muscular, Adipose, Nervous, Glandular), Level 2 (23 sub-classes from Level 1), Level 3 (36 sub-classes from Level 2 classes)	Ensemble of different CNN architectures
[702]	Classification	Arteries, nerves, smooth muscle, fat	InceptionV3, Deep ranking network
[683]	Disease diagnosis	Duodenum/Celiac	CNN-based classifier
[261]	Disease diagnosis	Cervical cancer, Squamous cell carcinoma, adenocarcinoma	CNN-based patch classifier
[684]	Disease diagnosis	Duodenum/Celiac, environmental enteropathy, Esophagus/EoE, Ileum/Crohns disease	Hierarchical CNN classifier
[696]	Disease diagnosis	Squamous carcinoma	Combinations of CNN classifiers
[451]	Classification	Normal, Cervicitis, Squamous Intra-epithelial Lesion- Low and High, Cancer	Deep multiple instance learning
[354]	Classification, Segmentation	Bone marrow/Aplasia	SVM classifier with BoW
[633]	Detection	Tumor cells, stromal cells, lymphocytes, stromal fibroblasts	k-means, Hierarchical Clustering

(*continued*)

References	Tasks	Disease Specification	Methods
391	Classification	colorectal liver metastasis	Ensemble of 4 MLP and an encoder, supervised multitask learning (MTL)
378	Detection	Mitosis	Feature pyramid network
715	Detection	Acute Lymphoblastic (or Lymphocytic) Leukemia (ALL), normal/lymphoblast	Transfer Learning, CNN pretrained on a histopathology dataset, ResNet18 and VGG16 as the backbone

Compilation of information and Neural Network architectures found in different Co-Path papers categorized by task (see 9.11)

References	Disease/Organ Specification	Architecture	Datasets
Detection Task			
32,62,64,71,72,97,199,212,219,231,264,291,298,302,305, 322,366,376,419,427,478,486,586,629,635,654,685,704, 727,728,729,739,744,747,748,782	Breast cancer	Custom CNN {15}, Inception {6}, ResNet {14}, VGG {4}, U-Net {2}, Multi-stage CNN {1}, DenseNet {4}, GAN {1}, AlexNet {1}, E-D CNN {1}, CAS-CNN {1}, Attention CNN {3}, HoVer-Net {1}, MLV-DeepLabV3 + {1}, Xception {1}, Lightweight-CNN {1}	RUMC, CAMELYON16, CAMELYON17, MSK, HUP + CINJ, NHO-1, IDC-Moh, AJ-IDC, PCam, NMCSD, HASHI, TCGA, Cancer Imaging Archive, TCGA-BRCA, Yale HER2 dataset, Yale response dataset
62,71,73,267,302,418,587,665,659	Prostate cancer	Custom CNN {2}, Res Net {4}, Inception {1}, Non-DL {1}, NASNetLarge {1}	RUMC, MSK, HUH, Pro-Raciti, Pro-Doyle, CUH, UHB, Gleason 2019
62,259,302,594,606,710	Skin cancer	ResNet {3}, Inception {1}, Custom CNN {1}, E-D CNN {1}, ResNeXt {1}	SCMOI, YSM, GHS, MIP, MSK, BE-Cruz-Roa, Private
221,224,303,304,432,440,441,445,453,704,767	Colon cancer	Custom CNN {2}, Inception {1}, GAN {1}, Novel algorithm {1}, DenseNet {1}, ResNet {2}, Inception-ResNet {1}, U-Net {1}, VGG {1}, Swarm Learning {1}	SC-Xu, FAHZU, OSU, TCGA, CRC-Chikontwe, Novel Dataset, DigestPath 2019, Epi700, DACHS, TCGA-CRC, QUASAR trial, YCR-BCIP
224,236,269,338,685,686,704,	Stomach cancer	AlexNet {1}, ResNet {3}, Inception {3}, DenseNet {1}, DeepLab {1}, VGG {1}, DLA {1}, Custom CNN {1}	TCGA, SSMH-STAD, SC-Kong
271,302	Bladder cancer	Inception {1}, ResNet {2}	TCGA
302,696	Cervix cancer	Inception {1}, ResNet {2}, Inception-ResNet {1}	XH-FMMU
614	Kidney cancer	Custom CNN {1}	Pantomics
302,345,563,651,759	Lung cancer	Inception {2}, ResNet {1}, DT {1}, Ad-aBoost {1}, XGBoost {1}, U-Net {1}	TCGA(-LUAD,-LUSC), MedicineInsight, 22c3, Ventana PD-L1, Private
32	Oral cancer	Custom CNN {1}	LNM-OSCC
199,200,218,262,337,370–378	Mitosis	Custom CNN {7}, AlexNet {1}, U-Net {2}, Multi-stage CNN {2}, FCN {1}, R-CNN {1}, ResNet {2}	TUPAC16, RUMC, MITOS12, TNBC-JRC, AMIDA13, MITOS-ATYPIA14, CWRU
77,365,369,380,381,382,383,385,470,471,757,780	Nuclei	U-Net {2}, GAN {1}, Non-DL {2}, Custom CNN {2}, Hover-Net {2}, SC-CNN {1}, Robust-Self Trained Network (RSTN) {1}, RCNN {1}, VGG {1}, ResNet {2}, E-D CNN {1}	NHS-LTGU, TNBC-CI, MoNuSeg, UHZ, CRCHistoPhenotypes, TCGA, Private, BCFM, PanNuke, NuCLS, CoNSeP, NCT-CRC-HE-100K, Cleveland Clinic (CC)
80,386	Colorectal gland	FCN {2}	GLaS
199	Epithelial cell	Custom CNN {1}	PCa-Bulten, RUMC
387–389	Glomeruli	ResNet {1}, VGG {1}, AlexNet {1}, MobileNet {1}	Kid-Wu, Kid-Yang
709,712,787	Heart failure, Heart Transplant	Custom CNN {1}, K-Means {1}, SVM {1}, VGG {1}, PG-GAN {1}	UPenn, CHOA
364	Keratin pearl	Custom CNN {1}	BCRWC
554,593	Liver, Liver fibrous region	Non-DL {1}, Autoencoder CNN {1}	Liv-Atupelage, PAIP
234	Lymphocyte-richness	Autoencoder CNN {1}	TCGA
287	Microsatellite instability	ResNet {1}	TCGA, DACHS, KCCH
390,591	Tumor-infiltrating lymphocyte	U-Net {1}, IM-Net {1}, DRDIN {1}	TCGA, DUKE
74,239,302,309,450,601	Multi-organ tumor	KimiaNet {1}, Novel algorithm {1}, ResNet {3}, Inception {1}, DenseNet {1}, Custom CNN {1}, MLV-DeepLabV3 + {1}	AJ-Lymph, TCGA, ISIC2017, LUNA, COVID19-CT
195,196,790	WSI defect	ResNet {2}, DenseNet {1}, Novel algorithm {1}, Custom CNN {1}	Pro-Campanella, MO-Campanella, MGH, TCGA@Focus, FocusPath
715	Acute Lymphoblastic (or Lymphocytic) Leukemia (ALL)	Custom CNN {1}, ResNet {1}, VGG {1}	ADP, ALL-IDB2
Tissue Subtype Classification Task			
32,78,86,199,279,311,676,679,682,762–765	Colorectal cancer	Non-DL {1}, FCN {1}, ResNet {3}, VGG {3}, AlexNet {1}, Inception {1}, SqueezeNet {2}, BCNN {1}, Capsule CNN {1}, Custom CNN {5}, U-Net {2}	NCT-CRC-HE-100K, NCT-CRC-HE-7K, RUMC, RC-Ciompi, GLaS, CRC-TP, CRC-CDC, UMCM, DHMC-Korbar, TBB, HUH, Stanford Hospital, TCGA
27,327,429,438,632,676,769	Breast cancer	Custom CNN {1}, ResNet {1}, Novel algorithm {2}, Inception {2}, Novel CNN {1}	US-Biomax, ABCTB, TCGA, Bre-Chang, Bre-Steiner, BCSC, NKI-VGH, BACH
250,556,769	Brain cancer	VGG {1}, Novel algorithm {1}, ResNet {1}	UHN, TCGA
75,240,534	Lung cancer	ResNet {2}, AlexNet {1}, Inception {1}, Custom CNN {1}	DHMC, CSMC, MIMW, TCGA, NLST, SPORE, CHCAMS
204,289,666	Prostate cancer	Non-DL {2}, Custom CNN {1}, ResNet {1}	CPCTR, UHZ-PCa, UPenn
64,289,769	Kidney cancer	Novel algorithm {1}, ResNet {2}	TCGA, UHZ-RCC, BWH
146	Bladder cancer	ResNet {1}	CCC-EMN MIBC
681	Stomach cancer	Custom CNN {1}	SPSCI
65,167,202,289,448,628,703,771,783	Multi-organ	Non-DL {1}, Custom CNN {2}, VGG {2},	MO-Khan, KIMIA Path24, ADP, UHZ, TCGA,

(*continued on next page*)

(*continued*)

References	Disease/Organ Specification	Architecture	Datasets
		Inception {3}, ResNet {4}, K-Means {2}, XGBoost {1}, ViT {1}	KIMIA Path960, MO-Diao, BWH-TCGA-MO, CRC-100K, BCSS, BreastPathQ
77,263,277,365,470,554	Nuclei	Custom CNN {3}, ResNet {1}, Non-DL {1}, Hover-Net {2}	CRCHistoPhenotypes, CoNSeP, Liv-Atupelage, PHI, Private, PanNuke, NuCLS
224,365,717	Epithelial	Inception {1}, Custom CNN {1}, Hover-Net + {1}	HUH-HH, NKI-VGH, TCGA, Private
389	Glomeruli	AlexNet {1}	$AIDPATH_A$, $AIDPATH_B$
354,433,693	Bone marrow	VGG {1}, GAN {1}, FCN {1}	BM-MICCAI15, BM-Hu, FAHZU, RUMC, EUH
252,557,605	Lesion	Non-DL {2}, Inception {1}	UPMC, BE-Hart, Bre-Parvatikar
720	Oral cavity	AlexNet {1}	ECMC
Disease Diagnosis Task			
26,63,213,220,227–229,256,257,290,291,294,295, 298,299,301,321,323,324,414,416,417,422,437, 447,488,489,508,585,621,629,635,636,638,639, 722–725,730–738,740–742,749	Breast cancer	ResNet {14}, VGG {7}, Inception {9}, Custom CNN {12}, AlexNet {3}, XGBoost {1}, MobileNet {1}, Xception {1}, DenseNet {7}, Multi-stage CNN {3}, Capsule CNN {1}, SENet {1}, Inception-ResNet {1}, VGGNet {2}, Attention CNN {3}, RCNN {1}, CaffeNet {1}, TriResNet {1}, Class Structured Deep CNN {1}, Non-DL {1}	BACH18, BreakHis, BioImaging, Ext-BioImaging, CAMELYON16, CAMELYON17, CMTHis, AP, AJ-IDC, BIDMC-MGH, PUIH, BRACS, TCGA
200,208,382,442,659,661–664,667,751–753	Prostate cancer	Custom CNN {3}, U-Net {1}, ResNet {2}, VGG {2}, Inception {1}, AlexNet {2}, Non-DL {1}, MobileNet {1}, DenseNet {1}, DCNN {1}, NASNetLarge {1}	SUH, CSMC, TCGA, NMCSD-MML-TCGA, VPC, UPenn, RCINJ
82,142,296,675,678	Colon cancer	Inception {1}, ResNet {4}, SqueezeNet {1}, AlexNet {2}, MobileNet {1}, Xception {1}	Warwick-CRC, Ext-Warwick-CRC, SC-Holland, GLaS, ZU, ULeeds
64,251,332,491,650,756,758	Lung cancer	Inception {1}, ResNet {3}, Non-DL {2}, DenseNet {1}, GCNN {1}	TCGA, MICCAI17, Stanford-TMA, NYU LMC, BWH, DHMC, ES-NSCLC
76,142,718,719	Brain cancer	Non-DL {2}, Custom CNN {1}, AlexNet {1}	TCGA, MICCAI14
490,554	Liver cancer	DenseNet {1}, Non-DL {1}	TCGA, SUMC, Liv-Atupelage
328,439	Stomach cancer	Custom CNN {1}, Multi-stage CNN {1}	GNUCH, WSGI
172,297,604	Skin cancer	ResNet {2}, VGG {1}, Multi-stage CNN {1}	DKI, Y/CSUXH-TCGA, DLCS, BE-TF-Florida-MC
415	Bladder cancer	Custom CNN {1}, Inception {1}, Multi-stage CNN {1}	TCGA + UFHSH
261	Cervix cancer	VGG {1}	TCGA
288	Esophagus cancer	ResNet {1}, Attention CNN {1}	DHMC
447	Kidney cancer	Custom CNN {1}	TCGA
290,346	Multi-organ cancer	Inception {1}, ResNet {2}, Custom CNN {1}, U-Net {1}, VGG {1}	Stanford-TMA, BIDMC-MGH, Private
650	Oral cancer	Custom CNN {1}	OP-SCC-Vanderbilt
119	Ovarian cancer	VGG {1}, Multi-stage CNN {1}	VGH
293,683,684	Non-cancer GI tract disorder	ResNet {2}, VGG {1}	DHMC-Wei, UV, SC-Sali
558,654	Lymphoma	E-D CNN {1}, Custom CNN {1}	TUCI-DUH, AJ-Lymph
Segmentation Task			
168,207,214,234,258,277,330–335,350–352,356–358, 369,370,376,424,433,470,471,478,554,559,607, 630,699,757,782	Nuclei	U-Net {6}, Custom CNN {8}, FCN {1}, ResNet {5}, GAN {4}, Non-DL {2}, Multistage CNN {1}, E-D CNN {4}, Autoencoder CNN {1}, PangNet {1}, DeconvNet {1}, Hover-Net {3}, multi-branch CNN {1}, Attention(EP, SM) CNN {1}, HBANet {1}	MICCAI15-18, TCGA, TNBC-CI, MoNuSeg, CPM-15, CPM-17, CCB, CRCHistoPhenotypes, CoNSeP, BM-Hu, FAHZU, Liv-Atupelage, DHMC, MO-Khoshdeli, AJ-N, Kumar-TCGA, TCGA-Nuclei, SOX10, UrCyt, NLST, Pan-Bai, PanNuke, NuCLS, Cleveland Clinic (CC)
80-84,168,359,386,760,761,782	Gland	FCN {2}, Non-DL {1}, Custom CNN {5}, ResNet {2}, VGG {1}, multi-branch CNN {1}, E-D CNN {1}	GLaS, Bilkent, CRAG, Priv-IHC
278,305,323,353,360–362,366,367,560,631,726	Breast tumor	Custom CNN {2}, Inception {2}, U-Net {3}, FCN 1, E-D CNN {1}, RAN {1}, DA-RefineNet {1}, DeepLab {1}, MLV-DeepLabV3 {1}	CAMELYON16, CAMELYON17, BACH18, TCGA, UHCMC-CWRU, BC-Priego-Torres, TUPAC16, AMGrad, TCGA-BRCA, Yale HER2 dataset, Yale response dataset
142,304,363,368	Colon tumor	Custom CNN {1}, VGG {1}, U-Net {2}, Non-DL {1}, AlexNet {1}	Warwick-UHCW, Warwick-Osaka, ZU, DigestPath 2019, Yeouido
336,476,593	Liver tumor	PlexusNet {1}, U-Net {1}, Autoencoder CNN {1}	TCGA, IHC-Seg, PAIP
345	Lung tumor	U-Net {1}	22c3, Ventana PD-L1
347,476,561	Prostate tumor	PlexusNet {1}, Non-DL {1}, U-Net {1}	SMS-TCGA, UUH, Private
278,292	Stomach tumor	Inception {1}, U-Net {1}, ResNet {1}	SC-Takahama, SC-Liu
142	Brain tumor	AlexNet {1}	MICCAI14
339	Bone tumor	U-Net {1}	MSKCC
270,309	Skin tumor	FCN {1}, ResNet {1}, ResGANet {1}	TCGA, ISIC2018
444	Multi-organ tumor	ResNet {1}	TCGA
84,152,344,613	Kidney tissue structure	Custom CNN {1}, U-Net {1}, cascaded CNN {1}	WUPAX, M-Gadermayr, RUMC, Mayo, AIDPATH
354	Bone marrow cell	FCN {1}	RUMC
340	Breast tissue subtype	U-Net {1}	NHS
300	Histological tissue type	Custom CNN {1}	ADP
746	Liver steatosis	ResNet {1}	Liv-Guo
337,338	Mitosis	U-Net {1}, FCN {1}	MITOS12, MITOS-ATYPIA14, AMIDA13
364,365	Oral mucosa, Oral Epithelial Dysplasia	Custom CNN {1}, Hover-Net + {1}	BCRWC,Private

(*continued*)

References	Disease/Organ Specification	Architecture	Datasets
[205,259,591]	Lymphocytes (Tumor-infiltrating,segmentation)	E-D CNN {1}, IM-Net {1}, DRDIN {1}, U-Net {1}, SegNet {1}	TCGA, DUKE, Lymphocyte Detection(from Andrew Janowczyk and Anant Madabhushi)
[198,355]	Tissue region, Fluid Lesions	Custom CNN {1}, FCN {1}, IAUNet {1}	Bándi-Dev-Set, Bándi-Dis-Set, RETOUCH
WSI Processing Task			
[200,209,380,430,431,607,662]	Domain adaptation	GAN {5}, U-Net {1}, AlexNet {1}, Custom CNN {1}, ResNet {5}	NHS-LTGU, MITOS-ATYPIA14, RCINJ, Roche, Liv-Lahiani, TU-PAC16, TCGA, DHMC, SOX10, UrCyt
[202,203,208,210,318,352,646,785]	Stain normalization	Custom CNN {2}, ResNet {1}, VGG {1}, U-NET {1}, GAN {3}, E-D CNN {1}, Multistage CNN {1}, Non-DL {4}	SUH, Leica Biosystems, MO-Khan, MGH, Lym-Bejnordi, Salvi-SCAN, MITOS-ATYPIA14
[330,424–426,489,616,668]	Patch synthesis	Custom CNN {2}, GAN {5}, PG-GAN {2}, ResNet {1}, VGG {1}, U-Net {2}	MICCAI16/17/18, Kumar-TCGA, BreakHis, NKI-VGH, TCGA, OVCARE, ISIC 2020, ChestXray-NIHCC, CRAG, Digestpath
[199,352,427,745]	Processing technique comparison	U-Net {1}, Custom CNN {2}, GAN {2}	RUMC, CAMELYON16, MITOS-ATYPIA14
[212,391]	WSI compression	Custom CNN {2}, E-D CNN {1}, GAN {1}	N/A
[678]	Data cleaning	ResNet {1}	ULeeds
[770]	Stain augmentation	VGG {1}	Kid-Cicalese
[770]	Tissue component discrimination	Non-DL {1}	TCGA, MO-JHU/US/UB
[738]	WSI transformations	Custom CNN {1}	BreakHis
[689]	WSI Classification	MIL {1}	IMP Diagnostics Lab., BRIGHT, CAMELYON16
Patient Prognosis Task			
[85,238,477,556,608]	Brain cancer	Inception {1}, VGG {1}, Custom CNN {2}, Capsule CNN {1}, ResNet {1}	TCGA
[214,251,446,534,564,608,650]	Lung cancer	Custom CNN {2}, Non-DL {2}, AttentionMIL {1}, MI-FCN {1}, HANet {1}	Stanford-TMA, TCGA(-LUSC), CHCAMS, NLST, ES-NSCLC
[86,88,446,768]	Colon cancer	VGG {2}, Inception {1}, ResNet {1}, Non-DL {1}, AlexNet {1}, SqueezeNet {1}, AttentionMIL {1}, MI-FCN {1}	NCT-CRC-HE-100K, NCT-CRC-HE-7K, HUCH, WRH-WCH, MCO
[381,447,755]	Kidney cancer	Non-DL {2}, AttentionMIL {1}	UHZ, TCGA, HPA
[390,447]	Breast cancer	U-Net {1}, AttentionMIL {1}	AJ-Lymph, TCGA
[667]	Prostate cancer	Inception {1}	NMCSD + MML + TCGA
[259]	Melanoma	Multi-stage CNN {1}	MIP, YSM, GHS
[87]	Mesothelioma	ResNet {1}	MESOPATH, TCGA
[65,316]	Multi-Organ	AttentionMIL {1}, GCN {1}, ViT {1}	TCGA, CRC-100K, BCSS, BreastPathQ
[89,721]	Recurrence prediction	Custom CNN {1}, Non-DL {1}	NSCLC-Wang, ROOHNS
Other Tasks			
[27,297,343,418,490,669]	Clinical validation, Stress Test, Quality Control, Explainability	DenseNet {1}, ResNet {2}, Inception {1}, Inception-ResNet {1}, Extended U-Net {1}	SUMC, Bre-Steiner, Pro-Raciti, DKI, TCGA, Private
[167,206,213,260,266,273,299,307,348,349, 384,428,640,699]	Dataset creation/curation and annotation, IntegratedAPI and (End-to-End) Toolkits	Custom CNN {1}, GNN {1}, VGG {3}, Inception {3}, AlexNet {1}, FCN {2}, U-Net {4}, ResNet {6}, Hover-Net {1}, DenseNet {1}, MobileNet {1}, DeepLab {1}, SLAM {1}	CMTHis, ADP, TCGA, TCGA-Nuclei, PUIH, BRACS, BACH, UZH, SICAPv2, Lizard, GTEx Dataset(V8), BreaKHis, HF(Heart failure) Dataset, DACHS, YCR-BCIP, Diagset-A, Diagset-B, Diagset-C, Painter by Numbers, miniImageNet, CRC(DX), CAMELYON(16,17), DigestPath, PAIP, Private
[655,759,766]	Data deficiency study	Inception {1}, Custom CNN {1}, ResNet {1}	TCGA, GLaS, CAMELYON16, CAMELYON17, Thagaard
[368,420,449,452,702,750,753,771]	Image retrieval/compression, Representation Learning	ResNet {1}, Inception {1}, Non-DL {2}, GCN {1}, AttnMIL {1}, Custom CNN {2}, U-Net + + {1}, Barcodes {1}, XGBoost {1}, K-Means {1}	TCGA, CAMELYON16, SC-Zheng, CRA, Han-Wistar Rats
[120,268,269,306,308,316,391,428,451–456, 468,470,471,592,599,688,778,779,781,791]	Multi-(task,instance) learning (MT,MIL), (Weak,Semi,Self)-Supervised Learning, Contrastive Learning	ResNet {9}, GCN {1}, AttentionMIL {2}, MuSTMIL {1}, SimCLR {3}, MIL {2}, D(S)MIL {1}, Pretext-RSP {1}, MoCo {1}, MLP {1}, CLAM {1}, GAN {1}, VGG {2}, DenseNet {2}, Hover-Net {2}, Custom CNN {2}, SLAM {1}, DLA {1}, TransMIL {1}	UHC-WNHST, PanNuke, AJ-Epi-Seg, OSCC, TCGA(-CRC-DX, - THCA, -NSCLC, -RCC), CAMELYON16, CAMELYON17, NCT-CRC-HE-100K, NCT-CRC-HE-7K, CPM-17, AJ-Lymph, M-Qureshi, SKMCH&RC, SKMCH&RC-M, OV-Kobel, MT-Tellez, TUPAC16, SC-Galjart, CT-CRC-HE-100K, Munich AML, MSK, MHIST, CPTAC, Kather multi-class, BreastPathQ, CRC, Novel, PanNuke, NuCLS, GlaS, OAUTHC, DACHS, YCR-BCIP, BreakHis, DEC, TH-TMA17
[212,262,342]	Proliferation scoring	Custom CNN {2}, piNET {1}	TUPAC16, DeepSlides
[433]	Cell clustering	ResNet {1}	MICCAI15, BM-Hu, FAHZU
[433]	Chemosensitivity prediction	Non-DL {1}	TCGA
[479]	Neural Architecture Search	DARTS {1}	ADP,BCCS,BACH, Osteosarcoma
[250,469,471,593,601,750]	Feature extraction/analysis, Unsupervised Learning	VGG {1}, Custom CNN {2}, Hover-Net {1}, PixelCNN {1}, AutoEncoder CNN {1}	CAMELYON16, UHN, TCGA, Private
[454,455,491,688]	Gene mutation prediction	VGG {1}, Inception {1}, AttentionMIL {2}, DenseNet {1}, ResNet {1}, Hover-Net {1}	TCGA(-CRC-DX, -THCA), DEC, PAIP, TH-TMA17, Private
[304,379,385,387,735]	Novel loss function, Novel optimizer	ResNet {3}, VGG {3}, MobileNet {1}, DenseNet {1}, U-Net {1}	BACH18, AJ-Lymphocyte, CRCHistoPhenotypes, CoNSeP, ICPR12, AMIDA13, Kather Multi-class, DigestPath 2019, CT-CRC-HE-100K
[599,676]	Patch triaging	Non-DL {1}, ResNet {1}, Pretext-RSP {1}, MoCo	BIRL-SRI, CAMEYLON16, MSK, MHIST

(*continued on next page*)

(*continued*)

References	Disease/Organ Specification	Architecture	Datasets
		{1}, MLP {1}	
392,788	Pathology report information extraction	BERT {1}, Custom CNN {1}	LTR
325	Receptor status prediction	Custom CNN {1}	TCGA
271	TMB prediction	Inception {1}	TCGA
262,641	Tumor grading	Mask R-CNN {1}, Custom CNN {1}, Non-DL {1}	TUPAC16, Post-NAT-BRCA, ILC
633	Visual analytic tool	Non-DL {1}	TCGA

A.12. Model card categorization

For comprehensive review on model cards and updated information, please refer to our GitHub repository for more information. The following lists examples of our model cards used in preparation of our survey paper.

A.12.1. Template

Model-Card for Categorizing Computational Pathology Papers

Step-1) Paper Summarization:

Summarize the paper in terms of (A) Goal/Problem of the paper to be solved; (B) Why the problem introduced by the authors is important to the community in terms of Technical Novelty, Comprehensive Experiment, New Insights, Explainability; and (C) Overall conclusion of the paper.

Step-2) Model Card Table Categorization:

The following is a model-card for each paper to populate the table accordingly. Find relevant information within each category that is reported in the paper. Try to compile it efficiently and populate each sub-type within each category.

Step-3) Citation: BibTeX Citation.

Keywords	comma separated list
Organ Application	**Organ:**
	Task:
Dataset Compilation	**Name:**
	Availability:
	Dataset Size: (#patches/#slides/#images)
	Image Resolution:
	Staining Type:
	Annotation Type: (region/patch/slide-level)
	Histological Type: (cellular/tissue ROI/etc, I.e., on what basis is it labeled)
	Label Structure: (single label/multi label)
	Class Balance: (is size of dataset balanced across each classes)
Technicality	**Model:** (architecture/transfer learning/output format)
	Training Algorithm: (end-to-end/separately staged)
	Code Availability: (give source)
Data Processing	**Image Pre-processing:** (patching, data augmentation, color normalization)
	Output Processing:
Performance Summary	**Evaluation Metrics:**
	Notable Results: Numerical result for strongest performing model.
	Comparison to Other Works: Comparison to state-of-the-art models (one sentence)
Novelty	**Medical Applications/Perspectives:**
	Technical Innovation: (algorithms for processing or deep learning, new metrics)
Explainability	**Visual Representations:** (feature distribution, heatmaps, tsne, gradCAM, pseudocode, etc.)
Clinical Validation	**Usage in Clinical Settings:** Has the work been used by pathologists in clinical setting?
	Suggested Usage: How can the work be used by pathologists?
	Performance Comparison: Has the model performance been compared to that of pathologists?
Caveats and Recommendations	• Personal comments on the paper
	• Relevant info from other papers
	• Criticism and limitations of the work

A.12.2. Samples

Paper: Pathologist-level classification of histologic patterns on resected lung adenocarcinoma slides with deep neural networks

Summary:

Classification of histological structures in lung adenocarcinoma tissue is important for patient prognosis and treatment plans. Some histological patterns (such as lepidic patterns) are associated with better survival rates, whereas others (micropapillary and solid patterns) are associated with poor prognoses. The identification of these histological patterns is a challenge, as 80% of adenocarcinoma tissue samples contain a mixture of different patterns, and the qualitative classification criteria can result in variance in diagnosis between different pathologists. Automated analysis and classification of tissue structures through convolutional neural networks has been a compelling area of research. This paper presents a variant of ResNet, ResNet18 to perform a patch-

based classification amongst the different lung adenocarcinoma histological patterns. A heatmap for the entire WSI is made using the probability score per patch, with low-confidence patches being discarded. The performance of the model is compared with 3 expert pathologists to determine relative performance. The study concludes that the model has high performance, with results on par with expert pathologists.

Categorization:

Keywords	Deep learning, convolutional neural networks, lung adenocarcinoma, multi class, ResNet
Organ Application	**Organ:** Lung
	Task: Histologic pattern classification in lung adenocarcinoma
Dataset Compilation	**Name:** Dartmouth-Hitchcock Medical Centre in Lebanon, New Hampshire
	Availability: Unavailable due to patient privacy constraints. Anonymized version available upon request.
	Dataset Size: 422 WSIs, 4 161 training ROIs, 1 068 validation patches
	Image Resolution: 20× magnification
	Staining Type: H&E
	Annotation Type: Region-level training set, patch-level validation set, slide-level test set
	Histological Type: Lepidic, acinar, papillary, micropapillary, solid, and benign.
	Label Structure: Single label
	Class Balance: Imbalanced, with significantly fewer papillary patterns in all data.
Technicality	**Model:** ResNet model with 18 layers
	Training Algorithm:
	• Multi-class cross-entropy loss
	• Initial learning rate of 0.001
	• Learning rate decay by factor of 0.9 per epoch
	Code Availability: https://github.com/BMIRDS/deepslide
Data Processing	**Image Pre-processing:**
	• Created training ROIs by selectively cropping regions of 245 WSIs.
	• Spliced 34 validation WSIs into 1 068 224x224 patches.
	• Colour channel normalization to mean and standard deviation of entire training set.
	• Data augmentation by rotation; flipping; and random colour jittering on brightness, contrast, hue, and saturation.
	Output Processing: Low-confidence predictions filtered out for predictions below a threshold. Thresholds are determined by a grid search over classes, optimizing for similarity between the trained model and the validation data.
Performance Summary	**Evaluation Metrics:** F1-Score, AUC
	Notable Results: F1-Score of 0.904 on validation set, AUC greater than 0.97 for all classes.
	Comparison to Other Works: ResNet18, 34, 50, 101, 152 compared for performance to choose optimal depth. All had similar accuracies on validation set, so chose ResNet18 for lower model complexity.
Novelty	**Medical Applications/Perspectives:** Potential platform for quality assurance of diagnosis and slide analysis.
	Technical Innovation: First paper to attempt to classify based on histological lung adenocarcinoma subtypes.
Explainability	**Visual Representations:** Heatmaps for patterns detected, AUC curve for each class
Clinical Validation	**Usage in Clinical Settings:** N/A
	Suggested Usage:
	• Could be integrated into existing lab information management systems to provide second opinions to diagnoses.
	• Visualization of a slide could highlight important tissue structures.
	• Could help facilitate tumour diagnosis process by automatically requesting genetic testing based on histological data for patient.
	Performance Comparison:
	• On par with pathologists for all evaluated metrics
	• Model in agreement 66.6% of the time with pathologists on average, with robust agreement (agreement with 2/3 of the pathologists) 76.7% of the time.
	• WSI region annotation differences between pathologist and model are compared for a sample slide.
Caveats and Recommendations	• Data taken from one medical centre, so may not be representative of lung adenocarcinoma morphology
	• Dataset relatively small compared to other deep learning datasets, with some classes having very few instances

Citation:

```
@article{wei2019pathologist,
title={Pathologist-level classification of histologic patterns on resected lung adenocarcinoma slides with deep neural networks},
author={Wei, Jason W and Tafe, Laura J and Linnik, Yevgeniy A and Vaickus, Louis J and Tomita, Naofumi and Hassanpour, Saeed},
journal={Scientific reports},
volume={9},
number={1},
pages={3358},
year={2019},
publisher={Nature Publishing Group UK London}
}
```

Paper: Classification of lung cancer histology images using patch-level summary statistics

Summary:

The classification of non-small cell lung cancer WSIs as either lung adenocarcinoma (LUAD) or lung squamous cell carcinoma (LUSC) is an important task in diagnosis and treatment planning. Manually classifying these WSIs is a laborious and subjective task that is often complicated by poorly differentiated tissue structures within the slide. Automated classification of WSIs may facilitate the analysis of non-small cell lung cancers. This paper proposes a new 3-class network for effective classification of tissue regions within a WSI. It uses a modification of the ResNet50 architecture, ResNet32 to create probability maps of LUAD/LUSC/non-diagnostic pixels in the WSI. Features from these probability maps are next extracted and fed into a random forest classifier for the final classification. The model achieves the greatest accuracy of 0.81 in the Computational Precision Medicine Challenge and provides a new method of classification for non-small lung cancer histological images.

Categorization:

Keywords	Non-small cell lung cancer, histology image classification, computational pathology, deep learning
Organ Application	**Organ:** Lung
	Task: Classification between non-small cell lung cancer types
Dataset Compilation	**Name:** Computational Precision Medicine at MICCAI 2017
	Availability: Unavailable, link on MICCAI 2017 website unreachable
	Dataset Size: 64 WSIs
	Image Resolution: 20× magnification
	Staining Type: H&E
	Annotation Type: Pixel-level and Slide-level
	Histological Type:
	• At pixel-level, classifies as lung adenocarcinoma (LUAD), lung squamous cell carcinoma (LUSC), and non-diagnostic (ND)
	• At slide-level, LUAD or LUSC
	Label Structure: Single label
	Class Balance: Balanced dataset at the slide level, 32 LUAD and 32 LUSC
Technicality	**Model:**
	• Ensemble ML model
	• Variant of ResNet50, called ResNet32 with 32 layers and 3x3 kernel, as compared to 7x7 kernel with ResNet50.
	• 50 statistical and morphological features extracted from probability maps generated by ResNet32. The top 25 are selected for best class separability and used as input to a random forest.
	Training Algorithm: Separately staged, ResNet32 creates probability maps, then random forest generates final prediction for each WSI
	Code Availability: Unavailable
Data Processing	**Image Pre-processing:**
	• Splicing of slides into 256×256 patches, then random cropping into 224×224 patches
	• Reinhard stain normalization
	• Random crop, flip, rotation data augmentation
	Output Processing: N/A
Performance Summary	**Evaluation Metrics:** Accuracy
	Notable Results:
	• ResNet32 with Random Forest achieves 0.81 accuracy over WSI
	• Results superior to ResNet32 with Maximum Vote, which had 0.78 accuracy. Features for the random forest are tailored for WSI classification, and so can achieve higher performance.
	Comparison to Other Works: Compared ResNet32 to VGG, GoogLeNet, and ResNet50, with higher average classification accuracy.
Novelty	**Medical Applications/Perspectives:** Automated distinguishing of LUAD tissue from LUSC could be done at scale to assist pathologists in diagnosis and treatment planning for patients.
	Technical Innovation:
	• First 3-class network for classification of WSI into diagnostic/nondiagnostic areas
	• Ensemble method resulted in greatest accuracy at the MICCAI 2017 competition.
Explainability	**Visual Representations:** Probability maps for each pixel-level class
Clinical Validation	**Usage in Clinical Settings:** N/A
	Suggested Usage: Automated distinguishing of LUAD and LUSC slides could aid pathologists in treatment planning.
	Performance Comparison: N/A
Caveats and Recommendations	• Because features for random forest training are chosen based on categorization of lung tissue samples, may not be able to generalize well to other tissue types.

Citation:

```
@inproceedings{graham2018classification,
title={Classification of lung cancer histology images using patch-level summary statistics},
author={Graham, Simon and Shaban, Muhammad and Qaiser, Talha and Koohbanani, Navid Alemi and Khurram, Syed Ali and Rajpoot, Nasir},
booktitle={Medical Imaging 2018: Digital Pathology},
volume={10581},
pages={327–334},
year={2018},
organization={SPIE}
}
```

Paper: Digital pathology and artificial intelligence (Review)

Summary:

The advent of cheaper storage solutions, faster network speed, and digitized WSIs has greatly facilitated the presence of digital pathology in modern pathology. Particularly, WSIs allow for the development and integration of automated AI tools for histopathological analysis into the pathologist's workflow. AI tools have the potential to increase the efficiency of diagnostics and improve patient safety and care. However, histological analysis comes with several challenges, including the large size, different potential image magnifications, presence, and variation of stain color information, and z-axis information (in the thickness of the slide). These challenges make it difficult for a human viewer to extract all available information and provide important issues that an AI tool must overcome. This paper outlines several different areas in which AI may be applied in digital pathology, namely education, quality assurance (QA), clinical diagnosis, and image analysis. The potential uses are outlined as follows:

- Education: Through the digitization of slides, education can be enhanced. As slides no longer need to be viewed through a microscope, and images can be zoomed into and panned, convenience can be increased without sacrificing the quality of education. Synthetic tissue sample images using GANs can be used to easily create test material in trainees, as well as evaluate cognitive biases in practicing pathologists.
- Quality Assurance: Can help pathologists remain updated in their field and check for lab proficiency of diagnoses, as well as monitor for inter-observer variance.
- Clinical Diagnosis: AI can aid in the preparation of digital slide imagery, such as in reducing the frequency of out-of-focus areas in slides. Color and stain normalization methods using AI-based models are another possible area of application.
- Image Analysis: AI can be used to process the data, including in nuclear segmentation and ROI detection.

AI systems have several different limitations. AI models have been criticized as being black box models. Explainability of decisions will need to be increased. While visualization techniques are being developed, these tend to reduce performance. Additionally, regulatory and economic effects of AI-based systems are unknown at this time. Some areas of future research for AI applications in computational pathology include one-shot learning and reinforcement learning.

Citation:

```
@article{niazi2019digital,
title = {Digital pathology and artificial intelligence},
author = {Niazi, Muhammad Khalid Khan and Parwani, Anil V and Gurcan, Metin N},
journal = {The lancet oncology},
volume = {20},
number = {5},
pages = {e253–e261},
year = {2019},
publisher = {Elsevier}
}
```

References

1. FDA News Release. Fda allows marketing of first whole slide imaging system for digital pathology. https://www.fda.gov/news-events/press-announcements/fda-allows-marketing-first-whole-slide-imaging-system-digital-pathology 2017.
2. Evans Andrew J, Bauer Thomas W, Bui Marilyn M, et al. Us food and drug administration approval of whole slide imaging for primary diagnosis: a key milestone is reached and new questions are raised. Arch Pathol Lab Med 2018;142(11):1383–1387.
3. Araújo Anna Luíza Damaceno, Arboleda Lady Paola Aristizábal, Palmier Natalia Rangel, et al. The performance of digital microscopy for primary diagnosis in human pathology: a systematic review. Virchows Arch 2019;474(3):269–287.
4. Williams Bethany Jill, Hanby Andrew, Millican-Slater Rebecca, Nijhawan Anju, Verghese Eldo, Treanor Darren. Digital pathology for the primary diagnosis of breast histopathological specimens: an innovative validation and concordance study on digital pathology validation and training. Histopathology 2018;72(4):662–671.
5. Großerueschkamp Frederik, Jütte Hendrik, Gerwert Klaus, Tannapfel Andrea. Advances in digital pathology: from artificial intelligence to label-free imaging. Visceral Med 2021:1–9.
6. Kuo Kuo-Hsing, Leo Joyce M. Optical versus virtual microscope for medical education: a systematic review. Anat Sci Educ 2019;12(6):678–685.
7. Pell Robert, Oien Karin, Robinson Max, et al. UK National Cancer Research Institute (NCRI) Cellular-Molecular Pathology (CM-Path) quality assurance working group, Owen J Driskell, et al. The use of digital pathology and image analysis in clinical trials. J Pathol Clin Res 2019;5(2):81–90.
8. Al-Janabi Shaimaa, Huisman André, Van Diest Paul J. Digital pathology: current status and future perspectives. Histopathology 2012;61(1):1–9.
9. Griffin Jon, Treanor Darren. Digital pathology in clinical use: where are we now and what is holding us back? Histopathology 2017;70(1):134–145.
10. Saco Adela, Bombi Jose Antoni, Garcia Adriana, Ramírez Jose, Ordi Jaume. Current status of whole-slide imaging in education. Pathobiology 2016;83(2-3):79–88.
11. Kaushal Rajiv Kumar, Rajaganesan Sathyanarayanan, Rao Vidya, Sali Akash, More Balaji, Desai Sangeeta B. Validation of a portable whole-slide imaging system for frozen section diagnosis. J Pathol Inform 2021;12(1):33.
12. Van der Laak Jeroen, Litjens Geert, Ciompi Francesco. Deep learning in histopathology: the path to the clinic. Nat Med 2021;27(5):775–784.
13. Cui Miao, Zhang David Y. Artificial intelligence and computational pathology. Lab Invest 2021;101(4):412–422.
14. Echle Amelie, Rindtorff Niklas Timon, Brinker Titus Josef, Luedde Tom, Pearson Alexander Thomas, Kather Jakob Nikolas. Deep learning in cancer pathology: a new generation of clinical biomarkers. Br J Cancer 2021;124(4):686–696.
15. Acs Balázs, Rantalainen Mattias, Hartman Johan. Artificial intelligence as the next step towards precision pathology. J Intern Med 2020;288(1):62–81.
16. Massimo Salvi U, Acharya Rajendra, Molinari Filippo, Meiburger Kristen M. The impact of pre- and post-image processing techniques on deep learning frameworks: A comprehensive review for digital pathology image analysis. Comput Biol Med 2021;128, 104129.
17. Srinidhi Chetan L, Ciga Ozan, Martel Anne L. Deep neural network models for computational histopathology: A survey. Med Image Anal 2021;67, 101813.
18. Lujan Giovani, Li Zaibo, Parwani Anil V. Challenges in implementing a digital pathology workflow in surgical pathology. Human Pathol Rep 2022;29, 300673.
19. Liu Yingci, Pantanowitz Liron. Digital pathology: Review of current opportunities and challenges for oral pathologists. J Oral Pathol Med 2019;48(4):263–269.
20. Jara-Lazaro Ana Richelia, Thamboo Thomas Paulraj, Teh Ming, Tan Puay Hoon. Digital pathology: exploring its applications in diagnostic surgical pathology practice. Pathology 2010;42(6):512–518.

21. Smith Julie, Johnsen Sys, Zeuthen Mette Christa, et al. On the road to digital pathology in denmark—national survey and interviews. J Digit Imaging 2022:1-18.
22. Sundar Sandhya, Ramani Pratibha, Sherlin Herald J, Ranjith Gheena, Ramasubramani Abilasha, Jayaraj Gifrina. Awareness about whole slide imaging and digital pathology among pathologists-cross sectional survey. Indian. J For Med Toxicol 2020;14(2).
23. Buabbas Ali Jasem, Mohammad Tareq, Ayed Adel K, Mallah Hawraa, Al-Shawaf Hamza, Khalfan Abdulwahed Mohammed. Evaluating the success of the tele-pathology system in governmental hospitals in kuwait: an explanatory sequential mixed methods design. BMC Med Inform Decis Mak 2021;21(1):1-12.
24. Baidoshvili Alexi, Bucur Anca, van Leeuwen Jasper, van der Laak Jeroen, Kluin Philip, van Diest Paul J. Evaluating the benefits of digital pathology implementation: time savings in laboratory logistics. Histopathology 2018;73(5):784–794.
25. Dennis T, Start RD, Cross Simon S. The use of digital imaging, video conferencing, and telepathology in histopathology: a national survey. J Clin Pathol 2005;58:254–258.
26. Dong Fei, Irshad Humayun, Eun-Yeong Oh, et al. Computational pathology to discriminate benign from malignant intraductal proliferations of the breast. PloS One 2014;9(12), e114885.
27. Steiner David F, MacDonald Robert, Liu Yun, et al. Impact of deep learning assistance on the histopathologic review of lymph nodes for metastatic breast cancer. Am J Surg Pathol 2018;42(12):1636.
28. Lee AD, Carter Alexis B, Farris Alton B, et al. Digital pathology: Data-intensive frontier in medical imaging. Proceedings of the IEEE, 100 (4). ; 2012. p. 991-1003.
29. Kim Inho, Kang Kyungmin, Song Youngjae, Kim Tae-Jung. Application of artificial intelligence in pathology: Trends and challenges. Diagnostics 2022;12(11):2794.
30. Abels Esther, Pantanowitz Liron, Aeffner Famke, et al. Computational pathology definitions, best practices, and recommendations for regulatory guidance: a white paper from the digital pathology association. J Pathol 2019;249(3):286–294.
31. Kumar Neeta, Gupta Ruchika, Gupta Sanjay. Whole slide imaging (wsi) in pathology: current perspectives and future directions. J Digit Imaging 2020;33(4):1034–1040.
32. Koohbanani Navid Alemi, Unnikrishnan Balagopal, Khurram Syed Ali, Krishnaswamy Pavitra, Rajpoot Nasir. Self-path: Self-supervision for classification of pathology images with limited annotations. IEEE Trans Med Imaging 2021;40(10):2845–2856.
33. Bera Kaustav, Schalper Kurt A, Rimm David L, Velcheti Vamsidhar, Madabhushi Anant. Artificial intelligence in digital pathology—new tools for diagnosis and precision oncology. Nat Rev Clin Oncol 2019;16(11):703–715.
34. Niazi Muhammad Khalid Khan, Parwani Anil V, Gurcan Metin N. Digital pathology and artificial intelligence. Lancet Oncol 2019;20 (5):e253–e261.
35. Sobhani Faranak, Robinson Ruth, Hamidinekoo Azam, Roxanis Ioannis, Somaiah Navita, Yuan Yinyin. Artificial intelligence and digital pathology: Opportunities and implications for immuno-oncology. Biochim Biophys Acta (BBA)-Rev Cancer 2021;1875(2), 188520.
36. Klein Christophe, Zeng Qinghe, Arbaretaz Floriane, et al. Artificial intelligence for solid tumour diagnosis in digital pathology. Br J Pharmacol 2021;178(21):4291–4315.
37. Go Heounjeong. Digital pathology and artificial intelligence applications in pathology. Brain Tumor Res Treat 2022;10(2):76.
38. Rony Jérôme, Belharbi Soufiane, Dolz Jose, Ayed Ismail Ben, McCaffrey Luke, Granger Eric. Deep weakly-supervised learning methods for classification and localization in histology images: a survey. arXiv preprint arXiv 2019.1909.03354.
39. Abinaya K, Sivakumar B. A systematic review: Intellectual detection and prediction of cancer using dl techniques. 2022 6th International Conference on Trends in Electronics and Informatics (ICOEI). IEEE; 2022. p. 1497–1504.
40. Bilal Mohsin, Nimir Mohammed, Snead David, Taylor Graham S, Rajpoot Nasir. Role of ai and digital pathology for colorectal immuno-oncology. Br J Cancer 2022:1–9.
41. Schneider Lucas, Laiouar-Pedari Sara, Kuntz Sara, et al. Integration of deep learning-based image analysis and genomic data in cancer pathology: A systematic review. Eur J Cancer 2022;160:80–91.
42. Jiang Yahui, Yang Meng, Wang Shuhao, Li Xiangchun, Sun Yan. Emerging role of deep learning-based artificial intelligence in tumor pathology. Cancer Commun 2020;40(4):154–166.
43. Lancellotti Cesare, Cancian Pierandrea, Savevski Victor, et al. Artificial intelligence & tissue biomarkers: advantages, risks and perspectives for pathology. Cells 2021;10(4):787.
44. Colling Richard, Pitman Helen, Oien Karin, Rajpoot Nasir, Macklin Philip. CM-Path AI in Histopathology Working Group, Velicia Bachtiar, Richard Booth, Alyson Bryant, Joshua Bull, et al. Artificial intelligence in digital pathology: a roadmap to routine use in clinical practice. J Pathol 2019;249(2):143–150.
45. Baxi Vipul, Edwards Robin, Montalto Michael, Saha Saurabh. Digital pathology and artificial intelligence in translational medicine and clinical practice. Mod Pathol 2022;35(1):23–32.
46. Sakamoto Taro, Furukawa Tomoi, Lami Kris, et al. A narrative review of digital pathology and artificial intelligence: focusing on lung cancer. Trans Lung Cancer Res 2020;9(5):2255.
47. Cheng Jerome Y, Abel Jacob T, Balis Ulysses GJ, McClintock David S, Pantanowitz Liron. Challenges in the development, deployment, and regulation of artificial intelligence in anatomic pathology. Am J Pathol 2021;191(10):1684–1692.
48. Brixtel Romain, Bougleux Sébastien, Lézoray Olivier, et al. Whole slide image quality in digital pathology: review and perspectives. IEEE Access 2022;10:131005–131035.
49. Shmatko Artem, Laleh Narmin Ghaffari, Gerstung Moritz, Kather Jakob Nikolas. Artificial intelligence in histopathology: enhancing cancer research and clinical oncology. Nat Cancer 2022;3(9):1026–1038.
50. Makhlouf Yasmine, Salto-Tellez Manuel, James Jacqueline, O'Reilly Paul, Maxwell Perry. General roadmap and core steps for the development of ai tools in digital pathology. Diagnostics 2022;12(5):1272.
51. Huo Yuankai, Deng Ruining, Liu Quan, Fogo Agnes B, Yang Haichun. Ai applications in renal pathology. Kidney Int 2021;99(6):1309–1320.
52. Serag Ahmed, Ion-Margineanu Adrian, Qureshi Hammad, et al. Translational ai and deep learning in diagnostic pathology. Front Med 2019;6:185.
53. Wong Alex Ngai Nick, He Zebang, Leung Ka Long, et al. Current developments of artificial intelligence in digital pathology and its future clinical applications in gastrointestinal cancers. Cancers 2022;14 (15):3780.
54. AlAmir Manal, AlGhamdi Manal. The role of generative adversarial network in medical image analysis: An in-depth survey. ACM Comput Surv 2022;55(5):1-36.
55. Cifci Didem, Foersch Sebastian, Kather Jakob Nikolas. Artificial intelligence to identify genetic alterations in conventional histopathology. J Pathol 2022;257(4):430–444.
56. Haggenmüller Sarah, Maron Roman C, Hekler Achim, et al. Skin cancer classification via convolutional neural networks: systematic review of studies involving human experts. Eur J Cancer 2021;156: 202–216.
57. Margaret Mitchell, Simone Wu, Andrew Zaldivar, Parker Barnes, Lucy Vasserman, Ben Hutchinson, Elena Spitzer, Inioluwa Deborah Raji, and Timnit Gebru. Model cards for model reporting. In Proceedings of the conference on fairness, accountability, and transparency, pages 220 – 229, 2019.
58. Hongyan Gu, Huang Jingbin, Hung Lauren, Chen Xiang Anthony. Lessons learned from designing an ai-enabled diagnosis tool for pathologists. Proceedings of the ACM on Human-Computer Interaction, 5(CSCW1). ; 2021. p. 1-25.
59. Tomaszewski John E. Overview of the role of artificial intelligence in pathology: the computer as a pathology digital assistant. Artificial Intelligence and Deep Learning in Pathology. Elsevier; 2021. p. 237–262.
60. Deng Jia, Dong Wei, Socher Richard, Li Li-Jia, Li Kai, Fei-Fei Li. Imagenet: A large-scale hierarchical image database. IEEE

Conference on Computer Vision and Pattern Recognition; 2009. p. 248–255.
61. Litjens Geert, Bandi Peter, Bejnordi Babak Ehteshami, et al. 1399 h&e-stained sentinel lymph node sections of breast cancer patients: the camelyon dataset. Gigascience 2018;7(6):giy065.
62. Campanella Gabriele, Hanna Matthew G, Geneslaw Luke, et al. Clinical-grade computational pathology using weakly supervised deep learning on whole slide images. Nat Med 2019;25(8):1301–1309.
63. Lu Ming Y, Chen Richard J, Mahmood Faisal. Semi-supervised breast cancer histology classification using deep multiple instance learning and contrast predictive coding. Medical Imaging: Digital Pathology. International Society for Optics and Photonics; 2020. p. 113200J.
64. Lu Ming Y, Williamson Drew FK, Chen Tiffany Y, Chen Richard J, Barbieri Matteo, Mahmood Faisal. Data-efficient and weakly supervised computational pathology on whole-slide images. Nature. Biomed Eng 2021;5(6):555–570.
65. Richard J, Chen Chengkuan, Li Yicong, et al. Scaling vision transformers to gigapixel images via hierarchical self-supervised learning. Proceedings of the IEEE/CVF Conference on Computer Vision and Pattern Recognition; 2022. p. 16144–16155.
66. Chen Ting, Kornblith Simon, Norouzi Mohammad, Hinton Geoffrey. A simple framework for contrastive learning of visual representations. International conference on machine learning. PMLR; 2020. p. 1597–1607.
67. Caron Mathilde, Touvron Hugo, Misra Ishan, et al. Emerging properties in self-supervised vision transformers. Proceedings of the IEEE/CVF International Conference on Computer Vision; 2021. p. 9650–9660.
68. Njoroge Sarah W, Nichols James H. Risk management in the clinical laboratory. Ann Lab Med 2014;34(4):274.
69. Renshaw Andrew A, Mena-Allauca Mercy, Gould Edwin W, Joseph Sirintrapun S. Synoptic reporting: Evidence-based review and future directions. JCO Clinical. Cancer Inform 2018;2):1–9.(PMID: 30652566).
70. Hewer Ekkehard. The oncologist's guide to synoptic reporting: a primer. Oncology 2020;98(6):396–402.
71. Litjens Geert, Sánchez Clara I, Timofeeva Nadya, et al. Deep learning as a tool for increased accuracy and efficiency of histopathological diagnosis. Sci Rep 2016;6:26286.
72. Liu Yun, Kohlberger Timo, Norouzi Mohammad, et al. Artificial intelligence–based breast cancer nodal metastasis detection: Insights into the black box for pathologists. Arch Pathol Lab Med 2019;143(7):859–868.
73. Khan Umair Akhtar Hasan, Stürenberg Carolin, Gencoglu Oguzhan, et al. Improving prostate cancer detection with breast histopathology images. European Congress on Digital Pathology. Springer; 2019. p. 91–99.
74. Noorbakhsh Javad, Farahmand Saman, Namburi Sandeep, et al. Deep learning-based cross-classifications reveal conserved spatial behaviors within tumor histological images. Nat Commun 2020;11(1):1-14.
75. Wei Jason W, Tafe Laura J, Linnik Yevgeniy A, Vaickus Louis J, Tomita Naofumi, Hassanpour Saeed. Pathologist-level classification of histologic patterns on resected lung adenocarcinoma slides with deep neural networks. Sci Rep 2019;9(1):1–8.
76. Barker Jocelyn, Hoogi Assaf, Depeursinge Adrien, Rubin Daniel L. Automated classification of brain tumor type in whole-slide digital pathology images using local representative tiles. Med Image Anal 2016;30:60–71.
77. Sirinukunwattana Korsuk, Ahmed Shan E, Raza Yee-Wah Tsang, Snead David RJ, Cree Ian A, Rajpoot Nasir M. Locality sensitive deep learning for detection and classification of nuclei in routine colon cancer histology images. IEEE Trans Med Imaging 2016;35(5):1196–1206.
78. Korbar Bruno, Olofson Andrea M, Miraflor Allen P, et al. Deep learning for classification of colorectal polyps on whole-slide images. J Pathol Inform 2017;8.
79. Chan Lyndon, Hosseini Mahdi S, Plataniotis Konstantinos N. A comprehensive analysis of weakly-supervised semantic segmentation in different image domains. Int J Comput Vision 2021;129:361–384.
80. Chen Hao, Qi Xiaojuan, Yu Lequan, Heng Pheng-Ann. Dcan: deep contour-aware networks for accurate gland segmentation. IEEE Conference on Computer Vision and Pattern Recognition; 2016. p. 2487–2496.
81. Nateghi Ramin, Danyali Habibollah, Helfroush Mohammad-Sadegh. A systematic approach for glandular structure segmentation from colon histopathology images. Iranian Conference on Electrical Engineering (ICEE). IEEE; 2016. p. 1505–1509.
82. Yan Chaoyang, Jun Xu, Xie Jiawei, Cai Chengfei, Haoda Lu. Prior-aware cnn with multi-task learning for colon images analysis. IEEE International Symposium on Biomedical Imaging. IEEE; 2020. p. 254–257.
83. Sirinukunwattana Korsuk, Snead David RJ, Rajpoot Nasir M. A stochastic polygons model for glandular structures in colon histology images. IEEE Trans Med Imaging 2015;34(11):2366–2378.
84. Marsh Jon N, Matlock Matthew K, Kudose Satoru, et al. Deep learning global glomerulosclerosis in transplant kidney frozen sections. IEEE Trans Med Imaging 2018;37(12):2718–2728.
85. Shirazi Amin Zadeh, Fornaciari Eric, Bagherian Narjes Sadat, Ebert Lisa M, Koszyca Barbara, Gomez Guillermo A. Deepsurvnet: deep survival convolutional network for brain cancer survival rate classification based on histopathological images. Med Biol Eng Comput 2020;58(5):1031–1045.
86. Kather Jakob Nikolas, Krisam Johannes, Charoentong Pornpimol, et al. Predicting survival from colorectal cancer histology slides using deep learning: A retrospective multicenter study. PLoS Med 2019;16(1), e1002730.
87. Courtiol Pierre, Maussion Charles, Moarii Matahi, et al. Deep learning-based classification of mesothelioma improves prediction of patient outcome. Nat Med 2019;25(10):1519–1525.
88. Bychkov Dmitrii, Linder Nina, Turkki Riku, et al. Deep learning based tissue analysis predicts outcome in colorectal cancer. Sci Rep 2018;8(1):1-11.
89. Wang Xiangxue, Andrew Janowczyk Yu, Zhou Rajat Thawani, et al. Prediction of recurrence in early stage non-small cell lung cancer using computer extracted nuclear features from digital h&e images. Sci Rep 2017;7(1):1-10.
90. Siegel Rebecca L, Miller Kimberly D, Jemal Ahmedin. Cancer statistics, 2020. CA Cancer J Clin 2020;70(1):7-30.
91. American Cancer Society. What is breast cancer? 2023. Available at: https://www.cancer.org/cancer/breast-cancer/about/what-is-breast-cancer.html. (accessed Jan 22, 2023).
92. Fitzgibbons Connolly. Protocol for the examination of resection specimens from patients with ductal carcinoma in situ (dcis) of the breast. College Am Pathol 2021;133:15–25.
93. Allison Kimberly H, Elizabeth M, Hammond H, et al. Estrogen and progesterone receptor testing in breast cancer: Asco/cap guideline update. J Clin Oncol 2020;38(12):1346–1366.
94. Wolff Antonio C, Elizabeth Hale Hammond M, Allison Kimberly H, Harvey Brittany E, McShane Lisa M, Dowsett Mitchell. Her2 testing in breast cancer: American society of clinical oncology/college of american pathologists clinical practice guideline focused update summary. J Oncol Pract 2018;14(7):437–441.
95. Dowsett Mitch, Nielsen Torsten O, A'Hern Roger, et al. Assessment of ki67 in breast cancer: recommendations from the international ki67 in breast cancer working group. J Natl Cancer Inst 2011;103(22):1656–1664.
96. Healey Megan A, Hirko Kelly A, Beck Andrew H, et al. Assessment of ki67 expression for breast cancer subtype classification and prognosis in the nurses' health study. Breast Cancer Res Treat 2017;166(2):613–622.
97. Liu Yun, Gadepalli Krishna, Norouzi Mohammad, et al. Detecting cancer metastases on gigapixel pathology images. arXiv preprint arXiv 2017.1703.02442.

98. American Cancer Society. What is prostate cancer? 2023. Available at: https://www.cancer.org/cancer/prostate-cancer/about/what-is-prostate-cancer.html. (accessed Jan 21, 2023).
99. Ito Yujiro, Vertosick Emily A, Sjoberg Daniel D, et al. In organ-confined prostate cancer, tumor quantitation not found to aid in prediction of biochemical recurrence. Am J Surg Pathol 2019;43(8):1061.
100. Epstein Jonathan I. Prognostic significance of tumor volume in radical prostatectomy and needle biopsy specimens. J Urol 2011;186(3):790–797.
101. Salomon Laurent, Levrel Olivier, Anastasiadis Aristotelis G, et al. Prognostic significance of tumor volume after radical prostatectomy: a multivariate analysis of pathological prognostic factors. Eur Urol 2003;43(1):39–44.
102. Stamey Thomas A, McNeal John E, Yemoto Cheryl M, Sigal Bronislava M, Johnstone Iain M. Biological determinants of cancer progression in men with prostate cancer. Jama 1999;281(15):1395–1400.
103. J Joy Lee, I-Chun Thomas, Rosalie Nolley, Michelle Ferrari, James D Brooks, and John T Leppert. Biologic differences between peripheral and transition zone prostate cancer. Prostate, 75(2):183–190, 2015.
104. Paner Srigley. *Protocol for the examination of radical prostatectomy specimens from patients with carcinoma of the prostate gland*. Nov 2021.
105. Wright Jonathan L, Dalkin Bruce L, True Lawrence D, et al. Positive surgical margins at radical prostatectomy predict prostate cancer specific mortality. J Urol 2010;183(6):2213–2218.
106. Varma Murali. Intraductal carcinoma of the prostate: a guide for the practicing pathologist. Adv Anat Pathol 2021;28(4):276–287.
107. Montironi Rodolfo, Zhou Ming, Magi-Galluzzi Cristina, Epstein Jonathan I. Features and prognostic significance of intraductal carcinoma of the prostate. European Urology. Oncology 2018;1(1):21–28.
108. Zhou Ming. Intraductal carcinoma of the prostate: the whole story. Pathology 2013;45(6):533–539.
109. Cohen Ronald J, Wheeler Thomas M, Bonkhoff Helmut, Rubin Mark A. A proposal on the identification, histologic reporting, and implications of intraductal prostatic carcinoma. Arch Pathol Lab Med 2007;131(7):1103–1109.
110. Guo Charles C, Epstein Jonathan I. Intraductal carcinoma of the prostate on needle biopsy: histologic features and clinical significance. Mod Pathol 2006;19(12):1528–1535.
111. American Cancer Society. Tests to diagnose and stage prostate cancer. 2023. Available at: https://www.cancer.org/cancer/prostate-cancer/detection-diagnosis-staging/how-diagnosed.html. (accessed Jan 21, 2023).
112. Kweldam Charlotte F, Wildhagen Mark F, Steyerberg Ewout W, Bangma Chris H, Van Der Kwast Theodorus H, Van Leenders Geert Jlh. Cribriform growth is highly predictive for postoperative metastasis and disease-specific death in gleason score 7 prostate cancer. Mod Pathol 2015;28(3):457–464.
113. Lee Thomas K, Ro Jae Y. Spectrum of cribriform proliferations of the prostate: from benign to malignant. Arch Pathol Lab Med 2018;142(8):938–946.
114. Emily Bachert S, Jr Anthony McDowell, Piecoro Dava, Branch Lauren Baldwin. Serous tubal intraepithelial carcinoma: a concise review for the practicing pathologist and clinician. Diagnostics 2020;10(2):102.
115. American Cancer Society. What is ovarian cancer? Available at: https://www.cancer.org/cancer/ovarian-cancer/about/what-is-ovarian-cancer.html. (accessed Jan 21, 2023).
116. Yang Shi-Ping, Hui-Luan Su, Chen Xiu-Bei, et al. Long-term survival among histological subtypes in advanced epithelial ovarian cancer: population-based study using the surveillance, epidemiology, and end results database. JMIR Public Health Surveill 2021;7(11), e25976.
117. Vermij Lisa, Léon-Castillo Alicia, Singh Naveena, et al. p53 immunohistochemistry in endometrial cancer: clinical and molecular correlates in the portec-3 trial. Mod Pathol 2022;35(10):1475–1483.
118. Zhang Yu, Cao Lan, Nguyen Daniel, Hua Lu. Tp53 mutations in epithelial ovarian cancer. Transl Cancer Res 2016;5(6):650.
119. Wang Yiping, Farnell David, Farahani Hossein, et al. Classification of epithelial ovarian carcinoma whole-slide pathology images using deep transfer learning. Medical Imaging with Deep Learning; 2020.
120. Gamper Jevgenij, Kooohbanani Navid Alemi, Rajpoot Nasir. Multitask learning in histo-pathology for widely generalizable model. arXiv preprint arXiv 2020.2005.08645.
121. National Cancer Institute. Common cancer types. Available at: https://www.cancer.gov/types/common-cancers#:~:text=The most common type of,are combined for the list/. (accessed June 10, 2021).
122. American Cancer Society. Tests to diagnose and stage prostate cancer. Available at: https://www.cancer.org/cancer/lung-cancer/about/what-is.html. (accessed Jan 21, 2023).
123. Yoshizawa Akihiko, Motoi Noriko, Riely Gregory J, et al. Impact of proposed iaslc/ats/ers classification of lung adenocarcinoma: prognostic subgroups and implications for further revision of staging based on analysis of 514 stage i cases. Mod Pathol 2011;24(5):653–664.
124. Moreira Andre L, Ocampo Paolo SS, Xia Yuhe, et al. A grading system for invasive pulmonary adenocarcinoma: a proposal from the international association for the study of lung cancer pathology committee. J Thorac Oncol 2020;15(10):1599–1610.
125. Tsutani Yasuhiro, Miyata Yoshihiro, Nakayama Haruhiko, et al. Prognostic significance of using solid versus whole tumor size on high-resolution computed tomography for predicting pathologic malignant grade of tumors in clinical stage ia lung adenocarcinoma: a multicenter study. J Thorac Cardiovasc Surg 2012;143(3):607–612.
126. Maeyashiki Tatsuo, Suzuki Kenji, Hattori Aritoshi, Matsunaga Takeshi, Takamochi Kazuya, Shiaki Oh. The size of consolidation on thin-section computed tomography is a better predictor of survival than the maximum tumour dimension in resectable lung cancer. Eur J Cardiothorac Surg 2013;43(5):915–918.
127. Mahul B, Greene Frederick L, Edge Stephen B, et al. The eighth edition ajcc cancer staging manual: continuing to build a bridge from a population-based to a more "personalized" approach to cancer staging. CA Cancer J Clin 2017;67(2):93–99.
128. Wang Liang, Dou Xuejun, Liu Tao, Weiqiang Lu, Ma Yunlei, Yang Yue. Tumor size and lymph node metastasis are prognostic markers of small cell lung cancer in a chinese population. Medicine 2018;97(31).
129. Zhang Jianjun, Gold Kathryn A, Lin Heather Y, et al. Relationship between tumor size and survival in non–small-cell lung cancer (nsclc): an analysis of the surveillance, epidemiology, and end results (seer) registry. J Thorac Oncol 2015;10(4):682–690.
130. Gao Yina, Dong Yangyang, Zhou Yingxu, et al. Peripheral tumor location predicts a favorable prognosis in patients with resected small cell lung cancer. Int J Clin Pract 2022;2022.
131. Amin Mahul B, Edge Stephen B, Greene Frederick L, et al. *AJCC cancer staging manual*. , 1024Springer. 2017.
132. American Cancer Society. *Colorectal cancer facts & figures 2020–2022*. American Cancer Society. 2020:48.
133. American Cancer Society. What is colorectal cancer? 2023. Available at: https://www.cancer.org/cancer/colon-rectal-cancer/about/what-is-colorectal-cancer.html. (accessed Jan 21, 2023).
134. Nancy You Y, Hardiman Karin M, Bafford Andrea, et al. The american society of colon and rectal surgeons clinical practice guidelines for the management of rectal cancer. Dis Colon Rectum 2020;63(9):1191–1222.
135. Lim Seok-Byung, Chang Sik Yu, Jang Se Jin, Kim Tae Won, Kim Jong Hoon, Kim Jin Cheon. Prognostic significance of lymphovascular invasion in sporadic colorectal cancer. Dis Colon Rectum 2010;53(4):377–384.
136. Santos C, López-Doriga A, Navarro M, et al. Clinicopathological risk factors of stage ii colon cancer: results of a prospective study. Colorectal Dis 2013;15(4):414–422.
137. Gomez Dhanwant, Zaitoun Abed M, De Rosa Antonella, et al. Critical review of the prognostic significance of pathological variables in patients undergoing resection for colorectal liver metastases. HPB 2014;16(9):836–844.

138. Liebig Catherine, Ayala Gustavo, Wilks Jonathan, et al. Perineural invasion is an independent predictor of outcome in colorectal cancer. J Clin Oncol 2009;27(31):5131.
139. Ueno H, Shirouzu K, Eishi Y, et al. Study group for perineural invasion projected by the japanese society for cancer of the colon and rectum (jsccr). characterization of perineural invasion as a component of colorectal cancer staging. Am J Surg Pathol 2013;37(10):1542–1549.
140. Phipps Amanda I, Lindor Noralane M, Jenkins Mark A, et al. Colon and rectal cancer survival by tumor location and microsatellite instability: the colon cancer family registry. Dis Colon Rectum 2013;56 (8):937.
141. Vacante Marco, Borzì Antonio Maria, Basile Francesco, Biondi Antonio. Biomarkers in colorectal cancer: Current clinical utility and future perspectives. World J Clin Cases 2018;6(15):869.
142. Yan Xu, Jia Zhipeng, Wang Liang-Bo, et al. Large scale tissue histopathology image classification, segmentation, and visualization via deep convolutional activation features. BMC Bioinforma 2017;18 (1):1-17.
143. American Cancer Society. What is bladder cancer? Available at: https://www.cancer.org/cancer/bladder-cancer/about/what-is-bladder-cancer.html 2023. (accessed Jan 25, 2023).
144. Chalasani Venu, Chin Joseph L, Izawa Jonathan I. Histologic variants of urothelial bladder cancer and nonurothelial histology in bladder cancer. Can Urol Assoc J 2009;3(6 Suppl 4):S193.
145. Lotan Yair, Gupta Amit, Shariat Shahrokh F, et al. Lymphovascular invasion is independently associated with overall survival, cause-specific survival, and local and distant recurrence in patients with negative lymph nodes at radical cystectomy. J Clin Oncol 2005;23 (27):6533–6539.
146. Woerl Ann-Christin, Eckstein Markus, Geiger Josephine, et al. Deep learning predicts molecular subtype of muscle-invasive bladder cancer from conventional histopathological slides. Eur Urol 2020;78 (2):256–264.
147. American Cancer Society. What is kidney cancer? Available at: https://www.cancer.org/cancer/kidney-cancer/about/what-is-kidney-cancer 2023. (accessed Jan 25, 2023).
148. John R, Zhou M, Allan R, et al. Protocol for the examination of resection specimens from patients with invasive carcinoma of renal tubular origin. College American Pathologists (CAP) Cancer Protocols 2020;1(0).v4.
149. Bonsib Stephen M. Renal lymphatics, and lymphatic involvement in sinus vein invasive (pt3b) clear cell renal cell carcinoma: a study of 40 cases. Mod Pathol 2006;19(5):746–753.
150. Muglia Valdair F, Prando Adilson. Renal cell carcinoma: histological classification and correlation with imaging findings. Radiol Bras 2015;48:166–174.
151. Kannan Shruti, Morgan Laura A, Liang Benjamin, et al. Segmentation of glomeruli within trichrome images using deep learning. Kidney Int Rep 2019;4(7):955–962.
152. Hermsen Meyke, de Bel Thomas, Den Boer Marjolijn, et al. Deep learning–based histopathologic assessment of kidney tissue. J Am Soc Nephrol 2019;30(10):1968–1979.
153. Gehan Edmund A, Walker Michael D. Prognostic factors for patients with brain tumors. Nat Cancer Inst Monogr 1977;46:189–195.
154. Li Yao, Zhang Zuo-Xin, Huang Guo-Hao, et al. A systematic review of multifocal and multicentric glioblastoma. J Clin Neurosci 2021;83: 71–76.
155. American Cancer Society. Brain tumors – classifications, symptoms, diagnosis and treatments. Available at: https://www.aans.org/en/Patients/Neurosurgical-Conditions-and-Treatments/Brain-Tumors 2023. (accessed Jan 30, 2023).
156. Louis David N, Perry Arie, Wesseling Pieter, et al. The 2021 who classification of tumors of the central nervous system: a summary. Neuro-oncology 2021;23(8):1231–1251.
157. WHO Classification of Tumours Editorial Board. *Central Nervous System Tumours*. World Health Organization. 2021.
158. Canadian Cancer Society. Survival statistics for brain and spinal cord tumours. Available at: https://www.cancer.ca/en/cancer-information/cancer-type/brain-spinal/prognosis-and-survival/survival-statistics/?region=on#:~:text=In Canada, the 5-year,survive at least 5 years. (accessed June 10, 2021).
159. World Health Organization. Cancer. Available at: https://www.who.int/news-room/fact-sheets/detail/cancer. (accessed June 10, 2021).
160. Kim Haeryoung, Jang Mi, Park Young Nyun. Histopathological variants of hepatocellular carcinomas: an update according to the 5th edition of the who classification of digestive system tumors. J Liver Cancer 2020;20(1):17–24.
161. Lauwers Gregory Y, Terris Benoit, Balis Ulysses J, et al. Prognostic histologic indicators of curatively resected hepatocellular carcinomas: a multi-institutional analysis of 425 patients with definition of a histologic prognostic index. Am J Surg Pathol 2002;26(1):25–34.
162. Spolverato Gaya, Kim Yuhree, Alexandrescu Sorin, et al. Is hepatic resection for large or multifocal intrahepatic cholangiocarcinoma justified? results from a multi-institutional collaboration. Ann Surg Oncol 2015;22:2218–2225.
163. Wanless Ian R, et al. Terminology of nodular hepatocellular lesions. Hepatology 1995;22(3):983–993.
164. Martins-Filho Sebastiao N, Paiva Caterina, Azevedo Raymundo Soares, Alves Venancio Avancini Ferreira. Histological grading of hepatocellular carcinoma—a systematic review of literature. Front Med 2017;4:193.
165. American Cancer Society. Lymph nodes and cancer. Available at: https://www.cancer.org/treatment/understanding-your-diagnosis/lymph-nodes-and-cancer.html 2023. (accessed Jan 25, 2023).
166. Wang Zhihua, Lequan Yu, Ding Xin, Liao Xuehong, Wang Liansheng. Lymph node metastasis prediction from whole slide images with transformer-guided multi-instance learning and knowledge transfer. IEEE Trans Med Imaging 2022;41(10):2777–2787.
167. Mahdi S, Chan Lyndon, Tse Gabriel, et al. Atlas of digital pathology: A generalized hierarchical histological tissue type-annotated database for deep learning. IEEE Conference on Computer Vision and Pattern Recognition; 2019. p. 11747–11756.
168. Koohbanani Navid Alemi, Jahanifar Mostafa, Tajadin Neda Zamani, Rajpoot Nasir. Nuclick: a deep learning framework for interactive segmentation of microscopic images. Med Image Anal 2020;65, 101771.
169. Awan Ruqayya, Sirinukunwattana Korsuk, Epstein David, et al. Glandular morphometrics for objective grading of colorectal adenocarcinoma histology images. Sci Rep 2017;7(1):1-12.
170. Li Wenyuan, Li Jiayun, Wang Zichen, et al. Pathal: An active learning framework for histopathology image analysis. IEEE Trans Med Imaging 2021;41(5):1176–1187.
171. Ghaznavi Farzad, Evans Andrew, Madabhushi Anant, Feldman Michael. Digital imaging in pathology: whole-slide imaging and beyond. Ann Rev Pathol Mech Dis 2013;8:331–359.
172. Ianni Julianna D, Soans Rajath E, Sankarapandian Sivaramakrishnan, et al. Tailored for real-world: a whole slide image classification system validated on uncurated multi-site data emulating the prospective pathology workload. Sci Rep 2020;10(1):1-12.
173. Rolls Geoffrey. *101 Steps to Better Histology - a Practical Guide to Good Histology Practice. Leica. Biosystems*. 2016.
174. Kim Suvarna S, Layton Christopher, Bancroft John D. *Bancroft's theory and practice of histological techniques. 8 ed.* Elsevier. 2019.
175. Stephen R. *A Practical guide to Frozen Section Technique.* SPRINGER. 2016.
176. Yagi Yukako. Color standardization and optimization in whole slide imaging. Diagnostic pathology. Springer; 2011. p. 1-12.
177. Bejnordi Babak Ehteshami, Litjens Geert, Timofeeva Nadya, et al. Stain specific standardization of whole-slide histopathological images. IEEE Trans Med Imaging 2015;35(2):404–415.
178. Bejnordi Babak Ehteshami, Timofeeva Nadya, Otte-Höller Irene, Karssemeijer Nico, van der Laak Jeroen AWM. Quantitative analysis of stain variability in histology slides and an algorithm for standardization. Medical Imaging: Digital Pathology. International Society for Optics and Photonics; 2014. p. 904108.
179. Komura Daisuke, Ishikawa Shumpei. Machine learning methods for histopathological image analysis. Comput Struct Biotechnol J 2018;16:34–42.

180. Zarella Mark D, Bowman Douglas, Aeffner Famke, et al. A practical guide to whole slide imaging: a white paper from the digital pathology association. Arch Pathol Lab Med 2019;143(2):222–234.
181. Pantanowitz Liron. Digital images and the future of digital pathology. J Pathol Inform 2010;1.
182. Pantanowitz Liron, Sharma Ashish, Carter Alexis B, Kurc Tahsin, Sussman Alan, Saltz Joel. Twenty years of digital pathology: an overview of the road travelled, what is on the horizon, and the emergence of vendor-neutral archives. J Pathol Inform 2018;9.
183. Hossain Md Shakhawat, Nakamura Toyama, Kimura Fumikazu, Yagi Yukako, Yamaguchi Masahiro. Practical image quality evaluation for whole slide imaging scanner. Biomedical Imaging and Sensing Conference. International Society for Optics and Photonics; 2018. p. 107111S.
184. Tabata Kazuhiro, Uraoka Naohiro, Benhamida Jamal, et al. Validation of mitotic cell quantification via microscopy and multiple whole-slide scanners. Diagn Pathol 2019;14(1):1–9.
185. Cheng Wei-Chung, Saleheen Firdous, Badano Aldo. Assessing color performance of whole-slide imaging scanners for digital pathology. Color Res Appl 2019;44(3):322–334.
186. Lemaillet Paul, Takeda Kazuyo, Lamont Andrew C, Agrawal Anant. Colorimetrical uncertainty estimation for the performance assessment of whole slide imaging scanners. Journal of Medical. Imaging 2021;8(5), 057501.
187. Indu M, Rathy R, Binu MP. “slide less pathology”: Fairy tale or reality? J Oral Maxillofacial Pathol 2016;20(2):284.
188. Herrmann Markus D, Clunie David A, Fedorov Andriy, et al. Implementing the dicom standard for digital pathology. J Pathol Inform 2018;9.
189. Godinho Tiago Marques, Lebre Rui, Silva Luís Bastião, Costa Carlos. An efficient architecture to support digital pathology in standard medical imaging repositories. J Biomed Inform 2017;71:190–197.
190. Clunie David A. Dicom format and protocol standardization—a core requirement for digital pathology success. Toxicol Pathol 2021;49 (4):738–749.
191. Fusheng Wang, Tae W Oh, Cristobal Vergara-Niedermayr, Tahsin Kurc, and Joel Saltz. Managing and querying whole slide images. In Medical Imaging 2012: Advanced PACS-Based Imaging Informatics and Therapeutic Applications, volume 8319, pages 137–148. SPIE, 2012.
192. Daniel E Lopez Barron, Dig Vijay Kumar Yarlagadda, Praveen Rao, Ossama Tawfik, and Deepthi Rao. Scalable storage of whole slide images and fast retrieval of tiles using apache spark. In Medical Imaging: Digital Pathology, volume 10581, page 1058113 International Society for Optics and Photonics, 2018.
193. Singh Rajendra, Chubb Lauren, Pantanowitz Liron, Parwani Anil. Standardization in digital pathology: Supplement 145 of the dicom standards. J Pathol Inform 2011;2.
194. Kanwal Neel, Pérez-Bueno Fernando, Schmidt Arne, Engan Kjersti, Molina Rafael. The devil is in the details: Whole slide image acquisition and processing for artifacts detection, color variation, and data augmentation: A review. IEEE Access 2022;10:58821–58844.
195. Campanella Gabriele, Rajanna Arjun R, Corsale Lorraine, Schüffler Peter J, Yagi Yukako, Fuchs Thomas J. Towards machine learned quality control: A benchmark for sharpness quantification in digital pathology. Comput Med Imaging Graph 2018;65:142–151.
196. Wang Zhongling, Hosseini Mahdi S, Miles Adyn, Plataniotis Konstantinos N, Wang Zhou. Focuslitenn: High efficiency focus quality assessment for digital pathology. In: *Martel Anne L, Abolmaesumi Purang, Stoyanov Danail, Mateus Diana, Zuluaga Maria A, eds. Medical Image Computing and Computer-Assisted Intervention – MICCAI, volume 12265 of Lecture Notes in Computer Science. Springer; 2020. p. 403–413.*
197. Cross Simon, Furness Peter, Igali Laszlo, Snead David, Treanor Darren. Best practice recommendations for implementing digital pathology. Technical Report G162, The Royal College of Pathologists, 4th Floor 21 Prescott Street, London, United Kingdom E1 8BB; 2018.
198. Bándi Péter, Balkenhol Maschenka, van Ginneken Bram, van der Laak Jeroen, Litjens Geert. Resolution-agnostic tissue segmentation in whole-slide histopathology images with convolutional neural networks. PeerJ 2019;7, e8242.
199. Tellez David, Litjens Geert, Bándi Péter, et al. Quantifying the effects of data augmentation and stain color normalization in convolutional neural networks for computational pathology. Med Image Anal 2019;58, 101544.
200. Otálora Sebastian, Atzori Manfredo, Andrearczyk Vincent, Khan Amjad, Müller Henning. Staining invariant features for improving generalization of deep convolutional neural networks in computational pathology. Front Bioeng Biotechnol 2019:198.
201. Duenweg Savannah R, Bobholz Samuel A, Lowman Allison K, et al. Whole slide imaging (wsi) scanner differences influence optical and computed properties of digitized prostate cancer histology. J Pathol Inform 2023;14, 100321.
202. Khan Adnan Mujahid, Rajpoot Nasir, Treanor Darren, Magee Derek. A nonlinear mapping approach to stain normalization in digital histopathology images using image-specific color deconvolution. IEEE Trans Biomed Eng 2014;61(6):1729–1738.
203. Zanjani Farhad Ghazvinian, Zinger Svitlana, Bejnordi Babak E, et al. Histopathology stain-color normalization using deep generative models. 1st Conference on Medical Imaging with Deep Learning (MIDL); 2018. p. 1-11.
204. Sethi Amit, Sha Lingdao, Vahadane Abhishek Ramnath, et al. Empirical comparison of color normalization methods for epithelial-stromal classification in h and e images. J Pathol Inform 2016;7.
205. Guerrero Rodrigo Escobar Díaz, Oliveira José Luís. *Improvements in Lymphocytes Detection Using Deep Learning with a Preprocessing Stage*. 2021:178–182.
206. Yamashita Rikiya, Long Jin, Banda Snikitha, Shen Jeanne, Rubin Daniel L. Learning domain-agnostic visual representation for computational pathology using medically-irrelevant style transfer augmentation. IEEE Trans Med Imaging 2021;40(12):3945–3954.
207. Vahadane Abhishek, Atheeth B, Majumdar Shantanu. *Dual Encoder Attention u-net for Nuclei Segmentation*. 2021:3205–3208.
208. Arvidsson Ida, Overgaard Niels Christian, Åström Kalle, Heyden Anders. Comparison of different augmentation techniques for improved generalization performance for gleason grading. IEEE International Symposium on Biomedical Imaging. IEEE; 2019. p. 923–927.
209. Tarek Shaban M, Baur Christoph, Navab Nassir, Albarqouni Shadi. Staingan: Stain style transfer for digital histological images. IEEE International Symposium on Biomedical Imaging. IEEE; 2019. p. 953–956.
210. Mahapatra Dwarikanath, Bozorgtabar Behzad, Thiran Jean-Philippe, Shao Ling. Structure preserving stain normalization of histopathology images using self supervised semantic guidance. International Conference on Medical Image Computing and Computer-Assisted Intervention. Springer; 2020. p. 309–319.
211. Mehmood Shahid, Ghazal Taher M, Khan Muhammad Adnan, et al. Malignancy detection in lung and colon histopathology images using transfer learning with class selective image processing. IEEE Access 2022;10:25657–25668.
212. Tellez David, Litjens Geert, van der Laak Jeroen, Ciompi Francesco. Neural image compression for gigapixel histopathology image analysis. IEEE Trans Pattern Anal Mach Intell 2019;43(2):567–578.
213. Yan Rui, Ren Fei, Wang Zihao, et al. Breast cancer histopathological image classification using a hybrid deep neural network. Methods 2020;173:52–60.
214. Wang Shidan, Rong Ruichen, Yang Donghan M, et al. Computational staining of pathology images to study the tumor microenvironment in lung cancer. Cancer Res 2020;80(10):2056–2066.
215. Lin Yiyang, Zeng Bowei, Wang Yifeng, et al. *Unpaired multi-Domain Stain Transfer for Kidney Histopathological Images*. 2022.
216. Wei Jerry, Suriawinata Arief, Ren Bing, et al. Learn like a pathologist: curriculum learning by annotator agreement for histopathology image classification. IEEE/CVF Conference on Computer Vision; 2021. p. 2473–2483.
217. Kohli Marc D, Summers Ronald M, Raymond J, Geis. Medical image data and datasets in the era of machine learning—whitepaper from

the 2016 c-mimi meeting dataset session. J Digit Imaging 2017;30 (4):392–399.
218. Wahab Noorul, Khan Asifullah, Lee Yeon Soo. Two-phase deep convolutional neural network for reducing class skewness in histopathological images based breast cancer detection. Comput Biol Med 2017;85:86–97.
219. Cruz-Roa Angel, Gilmore Hannah, Basavanhally Ajay, et al. High-throughput adaptive sampling for whole-slide histopathology image analysis (hashi) via convolutional neural networks: Application to invasive breast cancer detection. PloS One 2018;13(5), e0196828.
220. Aresta Guilherme, Araújo Teresa, Kwok Scotty, et al. Bach: Grand challenge on breast cancer histology images. Med Image Anal 2019;56:122–139.
221. Saldanha Oliver Lester, Quirke Philip, West Nicholas P, et al. Swarm learning for decentralized artificial intelligence in cancer histopathology. Nat Med 2022:1–8.
222. Willemink Martin J, Koszek Wojciech A, Hardell Cailin, et al. Preparing medical imaging data for machine learning. Radiology 2020;295 (1):4-15.
223. Ali Sharib, Alham Nasullah Khalid, Verrill Clare, Rittscher Jens. Ink removal from histopathology whole slide images by combining classification, detection and image generation models. IEEE International Symposium on Biomedical Imaging. IEEE; 2019. p. 928–932.
224. Iizuka Osamu, Kanavati Fahdi, Kato Kei, Rambeau Michael, Arihiro Koji, Tsuneki Masayuki. Deep learning models for histopathological classification of gastric and colonic epithelial tumours. Sci Rep 2020;10(1):1-11.
225. Deng J, Dong W, Socher R, Li L-J, Li K, Fei-Fei L. ImageNet: a large-scale hierarchical image database. CVPR09; 2009.
226. Spanhol Fabio A, Oliveira Luiz S, Petitjean Caroline, Heutte Laurent. A dataset for breast cancer histopathological image classification. IEEE Trans Biomed Eng 2015;63(7):1455–1462.
227. Bardou Dalal, Zhang Kun, Ahmad Sayed Mohammad. Classification of breast cancer based on histology images using convolutional neural networks. IEEE Access 2018;6:24680–24693.
228. Bayramoglu Neslihan, Kannala Juho, Heikkilä Janne. Deep learning for magnification independent breast cancer histopathology image classification. International Conference on Pattern Recognition. IEEE; 2016. p. 2440–2445.
229. Li Xia, Shen Xi, Zhou Yongxia, Wang Xiuhui, Li Tie-Qiang. Classification of breast cancer histopathological images using interleaved densenet with senet (idsnet). PloS One 2020;15(5), e0232127.
230. Hartman Douglas Joseph, Van Der Laak Jeroen AWM, Gurcan Metin N, Pantanowitz Liron. Value of public challenges for the development of pathology deep learning algorithms. J Pathol Inform 2020;11.
231. Bejnordi Babak Ehteshami, Veta Mitko, Van Diest Paul Johannes, et al. Diagnostic assessment of deep learning algorithms for detection of lymph node metastases in women with breast cancer. JAMA Netw Open 2017;318(22):2199–2210.
232. Bándi Péter, Geessink Oscar, Manson Quirine, et al. Bram van Ginneken, Jeroen van der Laak, and Geert Litjens. From detection of individual metastases to classification of lymph node status at the patient level: The camelyon17 challenge. IEEE Trans Med Imaging 2019;38(2):550–560.
233. Sirinukunwattana Korsuk, Pluim Josien PW, Chen Hao, et al. Gland segmentation in colon histology images: The glas challenge contest. Med Image Anal 2017;35:489–502.
234. Le Hou Vu, Nguyen Ariel B, Kanevsky Dimitris Samaras, et al. Sparse autoencoder for unsupervised nucleus detection and representation in histopathology images. Pattern Recogn Lett 2019;86:188–200.
235. Grossman Robert L, Heath Allison P, Ferretti Vincent, et al. Toward a shared vision for cancer genomic data. N Engl J Med 2016;375(12): 1109–1112.
236. Cho Kyung-Ok, Lee Sung Hak, Jang Hyun-Jong. Feasibility of fully automated classification of whole slide images based on deep learning. Korean J Physiol & Pharmacol 2020;24(1):89–99.
237. Hou Le, Gupta Rajarsi, Van Arnam John S, et al. Dataset of segmented nuclei in hematoxylin and eosin stained histopathology images of ten cancer types. Sci Data 2020;7(1):1-12.
238. Mobadersany Pooya, Yousefi Safoora, Amgad Mohamed, et al. Predicting cancer outcomes from histology and genomics using convolutional networks. Natl Acad Sci 2018;115(13):E2970–E2979.
239. Fischer Will, Moudgalya Sanketh S, Cohn Judith D, Nguyen Nga TT, Kenyon Garrett T. Sparse coding of pathology slides compared to transfer learning with deep neural networks. BMC Bioinform 2018;19(18):9-17.
240. Gertych Arkadiusz, Swiderska-Chadaj Zaneta, Ma Zhaoxuan, et al. Convolutional neural networks can accurately distinguish four histologic growth patterns of lung adenocarcinoma in digital slides. Sci Rep 2019;9(1):1-12.
241. Nakagawa Keisuke, Moukheiber Lama, Celi Leo A, et al. Ai in pathology: What could possibly go wrong? Semin Diagn Pathol 2023;40(2): 100–108.Artificial Intelligence (AI) , machine learning ML) and digital pathology integration are the next major chapter in our diagnostic pathology and laboratory medicine arena.
242. Chauhan Chhavi, Gullapalli Rama. Ethics of ai in pathology: Current paradigms and emerging issues. Am J Pathol 2021;191(10):1673–1683.
243. Wang Zeyu, Qinami Klint, Karakozis Ioannis Christos, et al. Towards fairness in visual recognition: Effective strategies for bias mitigation. Proceedings of the IEEE/CVF Conference on Computer Vision and Pattern Recognition (CVPR); June 2020.
244. Tian Xu, White Jennifer, Kalkan Sinan, Gunes Hatice. Investigating bias and fairness in facial expression recognition. In: *Bartoli Adrien, Fusiello Andrea, eds. Computer Vision – ECCV 2020 Workshops. Cham: Springer International Publishing; 2020. p. 506–523.*
245. Fabbrizzi Simone, Papadopoulos Symeon, Ntoutsi Eirini, Kompatsiaris Ioannis. A survey on bias in visual datasets. Comput Vis Image Underst 2022;223, 103552.
246. Georgopoulos Markos, Panagakis Yannis, Pantic Maja. Investigating bias in deep face analysis: The kanface dataset and empirical study. Image Vis Comput 2020;102, 103954.
247. Mehrabi Ninareh, Morstatter Fred, Saxena Nripsuta, Lerman Kristina, Galstyan Aram. A survey on bias and fairness in machine learning. ACM Comput Surv Jul 2021;54(6).
248. Dehkharghanian Taher, Bidgoli Azam Asilian, Riasatian Abtin, et al. Biased data, biased ai: Deep networks predict the acquisition site of tcga images. Diagn Pathol May 2023;18(67).
249. Howard Frederick M, Dolezal James, Kochanny Sara, et al. The impact of site-specific digital histology signatures on deep learning model accuracy and bias. Nat Commun 2021;12(1).
250. Faust Kevin, Bala Sudarshan, Van Ommeren Randy, et al. Intelligent feature engineering and ontological mapping of brain tumour histomorphologies by deep learning. Nat Mach Intell 2019;1(7): 316–321.
251. Kun-Hsing Yu, Zhang Ce, Berry Gerald J, et al. Predicting non-small cell lung cancer prognosis by fully automated microscopic pathology image features. Nat Commun 2016;7(1):1-10.
252. Parvatikar Akash, Choudhary Om, Ramanathan Arvind, et al. Modeling histological patterns for differential diagnosis of atypical breast lesions. Medical Image Computing and Computer Assisted Intervention – MICCAI, volume 12265 of Lecture Notes in Computer Science. Springer; 2020. p. 550–560.
253. Naylor Peter, Laé Marick, Reyal Fabien, Walter Thomas. Segmentation of nuclei in histopathology images by deep regression of the distance map. IEEE Trans Med Imaging 2018;38(2):448–459.
254. Breast Cancer Surveillance Consortium. Available at: https://www.bcsc-research.org/ 2024. (accessed June 10, 2021).
255. Wei Jerry, Suriawinata Arief, Ren Bing, et al. A petri dish for histopathology image analysis. International Conference on Artificial Intelligence in Medicine. Springer; 2021. p. 11–24.
256. Araújo Teresa, Aresta Guilherme, Castro Eduardo, et al. Classification of breast cancer histology images using convolutional neural networks. PloS One 2017;12(6), e0177544.

257. Yan Rui, Ren Fei, Wang Zihao, et al. A hybrid convolutional and recurrent deep neural network for breast cancer pathological image classification. IEEE International Conference on Bioinformatics and Biomedicine (BIBM). IEEE; 2018. p. 957–962.
258. Kumar Neeraj, Verma Ruchika, Sharma Sanuj, Bhargava Surabhi, Vahadane Abhishek, Sethi Amit. A dataset and a technique for generalized nuclear segmentation for computational pathology. IEEE Trans Med Imaging 2017;36(7):1550–1560.
259. Saltz Joel, Gupta Rajarsi, Hou Le, et al. Spatial organization and molecular correlation of tumor-infiltrating lymphocytes using deep learning on pathology images. Cell Rep 2018;23(1):181–193.
260. Graham Simon, Jahanifar Mostafa, Azam Ayesha, et al. Lizard: A large-scale dataset for colonic nuclear instance segmentation and classification. IEEE/CVF International Conference on Computer Vision; 2021. p. 684–693.
261. Idlahcen Ferdaous, Himmi Mohammed Majid, Mahmoudi Abdelhak. Cnn-based approach for cervical cancer classification in whole-slide histopathology images. arXiv preprint 2020.arXiv:2005.13924.
262. Tellez David, Balkenhol Maschenka, Otte-Höller Irene, et al. Whole-slide mitosis detection in h&e breast histology using phh3 as a reference to train distilled stain-invariant convolutional networks. IEEE Trans Med Imaging 2018;37(9):2126–2136.
263. Chang Young Hwan, Thibault Guillaume, Madin Owen, et al. Deep learning based nucleus classification in pancreas histological images. International Conference of the IEEE Engineering in Medicine and Biology Society (EMBC). IEEE; 2017. p. 672–675.
264. Bandi Peter, Geessink Oscar, Manson Quirine, et al. From detection of individual metastases to classification of lymph node status at the patient level: the camelyon17 challenge. IEEE Trans Med Imaging 2018;38(2):550–560.
265. Veta Mitko, Heng Yujing J, Stathonikos Nikolas, et al. Predicting breast tumor proliferation from whole-slide images: the tupac16 challenge. Med Image Anal 2019;54:111–121.
266. Koziarski Michał, Cyganek Bogusław, Olborski Bogusław, et al. Diagset: a dataset for prostate cancer histopathological image classification. arXiv preprint arXiv 2021.2105.04014.
267. Pinckaers Hans, Bulten Wouter, van der Laak Jeroen, Litjens Geert. Detection of prostate cancer in whole-slide images through end-to-end training with image-level labels. IEEE Trans Med Imaging 2021;40(7):1817–1826.
268. Li Bin, Li Yin, Eliceiri Kevin W. Dual-stream multiple instance learning network for whole slide image classification with self-supervised contrastive learning. IEEE/CVF Conference on Computer Vision and Pattern Recognition; 2021. p. 14318–14328.
269. Li Jiahui, Chen Wen, Huang Xiaodi, et al. Hybrid supervision learning for pathology whole slide image classification. International Conference on Medical Image Computing and Computer-Assisted Intervention. Springer; 2021. p. 309–318.
270. Phillips Adon, Teo Iris, Lang Jochen. Fully convolutional network for melanoma diagnostics. arXiv preprint arXiv 2018.1806.04765.
271. Hongming Xu, Park Sunho, Clemenceau Jean René, Radakovich Nathan, Lee Sung Hak, Hwang Tae Hyun. *Deep transfer learning approach to predict tumor mutation burden (tmb) and delineate spatial heterogeneity of tmb within tumors from whole slide images.* , 1Cold Spring Harbor Lab. 2020:554527.
272. Diao James A, Chen Richard J, Kvedar Joseph C. Efficient cellular annotation of histopathology slides with real-time ai augmentation. NPJ Digit Medi 2021;4(1):161.
273. Miao Runtian, Robert Toth Yu, Zhou Anant Madabhushi, Janowczyk Andrew. Quick annotator: an open-source digital pathology based rapid image annotation tool. J Pathol 2021;7(6):542–547.
274. Zhang Ziyu, Fidler Sanja, Urtasun Raquel. Instance-level segmentation for autonomous driving with deep densely connected mrfs. IEEE Conference on Computer Vision and Pattern Recognition; 2016. p. 669–677.
275. Zhang Yuxuan, Ling Huan, Gao Jun, et al. Datasetgan: Efficient labeled data factory with minimal human effort. IEEE/CVF Conference on Computer Vision and Pattern Recognition; 2021. p. 10145–10155.
276. Chen Bowen, Ling Huan, Zeng Xiaohui, Gao Jun, Ziyue Xu, Fidler Sanja. Scribblebox: Interactive annotation framework for video object segmentation. European Conference on Computer Vision. Springer; 2020. p. 293–310.
277. Graham Simon, Quoc Dang Vu, Ahmed Shan E, et al. Hover-net: Simultaneous segmentation and classification of nuclei in multi-tissue histology images. Med Image Anal 2019;58, 101563.
278. Takahama Shusuke, Kurose Yusuke, Mukuta Yusuke, et al. Multi-stage pathological image classification using semantic segmentation. IEEE/CVF International Conference on Computer Vision; 2019. p. 10702–10711.
279. Javed Sajid, Mahmood Arif, Fraz Muhammad Moazam, et al. Cellular community detection for tissue phenotyping in colorectal cancer histology images. Med Image Anal 2020;63, 101696.
280. Roh Yuji, Heo Geon, Whang Steven Euijong. A survey on data collection for machine learning: a big data-ai integration perspective. IEEE Trans Knowl Data Eng 2019;33(4):1328–1347.
281. Wahab Noorul, Miligy Islam M, Dodd Katherine, et al. Semantic annotation for computational pathology: Multidisciplinary experience and best practice recommendations. J Pathol Clin Res 2022;8(2):116–128.
282. Sambasivan Nithya, Kapania Shivani, Highfill Hannah, Akrong Diana, Paritosh Praveen Kumar, Aroyo Lora Mois. Everyone wants to do the model work, not the data work. Data Cascades in High-Stakes Ai 2021:1-15.
283. O'Neil Cathy. *Weapons of Math Destruction: How Big Data Increases Inequality and Threatens Democracy*. USA: Crown Publishing Group. 2016.
284. Lones Michael A. How to avoid machine learning pitfalls: a guide for academic researchers. arXiv preprint arXiv 2021.2108.02497.
285. Bengio Yoshua, Courville Aaron, Vincent Pascal. *Representation Learning: A Review and New Perspectives*. 2012.
286. LeCun Yann, Bengio Yoshua, Hinton Geoffrey. Deep learning. Nature 2015;521(7553):436–444.
287. Kather Jakob Nikolas, Pearson Alexander T, Halama Niels, et al. Deep learning can predict microsatellite instability directly from histology in gastrointestinal cancer. Nat Med 2019;25(7):1054–1056.
288. Tomita Naofumi, Abdollahi Behnaz, Wei Jason, Ren Bing, Suriawinata Arief, Hassanpour Saeed. Attention-based deep neural networks for detection of cancerous and precancerous esophagus tissue on histopathological slides. JAMA Netw Open 2019;2(11). e1914645–e1914645.
289. Bauer Stefan, Carion Nicolas, Schüffler Peter, Fuchs Thomas, Wild Peter, Buhmann Joachim M. Multi-organ cancer classification and survival analysis. arXiv preprint arXiv 2016.1606.00897.
290. Motlagh Mehdi Habibzadeh, Jannesari Mahboobeh, Aboulkheyr HamidReza, et al. Breast cancer histopathological image classification: A deep learning approach. BioRxiv 2018:242818.
291. Celik Yusuf, Talo Muhammed, Yildirim Ozal, Karabatak Murat, Rajendra U, Acharya. Automated invasive ductal carcinoma detection based using deep transfer learning with whole-slide images. Pattern Recogn Lett 2020;133:232–239.
292. Liu Bo, Yao Kelu, Huang Mengmeng, Zhang Jiahui, Li Yong, Li Rong. Gastric pathology image recognition based on deep residual networks. IEEE Annual Computer Software and Applications Conference (COMPSAC). IEEE; 2018. p. 408–412.
293. Wei Jason W, Wei Jerry W, Jackson Christopher R, Ren Bing, Suriawinata Arief A, Hassanpour Saeed. Automated detection of celiac disease on duodenal biopsy slides: A deep learning approach. J Pathol Inform 2019;10.
294. Saxena Shweta, Shukla Sanyam, Gyanchandani Manasi. Pre-trained convolutional neural networks as feature extractors for diagnosis of breast cancer using histopathology. Int J Imaging Syst Technol 2020;30(3):577–591.
295. Bidart Rene, Wong Alexander. Triresnet: A deep triple-stream residual network for histopathology grading. International Conference on Image Analysis and Recognition. Springer; 2019. p. 369–382.
296. Holland Lorne, Wei Dongguang, Olson Kristin A, et al. Limited number of cases may yield generalizable models, a proof of concept in deep learning for colon histology. J Pathol Inform 2020;11.

297. Hekler Achim, Utikal Jochen S, Enk Alexander H, et al. Deep learning outperformed 11 pathologists in the classification of histopathological melanoma images. Eur J Cancer 2019;118:91–96.
298. Lee Byungjae, Paeng Kyunghyun. A robust and effective approach towards accurate metastasis detection and pn-stage classification in breast cancer. International Conference on Medical Image Computing and Computer-Assisted Intervention. Springer; 2018. p. 841–850.
299. Kumar Abhinav, Singh Sanjay Kumar, Sonal Saxena K, et al. Deep feature learning for histopathological image classification of canine mammary tumors and human breast cancer. Inform Sci 2020;508: 405–421.
300. Chan Lyndon, Hosseini Mahdi S, Rowsell Corwyn, Plataniotis Konstantinos N, Damaskinos Savvas. Histosegnet: Semantic segmentation of histological tissue type in whole slide images. IEEE/CVF International Conference on Computer Vision; 2019. p. 10662–10671.
301. Wang Zeya, Dong Nanqing, Dai Wei, Rosario Sean D, Xing Eric P. Classification of breast cancer histopathological images using convolutional neural networks with hierarchical loss and global pooling. International Conference Image Analysis and Recognition. Springer; 2018. p. 745–753.
302. Lu Ming Y, Chen Tiffany Y, Williamson Drew FK, et al. Ai-based pathology predicts origins for cancers of unknown primary. Nature 2021;594(7861):106–110.
303. Gupta Pushpanjali, Huang Yenlin, Sahoo Prasan Kumar, et al. Colon tissues classification and localization in whole slide images using deep learning. Diagnostics 2021;11(8):1398.
304. Feng Ruiwei, Liu Xuechen, Chen Jintai, Chen Danny Z, Gao Honghao, Jian Wu. A deep learning approach for colonoscopy pathology wsi analysis: accurate segmentation and classification. IEEE J Biomed Health Inform 2020;25(10):3700–3708.
305. Farahmand Saman, Fernandez Aileen I, Ahmed Fahad Shabbir, et al. Deep learning trained on hematoxylin and eosin tumor region of interest predicts her2 status and trastuzumab treatment response in her2+ breast cancer. Mod Pathol 2022;35(1):44–51.
306. Ciga Ozan, Tony Xu, Martel Anne Louise. Self supervised contrastive learning for digital histopathology. Mach Learn Appl 2022;7, 100198.
307. Bussola Nicole, Marcolini Alessia, Maggio Valerio, Jurman Giuseppe, Furlanello Cesare. Ai slipping on tiles: Data leakage in digital pathology. International Conference on Pattern Recognition. Springer; 2021. p. 167–182.
308. Alharbi Afaf, Wang Yaqi, Zhang Qianni. Trans-attention multiple instance learning for cancer tissue classification in digital histopathology images. International Conference on Biomedical Signal and Image Processing; 2021. p. 79–84.
309. Cheng Junlong, Tian Shengwei, Long Yu, et al. Resganet: Residual group attention network for medical image classification and segmentation. Med Image Anal 2022;76, 102313.
310. Teh Eu Wern, Taylor Graham W. Learning with less labels in digital pathology via scribble supervision from natural images. arXiv preprint arXiv 2022.2201.02627.
311. Andrew Su, Lee HoJoon, Tan Xiao, et al. A deep learning model for molecular label transfer that enables cancer cell identification from histopathology images. NPJ Precis Oncol 2022;6(1):1-11.
312. Yang Jiawei, Chen Hanbo, Liang Yuan, Huang Junzhou, He Lei, Yao Jianhua. Concl: Concept contrastive learning for dense prediction pre-training in pathology images. European Conference on Computer Vision. Springer; 2022. p. 523–539.
313. Tan Chuanqi, Sun Fuchun, Kong Tao, Zhang Wenchang, Yang Chao, Liu Chunfang. A survey on deep transfer learning. International conference on artificial neural networks. Springer; 2018. p. 270–279.
314. Kipf Thomas N, Welling Max. Semi-supervised classification with graph convolutional networks. International Conference on Learning Representations. OpenReview.net; 2017.
315. Guan Yonghang, Zhang Jun, Tian Kuan, et al. Node-aligned graph convolutional network for whole-slide image representation and classification. Proceedings of the IEEE/CVF Conference on Computer Vision and Pattern Recognition; 2022. p. 18813–18823.
316. Chen Richard J, Lu Ming Y, Shaban Muhammad, et al. Whole slide images are 2d point clouds: Context-aware survival prediction using patch-based graph convolutional networks. International Conference on Medical Image Computing and Computer-Assisted Intervention. Springer; 2021. p. 339–349.
317. Dosovitskiy Alexey, Beyer Lucas, Kolesnikov Alexander, et al. An image is worth 16x16 words: Transformers for image recognition at scale. International Conference on Learning Representations; 2024.
318. Bug Daniel, Schneider Steffen, Grote Anne, et al. Context-based normalization of histological stains using deep convolutional features. Deep Learning in Medical Image Analysis and Multimodal Learning for Clinical Decision Support. Springer; 2017. p. 135–142.
319. Gao Zeyu, Hong Bangyang, Zhang Xianli, et al. Instance-based vision transformer for subtyping of papillary renal cell carcinoma in histopathological image. International Conference on Medical Image Computing and Computer-Assisted Intervention. Springer; 2021. p. 299–308.
320. He Kelei, Gan Chen, Li Zhuoyuan, et al. Transformers in medical image analysis. Intell Med 2023;3(1):59–78.
321. Jiang Yun, Chen Li, Zhang Hai, Xiao Xiao. Breast cancer histopathological image classification using convolutional neural networks with small se-resnet module. PloS One 2019;14(3), e0214587.
322. Li Yi, Ping Wei. Cancer metastasis detection with neural conditional random field. arXiv preprint arXiv 2018.1806.07064.
323. Pimkin Artem, Makarchuk Gleb, Kondratenko Vladimir, Pisov Maxim, Krivov Egor, Belyaev Mikhail. Ensembling neural networks for digital pathology images classification and segmentation. International Conference Image Analysis and Recognition. Springer; 2018. p. 877–886.
324. Kassani Sara Hosseinzadeh, Kassani Peyman Hosseinzadeh, Wesolowski Michal J, Schneider Kevin A, Deters Ralph. Classification of histopathological biopsy images using ensemble of deep learning networks. International Conference on Computer Science and Software Engineering; 2019. p. 92–99.
325. Lu Wenqi, Graham Simon, Bilal Mohsin, Rajpoot Nasir, Minhas Fayyaz. Capturing cellular topology in multi-gigapixel pathology images. IEEE/CVF Conference on Computer Vision and Pattern Recognition Workshops; 2020. p. 260–261.
326. Lin Jiatai, Han Guoqiang, Pan Xipeng, et al. Pdbl: Improving histopathological tissue classification with plug-and-play pyramidal deep-broad learning. IEEE Transactions on Medical Imaging 2022;41: 2252–2262.
327. Senousy Zakaria, Abdelsamea Mohammed M, Gaber Mohamed Medhat, et al. Mcua: Multi-level context and uncertainty aware dynamic deep ensemble for breast cancer histology image classification. IEEE Trans Biomed Eng 2021;69(2):818–829.
328. Kosaraju Sai Chandra, Hao Jie, Koh Hyun Min, Kang Mingon. Deephipo: Multi-scale receptive field deep learning for histopathological image analysis. Methods 2020;179:3-13.
329. Ronneberger Olaf, Fischer Philipp, Brox Thomas. U-net: Convolutional networks for biomedical image segmentation. International Conference on Medical Image Computing and Computer-Assisted Intervention. Springer; 2015. p. 234–241.
330. Hou Le, Agarwal Ayush, Samaras Dimitris, Kurc Tahsin M, Gupta Rajarsi R, Saltz Joel H. *Robust Histopathology Image Analysis: To Label or to Synthesize?*. 2019:8533–8542.
331. Shin Hoo-Chang, Roth Holger R, Gao Mingchen, et al. Deep convolutional neural networks for computer-aided detection: Cnn architectures, dataset characteristics and transfer learning. IEEE Trans Med Imaging 2016;35(5):1285–1298.
332. Quoc Dang Vu, Graham Simon, Kurc Tahsin, et al. Methods for segmentation and classification of digital microscopy tissue images. Front Bioeng Biotechnol 2019:53.
333. Chen Kemeng, Zhang Ning, Powers Linda, Roveda Janet. Cell nuclei detection and segmentation for computational pathology using deep learning. Spring Simulation Conference (SpringSim). IEEE; 2019. p. 1–6.

334. Bai Tian, Jiayu Xu, Xing Fuyong. Multi-field of view aggregation and context encoding for single-stage nucleus recognition. International Conference on Medical Image Computing and Computer-Assisted Intervention. Springer; 2020. p. 382–392.
335. Xie Xinpeng, Chen Jiawei, Li Yuexiang, Shen Linlin, Ma Kai, Zheng Yefeng. Instance-aware self-supervised learning for nuclei segmentation. International Conference on Medical Image Computing and Computer-Assisted Intervention. Springer; 2020. p. 341–350.
336. Lahiani Amal, Gildenblat Jacob, Klaman Irina, Navab Nassir, Klaiman Eldad. Generalizing multistain immunohistochemistry tissue segmentation using one-shot color deconvolution deep neural networks. arXiv preprint arXiv 2018.1805.06958.
337. Jiménez Gabriel, Racoceanu Daniel. Deep learning for semantic segmentation versus classification in computational pathology: Application to mitosis analysis in breast cancer grading. Front Bioeng Biotechnol 2019;7:145.
338. Kausar Tasleem, MingJiang Wang, Ashraf M Adnan, Kausar Adeeba. Smallmitosis: Small size mitotic cells detection in breast histopathology images. IEEE Access 2020;9:905–922.
339. Ho David Joon, Agaram Narasimhan P, Schüffler Peter J, et al. Deep interactive learning: an efficient labeling approach for deep learning-based osteosarcoma treatment response assessment. International Conference on Medical Image Computing and Computer-Assisted Intervention. Springer; 2020. p. 540–549.
340. Wetstein Suzanne C, Onken Allison M, Luffman Christina, et al. Deep learning assessment of breast terminal duct lobular unit involution: Towards automated prediction of breast cancer risk. PloS One 2020;15(4), e0231653.
341. Qureshi Hammad, Sertel Olcay, Rajpoot Nasir, Wilson Roland, Gurcan Metin. Adaptive discriminant wavelet packet transform and local binary patterns for meningioma subtype classification. International Conference on Medical Image Computing and Computer-Assisted Intervention. Springer; 2008. p. 196–204.
342. Geread Rokshana Stephny, Sivanandarajah Abishika, Brouwer Emily Rita, et al. pinet–an automated proliferation index calculator framework for ki67 breast cancer images. Cancers 2021;13(1):11.
343. Schuhmacher D, Schörner S, Küpper C, et al. A framework for falsifiable explanations of machine learning models with an application in computational pathology. Medical Image Analysis 2022 Nov 1;82:102594.
344. Gallego Jaime, Swiderska-Chadaj Zaneta, Markiewicz Tomasz, Michifumi Yamashita M, Gabaldon Alejandra, Gertych Arkadiusz. A u-net based framework to quantify glomerulosclerosis in digitized pas and h&e stained human tissues. Comput Med Imaging Graph 2021;89, 101865.
345. Jianghua Wu, Liu Changling, Liu Xiaoqing, et al. Artificial intelligence-assisted system for precision diagnosis of pd-l1 expression in non-small cell lung cancer. Mod Pathol 2021:1–9.
346. Chen Pingjun, Liang Yun, Shi Xiaoshuang, Yang Lin, Gader Paul. Automatic whole slide pathology image diagnosis framework via unit stochastic selection and attention fusion. Neurocomputing 2021;453:312–325.
347. Nour Abdala, Saad Sherif, Boufama Boubakeur. Prostate biomedical images segmentation and classification by using u-net cnn model. ACM Conference on Bioinformatics, Computational Biology, and Health Informatics, 1–7. ; 2021.
348. Bayat Akram, Anderson Connor, Shah Pratik. *Automated End-to-End Deep Learning Framework for Classification and Tumor Localization From Native Non-Stained Pathology Images*, 11596. 2021:115960A.
349. Khened Mahendra, Kori Avinash, Rajkumar Haran, Krishnamurthi Ganapathy, Srinivasan Balaji. A generalized deep learning framework for whole-slide image segmentation and analysis. Sci Rep 2021;11(1):1-14.
350. Naylor Peter, Laé Marick, Reyal Fabien, Walter Thomas. *Nuclei Segmentation in Histopathology Images Using Deep Neural Networks*. 2017:933–936.
351. Sahasrabudhe Mihir, Christodoulidis Stergios, Salgado Roberto, et al. Self-supervised nuclei segmentation in histopathological images using attention. International Conference on Medical Image Computing and Computer-Assisted Intervention. Springer; 2020. p. 393–402.
352. Nadeem Saad, Hollmann Travis, Tannenbaum Allen. Multimarginal wasserstein barycenter for stain normalization and augmentation. International Conference on Medical Image Computing and Computer-Assisted Intervention. Springer; 2020. p. 362–371.
353. Dong Nanqing, Kampffmeyer Michael, Liang Xiaodan, Wang Zeya, Dai Wei, Xing Eric. Reinforced auto-zoom net: Towards accurate and fast breast cancer segmentation in whole-slide images. Deep Learning in Medical Image Analysis and Multimodal Learning for Clinical Decision Support. Springer; 2018. p. 317–325.
354. van Eekelen Leander, Pinckaers Hans, Hebeda Konnie M, Litjens Geert. *Multi-Class Semantic Cell Segmentation and Classification of Aplasia in Bone Marrow Histology Images*, 11320. 2020:113200B.
355. Xing Gang, Lei Jianqin, Xu Xiayu. Fluid segmentation in oct with an improved convolutional neural network. The Fifth International Conference on Biological Information and Biomedical Engineering; 2021. p. 1–5.
356. Khoshdeli Mina, Winkelmaier Garrett, Parvin Bahram. Fusion of encoder-decoder deep networks improves delineation of multiple nuclear phenotypes. BMC Bioinform 2018;19(1):1-11.
357. Abdel-Nasser Mohamed, Saleh Adel, Puig Domenec. Channel-wise aggregation with self-correction mechanism for multi-center multi-organ nuclei segmentation in whole slide imaging. VISIGRAPP; 2020. p. 466–473.
358. Chen Shengcong, Ding Changxing, Tao Dacheng. *Boundary-Assisted Region Proposal Networks for Nucleus Segmentation*. 2020:279–288.
359. Graham Simon, Chen Hao, Gamper Jevgenij, et al. Mild-net: Minimal information loss dilated network for gland instance segmentation in colon histology images. Med Image Anal 2019;52:199–211.
360. Agarwalla Abhinav, Shaban Muhammad, Rajpoot Nasir M. Representation-aggregation networks for segmentation of multi-gigapixel histology images. ArXiv 2017.abs/1707.08814.
361. Li Ziqiang, Tao Rentuo, Wu Qianrun, Li Bin. Da-refinenet: A dual input whole slide image segmentation algorithm based on attention. arXiv 2019.arXiv–1907.
362. Pati Pushpak, Andani Sonali, Pediaditis Matthew, et al. Deep positive-unlabeled learning for region of interest localization in breast tissue images. Medical Imaging: Digital Pathology. International Society for Optics and Photonics; 2018. p. 1058107.
363. Qaiser Talha, Tsang Yee-Wah, Taniyama Daiki, et al. Fast and accurate tumor segmentation of histology images using persistent homology and deep convolutional features. Med Image Anal 2019;55:1-14.
364. Das Dev Kumar, Bose Surajit, Maiti Asok Kumar, Mitra Bhaskar, Mukherjee Gopeswar, Dutta Pranab Kumar. Automatic identification of clinically relevant regions from oral tissue histological images for oral squamous cell carcinoma diagnosis. Tissue Cell 2018;53:111–119.
365. Adam J, Shephard Simon Graham, Bashir Saad, et al. Simultaneous nuclear instance and layer segmentation in oral epithelial dysplasia. IEEE/CVF International Conference on Computer Vision; 2021. p. 552–561.
366. Wang Liuan, Sun Li, Zhang Mingjie, et al. Exploring pathologist knowledge for automatic assessment of breast cancer metastases in whole-slide image. ACM International Conference on Multimedia; 2021. p. 255–263.
367. Jahanifar Mostafa, Tajeddin Neda Zamani, Koohbanani Navid Alemi, Rajpoot Nasir M. Robust interactive semantic segmentation of pathology images with minimal user input. IEEE/CVF International Conference on Computer Vision; 2021. p. 674–683.
368. Kim Hyeongsub, Yoon Hongjoon, Thakur Nishant, et al. Deep learning-based histopathological segmentation for whole slide images of colorectal cancer in a compressed domain. Sci Rep 2021;11(1):1-14.
369. Dogar G Murtaza, Fraz Muhammad Moazam, Javed Sajid. *Feature Attention Network for Simultaneous Nuclei Instance Segmentation and Classification in Histology Images*. 2021:1–6.
370. Lafarge Maxime W, Pluim Josien PW, Eppenhof Koen AJ, Veta Mitko. Learning domain-invariant representations of histological images. Front Med 2019;6:162.

371. Wang Haibo, Roa Angel Cruz, Basavanhally Ajay N, et al. Mitosis detection in breast cancer pathology images by combining handcrafted and convolutional neural network features. J Med Imag 2014;1(3), 034003.
372. Li Chao, Wang Xinggang, Liu Wenyu, Latecki Longin Jan. Deepmitosis: Mitosis detection via deep detection, verification and segmentation networks. Med Image Anal 2018;45:121–133.
373. Li Chao, Wang Xinggang, Liu Wenyu, Latecki Longin Jan, Wang Bo, Huang Junzhou. Weakly supervised mitosis detection in breast histopathology images using concentric loss. Med Image Anal 2019;53: 165–178.
374. Sebai Meriem, Wang Xinggang, Wang Tianjiang. Maskmitosis: a deep learning framework for fully supervised, weakly supervised, and unsupervised mitosis detection in histopathology images. Med Biol Eng Comput 2020;58(7):1603–1623.
375. Akram Saad Ullah, Qaiser Talha, Graham Simon, Kannala Juho, Heikkilä Janne, Rajpoot Nasir. *Leveraging Unlabeled Whole-Slide-Images for Mitosis Detection*. 2018:69–77.
376. Lafarge Maxime W, Bekkers Erik J, Pluim Josien PW, Duits Remco, Veta Mitko. Roto-translation equivariant convolutional networks: Application to histopathology image analysis. Med Image Anal 2021;68, 101849.
377. Alom Md Zahangir, Aspiras Theus, Taha Tarek M, Bowen Tj, Asari Vijayan K. Mitosisnet: End-to-end mitotic cell detection by multi-task learning. IEEE Access 2020;8:68695–68710.
378. Li Hansheng, Han Xin, Kang Yuxin, et al. A novel loss calibration strategy for object detection networks training on sparsely annotated pathological datasets. International Conference on Medical Image Computing and Computer-Assisted Intervention. Springer; 2020. p. 320–329.
379. Pati Pushpak, Foncubierta-Rodríguez Antonio, Goksel Orcun, Gabrani Maria. Reducing annotation effort in digital pathology: A co-representation learning framework for classification tasks. Med Image Anal 2021;67, 101859.
380. Brieu Nicolas, Meier Armin, Kapil Ansh, et al. Domain adaptation-based augmentation for weakly supervised nuclei detection. arXiv preprint arXiv 2019.1907.04681.
381. Thomas J Fuchs, Wild Peter J, Moch Holger, Buhmann Joachim M. *Computational Pathology Analysis of Tissue Microarrays Predicts Survival of Renal Clear Cell Carcinoma Patients*. 2008:1–8.
382. Li Wenyuan, Li Jiayun, Sarma Karthik V, et al. Path r-cnn for prostate cancer diagnosis and gleason grading of histological images. IEEE Trans Med Imaging 2018;38(4):945–954.
383. Kashif Muhammad Nasim, Ahmed Shan E, Raza Korsuk Sirinukunwattana, Arif Muhammmad, Rajpoot Nasir. Handcrafted features with convolutional neural networks for detection of tumor cells in histology images. IEEE International Symposium on Biomedical Imaging. IEEE; 2016. p. 1029–1032.
384. Jaume Guillaume, Pati Pushpak, Anklin Valentin, Foncubierta Antonio, Gabrani Maria. Histocartography: A toolkit for graph analytics in digital pathology. MICCAI Workshop on Computational Pathology. PMLR; 2021. p. 117–128.
385. Javed Sajid, Mahmood Arif, Dias Jorge, Werghi Naoufel, Rajpoot Nasir. Spatially constrained context-aware hierarchical deep correlation filters for nucleus detection in histology images. Med Image Anal 2021;72, 102104.
386. Wang Linbo, Zhen Hui, Fang Xianyong, Wan Shaohua, Ding Weiping, Guo Yanwen. A unified two-parallel-branch deep neural network for joint gland contour and segmentation learning. Futur Gener Comput Syst 2019;100:316–324.
387. Wu Bingzhe, Zhao Shiwan, Sun Guangyu, et al. P3sgd: Patient privacy preserving sgd for regularizing deep cnns in pathological image classification. IEEE/CVF Conference on Computer Vision and Pattern Recognition; 2019. p. 2099–2108.
388. Yang Haichun, Deng Ruining, Yuzhe Lu, et al. Circlenet: Anchor-free glomerulus detection with circle representation. International Conference on Medical Image Computing and Computer-Assisted Intervention. Springer; 2020. p. 35–44.
389. Gloria Bueno M, Fernandez-Carrobles Milagro, Gonzalez-Lopez Lucia, Deniz Oscar. Glomerulosclerosis identification in whole slide images using semantic segmentation. Comput Methods Programs Biomed 2020;184, 105273.
390. Zixiao Lu, Siwen Xu, Shao Wei, et al. Deep-learning–based characterization of tumor-infiltrating lymphocytes in breast cancers from histopathology images and multiomics data. JCO Clin Cancer Inform 2020;4:480–490.
391. Tellez David, Höppener Diederik, Verhoef Cornelis, et al. *Extending Unsupervised Neural Image Compression with Supervised Multitask Learning*. 2020:770–783.
392. Alawad Mohammed, Gao Shang, Qiu John X, et al. Automatic extraction of cancer registry reportable information from free-text pathology reports using multitask convolutional neural networks. J Am Med Inform Assoc 2020;27(1):89–98.
393. Feng Zunlei, Wang Zhonghua, Wang Xinchao, et al. Mutual-complementing framework for nuclei detection and segmentation in pathology image. Proceedings of the IEEE/CVF International Conference on Computer Vision; 2021. p. 4036–4045.
394. Sener Ozan, Koltun Vladlen. Multi-task learning as multi-objective optimization. In: *Bengio S, Wallach H, Larochelle H, Grauman K, Cesa-Bianchi N, Garnett R, eds. Advances in Neural Information Processing Systems*. Curran Associates, Inc; 2018.
395. Royer Amelie, Blankevoort Tijmen, Bejnordi Babak Ehteshami Bejnordi. Scalarization for multi-task and multi-domain learning at scale. Advances in Neural Information Processing Systems; 2023.
396. Ngiam Jiquan, Khosla Aditya, Kim Mingyu, Nam Juhan, Lee Honglak, Ng Andrew Y. Multimodal deep learning. ICML; 2011.
397. Mi Haoyang, Bivalacqua Trinity J, Kates Max, et al. Predictive models of response to neoadjuvant chemotherapy in muscle-invasive bladder cancer using nuclear morphology and tissue architecture. Cell Rep Med 2021;2(9).
398. Foersch Sebastian, Glasner Christina, Woerl Ann-Christin, et al. Multistain deep learning for prediction of prognosis and therapy response in colorectal cancer. Nat Med 2023;29(2):430–439.
399. Huang Zhi, Shao Wei, Han Zhi, et al. Artificial intelligence reveals features associated with breast cancer neoadjuvant chemotherapy responses from multi-stain histopathologic images. NPJ Precis Oncol 2023;7(1):14.
400. Li Chunyuan, Zhu Xinliang, Yao Jiawen, Huang Junzhou. Hierarchical transformer for survival prediction using multimodality whole slide images and genomics. In 2022 26th International Conference on Pattern Recognition (ICPR). IEEE; 2022. p. 4256–4262.
401. Yawen Wu, Michael Cheng, Shuo Huang, Zongxiang Pei, Yingli Zuo, Jianxin Liu, Kai Yang, Qi Zhu, Jie Zhang, Honghai Hong, Daoqiang Zhang, Kun Huang, Liang Cheng, and Wei Shao. Recent advances of deep learning for computational histopathology: principles and applications. Cancers (Basel), 14(5):1199, February 2022.
402. Xinrui Huang, Zhaotong Li, Minghui Zhang, and Song Gao. Fusing hand-crafted and deep-learning features in a convolutional neural network model to identify prostate cancer in pathology images. Front Oncol, 12:994950, September 2022.
403. Rehman Mobeen Ur, Akhtar Suhail, Zakwan Muhammad, Mahmood Muhammad Habib. Novel architecture with selected feature vector for effective classification of mitotic and non-mitotic cells in breast cancer histology images. Biomed Signal Process Control 2022;71, 103212.
404. Sigirci I Onur, Albayrak Abdulkadir, Bilgin Gokhan. Detection of mitotic cells in breast cancer histopathological images using deep versus handcrafted features. Multimed Tools Appl 2021:1-24.
405. Weng Wei-Hung, Cai Yuannan, Lin Angela, Tan Fraser, Chen Po-Hsuan Cameron. Multimodal multitask representation learning for pathology biobank metadata predictionarXiv preprint arXiv: 1909.07846. . 2019.
406. Boehm Kevin M, Khosravi Pegah, Vanguri Rami, Gao Jianjiong, Shah Sohrab P. Harnessing multimodal data integration to advance precision oncology. Nat Rev Cancer 2021:1-13.

407. Shao Wei, Wang Tongxin, Sun Liang, et al. Multi-task multi-modal learning for joint diagnosis and prognosis of human cancers. Med Image Anal 2020;65, 101795.
408. Wang Zhiqin, Li Ruiqing, Wang Minghui, Li Ao. Gpdbn: deep bilinear network integrating both genomic data and pathological images for breast cancer prognosis prediction. Bioinformatics 2021;37(18): 2963–2970.
409. Huang Zhi, Bianchi Federico, Yuksekgonul Mert, Montine Thomas J, Zou James. A visual–language foundation model for pathology image analysis using medical twitter. Nat Med 2023:1-10.
410. Ikezogwo Wisdom Oluchi, Seyfioglu Mehmet Saygin, Ghezloo Fatemeh, et al. Quilt-1m: One million image-text pairs for histopathologyarXiv preprint arXiv:2306.11207. . 2023.
411. Linhao Qu, Luo Xiaoyuan, Fu Kexue, Wang Manning, Song Zhijian. The rise of ai language pathologists: Exploring two-level prompt learning for few-shot weakly-supervised whole slide image classification. Conference on Computer Vision and Pattern Recognition (CVPR); 2023.
412. Lu Ming Y, Chen Bowen, Zhang Andrew, et al. Visual language pretrained multiple instance zero-shot transfer for histopathology images. Proceedings of the IEEE/CVF Conference on Computer Vision and Pattern Recognition (CVPR); June 2023. p. 19764–19775.
413. LeCun Yann, Bengio Yoshua, Hinton Geoffrey. Deep learning. Nature 2015;521(7553):436–444.
414. Nahid AA, Mehrabi MA, Kong Y. Histopathological Breast Cancer Image Classification by Deep Neural Network Techniques Guided by Local Clustering. Biomed Research International 2018 Mar 7;2018.2362108-2362108.
415. Zhang Zizhao, Chen Pingjun, McGough Mason, et al. Pathologist-level interpretable whole-slide cancer diagnosis with deep learning. Nat Mach Intell 2019;1(5):236–245.
416. Yao Hongdou, Zhang Xuejie, Zhou Xiaobing, Liu Shengyan. Parallel structure deep neural network using cnn and rnn with an attention mechanism for breast cancer histology image classification. Cancers 2019;11(12):1901.
417. Bolei Xu, Liu Jingxin, Hou Xianxu, et al. Look, investigate, and classify: A deep hybrid attention method for breast cancer classification. IEEE International Symposium on Biomedical Imaging. IEEE; 2019. p. 914–918.
418. Raciti Patricia, Sue Jillian, Ceballos Rodrigo, et al. Novel artificial intelligence system increases the detection of prostate cancer in whole slide images of core needle biopsies. Mod Pathol 2020;33(10):2058–2066.
419. BenTaieb Aïcha, Hamarneh Ghassan. Predicting cancer with a recurrent visual attention model for histopathology images. International Conference on Medical Image Computing and Computer-Assisted Intervention. Springer; 2018. p. 129–137.
420. Zheng Yushan, Jiang Zhiguo, Zhang Haopeng, Xie Fengying, Shi Jun. Tracing diagnosis paths on histopathology wsis for diagnostically relevant case recommendation. In: *Martel Anne L, Abolmaesumi Purang, Stoyanov Danail, Mateus Diana, Zuluaga Maria A, eds. Medical Image Computing and Computer Assisted Intervention – MICCAI, Volume 12265 of Lecture Notes in Computer Science. Springer; 2020. p. 459–469.*
421. Qi Jing, Burnside Girvan, Charnley Paul, Coenen Frans. Event-based pathology data prioritisation: a study using multi-variate time series classification. Proceedings of the 13th International Joint Conference On Knowledge Discovery, Knowledge Engineering and Knowledge Management (KDIR). Scitepress-Science and Technology Publications; 2021. p. 121–128.
422. Bolei Xu, Liu Jingxin, Hou Xianxu, et al. Attention by selection: a deep selective attention approach to breast cancer classification. IEEE Trans Med Imaging 2019;39(6):1930–1941.
423. Vaswani Ashish, Shazeer Noam, Parmar Niki, et al. Attention is all you need. Adv Neural Inform Process Syst 2017;30.
424. Mahmood Faisal, Borders Daniel, Chen Richard J, et al. Deep adversarial training for multi-organ nuclei segmentation in histopathology images. IEEE Trans Med Imaging 2019;39(11):3257–3267.
425. Quiros Adalberto Claudio, Murray-Smith Roderick, Yuan Ke. Pathologygan: learning deep representations of cancer tissue. J Mach Learn Biomed Imaging 2021;2021(4):1-48.
426. Deshpande Srijay, Minhas Fayyaz, Graham Simon, Rajpoot Nasir. Safron: stitching across the frontier network for generating colorectal cancer histology images. Med Image Anal 2022;77, 102337.
427. Hyungjoo Cho, Sungbin Lim, Gunho Choi, and Hyunseok Min. Neural stain-style transfer learning using gan for histopathological images. arXiv preprint arXiv:1710.08543, 2017.
428. Schrammen Peter Leonard, Laleh Narmin Ghaffari, Echle Amelie, et al. Weakly supervised annotation-free cancer detection and prediction of genotype in routine histopathology. J Pathol 2022;256(1): 50–60.
429. Rawat Rishi R, Ortega Itzel, Roy Preeyam, et al. Deep learned tissue "fingerprints" classify breast cancers by er/pr/her2 status from h&e images. Sci Rep 2020;10(1):1-13.
430. Lahiani Amal, Gildenblat Jacob, Klaman Irina, Albarqouni Shadi, Navab Nassir, Klaiman Eldad. Virtualization of tissue staining in digital pathology using an unsupervised deep learning approach. European Congress on Digital Pathology. Springer; 2019. p. 47–55.
431. Lahiani Amal, Navab Nassir, Albarqouni Shadi, Klaiman Eldad. Perceptual embedding consistency for seamless reconstruction of tilewise style transfer. International Conference on Medical Image Computing and Computer-Assisted Intervention. Springer; 2019. p. 568–576.
432. Tavolara Thomas E, Khalid Khan Niazi M, Arole Vidya, Chen Wei, Frankel Wendy, Gurcan Metin N. A modular cgan classification framework: application to colorectal tumor detection. Sci Rep 2019;9(1):1–8.
433. Bo Hu, Ye Tang I, Eric Chao Chang, Fan Yubo, Lai Maode, Yan Xu. Unsupervised learning for cell-level visual representation in histopathology images with generative adversarial networks. IEEE J Biomed Health Inform 2018;23(3):1316–1328.
434. Xu Zhaoyang, Moro Carlos Fernández, Bozóky Béla, Zhang Qianni. Gan-based virtual re-staining: a promising solution for whole slide image analysisarXiv preprint arXiv:1901.04059. . 2019.
435. Abousamra Shahira, Gupta Rajarsi, Kurc Tahsin, Samaras Dimitris, Saltz Joel, Chen Chao. Topology-guided multi-class cell context generation for digital pathology. Proceedings of the IEEE/CVF Conference on Computer Vision and Pattern Recognition (CVPR); 2023. p. 3323–3333.
436. Aversa Marco, Nobis Gabriel, Hägele Miriam, et al. Diffinfinite: Large mask-image synthesis via parallel random patch diffusion in histopathologyarXiv preprint arXiv:2306.13384. . 2023.
437. Patil Abhijeet, Tamboli Dipesh, Meena Swati, Anand Deepak, Sethi Amit. Breast cancer histopathology image classification and localization using multiple instance learning. IEEE International WIE Conference on Electrical and Computer Engineering (WIECON-ECE). IEEE; 2019. p. 1–4.
438. Mercan Caner, Aksoy Selim, Mercan Ezgi, Shapiro Linda G, Weaver Donald L, Elmore Joann G. Multi-instance multi-label learning for multi-class classification of whole slide breast histopathology images. IEEE Trans Med Imaging 2017;37(1):316–325.
439. Wang Shujun, Zhu Yaxi, Lequan Yu, et al. Rmdl: recalibrated multi-instance deep learning for whole slide gastric image classification. Med Image Anal 2019;58, 101549.
440. Yan Xu, Mo Tao, Feng Qiwei, Zhong Peilin, Maode Lai I, Eric, and Chao Chang. Deep learning of feature representation with multiple instance learning for medical image analysis. IEEE International Conference on Acoustics, Speech and Signal Processing (ICASSP). IEEE; 2014. p. 1626–1630.
441. Yan Xu, Li Yeshu, Shen Zhengyang, et al. Parallel multiple instance learning for extremely large histopathology image analysis. BMC Bioinforma 2017;18(1):1-15.
442. Li Jiayun, Li Wenyuan, Gertych Arkadiusz, Knudsen Beatrice S, Speier William, Arnold Corey W. An attention-based multi-resolution model for prostate whole slide image classification and localizationArXiv, abs/1905.13208. . 2019.

443. Yaar Asfand, Asif Amina, Ahmed Raza Shan E, Rajpoot Nasir, Minhas Fayyaz. Cross-domain knowledge transfer for prediction of chemosensitivity in ovarian cancer patients. IEEE/CVF Conference on Computer Vision and Pattern Recognition Workshops; 2023. p. 928–929.
444. Lerousseau Marvin, Vakalopoulou Maria, Classe Marion, et al. Weakly supervised multiple instance learning histopathological tumor segmentation. International Conference on Medical Image Computing and Computer-Assisted Intervention. Springer; 2020. p. 470–479.
445. Chikontwe Philip, Kim Meejeong, Nam Soo Jeong, Go Heounjeong, Park Sang Hyun. Multiple instance learning with center embeddings for histopathology classification. International Conference on Medical Image Computing and Computer-Assisted Intervention. Springer; 2020. p. 519–528.
446. Yao Jiawen, Zhu Xinliang, Jonnagaddala Jitendra, Hawkins Nicholas, Huang Junzhou. Whole slide images based cancer survival prediction using attention guided deep multiple instance learning networks. Med Image Anal 2020;65, 101789.
447. Lu Ming Y, Chen Richard J, Kong Dehan, et al. Federated learning for computational pathology on gigapixel whole slide images. Med Image Anal 2022;76, 102298.
448. Lu Ming Y, Chen Tiffany Y, Williamson Drew FK, et al. Ai-based pathology predicts origins for cancers of unknown primary. Nature 2021;594(7861):106–110.
449. Jewsbury Robert, Bhalerao Abhir, Rajpoot Nasir M. A quadtree image representation for computational pathology. IEEE/CVF International Conference on Computer Vision; 2021. p. 648–656.
450. Riasatian Abtin, Babaie Morteza, Maleki Danial, et al. Fine-tuning and training of densenet for histopathology image representation using tcga diagnostic slides. Med Image Anal 2021;70, 102032.
451. Pal Anabik, Xue Zhiyun, Desai Kanan, et al. Deep multiple-instance learning for abnormal cell detection in cervical histopathology images. Comput Biol Med 2021;138, 104890.
452. Freyre Christophe AC, Spiegel Stephan, Keller Caroline Gubser, et al. Biomarker-based classification and localization of renal lesions using learned representations of histology—a machine learning approach to histopathology. Toxicol Pathol 2021;49(4):798–814.
453. Marini Niccolò, Otálora Sebastian, Ciompi Francesco, et al. Multi-scale task multiple instance learning for the classification of digital pathology images with global annotations. MICCAI Workshop on Computational Pathology. PMLR; 2021. p. 170–181.
454. Höhne Johannes, de Zoete Jacob, Schmitz Arndt A, Bal Tricia, di Tomaso Emmanuelle, Lenga Matthias. Detecting genetic alterations in braf and ntrk as oncogenic drivers in digital pathology images: towards model generalization within and across multiple thyroid cohorts. MICCAI Workshop on Computational Pathology. PMLR; 2021. p. 105–116.
455. Anand Deepak, Yashashwi Kumar, Kumar Neeraj, Rane Swapnil, Gann Peter H, Sethi Amit. Weakly supervised learning on unannotated h&e-stained slides predicts braf mutation in thyroid cancer with high accuracy. J Pathol 2021;255(3):232–242.
456. Shao Zhuchen, Bian Hao, Chen Yang, et al. Transmil: transformer based correlated multiple instance learning for whole slide image classification. Adv Neural Inform Process Syst 2021;34:2136–2147.
457. Li Kailu, Qian Ziniu, Han Yingnan, et al. Weakly supervised histopathology image segmentation with self-attention. Med Image Anal 2023;86(102791), 102791.
458. Li Fei, Wang Mingyu, Huang Bin, et al. Patients and slides are equal: A multi-level multi-instance learning framework for pathological image analysis. International Conference on Medical Image Computing and Computer-Assisted Intervention. Springer; 2023. p. 63–71.
459. Nakhli Ramin, Zhang Allen, Mirabadi Ali, et al. Co-pilot: Dynamic top-down point cloud with conditional neighborhood aggregation for multi-gigapixel histopathology image representation. Proceedings of the IEEE/CVF International Conference on Computer Vision (ICCV); October 2023. p. 21063–21073.
460. Abbas Syed Farhan, Le Vuong Trinh Thi, Kim Kyungeun, Song Boram, Kwak Jin Tae. Multi-cell type and multi-level graph aggregation network for cancer grading in pathology images. Med Image Anal 2023;90(102936), 102936.
461. Lee Jaeung, Byeon Keunho, Kwak Jin Tae. Centroid-aware feature recalibration for cancer grading in pathology images. International Conference on Medical Image Computing and Computer-Assisted Intervention. Springer; 2023. p. 212–221.
462. Azadi Puria, Suderman Jonathan, Nakhli Ramin, et al. ALL-IN: A local GLobal graph-based DIstillatioN model for representation learning of gigapixel histopathology images with application in cancer risk assessment. Lecture Notes in Computer Science. Switzerland, Cham: Springer Nature; 2023. p. 765–775.
463. Nakhli Ramin, Moghadam Puria Azadi, Mi Haoyang, et al. Sparse multi-modal graph transformer with shared-context processing for representation learning of giga-pixel images. In 2023 IEEE/CVF Conference on Computer Vision and Pattern Recognition (CVPR). IEEE; 2023.
464. Campanella Gabriele, Silva Vitor Werneck Krauss, Fuchs Thomas J. Terabyte-scale deep multiple instance learning for classification and localization in pathologyarXiv preprint arXiv:1805.06983. . 2018.
465. Zhang Hongrun, Meng Yanda, Zhao Yitian, et al. Dtfd-mil: Double-tier feature distillation multiple instance learning for histopathology whole slide image classification. Proceedings of the IEEE/CVF Conference on Computer Vision and Pattern Recognition; 2022. p. 18802–18812.
466. Hadsell Raia, Chopra Sumit, LeCun Yann. Dimensionality reduction by learning an invariant mapping. IEEE Computer Society Conference on Computer Vision and Pattern Recognition (CVPR'06). IEEE; 2006. p. 1735–1742.
467. Schroff Florian, Kalenichenko Dmitry, Philbin James. Facenet: A unified embedding for face recognition and clustering. IEEE Conference on Computer Vision and Pattern Recognition; 2015. p. 815–823.
468. Tran Manuel, Wagner Sophia J, Boxberg Melanie, Peng Tingying. S5cl: Unifying fully-supervised, self-supervised, and semi-supervised learning through hierarchical contrastive learning. In: *Wang Linwei, Qi Dou P, Fletcher Thomas, Speidel Stefanie, Li Shuo, eds. Medical Image Computing and Computer Assisted Intervention – MICCAI 2022. Cham: Springer Nature Switzerland; 2022. p. 99-108.*
469. Carse Jacob, Carey Frank, McKenna Stephen. Unsupervised representation learning from pathology images with multi-directional contrastive predictive coding. IEEE International Symposium on Biomedical Imaging. IEEE; 2021. p. 1254–1258.
470. Dawood Muhammad, Branson Kim, Rajpoot Nasir M, Minhas Fayyaz. Albrt: Cellular composition prediction in routine histology images. IEEE/CVF International Conference on Computer Vision; 2021. p. 664–673.
471. Feng Chao, Vanderbilt Chad, Fuchs Thomas. Nuc2vec: Learning representations of nuclei in histopathology images with contrastive loss. Medical Imaging with Deep Learning. PMLR; 2021. p. 179–189.
472. Yang Jiawei, Chen Hanbo, Yan Jiangpeng, Chen Xiaoyu, Yao Jianhua. Towards better understanding and better generalization of few-shot classification in histology images with contrastive learningarXiv preprint arXiv:2202.09059. . 2022.
473. Cheng Jiang, Hou Xinhai, Kondepudi Akhil, et al. Hierarchical discriminative learning improves visual representations of biomedical microscopy. Proceedings of the IEEE/CVF Conference on Computer Vision and Pattern Recognition (CVPR); June 2023. p. 19798–19808.
474. Gildenblat Jacob, Yüce Anil, Abbasi-Sureshjani Samaneh, Korski Konstanty. Deep cellular embeddings: An explainable plug and play improvement for feature representation in histopathology. Proceedings of the International Conference on Medical Image Computing and Computer Assisted Intervention (MICCAI); October 2023.
475. Basak Hritam, Yin Zhaozheng. Pseudo-label guided contrastive learning for semi-supervised medical image segmentation. Proceedings of the IEEE/CVF Conference on Computer Vision and Pattern Recognition (CVPR); June 2023. p. 19786–19797.
476. Eminaga Okyaz, Abbas Mahmoud, Kunder Christian, et al. Plexus convolutional neural network (plexusnet): A novel neural network

architecture for histologic image analysisarXiv preprint arXiv:1908.09067. . 2019.
477. Hao Jie, Kosaraju Sai Chandra, Tsaku Nelson Zange, Song Dae Hyun, Kang Mingon. Page-net: Interpretable and integrative deep learning for survival analysis using histopathological images and genomic data. Pacific Symposium on Biocomputing. World Scientific; 2019. p. 355–366.
478. Yen Ting-An, Hsu Hung-Chun, Pati Pushpak, Gabrani Maria, Foncubierta-Rodríguez Antonio, Chung Pau-Choo. Ninepins: Nuclei instance segmentation with point annotationsarXiv preprint arXiv:2006.13556. . 2020.
479. Tang Sheyang, Hosseini Mahdi S, Chen Lina, et al. Probeable darts with application to computational pathology. IEEE/CVF International Conference on Computer Vision; 2021. p. 572–581.
480. Galván Edgar, Mooney Peter. Neuroevolution in deep neural networks: current trends and future challenges. IEEE Trans Artif Intell 2021;2(6):476–493.
481. Liu Yuqiao, Sun Yanan, Xue Bing, Zhang Mengjie, Yen Gary G, Tan Kay Chen. A survey on evolutionary neural architecture search. IEEE Transactions on Neural Networks and Learning Systems; 2021.
482. Balaprakash Prasanna, Egele Romain, Salim Misha, et al. Scalable reinforcement-learning-based neural architecture search for cancer deep learning research. International Conference for High Performance Computing, Networking, Storage and Analysis; 2019. p. 1-33.
483. Wolpert David H, Macready William G. No free lunch theorems for optimization. IEEE Trans Evol Comput 1997;1(1):67–82.
484. Adam Stavros P, Alexandropoulos Stamatios-Aggelos N, Pardalos Panos M, Vrahatis Michael N. No free lunch theorem: a review. Approx Optim 2019:57–82.
485. Laleh Narmin Ghaffari, Muti Hannah Sophie, Loeffler Chiara Maria Lavinia, et al. Benchmarking weakly-supervised deep learning pipelines for whole slide classification in computational pathology. Med Image Anal 2022;79, 102474.
486. Chen Richard, Jing Yating, Jackson Hunter. Identifying metastases in sentinel lymph nodes with deep convolutional neural networksarXiv preprint arXiv:1608.01658. . 2016.
487. Iandola Forrest N, Han Song, Moskewicz Matthew W, Ashraf Khalid, Dally William J, Keutzer Kurt. Squeezenet: Alexnet-level accuracy with 50x fewer parameters and <0.5mb model sizearXiv preprint arXiv:1602.07360. . 2016.
488. Alzubaidi Laith, Al-Shamma Omran, Fadhel Mohammed A, Farhan Laith, Zhang Jinglan, Duan Ye. Optimizing the performance of breast cancer classification by employing the same domain transfer learning from hybrid deep convolutional neural network model. Electronics 2020;9(3):445.
489. Thuy Mai Bui Huynh, Hoang Vinh Truong. Fusing of deep learning, transfer learning and GAN for breast cancer histopathological image classification. International Conference on Computer Science, Applied Mathematics and Applications. Springer; 2019. p. 255–266.
490. Kiani Amirhossein, Uyumazturk Bora, Rajpurkar Pranav, et al. Impact of a deep learning assistant on the histopathologic classification of liver cancer. NPJ Digit Med 2020;3(1):1–8.
491. Coudray Nicolas, Ocampo Paolo Santiago, Sakellaropoulos Theodore, et al. Classification and mutation prediction from non–small cell lung cancer histopathology images using deep learning. Nat Med 2018;24(10):1559–1567.
492. Benjamens Stan, Dhunnoo Pranavsingh, Meskó Bertalan. The state of artificial intelligence-based fda-approved medical devices and algorithms: an online database. NPJ Digit Med 2020;3(1):1–8.
493. Radford Alec, Kim Jong Wook, Hallacy Chris, et al. Learning transferable visual models from natural language supervision. International Conference on Machine Learning. PMLR; 2021. p. 8748–8763.
494. Zhai Xiaohua, Wang Xiao, Mustafa Basil, et al. Lit: Zero-shot transfer with locked-image text tuning. Proceedings of the IEEE/CVF Conference on Computer Vision and Pattern Recognition; 2022. p. 18123–18133.
495. Singh Amanpreet, Hu Ronghang, Goswami Vedanuj, et al. Flava: A foundational language and vision alignment model. Proceedings of the IEEE/CVF Conference on Computer Vision and Pattern Recognition; 2022. p. 15638–15650.
496. Bakker Michiel, Chadwick Martin, Sheahan Hannah, et al. Fine-tuning language models to find agreement among humans with diverse preferences. In: *Koyejo S, Mohamed S, Agarwal A, Belgrave D, Cho K, Oh A, eds. Advances in Neural Information Processing Systems.* Curran Associates, Inc; 2022. p. 38176–38189.
497. Dosovitskiy Alexey, Ros German, Codevilla Felipe, Lopez Antonio, Koltun Vladlen. Carla: An open urban driving simulator. Conference on Robot Learning. PMLR; 2017. p. 1-16.
498. Borkman Steve, Crespi Adam, Dhakad Saurav, et al. Unity perception: Generate synthetic data for computer visionarXiv preprint arXiv:2107.04259. . 2021.
499. Makoviychuk Viktor, Wawrzyniak Lukasz, Guo Yunrong, et al. Isaac gym: High performance gpu-based physics simulation for robot learningarXiv preprint arXiv:2108.10470. . 2021.
500. Griffin Gregory, Holub Alex, Perona Pietro. *Caltech-256 Object Category Dataset.* 2007.
501. Krizhevsky Alex, Sutskever Ilya, Hinton Geoffrey E. Imagenet classification with deep convolutional neural networks. Adv Neural Inform Process Syst 2012;25.
502. Guansong Pang, Chunhua Shen, Longbing Cao, and Anton Van Den Hengel. Deep learning for anomaly detection: a review. ACM Comput Surv, 54(2), mar 2021.
503. Hosseini Mahdi S, Chan Lyndon, Huang Weimin, et al. On transferability of histological tissue labels in computational pathology. European Conference on Computer Vision. Springer; 2020. p. 453–469.
504. Yuchen Lu, Peng Xu. Anomaly detection for skin disease images using variational autoencoderCoRR, abs/1807.01349. . 2018.
505. Esteva Andre, Kuprel Brett, Novoa Roberto A, et al. Dermatologist-level classification of skin cancer with deep neural networks. Nature 2017;542(7639):115–118.
506. Iakovidis Dimitris K, Georgakopoulos Spiros V, Vasilakakis Michael, Koulaouzidis Anastasios, Plagianakos Vassilis P. Detecting and locating gastrointestinal anomalies using deep learning and iterative cluster unification. IEEE Trans Med Imaging 2018;37(10):2196–2210.
507. CAMELYON16 ISBI challenge on cancer metastasis detection in lymph node. Available at: https://camelyon16.grand-challenge.org/ 2016. (accessed June 11, 2021).
508. Qi Qi, Li Yanlong, Wang Jitian, et al. Label-efficient breast cancer histopathological image classification. IEEE J Biomed Health Inform 2018;23(5):2108–2116.
509. Caron Mathilde, Touvron Hugo, Misra Ishan, et al. Emerging properties in self-supervised vision transformers. Proceedings of the IEEE/CVF International Conference on Computer Vision; 2021. p. 9650–9660.
510. Sun Chen, Shrivastava Abhinav, Singh Saurabh, Gupta Abhinav. Revisiting unreasonable effectiveness of data in deep learning era. Proceedings of the IEEE International Conference on Computer Vision; 2017. p. 843–852.
511. Althnian Alhanoof, AlSaeed Duaa, Al-Baity Heyam, et al. Impact of dataset size on classification performance: an empirical evaluation in the medical domain. Appl Sci 2021;11(2):796.
512. Abdollahi Alireza, Saffar Hiva, Saffar Hana. Types and frequency of errors during different phases of testing at a clinical medical laboratory of a teaching hospital in tehran, iran. North Am J Med Sci 2014;6(5):224.
513. Meier Frederick A, Varney Ruan C, Zarbo Richard J. Study of amended reports to evaluate and improve surgical pathology processes. Adv Anat Pathol 2011;18(5):406–413.
514. Darcy Teresa P, Barasch Samuel P, Souers Rhona J, Perrotta Peter L. Test cancellation: a college of american pathologists q-probes study. Arch Pathol Lab Med 2016;140(2):125–129.
515. Nakhleh Raouf E. A prelude to error reduction in anatomic pathology. Am J Clin Pathol 2005;124(4):489–490.
516. Nakhleh Raouf E. Error reduction in surgical pathology. Arch Pathol Lab Med 2006;130(5):630–632.

517. Nakhleh Raouf E. Patient safety and error reduction in surgical pathology. Arch Pathol Lab Med 2008;132(2):181–185.
518. Nakhleh Raouf E, Nosé Vania, Colasacco Carol, et al. Interpretive diagnostic error reduction in surgical pathology and cytology: guideline from the college of american pathologists pathology and laboratory quality center and the association of directors of anatomic and surgical pathology. Arch Pathol Lab Med 2016;140(1):29–40.
519. Nakhleh Raouf E. Role of informatics in patient safety and quality assurance. Surg Pathol Clin 2015;8(2):301–307.
520. Odisho Anobel Y, Park Briton, Altieri Nicholas, et al. Natural language processing systems for pathology parsing in limited data environments with uncertainty estimation. JAMIA Open 2020;3(3):431–438.
521. López-Úbeda Pilar, Martín-Noguerol Teodoro, Aneiros-Fernández José, Luna Antonio. Natural language processing in pathology: Current trends and future insights. Am J Pathol 2022;192(11):1486–1495.
522. Kim Yoojoong, Lee Jeong Hyeon, Choi Sunho, et al. Validation of deep learning natural language processing algorithm for keyword extraction from pathology reports in electronic health records. Sci Rep 2020;10(1):1–9.
523. Qiu John X, Yoon Hong-Jun, Fearn Paul A, Tourassi Georgia D. Deep learning for automated extraction of primary sites from cancer pathology reports. IEEE J Biomed Health Inform 2017;22(1):244–251.
524. Zamir Amir R, Sax Alexander, Shen William, Guibas Leonidas J, Malik Jitendra, Savarese Silvio. Taskonomy: Disentangling task transfer learning. Proceedings of the IEEE Conference on Computer Vision and Pattern Recognition; 2018. p. 3712–3722.
525. Zhang Yu, Yang Qiang. A survey on multi-task learning. IEEE Trans Knowl Data Eng 2021;34(12):5586–5609.
526. Bonawitz Keith, Eichner Hubert, Grieskamp Wolfgang, et al. Towards federated learning at scale: System design. Proceedings of Machine Learning and Systems, 1. ; 2019. p. 374–388.
527. Peter Kairouz H, McMahan Brendan, Avent Brendan, et al. Advances and open problems in federated learning. Found Trends Mach Learn 2021;14(1–2):1-210.
528. Veeling Bastiaan S, Linmans Jasper, Winkens Jim, Cohen Taco, Welling Max. Rotation equivariant cnns for digital pathology. In: *Frangi Alejandro F, Schnabel Julia A, Davatzikos Christos, Alberola-López Carlos, eds. Medical Image Computing and Computer Assisted Intervention – MICCAI, volume 11071 of Lecture Notes in Computer Science. Springer; 2018. p. 210–218.*
529. Schüffler Peter J, Luke Geneslaw D, Yarlagadda Vijay K, et al. Integrated digital pathology at scale: a solution for clinical diagnostics and cancer research at a large academic medical center. J Am Med Inform Assoc 2021;28(9):1874–1884.
530. Hanna Matthew G, Reuter Victor E, Hameed Meera R, et al. Whole slide imaging equivalency and efficiency study: experience at a large academic center. Mod Pathol 2019;32(7):916–928.
531. Hanna Matthew G, Reuter Victor E, Samboy Jennifer, et al. Implementation of digital pathology offers clinical and operational increase in efficiency and cost savings. Arch Pathol Lab Med 2019;143(12):1545–1555.
532. Ho Jonhan, Ahlers Stefan M, Stratman Curtis, et al. Can digital pathology result in cost savings? A financial projection for digital pathology implementation at a large integrated health care organization. J Pathol Inform 2014;5(1):33.
533. Evgenievna Rudenko Ekaterina, Alexandrovna Demura Tatiana, Andreevna Vekhova Ksenia, et al. Analysis of the three-year work of a digital pathomorphological laboratory built from the ground. J Pathol Inform 2022;13, 100111.
534. Wang Shidan, Wang Tao, Yang Lin, et al. Convpath: a software tool for lung adenocarcinoma digital pathological image analysis aided by a convolutional neural network. EBioMedicine 2019;50:103–110.
535. Isaacs Mike, Lennerz Jochen K, Yates Stacey, Clermont Walter, Rossi Joan, Pfeifer John D. Implementation of whole slide imaging in surgical pathology: a value added approach. J Pathol Inform 2011;2(1):39.
536. Pare Guy, Meyer Julien, Trudel Marie-Claude, Tetu Bernard. Impacts of a large decentralized telepathology network in canada. Telemed e-Health 2016;22(3):246–250.
537. Thorstenson Sten, Molin Jesper, Lundström Claes. Implementation of large-scale routine diagnostics using whole slide imaging in sweden: digital pathology experiences 2006-2013. J Pathol Inform 2014;5(1):14.
538. Cheng Chee Leong, Azhar Rafay, Sng Shi Hui Adeline, et al. Enabling digital pathology in the diagnostic setting: navigating through the implementation journey in an academic medical centre. J Clin Pathol 2016;69(9):784–792.
539. Stathonikos Nikolas, Veta Mitko, Huisman André, van Diest Paul J. Going fully digital: perspective of a dutch academic pathology lab. J Pathol Inform 2013;4(1):15.
540. Pantanowitz Liron, Sinard John H, Henricks Walter H, et al. Validating whole slide imaging for diagnostic purposes in pathology: guideline from the college of american pathologists pathology and laboratory quality center. Arch Pathol Lab Med 2013;137(12):1710–1722.
541. Abels Esther, Pantanowitz Liron. Current state of the regulatory trajectory for whole slide imaging devices in the usa. J Pathol Inform 2017;8(1):23.
542. Parwani Anil V, Hassell Lewis, Glassy Eric, Pantanowitz Liron. Regulatory barriers surrounding the use of whole slide imaging in the united states of america. J Pathol Inform 2014;5.
543. Janowczyk Andrew, Madabhushi Anant. Deep learning for digital pathology image analysis: a comprehensive tutorial with selected use cases. J Pathol Inform 2016;7.
544. Sankarapandian Sivaramakrishnan, Kohn Saul, Spurrier Vaughn, et al. A pathology deep learning system capable of triage of melanoma specimens utilizing dermatopathologist consensus as ground truth. Proceedings of the IEEE/CVF International Conference on Computer Vision; 2021. p. 629–638.
545. Alshieban Saeed, Al-Surimi Khaled. Reducing turnaround time of surgical pathology reports in pathology and laboratory medicine departments. BMJ Open Qual 2015;4(1):u209223-w3773.
546. Nakhleh Raouf E, Fitzgibbons Patrick L. *Quality Management in Anatomic Pathology: Promoting Patient Safety through Systems Improvement and Error Reduction.* College of American Pathologists. 2005.
547. Metter David M, Colgan Terence J, Leung Stanley T, Timmons Charles F, Park Jason Y. Trends in the us and canadian pathologist workforces from 2007 to 2017. JAMA Netw Open 2019;2(5):e194337.
548. Bulten Wouter, Kartasalo Kimmo, Chen Po-Hsuan Cameron, et al. Artificial intelligence for diagnosis and gleason grading of prostate cancer: the panda challenge. Nat Med 2022;28(1):154–163.
549. Peck Martyn, Moffat David, Latham Bruce, Badrick Tony. Review of diagnostic error in anatomical pathology and the role and value of second opinions in error prevention. J Clin Pathol 2018;71(11):995-1000.
550. Smith John HF. Cytology, liquid-based cytology and automation. Best Pract Res Clin Obstet Gynaecol 2011;25(5):585–596.
551. Brender Erin, Burke Alison, Glass Richard M. Frozen section biopsy. Jama 2005;294(24):3200.
552. Ayyagari Sudha, Potnuru Anusha, Saleem Sk Aamer, Marapaka Pavani. Analysis of frozen section compared to permanent section: a 2 year study in a single teritiary care hospital. J Pathol Nepal 2021;11(2):1854–1858.
553. Jahn Stephan W, Plass Markus, Moinfar Farid. Digital pathology: advantages, limitations and emerging perspective. J Clin Med 2020;9(11):3697.
554. Atupelage Chamidu, Nagahashi Hiroshi, Kimura Fumikazu, et al. Computational cell classification methodology for hepatocellular carcinoma. International Conference on Advances in ICT for Emerging Regions (ICTer). IEEE; 2013. p. 21–27.
555. Bankhead Peter, Loughrey Maurice B, Fernández José A, et al. Qupath: open source software for digital pathology image analysis. Sci Rep 2017;7(1):1–7.

556. Rathore S, Iftikhar M, Nasrallah M, Gurcan M, Rajpoot N, Mourelatos Z. Tmod-35. prediction of overall survival, and molecular markers in gliomas via analysis of digital pathology images using deep learning. Neuro-Oncology 2019;21(suppl 6).vi270–vi270.
557. Wang Wei, Ozolek John A, Rohde Gustavo K. Detection and classification of thyroid follicular lesions based on nuclear structure from histopathology images. Cytometry A 2010;77(5):485–494.
558. Syrykh Charlotte, Abreu Arnaud, Amara Nadia, et al. Accurate diagnosis of lymphoma on whole-slide histopathology images using deep learning. NPJ Digit Med 2020;3(1):1–8.
559. Cheng Yalu, Qiao Pengchong, He Hongliang, Song Guoli, Chen Jie. Hard-boundary attention network for nuclei instance segmentation. ACM Multimedia Asia; 2021. p. 1–7.
560. Priego-Torres Blanca Maria, Sanchez-Morillo Daniel, Fernandez-Granero Miguel Angel, Garcia-Rojo Marcial. Automatic segmentation of whole-slide h&e stained breast histopathology images using a deep convolutional neural network architecture. Expert Syst Appl 2020;151, 113387.
561. Avenel Christophe, Tolf Anna, Dragomir Anca, Carlbom Ingrid B. Glandular segmentation of prostate cancer: an illustration of how the choice of histopathological stain is one key to success for computational pathology. Front Bioeng Biotechnol 2019;7:125.
562. Chen Richard J, Lu Ming Y, Wang Jingwen, et al. Pathomic fusion: an integrated framework for fusing histopathology and genomic features for cancer diagnosis and prognosis. IEEE Trans Med Imaging 2020;41(4):757–770.
563. Ristanoski Goce, Emery Jon, Gutierrez Javiera Martinez, McCarthy Damien, Aickelin Uwe. Handling uncertainty using features from pathology: opportunities in primary care data for developing high risk cancer survival methods. Australasian Computer Science Week Multiconference; 2021. p. 1–7.
564. Chang Jia-Ren, Lee Ching-Yi, Chen Chi-Chung, Reischl Joachim, Qaiser Talha, Yeh Chao-Yuan. Hybrid aggregation network for survival analysis from whole slide histopathological images. International Conference on Medical Image Computing and Computer-Assisted Intervention. Springer; 2021. p. 731–740.
565. National Cancer Institute. Cancer stat facts: Common cancer sites. Available at: https://seer.cancer.gov/statfacts/html/common.html. (accessed Feb 12, 2023).
566. Kenfield Stacey A, Wei Esther K, Stampfer Meir J, Rosner Bernard A, Colditz Graham A. Comparison of aspects of smoking among the four histological types of lung cancer. Tob Control 2008;17(3):198–204.
567. American Cancer Society. Survival rates for breast cancer. Available at: https://www.cancer.org/cancer/breast-cancer/understanding-a-breast-cancer-diagnosis/breast-cancer-survival-rates.html. (accessed Feb 9, 2023).
568. Cancer Center. Bladder cancer types. Available at: https://www.cancercenter.com/cancer-types/bladder-cancer/types. (accessed Feb 10, 2023).
569. American Cancer Society. Survival rates for bladder cancer. m: https://www.cancer.org/cancer/bladder-cancer/detection-diagnosis-staging/survival-rates.html. (accessed Feb 10, 2023).
570. Andreassen BK, Aagnes B, Gislefoss R, Andreassen M, Wahlqvist R. Incidence and survival of urothelial carcinoma of the urinary bladder in norway 1981-2014. BMC Cancer 2016;16:1-11.
571. American Cancer Society. Liver cancer survival rates. Available at: https://www.cancer.org/cancer/liver-cancer/detection-diagnosis-staging/survival-rates.html. (accessed Feb 10, 2023).
572. Goodman Zachary D. Neoplasms of the liver. Mod Pathol 2007;20:S49–S60.
573. Ries LA Gloeckler, Young JL, Keel GE, et al. *Seer survival monograph: cancer survival among adults: US seer program, 1988-2001, patient and tumor characteristics.* , 7National Cancer Institute, SEER Program, NIH Pub. 2007:133–144.
574. National Cancer Institute. Cancer stat facts: Ovarian cancer. Available at: https://seer.cancer.gov/statfacts/html/ovary.html. (accessed Feb 14, 2023).
575. American Cancer Society. Survival Rates for Kidney Cancer. Available at: https://www.cancer.org/cancer/kidney-cancer/detection-diagnosis-staging/survival-rates.html. (accessed Feb 9, 2023).
576. Bottaro Donald P, Marston W, Linehan. Multifocal renal cancer: genetic basis and its medical relevance. Clin Cancer Res 2005;11(20):7206–7208.
577. Srougi Victor, Kato Raphael B, Salvatore Fernanda A, Ayres Pedro PM, Marcos F, Dall'Oglio, and Miguel Srougi. Incidence of benign lesions according to tumor size in solid renal masses. Int Braz J Urol 2009;35:427–431.
578. American Cancer Society. Survival rates for colorectal cancer. Available at: https://www.cancer.org/cancer/colon-rectal-cancer/detection-diagnosis-staging/survival-rates.html. (accessed Feb 9, 2023).
579. Remo Andrea, Fassan Matteo, Vanoli Alessandro, et al. Morphology and molecular features of rare colorectal carcinoma histotypes. Cancers 2019;11(7):1036.
580. American Cancer Society. Survival rates for prostate cancer. Available at: https://www.cancer.org/cancer/prostate-cancer/detection-diagnosis-staging/survival-rates.html. (accessed Feb 8, 2023).
581. Abbas Abul K, Aster Jon C, Kumar Vinay. *Robbins and Cotran Pathologic basis of Disease.* Saunders/Elsevier. 2010.
582. American Cancer Society. Lung cancer survival rates. Available at: https://www.cancer.org/cancer/lung-cancer/detection-diagnosis-staging/survival-rates.html. (accessed Feb 11, 2023).
583. World Health Organization. Cancer. Available at: https://www.who.int/news-room/fact-sheets/detail/cancer. (accessed Feb 13, 2023).
584. Clunie David, Hosseinzadeh Dan, Wintell Mikael, et al. Digital imaging and communications in medicine whole slide imaging connectathon at digital pathology association pathology visions 2017. J Pathol Inform 2018;9.
585. Nazeri Kamyar, Aminpour Azad, Ebrahimi Mehran. Two-stage convolutional neural network for breast cancer histology image classification. International Conference Image Analysis and Recognition. Springer; 2018. p. 717–726.
586. Turki Turki, Al-Sharif Anmar, Taguchi Yh. End-to-end deep learning for detecting metastatic breast cancer in axillary lymph node from digital pathology imagesmedRxiv. . 2021.
587. Xiong Zihan, Zheng Yixuan, Qiu Jiayue. Processing tissue microarray images using machine learning techniques as preparation for determining gleason grade of prostate cancer. International Conference on Bioinformatics Research and Applications; 2021. p. 34–41.
588. Xiangyu Zhang, Xinyu Zhou, Mengxiao Lin, and Jian Sun. Shufflenet: An extremely efficient convolutional neural network for mobile devices. In 2018 IEEE/CVF Conference on Computer Vision and Pattern Recognition, pages 6848–6856, 2018.
589. Gurcan Metin N, Madabhushi Anant, Rajpoot Nasir. Pattern recognition in histopathological images: An icpr 2010 contest. International Conference on Pattern Recognition. Springer; 2010. p. 226–234.
590. Pantanowitz Liron, Henricks Walter H, Beckwith Bruce A. Medical laboratory informatics. Clin Lab Med 2007;27(4):823–843.
591. Narayanan Priya Lakshmi, Ahmed Shan E, Raza Allison H, et al. Unmasking the tissue microecology of ductal carcinoma in situ with deep learning. BioRxiv 2019:812735.
592. Lai Zhengfeng, Wang Chao, Oliveira Luca Cerny, Dugger Brittany N, Cheung Sen-Ching, Chuah Chen-Nee. Joint semi-supervised and active learning for segmentation of gigapixel pathology images with cost-effective labeling. IEEE/CVF International Conference on Computer Vision; 2021. p. 591–600.
593. Roy Mousumi, Kong Jun, Kashyap Satyananda, et al. Convolutional autoencoder based model histocae for segmentation of viable tumor regions in liver whole-slide images. Sci Rep 2021;11(1):1-10.
594. Jiang YQ, Xiong JH, Li HY, et al. Recognizing basal cell carcinoma on smartphone-captured digital histopathology images with a deep neural network. Br J Dermatol 2020;182(3):754–762.
595. Wang Shidan, Yang Donghan M, Rong Ruichen, Zhan Xiaowei, Xiao Guanghua. Pathology image analysis using segmentation deep learning algorithms. Am J Pathol 2019;189(9):1686–1698.

596. Tokunaga Hiroki, Teramoto Yuki, Yoshizawa Akihiko, Bise Ryoma. Adaptive weighting multi-field-of-view cnn for semantic segmentation in pathology. IEEE/CVF Conference on Computer Vision and Pattern Recognition; 2019. p. 12597–12606.
597. Chang Hye Yoon, Jung Chan Kwon, Woo Junwoo Isaac, et al. Artificial intelligence in pathology. J Pathol Transl Med 2019;53(1):1.
598. Xiang Tiange, Yang Song, Zhang Chaoyi, et al. Dsnet: A dual-stream framework for weakly-supervised gigapixel pathology image analysis. IEEE Transactions on Medical ImagingarXiv 2022;41(8):2180–2190.
599. Chetan L Srinidhi and Anne L Martel. Improving self-supervised learning with hardness-aware dynamic curriculum learning: An application to digital pathology. In IEEE/CVF International Conference on Computer Vision, pages 562–571, 2021.
600. Shirazi Syed Hamad, Naz Saeeda, Razzak Muhammad Imran, Umar Arif Iqbal, Zaib Ahmad. Automated pathology image analysis. Soft Computing Based Medical Image Analysis. Elsevier; 2018. p. 13–29.
601. Diao James A, Wang Jason K, Chui Wan Fung, et al. Human-interpretable image features derived from densely mapped cancer pathology slides predict diverse molecular phenotypes. Nat Commun 2021;12(1):1-15.
602. Beck Andrew H, Sangoi Ankur R, Leung Samuel, et al. Systematic analysis of breast cancer morphology uncovers stromal features associated with survival. Sci Transl Med 2011;3(108):108ra113.
603. Kulkarni Prathamesh M, Robinson Eric J, Pradhan Jaya Sarin, et al. Deep learning based on standard h&e images of primary melanoma tumors identifies patients at risk for visceral recurrence and death. Clin Cancer Res 2020;26(5):1126–1134.
604. Xie Peizhen, Zuo Ke, Zhang Yu, Li Fangfang, Yin Mingzhu, Lu Kai. Interpretable classification from skin cancer histology slides using deep learning: A retrospective multicenter study. arXiv 2019.preprint arXiv:1904.06156.
605. Hart Steven N, Flotte William, Norgan Andrew P, et al. Classification of melanocytic lesions in selected and whole-slide images via convolutional neural networks. J Pathol Inform 2019;10.
606. Cruz-Roa Angel Alfonso, Ovalle John Edison Arevalo, Madabhushi Anant, Osorio Fabio Augusto González. *A deep learning architecture for image representation, visual interpretability and automated basal-cell carcinoma cancer detection*. 2013:403–410.
607. Levy Joshua J, Jackson Christopher R, Sriharan Aravindhan, Christensen Brock C, Vaickus Louis J. Preliminary evaluation of the utility of deep generative histopathology image translation at a mid-sized NCI cancer center. bioRxiv 2020.
608. Tang Bo, Li Ao, Li Bin, Wang Minghui. Capsurv: capsule network for survival analysis with whole slide pathological images. IEEE Access 2019;7:26022–26030.
609. Kirby Justin. MICCAI 2014 Grand Challenges. Available at: https://wiki.cancerimagingarchive.net/display/Public/MICCAI2014GrandChallenges. (accessed June 10, 2021).
610. Teikari Petteri, Santos Marc, Poon Charissa, Hynynen Kullervo. Deep learning convolutional networks for multiphoton microscopy vasculature segmentation. arXiv 2016.preprint arXiv:1606.02382.
611. Liechty Benjamin, Zhuoran Xu, Zhang Zhilu, et al. Machine learning can aid in prediction of idh mutation from h&e-stained histology slides in infiltrating gliomas. Sci Rep 2022;12(1):22623.
612. Bueno Gloria, Gonzalez-Lopez Lucia, Garcia-Rojo Marcial, Laurinavicius Arvydas, Deniz Oscar. Data for glomeruli characterization in histopathological images. Data Brief 2020;29, 105314.
613. Gadermayr Michael, Dombrowski Ann-Kathrin, Klinkhammer Barbara Mara, Boor Peter, Merhof Dorit. Cnn cascades for segmenting sparse objects in gigapixel whole slide images. Comput Med Imaging Graph 2019;71:40–48.
614. Tjio Gabriel, Yang Xulei, Hong Jia Mei, et al. Accurate tumor tissue region detection with accelerated deep convolutional neural networks. arXiv 2020.preprint arXiv:2004.08552.
615. Cicalese Pietro Antonio, Mobiny Aryan, Yuan Pengyu, Becker Jan, Mohan Chandra, Van Nguyen Hien. Stypath: Style-transfer data augmentation for robust histology image classification. Medical Image Computing and Computer Assisted Intervention – MICCAI. Springer; Sep 2020. p. 351–361.of Lecture Notes in Computer Science.
616. Chen Richard J, Lu Ming Y, Chen Tiffany Y, Williamson Drew FK, Mahmood Faisal. Synthetic data in machine learning for medicine and healthcare. Nat Biomed Eng 2021;5(6):493–497.
617. Borovec Jiří, Kybic Jan, Arganda-Carreras Ignacio, et al. Anhir: Automatic non-rigid histological image registration challenge. IEEE Trans Med Imaging 2020;39(10):3042–3052.
618. Wu Fei, Liu Pei, Fu Bo, Ye Feng. Deepgcnmil: Multi-head attention guided multi-instance learning approach for whole-slide images survival analysis using graph convolutional networks. 2022 14th International Conference on Machine Learning and Computing (ICMLC); 2022. p. 67–73.
619. Lutnick Brendon, Manthey David, Becker Jan U, et al. A user-friendly tool for cloud-based whole slide image segmentation with examples from renal histopathology. Commun Med 2022;2(1):105.
620. CAMELYON17. Available at: https://camelyon17.grand-challenge.org/Organisers/ 2017. (accessed June 11, 2021).
621. Yongxiang Huang and Albert Chi-shing Chung. Improving high resolution histology image classification with deep spatial fusion network. Computational Pathology and Ophthalmic Medical Image Analysis. Springer; 2018. p. 19–26.
622. MITOS-ATYPIA-14 Grand Challenge. Available online: https://mitos-atypia-14.grand-challenge.org/. (accessed June 10, 2021).
623. Roux Ludovic, Racoceanu Daniel, Loménie Nicolas, et al. Mitosis detection in breast cancer histological images an icpr 2012 contest. J Pathol Inform 2013;4.
624. Campanella Gabriele, Hanna Matthew G, Brogi Edi, Fuchs Thomas J. Breast metastases to axillary lymph nodes. Cancer Imaging Arch 2019.
625. Clark Kenneth, Vendt Bruce, Smith Kirk, et al. The cancer imaging archive (tcia): maintaining and operating a public information repository. J Digit Imaging 2013;26(6):1045–1057.
626. Dimitropoulos Kosmas, Barmpoutis Panagiotis, Zioga Christina, Kamas Athanasios, Patsiaoura Kalliopi, Grammalidis Nikos. Grading of invasive breast carcinoma through grassmannian vlad encoding. PloS One 2017;12(9), e0185110.
627. Zioga C, Kamas A, Patsiaoura K, Dimitropoulos K, Barmpoutis P, Grammalidis N. *Breast carcinoma histological images from the department of pathology,"agios pavlos" general hospital of thessaloniki. Greece*. July 2017.
628. Kieffer Brady, Babaie Morteza, Kalra Shivam, Tizhoosh Hamid R. Convolutional neural networks for histopathology image classification: Training vs. using pre-trained networks. International Conference on Image Processing Theory, Tools and Applications (IPTA). IEEE; 2017. p. 1–6.
629. Mohapatra Puspanjali, Panda Baldev, Swain Samikshya. Enhancing histopathological breast cancer image classification using deep learning. Int J Innov Technol Explor Eng 2019;8:2024–2032.
630. Janowczyk Andrew, Doyle Scott, Gilmore Hannah, Madabhushi Anant. A resolution adaptive deep hierarchical (radhical) learning scheme applied to nuclear segmentation of digital pathology images. Comput Methods Biomech Biomed Eng Imaging Vis 2018;6(3):270–276.
631. Cruz-Roa Angel, Gilmore Hannah, Basavanhally Ajay, et al. Accurate and reproducible invasive breast cancer detection in whole-slide images: a deep learning approach for quantifying tumor extent. Sci Rep 2017;7(1):1-14.
632. Jaber Mustafa I, Song Bing, Taylor Clive, et al. A deep learning image-based intrinsic molecular subtype classifier of breast tumors reveals tumor heterogeneity that may affect survival. Breast Cancer Res 2020;22(1):1-10.
633. Corvo Alberto, Caballero Humberto Simon Garcia, Westenberg Michel A, van Driel Marc A, van Wijk Jarke. *Visual analytics for hypothesis-driven exploration in computational pathology*. IEEE Transactions on Visualization and Computer Graphics. 2020.
634. Veta Mitko, Van Diest Paul J, Willems Stefan M, et al. Assessment of algorithms for mitosis detection in breast cancer histopathology images. Med Image Anal 2015;20(1):237–248.

635. Bejnordi Babak Ehteshami, Zuidhof Guido, Balkenhol Maschenka, et al. Context-aware stacked convolutional neural networks for classification of breast carcinomas in whole-slide histopathology images. J Med Imaging 2017;4(4), 044504.
636. Bejnordi Babak Ehteshami, Mullooly Maeve, Pfeiffer Ruth M, et al. Using deep convolutional neural networks to identify and classify tumor-associated stroma in diagnostic breast biopsies. Mod Pathol 2018;31(10):1502–1512.
637. Peikari Mohammad, Gangeh Mehrdad J, Zubovits Judit, Clarke Gina, Martel Anne L. Triaging diagnostically relevant regions from pathology whole slides of breast cancer: A texture based approach. IEEE Trans Med Imaging 2015;35(1):307–315.
638. Jaume Guillaume, Pati Pushpak, Foncubierta-Rodríguez Antonio, et al. Towards explainable graph representations in digital pathology. ICML; 2020. p. 1–5.
639. Jaume Guillaume, Pati Pushpak, Bozorgtabar Behzad, et al. Quantifying explainers of graph neural networks in computational pathology. IEEE/CVF Conference on Computer Vision and Pattern Recognition; 2021. p. 8106–8116.
640. Brancati N, Anniciello AM, Pati P, et al. A dataset for breast carcinoma subtyping in h&e histology images. Database 2022 Jan 1;2022:baac093.
641. Lagree Andrew, Shiner Audrey, Alera Marie Angeli, et al. Assessment of digital pathology imaging biomarkers associated with breast cancer histologic grade. Curr Oncol 2021;28(6):4298–4316.
642. Amgad Mohamed, Elfandy Habiba, Hussein Hagar, et al. Structured crowdsourcing enables convolutional segmentation of histology images. Bioinformatics 2019;35(18):3461–3467.
643. Uhlen Mathias, Zhang Cheng, Lee Sunjae, et al. A pathology atlas of the human cancer transcriptome. Science 2017;357(6352), eaan2507.
644. Thiagarajan Ponkrshnan, Khairnar Pushkar, Ghosh Susanta. Explanation and use of uncertainty quantified by bayesian neural network classifiers for breast histopathology images. IEEE Trans Med Imaging 2021;41(4):815–825.
645. Hameed Zabit, Garcia-Zapirain Begonya, Aguirre José Javier, Isaza-Ruget Mario Arturo. Multiclass classification of breast cancer histopathology images using multilevel features of deep convolutional neural network. Sci Rep 2022;12(1):1-21.
646. Bautista Pinky A, Yagi Yukako. Staining correction in digital pathology by utilizing a dye amount table. J Digit Imaging 2015;28(3):283–294.
647. Albertina B, Watson M, Holback C, et al. Radiology data from the cancer genome atlas lung adenocarcinoma [tcga-luad] collection. Cancer Imaging Arch 2016;10:k9.
648. National Lung Screening Trial Research Team. The national lung screening trial: overview and study design. Radiology 2011;258(1):243–253.
649. The Lung Cancer SPORE. Available at: https://www.mdanderson.org/research/departments-labs-institutes/spores/lung-cancer-spore.html 2023. (accessed June 10, 2021).
650. Cheng Lu, Koyuncu Can, Corredor German, et al. Feature-driven local cell graph (FLocK): New computational pathology-based descriptors for prognosis of lung cancer and hpv status of oropharyngeal cancers. Med Image Anal 2021;68, 101903.
651. Le Page Anne Laure, Ballot Elise, Truntzer Caroline, et al. Using a convolutional neural network for classification of squamous and non-squamous non-small cell lung cancer based on diagnostic histopathology hes images. Sci Rep 2021;11(1):1–8.
652. Swiderska-Chadaj Zaneta, Ciompi Francesco. Lyon19- lymphocyte detection test set (version v1) [data set]. https://zenodo.org/record/3385420#.XW-6JygzYuW 2019. (Accessed 18-Mar-2023).
653. Swiderska-Chadaj Zaneta, Pinckaers Hans, van Rijthoven Mart, et al. Learning to detect lymphocytes in immunohistochemistry with deep learning. Med Image Anal 2019;58, 101547.
654. Brancati Nadia, De Pietro Giuseppe, Frucci Maria, Riccio Daniel. A deep learning approach for breast invasive ductal carcinoma detection and lymphoma multi-classification in histological images. IEEE Access 2019;7:44709–44720.
655. Thagaard Jeppe, Hauberg Søren, van der Vegt Bert, Ebstrup Thomas, Hansen Johan D, Dahl Anders B. Can you trust predictive uncertainty under real dataset shifts in digital pathology?. International Conference on Medical Image Computing and Computer-Assisted Intervention. Springer; 2020. p. 824–833.
656. Shaban Muhammad, Khurram Syed Ali, Fraz Muhammad Moazam, et al. A novel digital score for abundance of tumour infiltrating lymphocytes predicts disease free survival in oral squamous cell carcinoma. Sci Rep 2019;9(1):1-13.
657. Bulten Wouter, Bándi Péter, Hoven Jeffrey, et al. Epithelium segmentation using deep learning in h&e-stained prostate specimens with immunohistochemistry as reference standard. Sci Rep 2019;9(1):864.
658. Köbel Martin, Kalloger Steve E, Baker Patricia M, et al. Diagnosis of ovarian carcinoma cell type is highly reproducible: A transcanadian study. Am J Surg Pathol 2010;34(7):984–993.
659. Tolkach Yuri, Dohmgörgen Tilmann, Toma Marieta, Kristiansen Glen. High-accuracy prostate cancer pathology using deep learning. Nat Mach Intell 2020;2(7):411–418.
660. Arvaniti Eirini, Fricker Kim S, Moret Michael, et al. Automated gleason grading of prostate cancer tissue microarrays via deep learning. Sci Rep 2018;8(1):1-11.
661. Arvaniti Eirini, Claassen Manfred. Coupling weak and strong supervision for classification of prostate cancer histopathology images. ArXiv 2018.abs/1811.07013.
662. Ren Jian, Hacihaliloglu Ilker, Singer Eric A, Foran David J, Qi Xin. Unsupervised domain adaptation for classification of histopathology whole-slide images. Front Bioeng Biotechnol 2019;7:102.
663. Karimi Davood, Nir Guy, Fazli Ladan, Black Peter C, Goldenberg Larry, Salcudean Septimiu E. Deep learning-based gleason grading of prostate cancer from histopathology images—role of multiscale decision aggregation and data augmentation. IEEE J Biomed Health Inform 2019;24(5):1413–1426.
664. Yan Chaoyang, Nakane Kazuaki, Wang Xiangxue, et al. Automated gleason grading on prostate biopsy slides by statistical representations of homology profile. Comput Methods Programs Biomed 2020;194, 105528.
665. Doyle Scott, Monaco James, Feldman Michael, Tomaszewski John, Madabhushi Anant. An active learning based classification strategy for the minority class problem: application to histopathology annotation. BMC Bioinforma 2011;12(1):1-14.
666. Doyle Scott, Feldman Michael D, Shih Natalie, Tomaszewski John, Madabhushi Anant. Cascaded discrimination of normal, abnormal, and confounder classes in histopathology: Gleason grading of prostate cancer. BMC Bioinforma 2012;13(1):1-15.
667. Nagpal Kunal, Foote Davis, Liu Yun, et al. Development and validation of a deep learning algorithm for improving gleason scoring of prostate cancer. NPJ Digit Med 2019;2(1):1-10.
668. Levine Adrian B, Peng Jason, Farnell David, et al. Synthesis of diagnostic quality cancer pathology images by generative adversarial networks. J Pathol 2020;252(2):178–188.
669. Schömig-Markiefka Birgid, Pryalukhin Alexey, Hulla Wolfgang, et al. Quality control stress test for deep learning-based diagnostic model in digital pathology. Mod Pathol 2021;34(12):2098–2108.
670. Silva-Rodríguez Julio, Colomer Adrián, Sales María A, Molina Rafael, Naranjo Valery. Going deeper through the gleason scoring scale: An automatic end-to-end system for histology prostate grading and cribriform pattern detection. Comput Methods Programs Biomed 2020;195, 105637.
671. Farahani Hossein, Boschman Jeffrey, Farnell David, et al. Deep learning-based histotype diagnosis of ovarian carcinoma whole-slide pathology images. Mod Pathol 2022;35(12):1983–1990.
672. Bulten Wouter, Litjens Geert, Pinckaers Hans, et al. *The PANDA challenge: Prostate cANcer graDe Assessment using the Gleason grading system.* March 2020.
673. Kather Jakob Nikolas, Zöllner FG, Bianconi F, et al. Collection of textures in colorectal cancer histology. Zenodo 2016;5281.

674. Sirinukunwattana Korsuk, Pluim Josien PW, Chen Hao, et al. Gland segmentation in colon histology images: The glas challenge contest. Med Image Anal 2017;35:489–502.
675. Shaban Muhammad, Awan Ruqayya, Fraz Muhammad Moazam, et al. Context-aware convolutional neural network for grading of colorectal cancer histology images. IEEE Trans Med Imaging 2020;39 (7):2395–2405.
676. Jun Xu, Luo Xiaofei, Wang Guanhao, Gilmore Hannah, Madabhushi Anant. A deep convolutional neural network for segmenting and classifying epithelial and stromal regions in histopathological images. Neurocomputing 2016;191:214–223.
677. University of Leeds. Welcome to the university of leeds virtual pathology project website. Available at: https://www.virtualpathology.leeds.ac.uk/ 2023. (accessed June 10, 2021).
678. Ponzio Francesco, Deodato Giacomo, Macii Enrico, Di Cataldo Santa, Ficarra Elisa. Exploiting "uncertain" deep networks for data cleaning in digital pathology. IEEE International Symposium on Biomedical Imaging. IEEE; 2020. p. 1139–1143.
679. Ciompi Francesco, Geessink Oscar, Bejnordi Babak Ehteshami, et al. The importance of stain normalization in colorectal tissue classification with convolutional networks. IEEE International Symposium on Biomedical Imaging. IEEE; 2017. p. 160–163.
680. Gunduz-Demir Cigdem, Kandemir Melih, Tosun Akif Burak, Sokmensuer Cenk. Automatic segmentation of colon glands using object-graphs. Med Image Anal 2010;14(1):1-12.
681. Kloeckner Jonas, Sansonowicz Tatiana K, Rodrigues Áttila L, Nunes Tatiana WN. Multi-categorical classification using deep learning applied to the diagnosis of gastric cancer. J Bras Patol Med Lab 2020;56.
682. Nguyen Huu-Giao, Blank Annika, Lugli Alessandro, Zlobec Inti. An effective deep learning architecture combination for tissue microarray spots classification of h&e stained colorectal images. IEEE International Symposium on Biomedical Imaging. IEEE; 2020. p. 1271–1274.
683. Sali Rasoul, Ehsan Lubaina, Kowsari Kamran, et al. Celiacnet: Celiac disease severity diagnosis on duodenal histopathological images using deep residual networks. IEEE International Conference on Bioinformatics and Biomedicine (BIBM). IEEE; 2019. p. 962–967.
684. Sali Rasoul, Adewole Sodiq, Ehsan Lubaina, et al. Hierarchical deep convolutional neural networks for multi-category diagnosis of gastrointestinal disorders on histopathological images. IEEE International Conference on Healthcare Informatics (ICHI). IEEE; 2020. p. 1–6.
685. Kong Bin, Sun Shanhui, Wang Xin, Song Qi, Zhang Shaoting. Invasive cancer detection utilizing compressed convolutional neural network and transfer learning. International Conference on Medical Image Computing and Computer-Assisted Intervention. Springer; 2018. p. 156–164.
686. Song Zhigang, Zou Shuangmei, Zhou Weixun, et al. Clinically applicable histopathological diagnosis system for gastric cancer detection using deep learning. Nat Commun 2020;11(1):1–9.
687. Wright Alexander Ian, Dunn Catriona Marie, Hale Michael, Hutchins Gordon, Treanor Darren. The effect of quality control on accuracy of digital pathology image analysis. IEEE J Biomed Health Inform 2020;25(2):307–314.
688. Bilal Mohsin, Ahmed Shan E, Raza Ayesha Azam, et al. Development and validation of a weakly supervised deep learning framework to predict the status of molecular pathways and key mutations in colorectal cancer from routine histology images: a retrospective study. Lancet Digit Health 2021;3(12):e763–e772.
689. Thandiackal K, Chen B, Pati P, et al. Differentiable Zooming for Multiple Instance Learning on Whole-Slide Images. 17th European Conference on Computer Vision (ECCV), OCT 23-27, 2022, Tel Aviv, ISRAEL. Springer Nature; 2022. p. 699–715.
690. Oliveira Sara P, Neto Pedro C, Fraga João, et al. Cad systems for colorectal cancer from wsi are still not ready for clinical acceptance. Sci Rep 2021;11(1):1-15.
691. Chuang Zhu, Wenkai Chen, Ting Peng, Ying Wang, and Mulan Jin. Hard sample aware noise robust learning for histopathology image classification. IEEE Trans Med Imaging.
692. Kainz Philipp, Urschler Martin, Schulter Samuel, Wohlhart Paul, Lepetit Vincent. You should use regression to detect cells. International Conference on Medical Image Computing and Computer-Assisted Intervention. Springer; 2015. p. 276–283.
693. Chandradevan Ramraj, Aljudi Ahmed A, Drumheller Bradley R, et al. Machine-based detection and classification for bone marrow aspirate differential counts: initial development focusing on nonneoplastic cells. Lab Invest 2020;100(1):98-109.
694. Frankel Arthur O, Lathara Melvin, Shaw Celine Y, et al. Machine learning for rhabdomyosarcoma histopathology. Mod Pathol 2022: 1-11.
695. Zheng Xueyi, Wang Ruixuan, Zhang Xinke, et al. A deep learning model and human-machine fusion for prediction of ebv-associated gastric cancer from histopathology. Nat Commun 2022;13(1):1-12.
696. Tian Ye, Yang Li, Wang Wei, et al. Computer-aided detection of squamous carcinoma of the cervix in whole slide images. arXiv 2019.preprint arXiv:1905.10959.
697. Gamper Jevgenij, Koohbanani Navid Alemi, Benet Ksenija, Khuram Ali, Rajpoot Nasir. Pannuke: an open pan-cancer histology dataset for nuclei instance segmentation and classification. European Congress on Digital Pathology. Springer; 2019. p. 11–19.
698. Gamper Jevgenij, Koohbanani Navid Alemi, Graham Simon, et al. Pannuke dataset extension, insights and baselines. CoRR 2020. abs/2003.10778.
699. Hou Le, Gupta Rajarsi, Van Arnam John S, et al. Dataset of segmented nuclei in hematoxylin and eosin stained histopathology images of ten cancer types. Sci Data 2020;7(1):1-12.
700. Jiang Cheng, Liao Jun, Dong Pei, et al. Blind deblurring for microscopic pathology images using deep learning networks. CoRR 2020. abs/2011.11879.
701. Marinelli Robert J, Montgomery Kelli, Liu Chih Long, et al. The stanford tissue microarray database. Nucleic Acids Res 2007;36 (suppl_1):D871–D877.
702. Hegde Narayan, Hipp Jason D, Liu Yun, et al. Similar image search for histopathology: Smily. NPJ Digit Med 2019;2(1):1–9.
703. Diao James A, Chui Wan Fung, Wang Jason K, et al. Dense, high-resolution mapping of cells and tissues from pathology images for the interpretable prediction of molecular phenotypes in cancer. bioRxiv 2020.
704. Shen Yiqing, Ke Jing. A deformable crf model for histopathology whole-slide image classification. International Conference on Medical Image Computing and Computer-Assisted Intervention. Springer; 2020. p. 500–508.
705. Schmauch Benoît, Romagnoni Alberto, Pronier Elodie, et al. A deep learning model to predict rna-seq expression of tumours from whole slide images. Nat Commun 2020;11(1):1-15.
706. Borkowski Andrew A, Bui Marilyn M, Thomas L Brannon, Wilson Catherine P, DeLand Lauren A, Mastorides Stephen M. Lung and colon cancer histopathological image dataset (lc25000). arXiv 2019.preprint arXiv:1912.12142.
707. Ryu Jeongun, Puche Aaron Valero, Shin JaeWoong, et al. Ocelot: Overlapped cell on tissue dataset for histopathology. Proceedings of the IEEE Conference on Computer Vision and Pattern Recognition; 2023.
708. Matek Christian, Schwarz Simone, Spiekermann Karsten, Marr Carsten. Human-level recognition of blast cells in acute myeloid leukaemia with convolutional neural networks. Nat Mach Intell 2019;1 (11):538–544.
709. Nirschl Jeffrey J, Janowczyk Andrew, Peyster Eliot G, et al. A deep-learning classifier identifies patients with clinical heart failure using whole-slide images of h&e tissue. PloS One 2018;13(4), e0192726.
710. Höhn Julia, Krieghoff-Henning Eva, Jutzi Tanja B, et al. Combining cnn-based histologic whole slide image analysis and patient data to improve skin cancer classification. Eur J Cancer 2021;149:94-101.
711. Giuste Felipe, Venkatesan Mythreye, Zhao Conan, et al. Automated classification of acute rejection from endomyocardial biopsies. Proceedings of the 11th ACM International Conference on Bioinformatics, Computational Biology and Health Informatics; 2020. p. 1–9.

712. Peyster Eliot G, Arabyarmohammadi Sara, Janowczyk Andrew, et al. An automated computational image analysis pipeline for histological grading of cardiac allograft rejection. Eur Heart J 2021;42(24):2356–2369.
713. Caicedo Juan C, Goodman Allen, Karhohs Kyle W, et al. Nucleus segmentation across imaging experiments: the 2018 data science bowl. Nat Methods 2019;16(12):1247–1253.
714. Labati Ruggero Donida, Piuri Vincenzo, Scotti Fabio. All-idb: The acute lymphoblastic leukemia image database for image processing. 2011 18th IEEE International Conference on Image Processing. IEEE; 2011. p. 2045–2048.
715. Genovese Angelo, Hosseini Mahdi S, Piuri Vincenzo, Plataniotis Konstantinos N, Scotti Fabio. Histopathological transfer learning for acute lymphoblastic leukemia detection. 2021 IEEE International Conference on Computational Intelligence and Virtual Environments for Measurement Systems and Applications (CIVEMSA). IEEE; 2021. p. 1–6.
716. Failmezger Henrik, Muralidhar Sathya, Rullan Antonio, de Andrea Carlos E, Sahai Erik, Yuan Yinyin. Topological tumor graphs: A graph-based spatial model to infer stromal recruitment for immunosuppression in melanoma histology. Cancer Res 2020;80(5):1199–1209.
717. Al-Milaji Zahraa, Ersoy Ilker, Hafiane Adel, Palaniappan Kannappan, Bunyak Filiz. Integrating segmentation with deep learning for enhanced classification of epithelial and stromal tissues in H&E images. Pattern Recogn Lett 2019;119:214–221.
718. Ertosun Mehmet Günhan, Rubin Daniel L. Automated grading of gliomas using deep learning in digital pathology images: a modular approach with ensemble of convolutional neural networks. AMIA Annual Symposium Proceedings. American Medical Informatics Association; 2015. p. 1899.
719. Rathore Saima, Niazi Tamim, Iftikhar Muhammad Aksam, Chaddad Ahmad. Glioma grading via analysis of digital pathology images using machine learning. Cancers 2020;12(3):578.
720. Folmsbee Jonathan, Liu Xulei, Brandwein-Weber Margaret, Doyle Scott. Active deep learning: Improved training efficiency of convolutional neural networks for tissue classification in oral cavity cancer. IEEE International Symposium on Biomedical Imaging. IEEE; 2018. p. 770–773.
721. Lewis Jr James S, Ali Sahirzeeshan, Luo Jingqin, Thorstad Wade L, Madabhushi Anant. A quantitative histomorphometric classifier (quhbic) identifies aggressive versus indolent p16-positive oropharyngeal squamous cell carcinoma. Am J Surg Pathol 2014;38(1):128.
722. Kassani Sara Hosseinzadeh, Kassani Peyman Hosseinzadeh, Wesolowski Michal J, Schneider Kevin A, Deters Ralph. Breast cancer diagnosis with transfer learning and global pooling. International Conference on Information and Communication Technology Convergence (ICTC). IEEE; 2019. p. 519–524.
723. Khan SanaUllah, Islam Naveed, Jan Zahoor, Din Ikram Ud, Rodrigues Joel JPC. A novel deep learning based framework for the detection and classification of breast cancer using transfer learning. Pattern Recogn Lett 2019;125:1–6.
724. Budak Ümit, Cömert Zafer, Rashid Zryan Najat, Şengür Abdulkadir, Çıbuk Musa. Computer-aided diagnosis system combining fcn and bi-lstm model for efficient breast cancer detection from histopathological images. Appl Soft Comput 2019;85, 105765.
725. Spanhol Fabio A, Oliveira Luiz S, Cavalin Paulo R, Petitjean Caroline, Heutte Laurent. Deep features for breast cancer histopathological image classification. IEEE International Conference on Systems, Man, and Cybernetics (SMC). IEEE; 2017. p. 1868–1873.
726. Ho David Joon, Yarlagadda Dig VK, D'Alfonso Timothy M, et al. Deep multi-magnification networks for multi-class breast cancer image segmentation. Comput Med Imaging Graph 2021;88, 101866.
727. Valkonen Mira, Kartasalo Kimmo, Liimatainen Kaisa, Nykter Matti, Latonen Leena, Ruusuvuori Pekka. Dual structured convolutional neural network with feature augmentation for quantitative characterization of tissue histology. IEEE International Conference on Computer Vision Workshops; 2017. p. 27–35.
728. Liang Yu, Yang Jinglong, Quan Xiongwen, Zhang Han. Metastatic breast cancer recognition in histopathology images using convolutional neural network with attention mechanism. Chinese Automation Congress (CAC). IEEE; 2019. p. 2922–2926.
729. Cruz-Roa Angel, Basavanhally Ajay, González Fabio, et al. Automatic detection of invasive ductal carcinoma in whole slide images with convolutional neural networks. Medical Imaging: Digital Pathology. International Society for Optics and Photonics; 2014. p. 904103.
730. Alom Md Zahangir, Yakopcic Chris, Nasrin Mst, et al. Breast cancer classification from histopathological images with inception recurrent residual convolutional neural network. J Digit Imaging 2019;32(4):605–617.
731. Nawaz Majid, Sewissy Adel A, Taysir Hassan A, Soliman. Multi-class breast cancer classification using deep learning convolutional neural network. Int J Adv Comput Sci Appl 2018;9(6):316–332.
732. Gandomkar Ziba, Brennan Patrick C, Mello-Thoms Claudia. Mudern: Multi-category classification of breast histopathological image using deep residual networks. Artif Intell Med 2018;88:14–24.
733. Han Zhongyi, Wei Benzheng, Zheng Yuanjie, Yin Yilong, Li Kejian, Li Shuo. Breast cancer multi-classification from histopathological images with structured deep learning model. Sci Rep 2017;7(1):1-10.
734. Alirezazadeh Pendar, Hejrati Behzad, Monsef-Esfahani Alireza, Fathi Abdolhossein. Representation learning-based unsupervised domain adaptation for classification of breast cancer histopathology images. Biocybernet Biomed Eng 2018;38(3):671–683.
735. Meng Zhu, Zhao Zhicheng, Fei Su. Multi-classification of breast cancer histology images by using gravitation loss. IEEE International Conference on Acoustics, Speech and Signal Processing (ICASSP). IEEE; 2019. p. 1030–1034.
736. Rakhlin Alexander, Shvets Alexey, Iglovikov Vladimir, Kalinin Alexandr A. Deep convolutional neural networks for breast cancer histology image analysis. International Conference Image Analysis and Recognition. Springer; 2018. p. 737–744.
737. Vang Yeeleng S, Chen Zhen, Xie Xiaohui. Deep learning framework for multi-class breast cancer histology image classification. International Conference Image Analysis and Recognition. Springer; 2018. p. 914–922.
738. Nahid Abdullah-Al, Kong Yinan. Histopathological breast-image classification using local and frequency domains by convolutional neural network. Information 2018;9(1):19.
739. Teh Eu Wern, Taylor Graham W. Metric learning for patch classification in digital pathology. International Conference on Medical Imaging with Deep Learning–Extended Abstract Track; 2019.
740. Awan Ruqayya, Koohbanani Navid Alemi, Shaban Muhammad, Lisowska Anna, Rajpoot Nasir. Context-aware learning using transferable features for classification of breast cancer histology images. International Conference Image Analysis and Recognition. Springer; 2018. p. 788–795.
741. Iesmantas Tomas, Alzbutas Robertas. Convolutional capsule network for classification of breast cancer histology images. International Conference Image Analysis and Recognition. Springer; 2018. p. 853–860.
742. Roy Kaushiki, Banik Debapriya, Bhattacharjee Debotosh, Nasipuri Mita. Patch-based system for classification of breast histology images using deep learning. Comput Med Imaging Graph 2019;71:90-103.
743. Lei Gaoyi, Xia Yuanqing, Zhai Di-Hua, Zhang Wei, Chen Duanduan, Wang Defeng. Staincnns: An efficient stain feature learning method. Neurocomputing 2020;406:267–273.
744. Khan Amjad, Atzori Manfredo, Otálora Sebastian, Andrearczyk Vincent, Müller Henning. Generalizing convolution neural networks on stain color heterogeneous data for computational pathology. Medical Imaging: Digital Pathology. International Society for Optics and Photonics; 2020. p. 113200R.
745. Ziaei Dorsa, Li Weizhe, Lam Samuel, Cheng Wei-Chung, Chen Weijie. Characterization of color normalization methods in digital pathology whole slide imaging. Medical Imaging: Digital Pathology. International Society for Optics and Photonics; 2020. p. 1132017.

746. Guo X, Wang F, Teodoro G, Farris AB, Kong J. Liver steatosis segmentation with deep learning methods. IEEE International Symposium on Biomedical Imaging; 2019. p. 24–27.
747. Huang Yongxiang, Chung Albert. Evidence localization for pathology images using weakly supervised learning. International Conference on Medical Image Computing and Computer-Assisted Intervention. Springer; 2019. p. 613–621.
748. Öztürk Şaban, Akdemir Bayram. Hic-net: A deep convolutional neural network model for classification of histopathological breast images. Comput Electric Eng 2019;76:299–310.
749. Stacke K, Eilertsen G, Unger J, Lundström C. Measuring domain shift for deep learning in histopathology. IEEE journal of biomedical and health informatics 2020 Oct 20;25(2):325–336.
750. Gildenblat Jacob, Klaiman Eldad. Self-supervised similarity learning for digital pathology. arXiv 2019.preprint arXiv:1905.08139.
751. Otálora Sebastian, Atzori Manfredo, Khan Amjad, Toro Oscar Jimenez-del, Andrearczyk Vincent, Müller Henning. Systematic comparison of deep learning strategies for weakly supervised gleason grading. Medical Imaging: Digital Pathology. International Society for Optics and Photonics; 2020. p. 113200L.
752. Li Jiayun, Sarma Karthik V, Ho King Chung, Gertych Arkadiusz, Knudsen Beatrice S, Arnold Corey W. *A multi-scale u-net for semantic segmentation of histological images from radical prostatectomies*, 1140. 2017:2017.
753. Lara Juan S, Victor H, Contreras O, Otálora Sebastián, Müller Henning, González Fabio A. Multimodal latent semantic alignment for automated prostate tissue classification and retrieval. Medical Image Computing and Computer Assisted Intervention – MICCAI. Springer; Sep 2020. p. 572–581.of Lecture Notes in Computer Science.
754. Nguyen Ethan H, Yang Haichun, Deng Ruining, et al. Circle representation for medical object detection. IEEE Trans Med Imaging 2021;41 (3):746–754.
755. Almansouri Saif, Zwyea Susan. *Early prognosis of human renal cancer with kaplan-meier plotter data analysis model. In Journal of physics: conference series.* , 1530IOP Publishing. 2020:012051.
756. Graham Simon, Shaban Muhammad, Qaiser Talha, Koohbanani Navid Alemi, Khurram Syed Ali, Rajpoot Nasir. Classification of lung cancer histology images using patch-level summary statistics. Medical Imaging: Digital Pathology. International Society for Optics and Photonics; 2018. p. 1058119.
757. Corredor Germán, Toro Paula, Bera Kaustav, et al. Computational pathology reveals unique spatial patterns of immune response in H&E images from covid-19 autopsies: preliminary findings. J Med Imaging 2021;8(S1), 017501.
758. Adnan Mohammed, Kalra Shivam, Tizhoosh Hamid R. Representation learning of histopathology images using graph neural networks. IEEE/CVF Conference on Computer Vision and Pattern Recognition Workshops; 2020. p. 988–989.
759. Hägele Miriam, Seegerer Philipp, Lapuschkin Sebastian, et al. Resolving challenges in deep learning-based analyses of histopathological images using explanation methods. Sci Rep 2020;10(1):1-12.
760. Van Eycke Yves-Rémi, Balsat Cédric, Verset Laurine, Debeir Olivier, Salmon Isabelle, Decaestecker Christine. Segmentation of glandular epithelium in colorectal tumours to automatically compartmentalise ihc biomarker quantification: A deep learning approach. Med Image Anal 2018;49:35–45.
761. Yan Xu, Li Yang, Wang Yipei, et al. Gland instance segmentation using deep multichannel neural networks. IEEE Trans Biomed Eng 2017;64(12):2901–2912.
762. Kather Jakob, Weis Cleo-Aron, Bianconi Francesco, et al. Multi-class texture analysis in colorectal cancer histology. Sci Rep 2016;6: 27988.
763. Wang Chaofeng, Shi Jun, Zhang Qi, Ying Shihui. Histopathological image classification with bilinear convolutional neural networks. International Conference of the IEEE Engineering in Medicine and Biology Society (EMBC). IEEE; 2017. p. 4050–4053.
764. Rączkowski Łukasz, Możejko Marcin, Zambonelli Joanna, Szczurek Ewa. Ara: accurate, reliable and active histopathological image classification framework with bayesian deep learning. Sci Rep 2019;9(1):1-12.
765. Jayachandran Srinath, Ghosh Ashlin. Deep transfer learning for texture classification in colorectal cancer histology. IAPR Workshop on Artificial Neural Networks in Pattern Recognition. Springer; 2020. p. 173–186.
766. Foucart Adrien, Debeir Olivier, Decaestecker Christine. Snow: Semi-supervised, noisy and/or weak data for deep learning in digital pathology. IEEE International Symposium on Biomedical Imaging. IEEE; 2019. p. 1869–1872.
767. Lahiani Amal, Klaman Irina, Navab Nassir, Albarqouni Shadi, Klaiman Eldad. Seamless virtual whole slide image synthesis and validation using perceptual embedding consistency. IEEE J Biomed Health Inform 2020;25(2):403–411.
768. Ji Meng-Yao, Yuan Lei, Shi-Min Lu, et al. Glandular orientation and shape determined by computational pathology could identify aggressive tumor for early colon carcinoma: a triple-center study. J Transl Med 2020;18(1):1-12.
769. Hang Chang Ju, Han Cheng Zhong, Snijders Antoine M, Mao Jian-Hua. Unsupervised transfer learning via multi-scale convolutional sparse coding for biomedical applications. IEEE Trans Pattern Anal Mach Intell 2017;40(5):1182–1194.
770. Sarnecki Jacob S, Burns Kathleen H, Wood Laura D, et al. A robust nonlinear tissue-component discrimination method for computational pathology. Lab Invest 2016;96(4):450–458.
771. Gueréndel Corentin, Arnold Phil, Torben-Nielsen Ben. Creating small but meaningful representations of digital pathology images. MICCAI Workshop on Computational Pathology. PMLR; 2021. p. 206–215.
772. Wu Huisi, Wang Zhaoze, Song Youyi, Lin Yang, Qin Jing. Cross-patch dense contrastive learning for semi-supervised segmentation of cellular nuclei in histopathologic images. Proceedings of the IEEE/CVF Conference on Computer Vision and Pattern Recognition; 2022. p. 11666–11675.
773. Belharbi Soufiane, Rony Jérôme, Dolz Jose, Ayed Ismail Ben, McCaffrey Luke, Granger Eric. Deep interpretable classification and weakly-supervised segmentation of histology images via max-min uncertainty. IEEE Trans Med Imaging 2021;41(3):702–714.
774. Ghahremani Parmida, Marino Joseph, Dodds Ricardo, Nadeem Saad. Deepliif: An online platform for quantification of clinical pathology slides. Proceedings of the IEEE/CVF Conference on Computer Vision and Pattern Recognition; 2022. p. 21399–21405.
775. Pati Pushpak, Foncubierta-Rodríguez Antonio, Goksel Orcun, Gabrani Maria. Reducing annotation effort in digital pathology: A co-representation learning framework for classification tasks. Med Image Anal 2021;67, 101859.
776. Shen Yiqing, Shen Dinggang, Ke Jing. Identify representative samples by conditional random field of cancer histology images. IEEE Trans Med Imaging 2022;41(12):3835–3848.
777. Zhu Chuang, Chen Wenkai, Peng Ting, Wang Ying, Jin Mulan. Hard sample aware noise robust learning for histopathology image classification. IEEE Trans Med Imaging 2021;41(4):881–894.
778. Lu Ming Y, Williamson Drew FK, Chen Tiffany Y, Chen Richard J, Barbieri Matteo, Mahmood Faisal. Data-efficient and weakly supervised computational pathology on whole-slide images. Nat Biomed Eng 2021;5(6):555–570.
779. Srinidhi Chetan L, Kim Seung Wook, Chen Fu-Der, Martel Anne L. Self-supervised driven consistency training for annotation efficient histopathology image analysis. Med Image Anal 2022;75, 102256.
780. Zhu Yu'Ang, Zheng Yuxin, Chen Zhao. Cell detection by robust self-trained networks. International Conference on Pattern Recognition and Intelligent Systems; 2021. p. 64–67.
781. Belharbi Soufiane, Rony Jérôme, Dolz Jose, Ayed Ismail Ben, McCaffrey Luke, Granger Eric. Deep interpretable classification and weakly-supervised segmentation of histology images via max-min uncertainty. IEEE Transactions on Medical Imaging; 2021.
782. Graham Simon, Epstein David, Rajpoot Nasir. Dense steerable filter cnns for exploiting rotational symmetry in histology images. IEEE Trans Med Imaging 2020;39(12):4124–4136.

783. Shamima Nasrin Md, Alom Zahangir, Taha Tarek M, Asari Vijayan K. Pcolornet: investigating the impact of different color spaces for pathological image classification. Medical Imaging: Digital Pathology. International Society for Optics and Photonics; 2020. p. 113201A.
784. Hou Le, Samaras Dimitris, Kurc Tahsin M, Gao Yi, Davis James E, Saltz Joel H. Patch-based convolutional neural network for whole slide tissue image classification. Proceedings of the IEEE Conference on Computer Vision and Pattern Recognition; 2016. p. 2424–2433.
785. Salvi Massimo, Michielli Nicola, Molinari Filippo. Stain color adaptive normalization (scan) algorithm: Separation and standardization of histological stains in digital pathology. Comput Methods Programs Biomed 2020;193, 105506.
786. Kalra Shivam, Tizhoosh Hamid R, Shah Sultaan, et al. Pan-cancer diagnostic consensus through searching archival histopathology images using artificial intelligence. NPJ Digit Med 2020;3(1):1-15.
787. Mirzazadeh Ali, Mohseni Arshawn, Ibrahim Sahar, et al. Improving heart transplant rejection classification training using progressive generative adversarial networks. IEEE EMBS International Conference on Biomedical and Health Informatics (BHI). IEEE; 2021. p. 1–4.
788. Youqing Mu, Tizhoosh Hamid R, Tayebi Rohollah Moosavi, et al. A bert model generates diagnostically relevant semantic embeddings from pathology synopses with active learning. Commun Med 2021;1(1):1-13.
789. Dastidar Tathagato Rai, Ethirajan Renu. Whole slide imaging system using deep learning-based automated focusing. Biomed Opt Express 2020;11(1):480–491.
790. Bautista Pinky A, Yagi Yukako. Detection of tissue folds in whole slide images. 2009 Annual International Conference of the IEEE Engineering in Medicine and Biology Society. IEEE; 2009. p. 3669–3672.
791. Boyd Joseph, Liashuha Mykola, Deutsch Eric, Paragios Nikos, Christodoulidis Stergios, Vakalopoulou Maria. Self-supervised representation learning using visual field expansion on digital pathology. IEEE/CVF International Conference on Computer Vision; 2021. p. 639–647.